TABLE OF CONTENTS

NOTATION

A	Cross-sectional area.
$\underline{A}$	Displacement deformation transformation matrix.
$\underline{\alpha}$	Transformation matrix from global displacements to element deformations.
A_s	Shear area.
$\overline{A}_s$	Embedded shaft area of the pile.
A_p	Gross end area of the pile.
A_w	External cross-sectional area of the member.
A_i	Internal cross-sectional area of the member.
$\underline{AM}$	Added mass matrix.
$\underline{AM'}$	Updated added mass matrix.
$\overline{A}$	Projected area of member.
α_n	Amplitude of the nth wave components.
$\underline{b}$, $\underline{b}_1$, $\underline{b}_2$, $\underline{b}_s$	Unit vectors.
$\underline{B}_L$	Linear strain displacement transformation matrix.
$\underline{B}_1$	Strain displacement transformation matrix at beginning of step.
$\underline{C}$	Damping matrix.
$\overline{\underline{C}}$	Constitutive matrix.
C_h	Radiation damping coefficient.
c	Numerical constant.

c_i	Convergence ratio of iteration i.
C_M	Inertia coefficient
C_D	Horizontal drag coefficient.
C_{DS}	Longitudinal drag coefficient.
D	Water depth.
d_w	Effective water diameter.
$d\underline{r}$	Infinitesimal displacement increment.
$d\underline{R}_I$	Infinitesimal increment of resisting forces.
d_s	Direction factor.
$\underline{d}$	Rotation matrix from x_k to x_{k+1} about x_k.
dv_x, dv_y, dv_z	Increments of gap element deformations along the local x, y, and z axes, respectively.
dF_x, dF_y	Components of increment of tangential resistance in the x and y directions.
dF_z	Increment of normal force in the gap element.
dv_t	Increment of displacement in the tangential direction of the slip circle for the gap element.
dv_r	Increment of displacement in the radial direction of the slip circle for the gap element.
dF_r	Force increment in the radial direction of the slip circle of the gap element.
dF_t	Force component in the tangential direction of the slip circle of the gap element.
dV	Volume increment.
d	Member diameter.

E_x	Green's strain in the x direction.
E	Young's modulus.
$\underline{e}$	Linear strain increment.
E_T	Tangent Young's Modulus
E_h	Accumulated energy absorbed within the hysteresis loops.
E_f	Cumulative flexural energy at plastic hinges.
E_s	Cumulative inelastic stretch energy.
E_{cf}	Reference flexural energy for failure.
E_{cs}	Reference inelastic stretch energy for failure.
f_s	Step factor.
$\underline{f}_s$	Shear flexibility matrix.
F_{yi}	Axial strength at yield surface i.
F_s	Tangential strength of the slip circle of the gap element.
f	Unit skin friction along the pile shaft.
F_1, F_2	Numerical constants.
F_{HS}	Hydrostatic force at the end of the member.
$\underline{F}$	Element relative forces in the local coordinates.
F_x, F_y, F_z	Element forces.
F_r, F_t	Force components radial and tangential to the slip circle.
G	Shear modulus.

$\bar{G}$	Amount of stiffness modification.
G_s	Soil shear modulus.
$\underline{G}_k$	Projection of stiffness matrix into a subspace.
g	Gravity acceleration.
H	Horizontal component of tension at top end of catenary.
$H(w)$	Transfer function.
$\underline{H}_k$	Projection of mass matrix into a subspace.
H_w	Wave height.
I	Number of iterations for convergence.
I_y, I_z	Cross-sectional moment of inertia about the local y and z axes, respectively.
I_2, I_3	Cross-sectional moment of inertia about the local 2 and 3 axes, respectively.
i	Unit vector in the global X direction.
I_p	Iteration at which prediction of convergence begins.
J	Cross-sectional torsional moment of inertia.
j	Unit vector in the global Y direction.
K_b	Scalar stiffness.
$\underline{K}$	Structure stiffness matrix.
$\underline{K}^*$	Effective stiffness matrix.
$\underline{k}_t$	Total element stiffness matrix.
$\underline{k}_e$	Material element stiffness matrix.

$\underline{K}_g$ Geometric stiffness matrix.

$\underline{K}_T$ Structure tangent stiffness.

$\underline{k}_T$ Element tangent stiffness matrix in the local coordinates.

$\underline{K}_o$ Structure initial stiffness.

$\underline{K}_s$ Structure secant stiffness.

$\underline{K}_m$ Modified structure stiffness matrix.

$\underline{k}_{get}$ Element external geometric stiffness (truss bar form).

$\underline{k}_{gei}$ Element external geometric stiffness (invariant form).

$\underline{k}_{gi}$ Element internal geometric stiffness.

$\underline{k}$ Linear element stiffness matrix in the local coordinates.

$\underline{\hat{k}}$ Element stiffness matrix in the global coordinates.

$\hat{k}$ Unit vector in the global z direction.

K_{Pi} Plastic stiffness after yield surface i.

K_{Fi} Axial stiffness of the complete inelastic beam column element before yield surface i.

K_{Ti} Torsional stiffness of the complete inelastic beam column element before yield surface i.

K_{Mi} Flexural stiffness of the complete inelastic beam column element before yield surface i.

K_f Stiffness of tangential resistance of the gap element.

K_z	Tangent stiffness of the normal force deformation relationship of the gap element.
$\underline{\hat{k}}_T$	Element tangent stiffness matrix in the global coordinates.
k_{xx}, k_{yy}, k_{zz}	Rotational springs around the global axes.
$\underline{K}^1$	Structural stiffness matrix at the beginning of the step.
K_M	Hydrodynamic added mass coefficient.
K_i	Stiffness before yield surface i.
$\underline{k}_g$	Element geometric stiffness matrix.
L	Current element length.
L_o	Undeformed element length.
l_i	Cosine the angle between the local axis i and the global X axis.
L_p	Length of plastic hinge.
L_h	Additional hinge length.
L_c	Catenary length.
$\underline{M}$	Mass matrix.
m_i	Cosine the angle between the local axis i and the global Y axis.
M_x	Torsional moment about the local x axis.
M_y, M_z	Bending moment about the local y and z axes, respectively.
M_{yi}	Bending strength of the hinge at yield surface i.
M_{fp}	Fully plastic moment.

$\underline{n}$	Unit normal to x_k and x_{k+1}.
n_i	Cosine the angle between the local axis i and the global z axis.
$\underline{n}_i$	Unit normal to yield surface i.
$\underline{N}^*$	Shape function matrix.
$\underline{N}$	Shape function vector.
$\underline{N}_j$	Derivatives of shape functions.
N_{so}	Number of pile load cycles required to cause 50 percent degradation in strength.
n	Maximum number of iterations.
P^1	Current element axial force.
$P-Y$	Lateral load deflection curves for PSAS element.
P_{min}	Fully degraded strength of PSAS element.
P_d	Dynamic pile resistance.
P_s	Static (at reference rate of load application) pile resistance.
P_i	Internal fluid pressure.
P_o	External water pressure.
$\underline{P}$	Element nodal forces in the local coordinates.
P_{yi}	Lateral load on a cantilever corresponding to flexural yield surface i.
$\underline{q}$	Element displacements.
$\underline{Q}$	Element internal resisting forces in the global coordinates.

$Q-Z$	Axial load deflection at the pile tip.
Q_d	Axial pile capacity.
Q_p	End bearing resistance.
$\overline{q}$	Unit end bearing capacity.
$\underline{r}, \dot{\underline{r}}, ,\ddot{\underline{r}}$	Displacement, velocity, and acceleration in the global coordinates, respectively.
$\underline{R}_u$	Unbalanced forces.
$\underline{R}_I$	Static internal resisting loads.
$\underline{R}_E$	External loads.
$\underline{R}$	Total load vector.
r_b	Scalar displacement
R_b	Scalar force.
$\underline{R}_{Uo}$	Orthogonalized vector of unbalanced loads.
$\underline{R}_{Eo}$	Orthogonalized vector of external loads.
r	Local element coordinates in the isoparametric formulation.
$\lvert \underline{R}_u \rvert$	Norm of unbalanced loads.
R_n	Unbalance measure.
$\underline{R}_w$	Vector of wave loads.
S_s	Step size.
s	Local element coordinates for the isoparametric formulation.

$\underline{S}^1$	Initial stress matrix.
$\underline{\bar{S}}^1$	Initial stress vector.
$\underline{S}$	Stress vector.
S	Normalized Resistance.
S_p	Current stiffness parameter.
S_{hh}	Wave height spectrum.
t	Time.
$(\ )^T$	Transpose of a vector or matrix.
$\underline{t}$	Direction cosine matrix.
$\underline{T}$	Coordinate transformation matrix.
$\underline{T}_{ms}$	Transformation matrix at the middle of step orientation of the element.
$\underline{t}_k$	Direction cosine matrix of element local axes for configuration k (beginning of step).
$\underline{t}_{k+1}$	Direction cosine matrix of element local axes for configuration k+1 (end of step).
$\underline{t}_{ms}$	Direction cosine matrix at middle of step.
Ty_i	Torsional strength at yield surface i.
$T-Z$	Axial load deflection curve at the pile shaft.
T_f	Pile shaft resistance.
T_c	Axial pile shaft compressive strength.
T_t	Axial pile shaft tensile strength.

$\overline{T}$	Tension in catenary.
i	
T_{rc}	Axial pile shaft residual compressive strength.
T_{rt}	Axial pile shaft residual tensile strength.
t_s	Standard (or reference) rate of pile loading.
t_r	Actual rate of pile loading.
T_A, T_B	Tension at end points of the catenary.
T	Wave period.
u_x^1, u_y^1, u_z^1	Displacement components at the beginning of the step.
Δu_x, Δu_y, Δu_z	Displacement increments.
$\underline{u_\partial}$	Derivatives of displacement increments.
U	Unbalance tolerance.
u_{wx}, u_{wy}, u_{wz}	Water particle velocities.
$\dot{u}_{wx}$, $\dot{u}_{wy}$, $\dot{u}_{wz}$	Water particle accelerations.
$\overline{U}$	Mean wind velocity.
$\underline{u}$	Element displacements in local coordinates.
V_s	Segment value.
V	Normalized deflection.
v_s	Shear wave velocity of soil.
V_{sc}	Segment value of critical vector.
$\forall$	Displaced volume

v_x, v_y, v_z	Local displacements of gap element.
v_r, v_t	Displacement components radial and tangential to the slip circle.
$\underline{v}$	Element deformations in the local coordinates.
$\underline{w}$	Vector of internal degrees of freedom.
W	Weighting factor for convergence rate.
$\overline{w}$	Weight per unit length of catenary.
x	Local cartesian coordinate (longitudinal axis for beam or truss element).
x_k	Local x axis at configuration k (beginning of step).
x_{k+1}	Local x axis at configuration k+1 (end of step).
$X(\omega)$	Irregular sea amplitude for frequency ω.
$\underline{X}_k$	Trial eigenvectors.
Y	Global cartesian coordinate.
y	Local cartesian coordinate.
YS_i	Yield surface i.
Y_D	Deflection defining cyclic degradation characteristics for piles.
$Y(\omega)$	Vessel motion for frequency ω.
Z	Global cartesian coordinate.
z	Local cartesian coordinate.
Z_c, Z_{dc}, Z_{rc}	Axial pile shaft displacements required to define the compressive cycle of the T-Z curve.

Z_t, Z_{dt}, Z_{rt}	Axial pile shaft displacements required to define the tensile cycle of the T-Z curve.
α	Correction factor for the Hilbert-Hughes-Taylor method for step-by-step time integration.
$\bar{\alpha}$	Governing event factor.
α_m	Mass proportional damping factor.
α_s	Scaling factor for load increment.
α_E	External load increment.
α^i	Load increment for step i.
α_k	Angle between local x axis in configuration k (beginning of step) and local x axis in configuration [k+1] (end of step).
α'	Angle between F_X and the tangential resistance of the gap element.
β	Constant used in Newmark β method.
β_o	Initial stiffness damping constant.
β_T	Tangent stiffness damping constant.
β_i, β_j	Rotations about the local x axis (longitudinal axis) at the element ends i and j.
$\bar{\beta}$	Average longitudinal rotation.
β_R	Loading rate factor.
β'	Line search method scaling factor.
$\underline{\beta}$	Longitudinal rotation matrix.
γ	Numerical constant.
γ_w	Unit weight of sea water.

γ_i Unit weight of internal fluid.

$\Delta \underline{R}_m$ Equilibrium error at mid step.

Δv Element deformations due to scaled displacement increment (event-to-event dynamic solution strategy).

$\Delta \underline{v}_o$ Element deformations due to unscaled displacement increment (event-to-event dynamic solution strategy).

$\Delta \underline{E}_I$ Internal energy increment.

$\Delta \underline{R}_I$ Increment of internal resisting forces.

$\Delta \underline{r}$ Finite displacement increment.

Δt Time step.

$\Delta \underline{R}_E$ Increment of external loads.

$\Delta \underline{q}$, $\Delta \underline{Q}$ Increments in element nodal displacements and forces referred to the global coordinate axes.

$\Delta \underline{u}$, $\Delta \underline{P}$ Increments in nodal displacements and forces referred to element local axes.

$\Delta \underline{V}$, $\Delta \underline{F}$ Increments in nodal relative deformations and forces referred to element local axes.

δx Extension in the local x direction.

$\Delta \underline{R}$ Total load increment.

$\Delta \underline{r}^i$ Displacement increment in iteration i.

$\Delta \underline{r}_c^i$ Conjugate displacement increment in iteration i.

$\Delta \underline{r}_u$ Displacement increment due to unbalanced load.

$\Delta \underline{r}_E$ Displacement increment due to external load.

$\Delta \underline{R}^*$	Effective load increment.
$\Delta \underline{r}$, $\Delta \underline{\dot{r}}$, $\Delta \underline{\ddot{r}}$	Displacement, velocity and acceleration increments in global coordinates.
Δy	Yield extension.
$\underline{\eta}$	Nonlinear strain increment.
η	Sea surface elevation.
θ_y	Rotation about the y axis.
θ_z	Rotation about the z axis.
θ_{hinge}	Plastic rotation at failure.
θ_{cr}	Critical curvature.
θ_A, θ_B	Angle with horizontal at ends of catenary.
θ	Catenary angle at any point.
$\bar{\theta}$	Angle between x axis and wave direction.
κ	Wave number.
λ	Cyclic degradation factor for PSAS element.
$\bar{\lambda}$	Lamé's constant.
λ_w	Wave length.
μ	Coefficient of friction.
μ_h	Energy ductility ratio.
ν	Poisson's ratio.
ρ_s	Soil mass density.
ρ_p	Pile mass density.

ρ_w Water mass density.

σ Specified shift for subspace evaluation of eigenvalues.

ϕ_2, ϕ_3 Shear deformation terms for the local axes 2 and 3, respectively.

ϕ_x Angle of twist about the local x axis.

ϕ_v Angle between member axis and vertical axis.

$\bar{\phi}$ Angle between member axis and global axis.

$\underline{\Phi}$ Eigenvector matrix.

ϕ Flow potential function.

ψ Stream Function.

ω Angular frequency.

1.0 INTRODUCTION

1.1 Purpose

This manual provides a description of the theoretical basis of the SEASTAR program. The mathematical formulations implemented in major aspects of the code are included. Due to the wide variety of topics discussed in this manual, the complete details of some algorithms are not provided and reference is made to the appropriate publications. For details of the program usage and descriptions of the input parameters, the user is referred to "SEASTAR Users' Manual."

1.2 Scope

This manual is organized into eight chapters. Chapter One is the introduction. Chapter Two describes the linear and nonlinear static solution algorithms used in SEASTAR. Chapter Three describes the dynamic solution algorithms. The eigensolution methods are described in Chapter Four. The theoretical formulation of the SEASTAR finite elements is given in Chapter Five. Chapter Six describes the different types of element loadings and the methods used to evaluate these loads. Chapter Seven deals with the available options for the calculation of wave and current kinematics and the wave-current interaction. Finally, Chapter Eight deals with the response of marine vessels to irregular seas.

2.0 SEASTAR STATIC SOLUTION

2.1 Introduction

A large number of solution strategies are available for solving nonlinear structures. The choice of a particular solution strategy depends on the characteristics of the problem. Many different types of behavior may be present in nonlinear structures, including stiffening, softening and instability with different post-buckling characteristics. The most efficient and reliable strategy for solving any nonlinear structure is obtained by anticipating the structure response and knowledge of the characteristics of different solution strategies. The description of the nonlinear solution scheme given in this chapter is directly based on Simons (1982) (a study sponsored by the National Science Foundation).

Sections 2.2 through 2.9 introduce the terms and concepts most commonly used in static nonlinear analysis. Sections 2.10 to 2.26 describe the solution scheme implemented in SEASTAR.

2.2 Definitions

2.2.1 Notations

For any type of nonlinear or time domain finite element analysis, the solution is carried out in an incremental fashion. In each increment, the solution starts from a known deformed state (Configuration 1), which is at equilibrium, and tries to advance to another state (Configuration 2) which is also at equilibrium. All the pertinent variables, such as displacements and forces, at Configuration 1 have the superscript 1 and those at Configuration 2 have the superscript 2. The increment by which the variable changes has the prefix Δ; thus, the incremental relationship for a vector $\underline{r}$ is written as

$$\underline{r}^2 = \underline{r}^1 + \Delta r$$

where the underscore indicates a vector or a matrix.

When a variable does not have a superscript, it should be taken as otherwise defined.

The cartesian coordinate system is used throughout the manual with X, Y and Z being the global cartesian axes which are fixed in space. Another set of local coordinates is also used which varies from one element type to another. The set of local coordinates could be cartesian (x, y, z) or natural coordinates (r, s). The local axes will be defined as each element type is discussed in Chapter 5.

2.2.2 Displacements

For analysis by the Displacement Method, the primary unknowns of the problem are a number of kinematic degrees of freedom (DOF). These degrees of freedom are typically translational and rotational displacements at nodes of the structure, and will be referred to as the structure displacements, or simply, the displacements. The complete set of displacements can be arranged in a displacement vector in the global coordinates, $\underline{r}$. Each element has associated with it a subset of the structure displacements, typically the displacements at the nodes to which the element connects. These are the element displacements, which may be arranged in an element displacement vector in the global coordinates, $\underline{q}$.

The current displacements are the most recently calculated displacements. A displacement increment is a finite ($\Delta\underline{r}$) or infinitesimal ($d\underline{r}$) change in the displacements.

2.2.3 Structure State

Each set of displacements corresponds to a deformed state, for the structure as a whole and for each element. The element deformations are related to the element displacements by shape functions which ideally (although not necessarily) ensure that geometric compatibility is satisfied. Element stresses or stress resultants (element actions) are related to corresponding strains or strain resultants (element deformations) by constitutive relationships of a variety of possible types.

For any set of element actions, there is a set of element resisting forces, $\underline{Q}$, which satisfies element equilibrium. These forces are external forces exerted on the element, corresponding to the element displacements. The term "force" includes both translational forces and moments. The element forces can be assembled into a vector of structure resisting forces, $\underline{R}_I$.

The structure displacements, element deformations, element actions and structure resisting forces constitute the structure state. The process of calculating the structure state for the current displacements is termed state determination. The calculation begins at a reference state and proceeds in the following steps:

1. The displacement increment from the reference state to the current state must be given.

2. The element deformation increments are calculated using the shape functions.

3. The element actions in the current state are calculated, considering the reference state, the deformation increments, and the constitutive relationships.

4. The element resisting forces are calculated by equilibrium and assembled to give the structure resisting forces.

The current state is an equilibrium state if the structure resisting forces are equal to the external forces on the structure, $\underline{R}_E$. The external forces consist of all applied forces and reactions acting externally on the structure, one force for each structure displacement. In a numerical solution, an exact equilibrium state will never be

reached. Rather, a converged state will be sought in which the equilibrium error is acceptably small. A measure of the equilibrium error is provided by the vector of unbalanced forces, $\underline{R}_U$, given by:

$$\underline{R}_U = \underline{R}_E - \underline{R}_I \qquad (2-1)$$

The criterion for convergence is commonly expressed as a tolerance on a norm of $\underline{R}_U$ (e.g., Euclidean norm, maximum absolute value).

If an iterative solution fails to arrive at a converged state, it may be necessary to restore the previous converged state and attempt a new solution. A converged state which is saved to permit restoration is called a backup state.

2.2.4 Stiffnesses

The structure tangent stiffness (or tangent stiffness matrix), $\underline{K}_T$, is defined by:

$$d\underline{R}_I = \underline{K}_T \, d\underline{r} \qquad (2-2)$$

in which $d\underline{r}$ is an infinitesimal increment of displacement and $d\underline{R}_I$ is the corresponding increment of resisting force. The process of calculating the tangent stiffness in any state may be termed linearization. It is performed by calculating and assembling the tangent stiffnesses, $\underline{k}_T$, of all the elements. The tangent stiffness in the initial undeformed state, $\underline{K}_O$, is the initial stiffness. A stiffness, $\underline{K}_S$, which satisfies the finite relationship

$$\Delta \underline{R}_I = \underline{K}_s \, \Delta \underline{r} \qquad (2-3)$$

is a secant stiffness. In Eq. (2-3), $\Delta \underline{R}_I$ is the increment in internal resistance.

2.2.5 Equilibrium Equations

For a linear structural analysis, the structure displacements are typically found by solving equilibrium equations of the form:

$$\underline{K} \, \underline{r} = \underline{R} \qquad (2-4)$$

where $\underline{K}$ is the stiffness matrix of a linear structure in which $\underline{r}$ defines the total displacements and $\underline{R}$ is the total load vector. For nonlinear analysis, the displacements are generally calculated in increments, frequently (but not necessarily) by solving equations of the form:

$$\underline{K}_T \, \Delta \underline{r} = \Delta \underline{R} \qquad (2-5)$$

in which $\Delta \underline{R}$ is the total load increment.

2.2.6 Loads

Displacement of a structure may be caused by applied loads of a variety of types. A static applied load is conveniently constructed as a combination of a number of separate load patterns, each multiplied by a load pattern magnitude. The set of load pattern magnitudes constitutes the load magnitude. A load pattern may define nodal loads, element loads, initial strain loads, or imposed displacement loads.

Nodal loads and element loads may consist of point forces, linear forces, surface forces, and/or body forces. A set of forces constitutes a nodal load if its contribution to the load vector, $\Delta \underline{R}$, can be determined without considering the stiffness and/or strength properties of the elements (e.g., point forces applied directly on a node). A set of forces constitutes an element load if the element properties must be considered in setting up $\Delta \underline{R}$ (e.g., distributed load along the length of a beam element, which produces "fixed end" forces on the nodes). Nodal and element loads contribute forces directly to both the load vector, $\Delta \underline{R}$, and the external force vector, $\underline{R}_E$.

Initial strain loads, (e.g., temperature change) contribute to the load vector, $\Delta \underline{R}$, but do not contribute directly to the external force vector, $\underline{R}_E$. As with element loads, the contributions to $\Delta \underline{R}$ depend on the stiffness and/or strength properties of the elements.

With imposed displacement loads, displacement increments are specified in particular directions at particular nodes. That is, in the equilibrium equation:

$$\underline{K}_T \, \Delta \underline{r} = \Delta \underline{R} \qquad (2-6)$$

certain terms in $\Delta \underline{r}$ are specified, and the corresponding terms in $\Delta \underline{R}$ are initially unknown. This is taken into account in the solution of the equilibrium equations. The nodal forces corresponding to the imposed displacements become external forces (in effect, reactions) on the structure, and hence contribute to $\underline{R}_E$.

A load pattern may be fixed or configuration dependent. The loads in a fixed pattern are independent of the displacements (e.g., forces with fixed magnitudes and directions). Configuration dependent loads vary as the structure deforms (e.g., hydrostatic pressure).

2.3 General Concepts and Techniques

2.3.1 General

A number of concepts and computational techniques are of general use in nonlinear structural analysis. Several of these are reviewed in this section.

2.3.2 Scalar Displacement and Scalar Force

The projection of a displacement vector, $\underline{r}$, on a unit vector, $\underline{b}$, in the displacement space defines a scalar displacement, r_b, along the direction $\underline{b}$. That is,

$$r_b = \underline{b}^T \underline{r} \tag{2-7}$$

Similarly, the projection of a force vector, $\underline{R}$, on a unit vector $\underline{b}$ in the force space defines a scalar force along the direction $\underline{b}$. That is,

$$R_b = \underline{b}^T \underline{R} \tag{2-8}$$

2.3.3 Scalar Stiffness

A scalar stiffness, K_b, is the ratio of a scalar force to a scalar displacement. That is,

$$K_b = \frac{\underline{b}_1^T \Delta \underline{R}}{\underline{b}_2^T \Delta \underline{r}} \tag{2-9}$$

in which $\underline{b}_1$ and $\underline{b}_2$ are unit vectors. Usually, $\underline{b}_1$ and $\underline{b}_2$ will be the same. The direction of interest will usually be the direction of either the displacement increment or the load increment.

2.3.4 Stiffness Ratio

A measure of the change in stiffness during an analysis can be expressed as the ratio of a scalar stiffness in the current state to a scalar stiffness in the initial state.

Bergan [1978, 1979] introduced the concept of a current stiffness parameter, S_p, to help control the nonlinear solution strategy. This parameter has the following properties.

1. The initial value of S_p is 1. Values greater than 1 indicate that the structure is stiffer than it was initially, and values of less than 1 indicate that it is more flexible.

2. Generally, for a stable structure S_p is positive, whereas for an unstable structure it is negative.

3. Where the load magnitude reaches a local maximum, the value of S_p is zero.

4. The rate of change of S_p is related to the nonlinearity of the response. For structures that are nearly linear, S_p changes slowly, whereas for structures that are highly nonlinear, S_p changes rapidly.

2.3.5 Rank One Stiffness Modification

A rank one stiffness matrix can be added to a structure stiffness matrix, $\underline{K}$, to change the stiffness in a particular direction, $\underline{b}$, by an amount $\hat{G}$. The modified stiffness matrix, $\underline{K}_m$, is given by:

$$\underline{K}_m = \underline{K} + \bar{G}\ \underline{b}\ \underline{b}^T \qquad (2-10)$$

The inverse of the modified stiffness matrix is given by the Sherman-Morrison formula as:

$$\underline{K}_m^{-1} = \underline{K}^{-1} - \frac{\underline{K}^{-1}\ \underline{b}\ \underline{b}^T\ \underline{K}^{-1}}{\frac{1}{\bar{G}} + \underline{b}^T\ \underline{K}^{-1}\ \underline{b}} \qquad (2-11)$$

Higher order modifications to a stiffness matrix can be made by a series of rank one modifications.

2.4 Newton-Raphson Iteration

2.4.1 General

The Newton-Raphson (NR) iteration scheme is well known as a method for the analysis of nonlinear structures. It is reviewed here as a basic solution scheme to introduce the concepts and operations found in the more general methods to be discussed later.

2.4.2 Algorithm

If the current state is an equilibrium state, the iterative sequence for NR iteration is as follows: (Figure 2-1):

1. The tangent stiffness is formed in the current state.

2. A load increment is added to the structure. A displacement increment is found by solving the equilibrium equations.

3. A state determination is carried out, and the structure resisting force is calculated.

4. The unbalanced force is calculated. Convergence is checked. If converged, go to Step 1. If not converged, continue.

5. The tangent stiffness is formed in the new current state.

6. The displacement increment due to the unbalanced load is calculated.

7. A state determination is carried out, and the structure resisting force is formed.

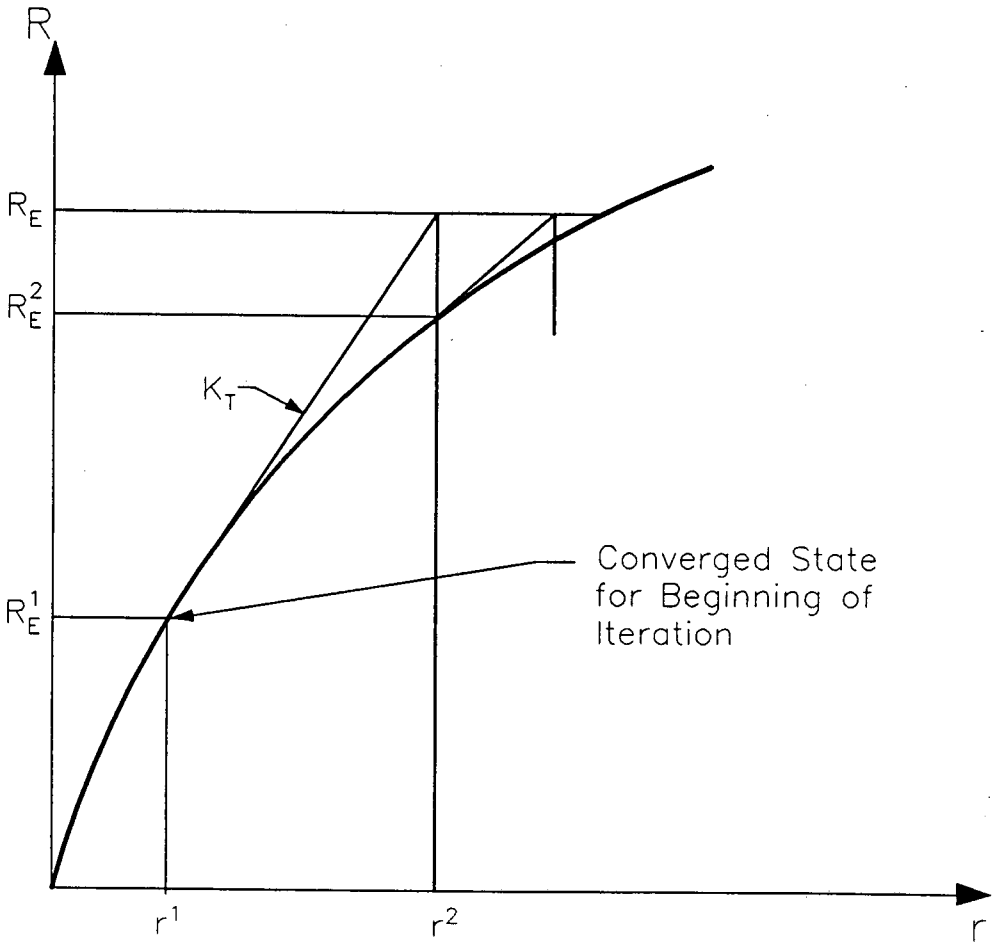

FIG. 2-1 NEWTON-RAPHSON ITERATION

8. The unbalanced force is calculated. Convergence is checked. If converged, go to Step 1. If not converged, go to Step 5.

2.4.3 Phases

There are two phases in the above sequence. In the advancing phase (Steps 1 to 4), a load increment is applied. In the correcting phase (Steps 4 to 8), the load magnitude is kept constant and the solution iterates in search of a converged state.

2.4.4 Tasks

The solution scheme can be separated into four distinct tasks, as follows, each of which is performed in both phases.

1. Linearization. The tangent stiffness is formed in the current state.

2. Displacement Prediction. A displacement increment is obtained by solving the equilibrium equations.

c. State Determination. The element deformation, element actions, element resisting forces, and structure resisting forces are calculated.

d. Convergence Check. The external force vector is formed, and the unbalanced force vector is checked for convergence.

2.4.5 Weaknesses

The basic NR scheme, although effective in many cases, is not necessarily the most economical solution scheme and does not always provide rapid or reliable convergence. Some weaknesses of the method are as follows:

1. Linearization Expense

   The computation involved in linearization and equation solving may be large. When the solution is nearly converged, only small changes will take place in the tangent stiffness, and a new linearization may not be needed.

2. Load Increments

   The size of each load increment must be predetermined. Because the structure stiffness varies throughout the analysis, equal load increments will produce unequal displacement increments and unequal unbalanced forces. A load increment that produces reasonable displacements with fast convergence initially may predict large displacement increments with slow or nonexistent convergence as the structure yields and becomes flexible. A substantial amount of trial and error may be needed to determine the appropriate load increments.

3. Step Direction

   The analyst will usually have no alternative but to specify positive load increments. In many structures, the strength can

reach a maximum and then decrease. In order to follow an equilibrium path in such cases, negative load increments must be applied.

4. Constant Load Iteration

The load is kept constant during iteration. If the structure strength reaches a maximum and then decreases, it is possible for the applied load to be greater than the structure strength, in which case convergence is impossible (at least near the predicted displaced state).

5. Sudden Nonlinearities

In some problems, distinct "events" occur that drastically alter the stiffness (for example, gap closure). If such an event occurs in either the advancing or correcting phase, the calculated displacement increment may be a poor estimate of the actual increment and results in a large unbalance.

6. Nonconvergence

If the analysis does not converge in a specified number of iterations, it is necessary either to quit or to continue from a nonconverged state.

7. Path Dependent State Determination

The structure state is updated at each iteration, and nonconverged states are thus used as reference states. Because

of the path dependent behavior of inelastic materials use of nonconverged reference states may cause the calculated material response to differ from the true response.

2.4.6 Variations on NR

To overcome some of the weaknesses of NR iteration, a number of modifications of the basic scheme have been proposed. These modifications can be classified into four categories, as follows:

1. Variations in the stiffness formation.
2. Variations in the advancing phase.
3. Variations in the correcting phase.
4. Special logic in case of large unbalance or nonconvergence.

The modifications are discussed in the following sections.

2.5 Variations in Stiffness Formation

2.5.1 Modified Newton Methods

If the analysis is not highly nonlinear, the structure stiffness will not change much between iterations. It is then possible to use the existing stiffness matrix to predict the displacement increment. Displacements predicted in this way may not converge as fast as those predicted with an updated stiffness, but because each iteration is cheaper, more iterations can be performed for the same cost. Variations on the NR scheme that do not reformulate the stiffness every iteration are commonly termed "modified Newton" methods. Some of these are described below and illustrated in Figure 2-2.

In initial stiffness iteration, the initial stiffness matrix, $\underline{K}_0$, is used for all the displacement increment calculations. In constant stiffness iteration, the stiffness matrix is updated for the advancing phase and then kept constant during the iteration. Other variations include (a) updating the stiffness in the advancing phase and at specified iterations during the correcting phase, and (b) reforming the stiffness when necessary according to some specified criteria (e.g., keep $\underline{K}$ constant after the solution converges to some preliminary tolerance).

2.5.2 Quasi-Newton Methods

An alternative to reformulating the stiffness every iteration or keeping the stiffness constant is modifying the stiffness in some way. This is the idea behind "quasi-Newton" methods. Modifications are typically done so that the following guidelines are met.

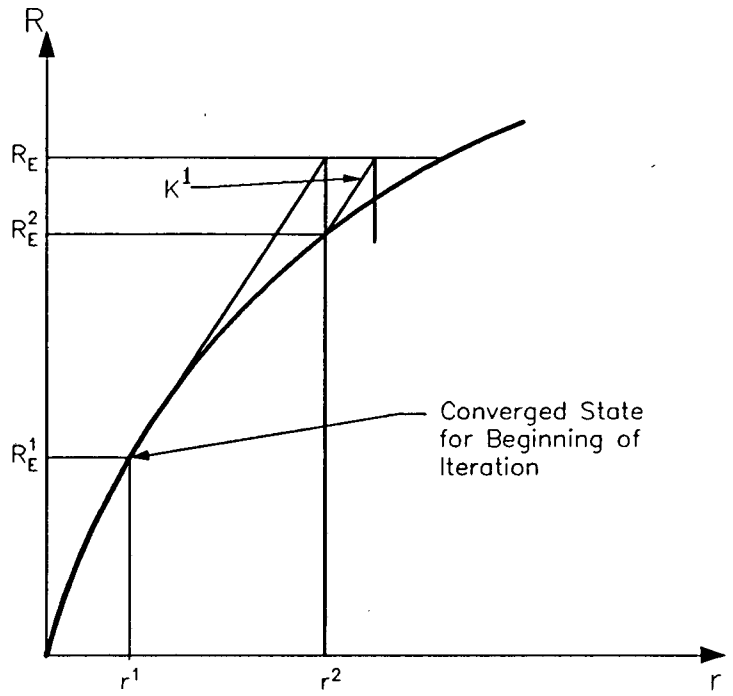

(a) = Constant Stiffness

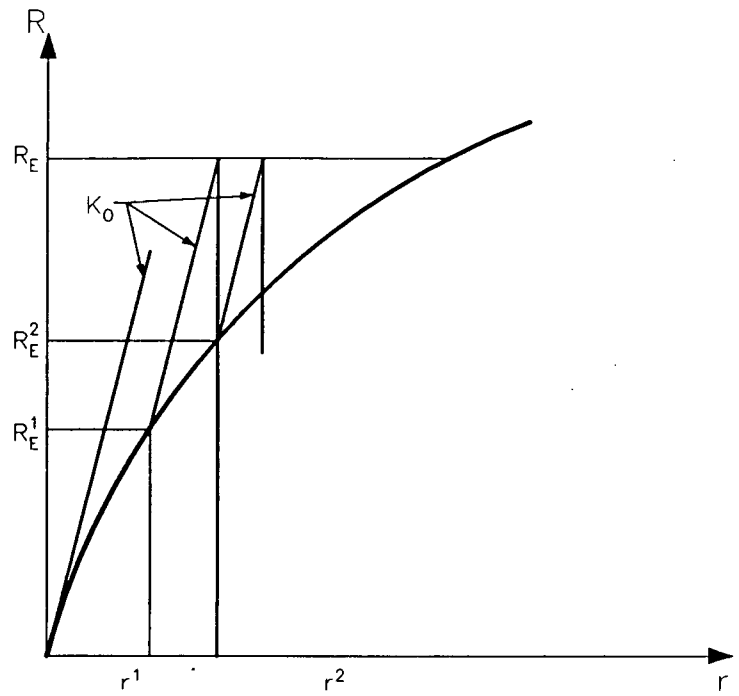

(b) = Initial Stiffness

FIG. 2-2 MODIFIED NEWTON METHODS

1. The modified stiffness matrix, $\underline{K}_m$, for any iteration, i, should be a secant stiffness matrix for the displacements calculated in the previous iteration.

2. If $\underline{K}$ is symmetric and positive definite, $\underline{K}_m$ should also be symmetric and positive definite.

3. Displacement increments using $\underline{K}_m$ should be cheap to calculate.

There is extensive literature on methods of stiffness modification, most of it from fields other than structural analysis. The method which has received the most attention for structural analysis is the Broyden-Fletcher-Goldfarb-Shanno (BFGS) method. (See Mattheis & Strang (1979).) It proposed modification of the stiffness matrix by addition of a rank two matrix. Rank one updates may not be numerically stable, and hence are not popular.

BFGS Correction

The BFGS modification is a rank two update. The stiffness is changed in two directions. The first of these is given by the change in the resisting force for the last iteration.

The second stiffness change is in the direction of the unbalanced force.

The inverse of the modified stiffness can be found by two applications of the Sherman-Morrison formulas, as discussed by Dennis and More (1977).

2.6 Variations in the Advancing Step

2.6.1 Variable Load Magnitude

Strategies that automatically select the load increment during the analysis have been developed to avoid having to specify the load increments in advance. Three strategies are described. In the first two, the aim is to keep the unbalance at the end of the advancing phase constant in each step. In the third, the aim is to keep the number of iterations in each step constant.

Bergan's Current Stiffness Parameter

Bergan (1978) uses the current stiffness parameter, S_p, as a guiding quantity for selecting the load increment. If the linearization is regarded as a first order Taylor series approximation, the truncation error in the advancing phase varies with (a) the load increment and (b) a norm measure of the second derivative of $\underline{r}$ with respect to the load magnitude.

Because S_p is an approximation to the first derivative of the displacements (with respect to the load magnitude), the change in S_p divided by the change in load magnitude is an approximation to the second derivative. Hence, the truncation error will be approximately constant in each step if the load increment is chosen so that the change in S_p is constant.

This method of step selection will result in small steps where the solution is strongly nonlinear and large steps in nearly linear regions.

Scaling Based on Unbalance

Step scaling based on the unbalance can be done directly if a state determination is added to the process. In this method, a trial step is taken, a state determination is performed, and the unbalance is calculated. If the unbalance is too large (based on some tolerance), the step is repeated with a reduced load increment.

The procedure is as follows:

1. Select a load increment (based on any method).
2. Solve for the displacement increment.
3. Perform a state determination.
4. Calculate the unbalance.
5. If the unbalance is greater than the specified tolerance, scale the load increment, according to

$$\alpha_s = \frac{U}{|\underline{R}_U|} \qquad (2-12)$$

where

α_s = scale factor for load increment.

U = unbalance tolerance.

$|\underline{R}U|$ = norm of unbalanced load.

and repeat from Step 3. If the unbalance is less than the tolerance, enter the correcting phase.

Because the unbalance varies approximately quadratically with the displacement increment (based on the truncation error), a linear scaling will, in most cases, be sufficient to reduce the unbalance below the allowable tolerance.

Scaling Based on Number of Iterations

A method in which the load increment is adjusted based on the number of iterations has been suggested by Crisfield (1981). The magnitude of each step (except the first, which must be specified) is calculated as follows for Step i:

$$\alpha^i = \frac{\alpha^{i-1} I}{I^{i-1}}$$

where

I^{i-1} = number of iterations for convergence in Step i-1.

α^{i-1} = load increment for Step i-1.

I = desired number of iterations for convergence.

2.6.2 Displacement Control

An alternative to varying the load increment is to control the size of the displacement increment directly. Various measures of the

displacement increment can be controlled, including (a) a single displacement degree of freedom, (b) a scalar displacement, and (c) the "arc length" of the increment.

Single Degree of Freedom Control

Haisler and Stricklin (1977) describe a step-by-step method without iteration in which a selected displacement (the controlled displacement) is increased by a specified amount in each step. In any step, the unbalanced load at the beginning of the step, plus some load increment, is applied. The magnitude of the load increment is initially unknown and is chosen to increase the controlled displacement by the specified amount. Because the displacement vector for any step consists of two parts, one due to the load increment and one due to the unbalance, the displacements cannot simply be scaled linearly to meet the displacement constraint, and a special computational procedure is needed to determine the required load magnitude. For details of the procedure, refer to Haisler and Stricklin (1977).

Scalar Displacement Steps

The method described in the preceding section has been presented in a generalized form by Powell and Simons (1981). In this method, the controlled displacement is not limited to a single DOF but is a scalar displacement characterized by a unit vector, $\underline{b}$.

Arc Length Steps

An alternative method of advancing the solution has been proposed by Riks (1974) and Crisfield (1981) and discussed by Ramm (1980). The "arc

length" of the step, $\bar{s}$, is defined by the Euclidean norm of a vector containing both the load increment and the displacement increment. That is,

$$\bar{s} = (\alpha_E^2 + \Delta \underline{r}^T \Delta \underline{r})^{1/2} \qquad (2-13)$$

in which

$\Delta \underline{r}$ = displacement increment.

α_E = load increment.

The arc length, in geometric terms, is an approximation to the length of the step in the displacement-load space.

Because both the load increment and the displacement increment are included in $\bar{s}$, the size of the load increment should be determined primarily by the largest of these quantities. When the structure is very flexible, the displacements will control the size, and when the structure is very stiff, the load increment will control.

This choice of load increment has some weaknesses, however. First, the quantities that make up the arc length do not have the same units (one is a load term and the rest are displacements). Because of this, the relative influence of the load term depends on the units which are chosen. Second, since the arc length contains all degrees of freedom, local nonlinearities tend to get lost or diluted, especially in analyses with many DOF.

From numerical experience, Crisfield recommends that the load increment not be included in the calculation (1981). The resulting strategy is then a displacement controlled method using the Euclidean norm of the displacement increment to control the size of the load increment.

Choice of Step Direction

In an analysis of a buckling structure, the load magnitude may increase up to a maximum value and then decrease as the structure continues to deform. This will be termed load reversal. For load stepping, negative load increments must be applied to follow the equilibrium path.

For displacement stepping a similar problem may occur, in which the controlled displacement reaches a maximum and then decreases. To continue the analysis past this displacement reversal, it is necessary to change from positive to negative displacement steps.

In general, if the controlled quantity (load or displacement) does not experience a reversal, then the step direction can simply be chosen as positive in each step. If, however, the controlled quantity is subject to reversals, a procedure to choose the step direction is necessary. Two procedures are considered here, the first based on the current stiffness parameter and the second on continuity of the displacement increment.

Current Stiffness Parameter

The current stiffness parameter, S_p, is used by Bergan to choose both the load magnitude and the step direction. When the load magnitude changes direction, S_p passes through zero. Monitoring S_p enables the direction of the load increment to be chosen as follows:

1. Initially S_p is equal to one and the load increment is positive.

2. As the stiffness deceases, S_p becomes smaller. As long as S_p remains positive, the load increment is chosen as positive.

3. If S_p passes through zero and changes sign, the load increment is chosen as negative, until S_p passes back through zero and becomes positive.

Continuity

Crisfield (1981) describes a method for choosing the step direction based on continuity of the displacement increments. The idea is that in order to keep the solution from going back on itself, consecutive displacement increments should be in the same direction. In each step, the displacement direction that makes the smaller angle with the previous displacement increment is the one chosen.

2.7 Variations in the Correcting Phase

As discussed in Section 2.4.6, the basic NR scheme has some weaknesses in the correcting phase. First, the iteration is done with constant load, which may lead to divergence. Second, path-dependent state determination is used, which can introduce errors in the material response. Third, no provision exists to alter the magnitude or direction of the displacement increment found by solving the equilibrium equations.

Several variations in the correcting phase have been proposed to overcome some of these weaknesses. Instead of iterating with constant load, schemes have been devised that (a) do not iterate, (b) do not iterate when the stiffness is very low, and (c) iterate with constant displacement. Schemes that alter the magnitude and/or direction of the calculated displacement increment in order to aid convergence have also been developed. Among these schemes are the line search methods to select the magnitude and the conjugate Newton method to alter the direction. Also, instead of path dependent state determination, path independent state determination is easily incorporated. These variations are discussed below.

2.7.1 No Iterations

The scheme proposed by Haisler and Stricklin (1977) is performed without iteration. The solution is carried out step-by-step with the unbalanced load and an increment of the load applied each step.

Bergan (1978) suggests that iteration be suspended only near critical points. He recommends the use of the current stiffness parameter, S_p, as a criterion for iteration, and iterations are performed only if S_p is not

near zero. Because S_p is a measure of the scalar stiffness of the structure, it will be close to zero when the structure stiffness is very low.

In schemes with iteration, it is usual to iterate until the unbalanced load is small so that only small unbalances are carried over from step to step. In schemes that do not iterate, substantial unbalances can be carried over, which may contribute to a drift from the equilibrium path.

2.7.2 Displacement Control

Methods that control displacements can be used in the correcting phase, and can be thought of as a special case of the method described in Section 2.6.2 for controlling the displacement increment in the advancing phase. In the correcting phase, iteration with some scalar displacement held constant corresponds to specifying the increment in that scalar displacement to be zero.

An important point to note is that if iteration is done at a constant displacement, the load magnitude varies during the iteration. For a softening structure, the load magnitude will typically decrease during iteration. For structures that reach a maximum load, the problem of iterating at a load magnitude greater than the structure strength is overcome, because the load magnitude is automatically reduced during the iteration.

2.7.3 Path Independent State Determination

In NR iteration, the state is updated in each iteration, so that the state determination is path dependent. It has been noted that path

dependent state determination can lead to significant errors if the path followed is far from the equilibrium path. An alternative scheme is to use path independent state determination.

If the element strains increase progressively during the iteration sequence, there will usually be little difference between the final states calculated by the two schemes. However, if the strains increase in early iterations and then decrease, the path dependent scheme may incorrectly unload yielded elements. Consider, for example, an analysis of a softening structure with constant displacement iteration. The load magnitude typically decreases in the iteration phase, although the accumulated load increment from the beginning of the step is positive. A path-dependent scheme will allow unloading of yielded elements as the load decreases, whereas a path independent scheme will not because it is based on the accumulated displacement increment. Path independent state determination is thus recommended for displacement controlled analysis.

2.7.4 Line Search

The displacement increment found by solving the equilibrium equations does not necessarily give the best estimate of the equilibrium state. Instead, some multiple of the displacement increment, $\beta' \Delta \underline{r}$, may be better. In line search methods, β' is chosen to minimize some measure of the unbalance, usually by a successive trial procedure.

Matheis and Strang (1979) discuss the use of a line search routine in conjunction with the BFGS stiffness modification scheme. The technique can be used with any method for choosing the displacement increment.

The line search is carried out as follows:

Phase 1: Upper and lower values of β' are sought which bound a zero value of unbalance.

1. A measure of the unbalance, R_n, at the beginning of the step ($\beta' = 0$) and for the calculated displacement increment ($\beta' = 1$) is calculated as follows:

$$R_n(\beta') = \Delta \underline{r}^T \ \underline{R}_U \ (\beta') \qquad (2-14)$$

$R_n(\beta')$ is a measure of the external work that the unbalanced load does on the structure.

2. If the unbalance measures are of opposite signs, the zero is bounded, so enter Phase 2. If the unbalance measures are of the same sign, the double the step size ($\beta' = 2$) and recalculate the unbalance, this time using $\beta'_1 = 1$ and $\beta'_2 = 2$ as the bounds. Repeat this step until a zero unbalance is bounded or until a maximum number of trails have been performed.

Phase 2: Find β' to minimize the unbalance.

1. Based on the values of $\beta'_1 = 1$ and $\beta'_2 = 2$ and the corresponding unbalances, use a linear approximation to choose the new value of β'. That is,

$$\beta' = \beta'_1 + \frac{R_n(\beta'_1)\ (\beta'_2 - \beta'_1)}{R_n(\beta'_2) - R_n(\beta'_1)} \qquad (2-15)$$

2. Evaluate the unbalance for this value. If it is less than a specified tolerance, then quit. If not, choose the two points with opposite signed unbalances and repeat Step (1). Convergence is obtained when the unbalance is less than a specified proportion of $R_n(0)$. That is, when

$$R_n(\beta') < c\, R_n(0) \qquad (2-16)$$

where c is a constant between zero and one.

2.7.5 Conjugate Newton

In all of the methods described so far, the search directions has been calculated by solving the equilibrium equations. Irons (1977) has introduced the conjugate Newton method in which the direction of the displacement increment is modified in each iteration. It is based on an idea from the conjugate gradient method (an iterative method of solving function minimization problems), in which a set of search directions that are conjugate result in an efficient search.

In the conjugate Newton method, a displacement increment $\Delta \underline{r}^i$ is first calculated as in the constant stiffness iteration. This increment is then modified so that it is conjugate to all previous directions, i.e., so that:

$$(\Delta \underline{r}^i)^T \; \underline{K}^1 \; \Delta \underline{r}^i = 0 \qquad j = i-1, i-2, \ldots, 1 \qquad (2-17)$$

where $\underline{K}^1$ is the stiffness matrix at the beginning of the step.

The steps are as follows for each iteration.

1. An unmodified displacement increment is obtained from:

$$\underline{K}^1 \, \Delta \underline{r}^i = \Delta \underline{R}^i \qquad (2-18)$$

2. The displacement increment is made conjugate to the previous displacement increments.

$$\Delta \underline{r}_c^i = \Delta \underline{r}^i - c \, \Delta \underline{r}_c^{i-1} \qquad (2-19)$$

where c is a constant determined so that:

$$\left(\Delta \underline{r}_c^i\right)^T \underline{K} \, \Delta \underline{r}_c^{i-1} = 0 \qquad (2-20)$$

where

$\Delta \underline{r}_c^i$ = modified displacement increment.

$\Delta \underline{r}_c^{i-1}$ = displacement increment from previous iteration.

3. The magnitude of the step is calculated by a line search.

2.8 Special Logic

In cases where large unbalances develop or the iteration fails to converge, it may be necessary to implement special logic in order to complete the analysis. Three schemes which have been developed to deal with these problems are considered in this section.

The first scheme aims to reduce the unbalance by making it orthogonal to the external force. The second scheme is applicable to problems in which a large unbalance may result from distinct "events" (e.g., gap closure). A strategy that advances the solution from event to event is described. Finally, for problems that do not converge within a specified number of iterations, a scheme to restart the analysis from the last converged state is described, along with a procedure to predict convergence.

2.8.1 Orthogonalized Unbalance

Bergan (1979) has introduced a method in which the unbalance force is orthogonalized with respect to the applied force in each iteration. The method is as follows for each iteration.

1. Calculate the displacement increment in the usual way.

2. Perform the state determination and calculation of the resisting force, $\underline{R}_I$.

3. Calculate the unbalanced force, $\underline{R}_U$.

4. Calculate the component $\underline{R}_U$ parallel to $\underline{R}_E$ and subtract it from both $\underline{R}_U$ and $\underline{R}_E$. That is:

$$\underline{R}_{EO} = (1.0 - \gamma)\ \underline{R}_E \qquad (2\text{-}21)$$

$$\underline{R}_{UO} = \underline{R}_U - \gamma\ \underline{R}_E \qquad (2\text{-}22)$$

where

$$\gamma = (\underline{R}_U^T\ \underline{R}_E) / (\underline{R}_E^T\ \underline{R}_E)$$

and the subscript 0 represents an orthogonalized vector.

5. Check convergence. If converged, go to the next step. If not, repeat from Step (1).

2.8.2 Event-to-Event Strategy

A strategy for problems that are linear (or nearly linear) between well-defined events is to advance the solution from event to event, rather than take specified steps with iteration. This strategy is discussed, for example, by Porter (1971). The purpose of the event-to-event strategy is to follow the equilibrium path closely at all times by updating the stiffness and state each time an event occurs. In this way the unbalance will, ideally, never get large.

The procedure is as follows, assuming the current state is an equilibrium state.

1. Linearize about the current state.

2. Calculate the displacements for an arbitrary load increment.

3. Predict the next event. Events typically correspond to changes of state in the elements, and event prediction calculations must be performed for each element to determine whether the calculated displacement increment will cause an event. If an event is predicted, a scale factor is determined that will bring the solution just to the predicted event.

4. Scale the displacement increment and add it to the current displacements. Update the structure state. Continue from Step 1.

2.8.3 Restepping if No Convergence

Despite the wide range of strategies available, convergence will not always occur. In such cases, it is helpful to have a restepping capability available. This means that if convergence is not obtained at the end of the correcting phase, the step size is reduced and the step is taken again from the backup state.

2.8.4 Convergence Prediction

The restepping option can be augmented by the use of a routine that predicts convergence, After a specified number of iterations, a prediction is made as to whether the solution will converge in the allowable number of iterations. If nonconvergence is predicted, the restepping option is exercised. This type of prediction can save doing futile iterations.

2.9 Desirable Features of a General Algorithm

It is possible to construct a general solution algorithm which retains the structure of NR iteration but which incorporates most of the variations described in the previous sections. The desirable features of such a general algorithm are those that overcome the difficulties of the standard NR iteration. Some of the features are as follows:

1. Strategies that avoid the high cost of linearization:

    a. Modified Newton methods, such as initial stiffness and constant stiffness iteration, that keep the stiffness constant for a number of iterations.

    b. Quasi-Newton methods, such as BFGS, that use simple modifications to the stiffness matrix.

2. Aids to convergence, especially for buckling and snap-through problems:

    a. Variable step size based on the current stiffness parameter or the unbalanced load.

    b. Line search in the correcting phase to minimize the unbalance.

    c. Direct control over the displacement increment.

    d. Iteration with constant displacement.

    e. Choice of path dependent or path independent state determination.

3. Special strategies, such as event-to-event, to deal with particular types of behavior.

4. Restepping capabilities combined with iteration prediction to deal with nonconvergence.

2.10 Tasks and Phases

The general solution scheme for static nonlinear analysis incorporated into the SEASTAR program is described in the remaining sections. The scheme is similar in structure to Newton-Raphson iteration. However, whereas there are four distinct tasks in NR iteration (linearization, calculation of the new displaced state, state determination, and convergence check), there are only three in the general scheme. Linearization, which is performed every iteration in NR iteration, is not considered as a separate task but only as an option for selecting a new displaced state. The three tasks are:

a. Selection of the new displaced state.
b. State determination.
c. Calculation of the unbalanced load and checking of convergence.

As in NR iteration, there are two phases in the analysis, namely, the advancing phase and the correcting phase. The three tasks are performed in each of the two phases.

2.11 Steps and Segments

An analysis is carried out in a series of analysis steps, each consisting of an advancing phase and a correcting phase. The step size (which defines the increments of load and displacement for the step) is controlled by a stepping parameter, which may be either a load or displacement quantity. For load stepping, the increment of load magnitude is controlled and the displacement follows. For displacement stepping, the increment in some displacement measure is controlled and the load magnitude follows. The displacement measure will usually be a specified scalar displacement but may also be (a) a displacement norm or (b) the most critical of a set of specified scalar displacements. Details are presented later.

A complete analysis is divided into a number of analysis segments, each of which is divided into a number of analysis steps. The amount of load or displacement applied in a segment is defined by the analyst in terms of a segment value, V_S. For load stepping, the segment value is the change in load magnitude for the segment. For displacement stepping, the segment value is the change in a scalar displacement or displacement norm. Within any analysis segment, stepping continues until the segment value is reached. The step size, S_S, is conveniently expressed as the produce of a step factor, f_S, (a number between 0 and 1), the segment value, and a direction factor, d_S (which is either 1 or -1). That is,

$$S_s = f_s \; V_s \; d_s \qquad (2-23)$$

The step factor may be specified in advance by the analyst, or it may be determined automatically to satisfy certain criteria, depending on the stepping options selected by the analyst.

2.12 Displacement Increment

For the advancing phase, and in each iteration of the correcting phase, a displacement increment must be determined. The basic procedure for calculating a displacement increment is as follows:

1. Displacements due to (a) the unbalanced load and (b) an arbitrary increment of applied load are calculated by solving the equilibrium equations:

$$\Delta \underline{r}_U = \underline{K}^{-1} \underline{R}_U \qquad (2-24)$$

$$\Delta \underline{r}_E = \underline{K}^{-1} \Delta \underline{R}_E \qquad (2-25)$$

   where $\underline{K}$ is the appropriate stiffness depending on the chosen solution strategy.

2. The displacement increment is formed as a linear combination of these two displacement vectors. That is,

$$\Delta \underline{r} = \Delta \underline{r}_U + \alpha_E \Delta \underline{r}_E \qquad (2-26)$$

A constraint equation on either a load or displacement quantity is used to select the increment of applied load, α_E. For load stepping, α_E is specified directly, whereas for displacement stepping it is calculated using a displacement constraint equation.

2.13 Advancing Phase

In the advancing phase, a load increment and a corresponding displacement increment must be determined to advance the solution along the equilibrium path. The nature of the step is determined by the stepping parameter, step factor, and direction factor.

2.13.1 Determination of Step Factor

The step factor is a fraction of the complete segment value (load or displacement) to be applied in the step. Similarly, for displacement stepping, a step factor of 0.5 means that half of the segment displacement is applied in the step.

The choice of step factor is an important consideration when advancing the solution. Too large a step may put the search far from the equilibrium path and may result in slow convergence or even divergence in the correcting phase. On the other hand, too small a step may be expensive because a large number of steps will be required to complete the analysis.

The step factor may remain constant throughout the analysis or it may vary. The available options are discussed in the following sections.

2.14 Equal Step

The analyst may specify that the solution is to be advanced in equal steps so that the stepping parameter is incremented by the same amount each step. For load stepping, the load increments will be equal and the displacement increments will generally be unequal. Conversely, for displacement stepping, the displacement increments will be equal (as measured by the stepping parameter) and the load increments will generally be unequal.

The disadvantage of using equal steps is that the step factor must be chosen in advance by the analyst, and it may be difficult to select an appropriate step factor. It may be advantageous, therefore, to allow steps of variable size.

2.15 Variable Steps

Two options for variable steps are included in the scheme, namely (a) scaling based on unbalance and (b) scaling based on speed of convergence. Other options could be added; for example, scaling based on Bergan's current stiffness parameter.

2.15.1 Scaling Based on Unbalance

Scaling the step size based on the unbalance ensures that some norm of the unbalance at the advancing phase never exceeds a specified value, U. An advancing step is taken using the current step factor, and the unbalance norm is calculated. If the unbalance exceeds U, the step size is reduced and the step is retaken. This procedure is repeated until the unbalance norm is below U.

Linear scaling is used, for which the step is scaled by:

$$S_s^i = S_s^{i-1} \; U / \; |\underline{R}_U^{i-1}| \qquad (2-27)$$

where $(\;)^i$ = i^{th} trial and $|R_u|$ is the unbalance norm.

This method results in smaller steps in regions of high nonlinearity. Scaling in one step does not alter the step factor for the following step.

2.15.2 Scaling Based on Convergence Rate

In the event of nonconvergence in a step, an option exists to take the step again from the backup state, with a reduced step size. The assumption is that if convergence is slow (or if divergence occurs), the

step size is too large and a smaller step would improve the chance of converging. The amount of the step reduction is specified by the analyst, by means of a reduction factor. For example, if the reduction factor is 0.25, the step factor is divided by four and the step is retaken.

If convergence is very rapid, the step size is assumed to be too small. The step factor is then increased by a specified multiple if the solution converges in less than some minimum number of iterations. Use of this option will result in large steps where the solution is nearly linear.

For scaling based on convergence, the modified step factor is used in the following step.

2.16 Stepping Parameter

The stepping parameter provides the analyst with the means of controlling the load and displacement increments. The best choice for the stepping parameter depends on the particular problem being solved.

2.16.1 Load Stepping

If the stepping parameter is the load magnitude (load stepping), then α_E in Eq. (2-26) is equal to the step factor and is thus specified directly. The load increment for the advancing phase is the step factor times the segment value. Typically, for load stepping the load magnitude will be kept constant during the correcting phase, so that the load magnitude for the step is specified. However, it is possible for the load magnitude to vary during the correcting phase.

2.16.2 Displacement Stepping

For displacement stepping, the stepping parameter may be chosen as (a) a displacement norm, (b) a scalar displacement, or (c) the most critical of a set of scalar displacements. The quantity α_E in Eq. (2-26) is then determined so that the stepping parameter is incremented an amount equal to the step size. The procedure is as follows:

Norms

If a displacement norm is chosen as the stepping parameter, α_E is chosen to make the norm of the displacement increment equal to the absolute value of the step size. Hence,

$$\alpha_E = \frac{(S_s - \underline{b}_s^T \Delta \underline{r}_U)}{\underline{b}_s^T \Delta \underline{r}_E} \qquad (2-28)$$

Some possible choices for the stepping vector are as follows:

1. Single degree of freedom: A single DOF, j, can be incremented by specifying $\underline{b}_S$ as a vector with all zero terms except term j = 1.

2. Strains: For an element such as a truss bar, displacement differences provide a measure of longitudinal strain. For example, consider a truss bar aligned parallel to the global X axis, with longitudinal degrees of freedom i and j. In this case, a stepping vector that measures the change in length is given by:

$$\underline{b}_s^T = [\ldots 0 \; -1 \; 0 \ldots + 1 \; 0 \ldots] \qquad (2-29)$$

in which the -1 value is for DOF i and the +1 value is for DOF j.

3. Rotations: Approximations to element rotations can be constructed as displacement differences. Consider, for example, a truss bar along the global X axis, and let degrees of freedom k and l be perpendicular to the bar. The rotation of the element, r_r, is given approximately by:

$$A_z = ((\Delta \underline{r})_l = (\Delta \underline{r})_k)/L \qquad (2-30)$$

in which

$(\Delta \underline{r})_k$ = component k of $\Delta \underline{r}$.

$(\Delta \underline{r})_l$ = component l of $\Delta \underline{r}$.

L = element length.

The appropriate stepping vector is

$$\underline{b}_s^T = [\ldots 0 \; -1/L \; 0 \ldots 0 \; +1/L \; 0 \ldots] \qquad (2\text{-}31)$$

in which the term -1/L is for DOF k and the term +1/L is for DOF l.

Critical Measure

In the above examples, the stepping parameter was a single predetermined quantity. In some analyses, there may be more than one quantity that needs to be controlled as the analysis progresses. Four scalar displacements can be specified as possible stepping parameters. In any step, the stepping parameter actually used is the most critical of these possible choices.

The procedure is as follows:

1. For each scalar displacement, a stepping vector, $\underline{b}_S$, and a corresponding segment value, V_S, are specified.

2. In any step, the vector that is the most "sensitive" to the applied load is used as the critical vector. Sensitivity is determined by a variable c, given by:

$$c = \underline{b}_s^T \; \Delta \underline{r}_E / V_s \qquad (2\text{-}32)$$

3. The value of α_E follows from the critical vector as:

$$\alpha_E = \frac{(V_{sc}\ f_s\ d_s - \underline{b}_{sc}^T\ \Delta\underline{r}_U)}{\underline{b}_{sc}^T\ \Delta\underline{r}_E} \qquad (2-33)$$

in which V_{SC} is the segment value for the critical vector, $\underline{b}_{SC}$.

The use of a critical vector to determine the step size has the advantage that the stepping parameter for the solution can change as the character of the solution changes. This feature allows control of local nonlinearities (assuming they can be reflected in appropriate stepping vectors).

2.17 Step Direction

The calculation of the quantity α_E in Eq. (2-26) has been discussed so far in terms of using the step size to scale the load or displacement increment. The sign of the step size, however, depends on the value of the direction factor, which is either one or minus one. The step direction must be chosen so that the solution advances in each step (i.e., so that the converged state found at the end of the step does not lie on a portion of the equilibrium path which has already been calculated). In general, the stepping parameter may reverse its direction during the analysis, and it is not always obvious in which direction the step should be taken.

Two methods are offered for the choice of the step direction. The first is to identify a direction parameter to guide the direction. If a direction parameter is specified, the step direction is chosen so that the value of the direction parameter increases in every step. The second method specifies the step direction indirectly, using Bergan's current stiffness parameter.

2.17.1 Direction Parameter

The best choice for the direction parameter in any analysis is not always known in advance. The essential requirement of a direction parameter is that it increases monotonically throughout the analysis. Even in the most complicated cases such parameters exist, but it may take trial and error by the analyst to find them. Possible choices include the load magnitude and various scalar displacements.

Load Magnitude

If the direction parameter is load magnitude, then the load is increased in every step (i.e., α_E is always positive). This option will work only for structures that do not buckle and lose strength.

Critical Vector

If the critical measure option is used to determine the stepping parameter, then the critical vector may be used to determine the step direction. The direction is chosen so that the scalar displacement r_s, defined by:

$$r_s = \underline{b}_{sc}^T \Delta \underline{r} \qquad (3-24)$$

is positive.

New Vector

A new vector, different from the stepping vectors, can be specified as the direction vector. Any of the scalar displacements discussed as stepping parameters are possible direction parameters.

2.17.2 Bergan's Current Stiffness Parameter

The second method for direction choice is automatic load step selection by use of Bergan's current stiffness parameter. In this method, the sign of α_E starts out positive and changes sign each time S_p passes through zero. Although the step direction is not specified directly, its value is determined once the sign of α_E is specified.

2.18 Correcting Phase

Following the advancing phase, one or more iterations are typically done to correct the solution in the region of the predicted state. Ideally, a converged state that is close to an equilibrium state (as measured by the unbalance) is found. However, specification of a large tolerance may allow significant unbalance.

Iterations are performed by holding an iteration parameter constant and adjusting the remaining degrees of freedom. The iteration parameter may be either the load magnitude or a displacement quantity.

2.18.1 Constant Load Iteration

For constant load iteration, the iteration parameter is the load magnitude. Keeping the load magnitude constant is accomplished by setting $\alpha_E = 0$. The displacement increment is thus:

$$\Delta \underline{r} = \Delta \underline{r}_U \qquad (2-35)$$

2.18.2 Constant Displacement Iteration

A displacement quantity can also be chosen as the iteration parameter. An iteration vector, $\underline{b}_I$, is specified to identify a scalar displacement (the iteration parameter) which is to be kept constant during the iteration. The magnitude of α_E is then chosen so that the change in the iteration parameter is zero. That is,

$$\alpha_E = \frac{-\underline{b}_I^T \Delta \underline{r}_U}{\underline{b}_I^T \Delta \underline{r}_E} \qquad (2-36)$$

Some possible choices for the iteration parameter are discussed below. These include external work, arc length, and specified scalar displacements.

Constant Work Iteration

If a vector equal to the applied load vector is chosen as the iteration vector, then the quantity held constant during iteration is the external work (i.e., the applied load does no external work on the structure during the correcting phase). For this case:

$$\underline{b}_I = \underline{R}_E \qquad (2-37)$$

Constant Arc Length

Iteration with constant "arc length" has been discussed by Riks (1979) and Crisfield (1981). It is based on keeping the arc length, s, defined by:

$$\bar{s} = (\alpha_E^2 + \Delta\underline{r}^T \Delta\underline{r})^{1/2} \qquad (2-38)$$

constant throughout the iteration. This leads to a quadratic equation for α_E.

A simpler method is to iterate in such a way that the displacement increment for any iteration is normal to the accumulated displacement increment for the step; this method is discussed by Ramm (1980). The iteration vector in this case is the displacement increment accumulated from the beginning of the current analysis step.

Constant Scalar Displacement

Several choices of scalar displacements for the advancing phase have been considered in Section 2.16.2. Any of these can be used for the correcting phase. For example, if the iteration vector is a unit vector with one in the j^{th} term and all other terms are zero, the j^{th} DOF will be held constant during the iteration.

2.19 Line Search

An option is provided to carry out a line search on the magnitude of the displacement increment in each iteration of the correcting phase. The purpose of the line search is to choose the magnitude of the displacement increment that produces the smallest unbalance for the current external forces. The magnitude of the displacement increment is varied by multiplication by a scalar, β', while the external forces are held constant. The scaled displacement increment, $\Delta \underline{r}_s$, still satisfies the iteration condition, namely, that the iteration parameter remains constant during iteration.

The procedure is as follows:

1. Perform state determination and unbalance calculations for three values of β', namely, $\beta' = 1$, $\beta' = \beta'_u$, and $\beta' = \beta'_l$, where β'_u and β'_l are upper and lower limits specified by the analyst. The lower limit, β_l, should be between 0 and 1 and the upper limit, β_u, should be greater than 1. Let the corresponding unbalance norms be $R_n(1)$, $R_n(\beta'_u)$ and $R_n(\beta'_l)$.

2. A new value of β' is predicted by choosing the value that corresponds to the minimum R_n, based on a parabolic approximation through the three known points.

3. Step 2 is repeated using the three most recently calculated points until one of the following conditions is met:

   a. Convergence is reached. That is,

$$R_n(\beta') < c\, R_n(0) \qquad (2-39)$$

in which $R_n(0)$ is the unbalance norm at the beginning of the iteration and c is a constant between zero and 1 that should be specified by the analyst.

b. The predicted value of β' is beyond the specified limits.

c. The allowable number of trials is exceeded.

If condition (a) applies, the next iteration is begun from the state corresponding to the latest value of β'. If condition (b) or (c) applies, the next iteration is begun from the state with the smallest unbalance.

2.20 Updating the Stiffness

It has been mentioned that the cost of reforming the stiffness each iteration can be high and that stiffness reformulation is not always necessary for convergence, especially if the change in stiffness between iterations is small. In general, the optimum frequency with which the stiffness matrix is reformed depends on the problem being solved. For this reason, the frequency with which the stiffness matrix is updated is left as a variable to be specified by the analyst. Because the stiffness is not necessarily updated each iteration, the stiffness matrix used in solving the displacement increment is not always the current tangent stiffness (although for optimal convergence, it should generally be a close approximation to the current tangent stiffness).

2.20.1 Update Frequency

The frequency with which the stiffness is updated may be specified at both the step level and the iteration level. Linearization is done only at the specified intervals and is always based on the current state. With appropriate choice of stiffness update frequencies, techniques such as initial stiffness iteration, constant stiffness iteration, and NR iteration can be specified, as follows:

Initial Stiffness Iteration

Initial stiffness iteration is obtained if the specified step frequency is greater than the maximum number of steps and if the specified iteration frequency is greater than the maximum number of iterations. Thus, the stiffness is reformed only once, at the beginning of the analysis.

Constant Stiffness Iteration

Constant stiffness iteration is obtained if the step frequency is one and the iteration frequency is greater than the maximum number of iterations per step. The stiffness is then formed only at the beginning of each step.

Newton-Raphson Iteration

Newton-Raphson iteration is obtained if both the step frequency and the iteration frequency are equal to one. The stiffness is then reformed every iteration.

2.21 BFGS Stiffness Modification

As a compromise between reforming the stiffness and keeping it constant for a given iteration, an option is included to modify the stiffness matrix. The modification used is the rank two update to the inverse of the stiffness matrix that was introduced in the discussion of the BFGS method.

2.22 Event Prediction

In analyses where event occurrences can cause large changes in stiffness, it may be advantageous to predict the next event, advance the solution just beyond it, and then update the state and stiffness. This procedure will keep the solution close to the equilibrium path.

2.22.1 Algorithm

The procedure used to predict events in the advancing phase is as follows:

1. The displacement increment is calculated.

2. If it is determined that the calculated displacement will cause an event, the displacement increment is scaled to bring the solution just beyond the first predicted event.

3. A state determination is performed, and $\underline{R}_U$ is calculated.

4. If it was determined in Step (2) that an event would occur, the state is updated and linearized. Since only a fraction of the step has been applied, the solution returns to Step 1 to apply the remainder of the step. If no event was predicted, the solution enters the correcting phase.

The same procedure is followed for events predicted in the correcting phase, but in Step 1 the increment is chosen to keep the iteration parameter constant.

2.23 State Determination

The structure resisting force is calculated by assembling the element resisting forces in the current displaced state. The element forces are obtained by state determination calculations, using the displacement increment accumulated from the reference state to the current state.

2.23.1 Frequency of Updating

The frequency with which the state is updated is specified by the analyst (in terms of number of iterations) and is independent of the stiffness update frequency. This allows the analyst to specify path dependent or path independent state determination, or any scheme in between.

In displacement stepping for softening structures, the load magnitude decreases during iteration. To avoid false unloading of yielded elements, path independent state determination should be used.

2.23.2 Path Dependent State Determination

Path dependent state determination is chosen by specifying that the state be updated every iteration.

2.23.3 Path Independent State Determination

Path independent state determination is chosen by specifying the state update frequency to be larger than the maximum number of iterations. The state at the beginning of the step is then used as the reference state for all state determinations in the step. Path independent state determination has the advantage that the reference states are all converged states.

2.24 External Load

The external load is the total load applied to the structure in the current state. It is calculated using the current values of the load pattern magnitudes, allowing for any configuration dependence.

2.25 Unbalance

The unbalanced force vector, $\underline{R}_U$, is calculated as the difference between the external applied forces and the structure resisting forces. A norm of the unbalance vector is typically used as the measure of the unbalance of the system. The Euclidean norm or the infinity norm of $\underline{R}_U$ can be chosen as the unbalance measure.

The rotational degrees of freedom may be excluded in calculation of the unbalance. This option is useful because it eliminates combining quantities with different units (i.e., forces and moments).

2.25.1 Convergence Rates

Extensive studies have been performed on the convergence properties of Newton-type methods. For standard NR iteration, it has been determined that the convergence rate is quadratic for continuously differentiable functions, provided the predicted displacement increment is not too large. The convergence rates for modified Newton and quasi-Newton methods tend to be linear or super-linear.

2.25.2 Predicting Convergence

Because the methods being used have the property of linear, super-linear, or quadratic convergence, it should be possible to predict whether or not a given iteration sequence is going to converge within the specified number of iterations. It may require a few iterations before a good prediction can be made, and these predictions will not always be correct. However, the advantage of predicting nonconvergence is that it can save computation if it appears that the solution will not converge.

Algorithm

The algorithm for convergence prediction is as follows:

Quantities Specified:

Iteration at which prediction begins = I_p.
Weighting factor for convergence rate = W.
Unbalance tolerance = U.
Maximum allowable iterations = n.

1. For iteration i, a convergence ratio, c_i, is computed by diving the unbalance at the end of the iteration, R_n^i, by the unbalance at the beginning of the iteration, R_n^{i-1}. That is,

$$c_i = \frac{R_n^i}{R_n^{i-1}} \qquad (2-39)$$

2. An estimated convergence rate, c_i, is calculated by taking a weighted average of the individual convergence ratios. The ratio is weighted so that the most recent iterations are counted more heavily. That is,

$$c_i = \frac{c_2 + Wc_3 + \cdots + W^{i-1} c_i}{1 + W^2 + \cdots + W^{i-1}} \qquad (2-40)$$

in which

c_i = i^{th} value of c.

W^i = W raised to the i^{th} power.

3. The unbalance is extrapolated using the current unbalance and the estimated convergence rate. The number of iterations, k, required to reach convergence is estimated as:

$$k = \ln (U/R_n^i)/C_i \qquad (2-41)$$

The value of k is truncated to an integer value, and the number of iterations to convergence is then predicted to be k + 1.

4. If the number of iterations is less than the maximum allowable, the iteration continues. If not, nonconvergence is predicted, and the restepping option is exercised.

Convergence prediction begins on an iteration number specified by the analyst. The use of an iteration other than the second allows the solution to settle down before the prediction begins. In general, the more information available for prediction, the more accurate the prediction will be.

A number of grace iterations is allowed so that the solution will continue if the predicted number of iterations to convergence is small, even if the total number is greater than the maximum allowable. The number of grace iterations is specified as a portion of the number of iterations completed. For example, a proportion of 0.5 means that if 8 iterations have been completed and a prediction of 3 iterations to convergence is made, the solution will continue even if the maximum number of iterations is 10.

3.0 SEASTAR DYNAMIC SOLUTION

The dynamic analysis procedures incorporated in SEASTAR are outlined in this chapter. Two separate analysis methods are incorporated in the program. The first method is based on a constant time step procedure using Newmark's integration procedure. The second method uses a step-by-step integration strategy which automatically varies the time step to ensure accuracy. This allows large steps to be used when possible, and small steps when necessary. An event-to-event strategy is also incorporated to modify step sizes during critical phases of the analysis, such as gap closure and yielding. The Hilber-Hughes-Taylor step-by-step integration method has been incorporated in addition to Newmark's method. This method introduces numerical damping and may improve the solution stability of certain types of nonlinear problems. A brief description of the computational steps involved in a dynamic analysis is included. For a complete background to the theory, refer to Oughourlian (1982).

3.1 Linear Step-by-Step Dynamic Analysis

3.1.1 Newmark, $\beta = 1/4$ Method

The most commonly used scheme for step-by-step dynamic analysis is the Newmark, $\beta = 1/4$ (constant average acceleration) scheme. This scheme is based on the following equations for the increments of acceleration and velocity in a time step.

$$\Delta \ddot{\underline{r}} = -2\ddot{\underline{r}}^{1} - \frac{4}{\Delta t}\dot{\underline{r}}^{1} + \frac{4}{\Delta t^{2}}\Delta \underline{r} \quad \checkmark \qquad (3-1)$$

$$\Delta \dot{\underline{r}} = -2\dot{\underline{r}}^{1} + \frac{2}{\Delta t}\Delta \underline{r} \quad \checkmark \qquad (3-2)$$

where

$\Delta \underline{r}$ = increment in displacement.

$\dot{\underline{r}}^{1}$, $\ddot{\underline{r}}^{1}$ = velocity and acceleration vectors at beginning of step.

Δt = time step.

With these relationships, an incremental equilibrium equation can be written as:

$$\left[\frac{4}{\Delta t^{2}}\underline{M} + \frac{2}{\Delta t}\underline{C} + \underline{K}\right]\Delta \underline{r} = \Delta \underline{R}_{E} + \underline{M}\left[2\ddot{\underline{r}}^{1} + \frac{4}{\Delta t}\dot{\underline{r}}^{1}\right] + 2\underline{C}\,\dot{\underline{r}}^{1} \quad (3-3) \quad \checkmark$$

There [illegible] many ~~software~~ computer codes [illegible] [illegible] for the solution of non-linear [illegible]. The details of the solution algorithms employed by the code can be quite different depending on the solution strategy, and [illegible] arrangement, [illegible].

or

$$\underline{K}^* \ \Delta \underline{r} \ = \ \Delta \underline{R}^* \qquad (3-4)$$

where

$\underline{K}^*$ = effective stiffness matrix.

$\Delta \underline{R}^*$ = effective load increment.

$\underline{M}$ = mass matrix.

$\underline{C}$ = damping matrix.

$\underline{K}$ = static stiffness matrix.

$\Delta \underline{R}_E$ = external load increment.

Hence, for step-by-step dynamic analysis, there are three major differences from linear static analysis, as follows:

1. Form the effective stiffness matrix:

$$\underline{K}^* = \frac{4}{\Delta t^2} \underline{M} + \frac{2}{\Delta t} \underline{C} + \underline{K} \qquad (3-5)$$

2. Form the effective load vector:

$$\Delta \underline{R}^* = \Delta \underline{R}_E + \underline{M} \ \ddot{r}^1 + \frac{4}{\Delta t} \underline{r}^1 + 2\underline{C} \dot{r}^1 \qquad (3-6)$$

3. Perform equilibrium check by calculating the equilibrium vector, $\underline{R}_U$:

$$\underline{R}_U = \underline{R}_E^2 - \underline{R}_I^2 + \underline{M}\,\ddot{\underline{r}}^2 + \underline{C}\,\dot{\underline{r}}^2 \qquad (3-7)$$

where

$\dot{\underline{r}}^2, \ddot{\underline{r}}^2$ = velocity and acceleration vectors at end of step.

$\underline{R}_E^2$ = external load vector at end of step.

$\underline{R}_I^2$ = static internal resisting load vector at end of step.

3.1.2 Hilber-Hughes-Taylor (HHT) Method

The HHT method (1977) adds numerical damping by solving the following modified equilibrium equation:

$$\left[\frac{4}{\Delta t^2}\underline{M} + \frac{2}{\Delta t}\underline{C} + (1+\alpha)\underline{K}\right]\Delta\underline{r} = \Delta\underline{R}_E + \underline{M}\left[\ddot{\underline{r}}^1 + \frac{4}{\Delta t}\dot{\underline{r}}^1\right] + 2\underline{C}\,\dot{\underline{r}}^1 \qquad (3-8)$$

where α is a damping parameter $\left(-\frac{1}{3} \le \alpha < 0\right)$.

For dynamic analysis using the HHT method, ther are two modifications from the Newmark β = 1/4 method, as follows:

1. Form the effective stiffness matrix:

$$\underline{K}^* = \frac{4}{\Delta t^2}\underline{M} + \frac{2}{\Delta t}\underline{C} + (1+\alpha)\underline{K} \qquad (3-9)$$

2. Perform equilibrium check:

$$\underline{R}_U = \underline{R}_E^2 - \underline{R}_I^2 + \underline{M}\,\ddot{\underline{r}}^2 + \underline{C}\,\dot{\underline{r}}^2 - \alpha\left(\underline{R}_I^2 - \underline{R}_I^1\right) \qquad (3-10)$$

where

$\underline{R}_I^1$ = static internal resisting load vector at beginning of step.

$\alpha(R_I^2 - R_I^1)$ = a correction which must be applied because true equilibrium is not satisfied.

3.2 Variable Time Step Dynamic Analysis

The variable time step approach requires additional logic to choose the variable time steps. The logic used in the midstep error calculations and event-to-event strategy is described in this section.

3.2.1 Midstep Error for Linear Problems

Hibbit and Karlsoon (1979) have proposed a criterion for the selection of the time step, Δt. This criterion assumes that if the equilibrium error, $\Delta \underline{R}_m$, at the middle of any time step is small, then overall equilibrium errors will also be small and the time step is acceptable. The midstep error can easily be calculated for a linear problem, as shown in Figure 3-1, as:

$$\Delta \underline{R}_m = \frac{\Delta t}{8} \cdot \underline{K} \cdot \Delta \dot{r} \qquad (3-10)$$

where

$\underline{K}$ = elastic stiffness matrix.

$\Delta \dot{\underline{r}}$ = increment in nodal velocities.

Δt = time step.

Within each step, a test is made to check whether the time step is too large for acceptable accuracy. This is done by comparing a norm of the midstep error with an upper tolerance. If the tolerance is exceeded, the time step Δt is reduced by a user-specified factor (usually 0.5). If the error is smaller than a lower tolerance for two consecutive steps,

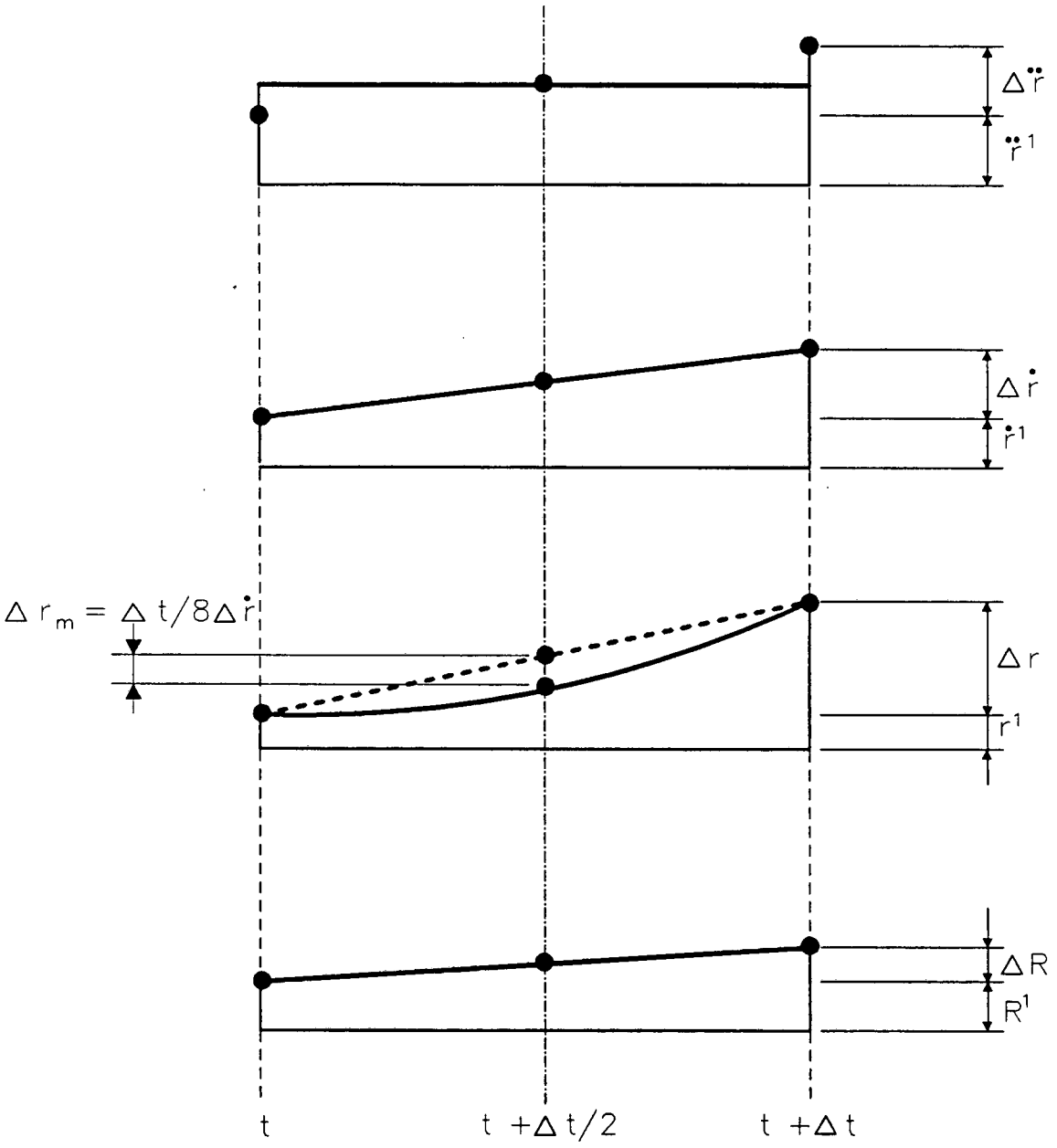

FIG. 3-1 CONSTANT AVERAGE ACCELERATION SCHEME

then Δt is increased by a second factor (usually 2). This algorithm thus controls the equilibrium error by automatically adjusting the time step.

3.2.2 Midstep Error for Nonlinear Problems

For a nonlinear problem, exact equilibrium is never, in general, satisfied either at the end of a step or within the step. Nevertheless, Eqn. (3-10) can still be used to estimate the midstep error, provided that it is recognized that the stiffness may change within the step. If the stiffness does not change, the tangent stiffness matrix must be used when calculating the midstep error, as follows:

$$\Delta \underline{R}_m = \frac{\Delta t}{8} \cdot \underline{K}_T \cdot \Delta \underline{\dot{r}} \qquad (3-11)$$

where $\underline{K}_T$ is the static tangent stiffness matrix.

With the event-to-event solution strategy (described in the following section), if any event occurs within a step, the midstep error, $\Delta \underline{R}_m$, is weighted by the governing event factor and accumulated over the entire step in the following manner:

$$\Delta \underline{R}_m = \sum_i \bar{\alpha}_i \ \underline{K}_{Ti} \Delta \dot{r}_i \qquad (3-12)$$

where $\bar{\alpha}_i$ is the governing event factor for substep i and i is the substep number. An alternative method for the computation of the midstep error would be to perform a state determination calculation, and hence, determine the equilibrium error exactly at midstep. With this procedure, however, it is essential to iterate to convergence at the end of the step

in order to eliminate any effect due to the unbalanced load $\underline{R}_U$. In general, the use of Eqn. (3-12) is preferred because it eliminates the need to iterate and is also more efficient.

The midstep error calculation could be carried out either at the element level (in which case $\Delta \underline{R}_m$ is assembled from the element contributions) or directly at the structure level. In the latter case, the static tangent stiffness matrix $\underline{K}_T$ must be available.

3.2.3 Event-to-Event Strategy

The event-to-event solution strategy for nonlinear analysis provides means of controlling the equilibrium error. Any significant "event" occurring within any element (such as yielding, nonlinear unloading, gap closure, etc.) determines a substep. The tangent stiffness is modified in each substep, and hence, the solution closely follows the exact response.

If the exact response of the structure is piecewise linear (Figure 3-2), and if no "overshoot" of the exact event is allowed, the solution will follow the exact load-deflection curve and no equilibrium unbalance result. In general, however, the response is not linear between well-defined events, and the type of behavior shown in Figure 3-3 is more likely to be present. In this case, the solution does not follow the exact response, with the result that there is an unbalanced load, $\underline{R}_U$, at the end of the step. This unbalanced load will be small if the events are well chosen (i.e., if they represent major nonlinearities in the behavior of the structure).

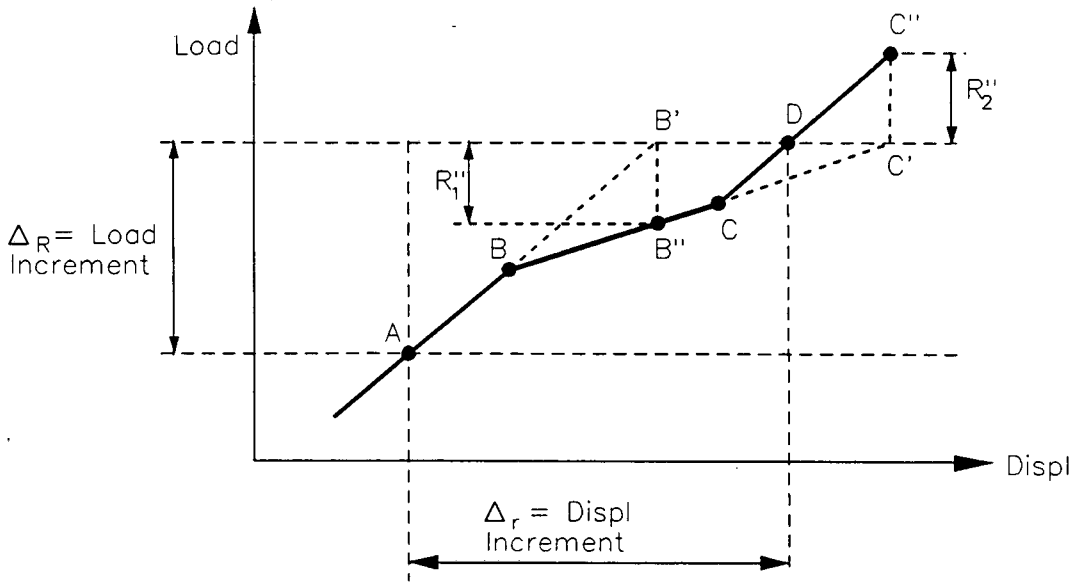

FIG. 3-2 ITERATION IN EVENT-TO-EVENT SOLUTIONS

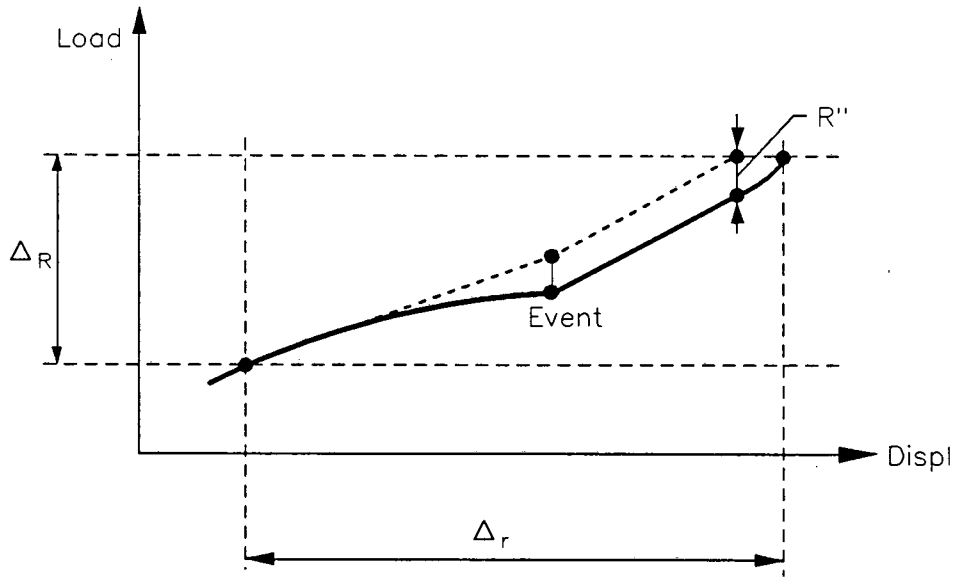

FIG. 3-3 UNBALANCE IN EVENT-TO-EVENT SOLUTION

To apply the event-to-event strategy, an event factor must be calculated for each element, and the minimum factor chosen to determine a scaling factor of the the displacement increment, $\Delta \underline{r}$, for the substep. An event could also be defined in terms of nodal displacement limits. Scaling the displacements $\Delta \underline{r}$ by the minimum event factor requires that the following complications be considered:

1. The state determination calculations for elements which have initial strain loadings require that the governing event factor be used to obtain the correct proportion of the initial deformations which are to be used. The state determination calculation is essentially:

$$\Delta \underline{Q} = \underline{k}_T \left(\Delta \underline{v} - \bar{\alpha} \Delta \underline{v}_o \right) \qquad (3-13)$$

where

$\Delta \underline{Q}$ = element force increment

$\underline{k}_T$ = element tangent stiffness matrix.

$\Delta \underline{v}$ = element deformations due to scaled displacement increment.

$\Delta \underline{v}_o$ = initial element deformations calculated assuming an unscaled load increment.

$\bar{\alpha}$ = governing event factor.

2. Path dependent state determination is consistent with the event-to-event strategy, whereas the path independent scheme can lead to inconsistencies. This is because the event factor is calculated from the current state. Hence, the state determination calculations should also begin using the current state.

3. After any event, the load vector may be multiplied by $(1 - \bar{\alpha})$ to obtain the remaining portion of the load to be applied in the next substep. If the initial strain effects are present, however, simply scaling the load vector, $\Delta \underline{R}^*$, is not consistent because the tangent stiffness, $\underline{k}_T$, may have changed, so that the initial strain loads may have to be recomputed. Hence, $\Delta \underline{R}$ must generally be recalculated at each substep and cannot be simply scaled.

3.2.4 Dynamic Load Scaling Using the Event-to-Event Strategy

The effective load vector for dynamic analysis contains contributions of initial stress type, and hence, recalculation of the load vector may strictly be necessary at each substep to account for changes in $\underline{k}_T$. For computational convenience, however, $\Delta \underline{R}^*$ can be assumed to be unaffected by changes in $\underline{k}_T$, so that it can be scaled by $(1 - \bar{\alpha})$ for each substep. In effect, the solution within the step is found as if the loading were static with no initial strain effects. This can introduce some inconsistencies during the state determination and some unbalanced loads $\underline{R}_U$ which are not corrected at the end of each substep. Hence, any accumulated unbalances must be corrected in the following step.

An alternative approach is to recalculate $\Delta \underline{R}^*$ at the end of each substep, including unbalanced load effects. This has the disadvantage of requiring an internal resisting force calculation at each substep, which requires the current velocities and accelerations. These quantities are not readily available in consistent form within the substep.

3.3 Energy Calculations

The different types of energy which can be calculated are as follows:

1. Work done by external loads.
2. Kinetic energy.
3. Viscous-damping work.
4. Internal work done by the elasto-plastic forces in the elements.
5. Work done by seismic base shear forces moving through support displacements.

Ideally, the internal and viscous-damping energies should be calculated exactly in the elements during the state determination phase. However, an alternative and simpler approach is to calculate these energies at the structure level using nodal forces and displacements. With this procedure, the internal energy increment, $\Delta \underline{E}_I$, is calculated as:

$$\Delta \underline{E}_I = \frac{1}{2} \left(\underline{R}_I^2 + \underline{R}_I^1 \right)^T \cdot \Delta \underline{r} \qquad (3-14)$$

The elastic-plastic work is calculated if $\underline{R}_I$ = resisting forces due to element elastic-plastic actions only, and the viscous damping work is calculated if $\underline{R}_I$ = resisting forces due to viscous damping effects within the elements. Other energies can be calculated similarly. The base shear energy can be obtained using the imposed nodal displacements and the corresponding nodal forces in the $\underline{R}_I$ vector. The kinetic energy is conveniently calculated as the work done by the inertia forces moving through the corresponding nodal displacements.

After all energies have been computed, a check on the energy balance can provide both a measure of the error produced during a nonlinear dynamic analysis and an idea of the contributions of the different types of energy.

3.4 Viscous Damping

The viscous damping in SEASTAR has the form

$$\underline{C} = \alpha_m \underline{M} + \beta_o \underline{K}_o + \beta_T \underline{K}_T \qquad (3-15)$$

where α_m, β_o and β_T are proportionality constants. Because the term $\beta_T \underline{K}_T$ changes as the structure becomes nonlinear, it is recommended that β_T be specified as zero.

4.0 SEASTAR EIGENSOLUTION

4.1 Introduction

The period and mode shape of vibrations of a structural system provide a significant insight to dynamic response of the system.

The frequency and mode shapes of the structure are obtained by solving the generalized eigenproblem of the form

$$\underline{K}\ \underline{\Phi} = \underline{M}\ \underline{\Phi}\ \underline{\Lambda} \quad . \tag{4-1}$$

in which

$\underline{K}$ = the structure's stiffness matrix.

$\underline{M}$ = the structure's mass matrix.

$\underline{\Phi}$ = the structure's eigenvector matrix.

$\underline{\Lambda}$ = the structure's eigenvalue matrix.

$\underline{\Phi}$ is the matrix of mode shapes of the structure, and the diagonal terms of the matrix $\underline{\Lambda}$ are the square of the natural frequencies of vibration of the structure.

The procedure used in SEASTAR to perform the eigensolution is outlined in the next section.

4.2 Procedure

The solution of an eigenvalue problem requires computation of mass and stiffness matrices. The structural mass matrix in SEASTAR has contributions from input concentrated mass and generated structural and hydrodynamic added mass. Lumped mass formulation is used in SEASTAR; hence, the mass matrix is diagonal. Lumped mass formulation is preferred to consistent mass formulation due to its computational efficiency.

The structural stiffness in SEASTAR has contributions from elastic and geometric stiffness. In riser analysis the effect of tension in the risers contributes significantly to the riser stiffness. After the application of static loads, the forces in the elements are used to evaluate the geometric stiffness of the structure. The geometric stiffness is added to the structure's elastic stiffness to obtain the total stiffness. At least one stiffness reformation should be performed after application of static loads and prior to an eigensolution.

The subspace iteration procedure is used in the eigensolution analysis of SEASTAR. This procedure allows the user to find a few required eigenvalues efficiently.

4.3 Subspace Iteration

Subspace iteration is from the family of iteration methods. In this method, the stiffness and mass matrices are projected into a smaller subspace depending on the number of trial subspace vectors. The projected matrices are given by

$$\underline{G}_k = \underline{X}_k^T \ \underline{M} \ (\underline{K} - \sigma \ \underline{M})^{-1} \ \underline{M} \ \underline{X}_k \qquad (4-2)$$

and

$$\underline{H}_k = \underline{X}_k^T \ \underline{M} \ \underline{X}_k \qquad (4-3)$$

in which

$\underline{X}_k^T$ = a set of trial vectors.

σ = a specified shift (σ = 0 gives the smallest eigenvalue).

$\underline{G}_k$ = projection of stiffness matrix.

$\underline{H}_k$ = projection of mass matrix.

The reduced problem is then solved in SEASTAR by the Q-L algorithm, and the solution of the reduced problem is projected into the original space. The shifting strategy allows the user to find the eigenvalues closest to a prespecified shift σ. This prevents unnecessary computation of unwanted eigenvalues and eigenvector. For more details on sub-space iteration, refer to Wilson (1976).

4.4 Subspace Iteration Algorithm

The steps carried during an eigenvalue analysis can be summarized as follows:

Given a pair of matrices $\underline{K}$ and $\underline{M}$ and a set of m vectors

$$X^{(1)} = [x_1^{(1)}, \ \ldots, \ x_m^{(1)}] \qquad (4-4)$$

where m is the subspace size,

1. Factor $(\underline{K} - \sigma \underline{M})$ into LDL^T for a specified shift.

2. For i = 1, until convergence perform

   i) Solve $(\underline{K} - \sigma \underline{M}) \ \underline{X}^{(i)} = \underline{M} \underline{X}^{(i)}$.

   ii) $\underline{G}_i = [\underline{X}^{(i)}]^T \underline{M} (\underline{K} - \sigma \underline{M})^{-1} \underline{M} [\underline{X}^{(i)}]$.

   iii) $\underline{H}_i = [\underline{X}^{(i)}]^T \underline{M} [\underline{X}^{(i)}]$.

   iv) Solve $(\underline{G}_i - \lambda^{(i)} \underline{H}_i) Y^{(i)} = 0$.

   v) $X^{(i+1)} = X^{(i)} \ Y^{(i)}$.

   vi) Check for convergence of $\lambda^{(i)}$.

4.5 Sturm Sequence

A Sturm sequence check is provided into the subspace iteration method. The Sturm sequence check gives the number of eigenvalues skipped when a shift σ is made. This procedure is useful as a check to prevent skipping eigenvalues when a shift is performed.

5.0 SEASTAR FINITE ELEMENTS

5.1 Nonlinear Truss Elements

The nonlinear truss element possesses a bilinear material model coupled with a rigorous 3D large displacement geometric stiffness formulation capable of predicting complete rigid body motions as well as accommodating large element deformations.

5.1.1 Applications

The element is very effective in modeling structural systems governed by axial material and geometric stiffness nonlinearities. The element of course cannot provide direct prediction of flexural behavior. It does, however, possess a higher order axial strain formulation not contained in the beam elements which allows the truss to predict the behavior of systems that undergo very large internal strains or stretch.

The element does have a nonlinear material model which can represent observed behavior of steel type materials. For computation purposes, this bilinear stress-strain relationship is considered to be the sum of two parallel elements; one an elastic-perfectly plastic component, the other a linear component.

5.1.2 Stiffness Terms

The element has six degrees of freedom, three translations at each end as shown in Figure 5.1-1. The element displacements in the local coordinates are written as

$$\underline{u} = \{u_1 \quad u_2 \quad u_3 \quad u_4 \quad u_5 \quad u_6\}^T$$

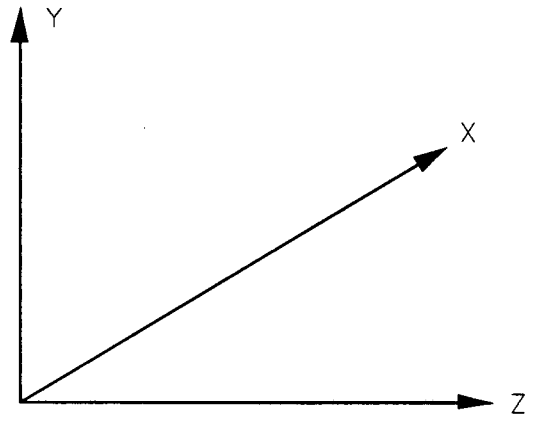

a) Global Coordinates

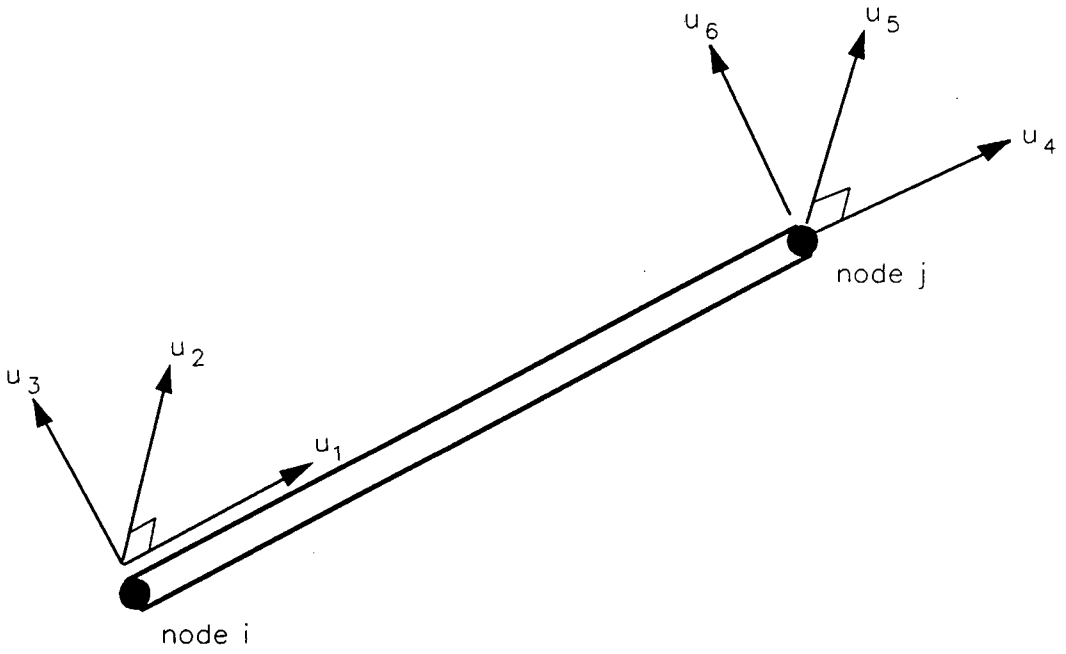

b: Local Coordinates

FIG. 5.1-1 NONLINEAR TRUSS ELEMENT

The total element stiffness matrix consists of two distinctive contributions, the material and the geometric matrices, and can be written as

$$\underline{k}_t = \underline{k}_e + \underline{k}_g$$

$\underline{k}_e$, Material Element Stiffness

The basic truss bar material stiffness is

$$\underline{k}_e = \frac{AE}{L}$$

where E is the Young's Modulus, A is the cross-sectional area, and L is the element length. Young's Modulus can vary according to the bilinear model shown in Figure 5-2.

$\underline{k}_g$, Geometric Element Stiffness

The formulation of a complete geometric stiffness centers on a higher order strain definition than the conventional engineering strain definition.

The Green strains applicable to large deformation problems are used.

For the truss element, the important strain is E_x and is given by

$$E_x = \frac{\partial u}{\partial x} + \frac{1}{2}\left[\left(\frac{\partial u}{\partial x}\right)^2 + \left(\frac{\partial v}{\partial x}\right)^2 + \left(\frac{\partial w}{\partial x}\right)^2\right]$$

The strain increment, ΔE_x, is given by

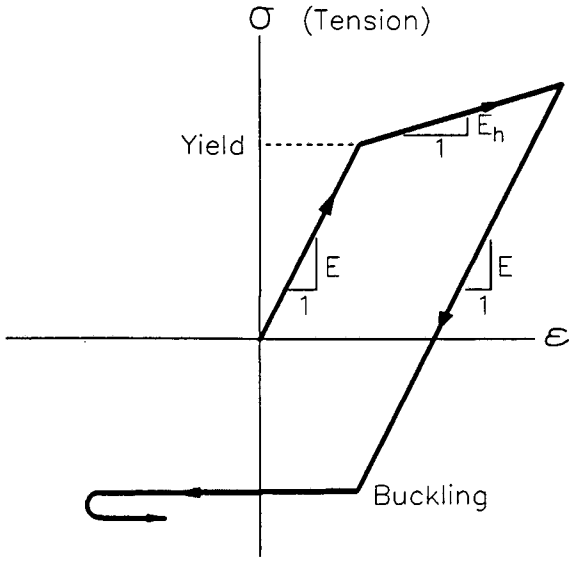

(a) Elastic Buckling and Tensile Yield

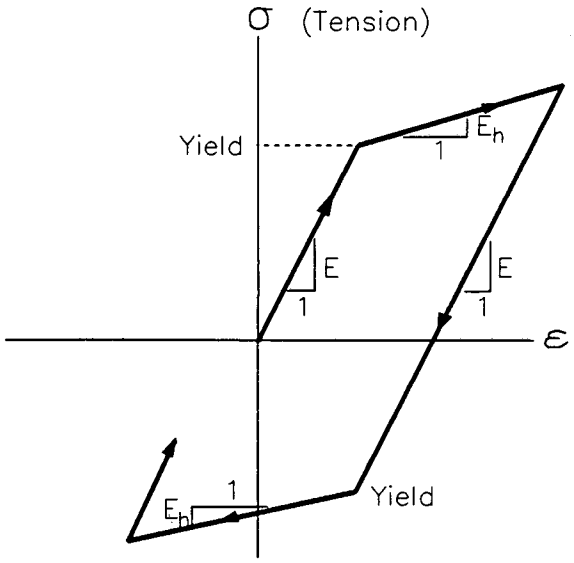

(b) Tensile and Compressive Yield

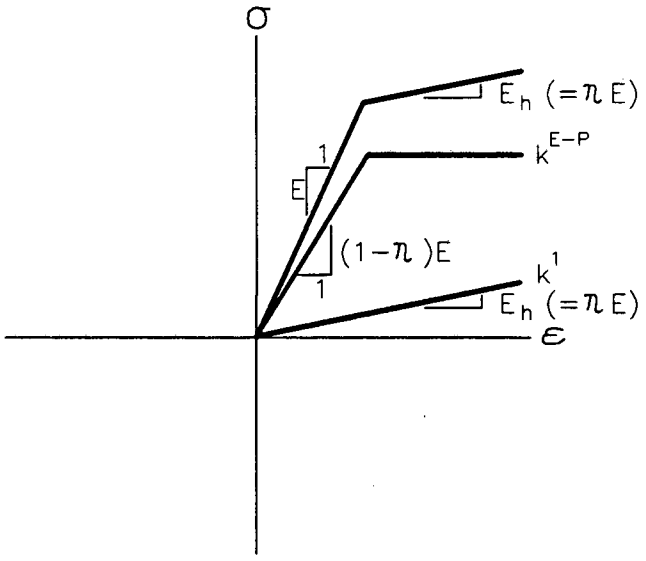

(c) Addition of Components to Form Element

FIG. 5.1-2 NONLINEAR TRUSS ELEMENT

$$\Delta E_x = E_x^2 - E_x^1$$

where E_x^1 and E_x^2 are the strains at the beginning and the end of the increment, respectively. The strain increment can be written as a sum of a linear and nonlinear strain, i.e.,

$$\Delta E_x = e_x + \eta_x$$

where

$$e_x = \left[1 + \frac{\partial u^1}{\partial x}\right] \frac{\partial (\Delta u)}{\partial x} + \frac{\partial v^1}{\partial x} \frac{\partial (\Delta v)}{\partial x} + \frac{\partial w^1}{\partial x} \frac{\partial (\Delta w)}{\partial x}$$

and

$$\eta_x = \frac{1}{2}\left[\left(\frac{\partial(\Delta u)}{\partial x}\right)^2 + \left(\frac{\partial (\Delta v)}{\partial x}\right)^2 = \left(\frac{\partial (\Delta w)}{\partial x}\right)^2\right]$$

The linear strain can be written in the following form

$$e_x = \frac{1}{L_o} \underline{B}_L \Delta \underline{r}$$

where L_0 is the undeformed element length and $\underline{B}_L$ is given by.

$$\underline{B}_L = \left[-\left(1 + \frac{\partial u^1}{\partial x}\right), \frac{\partial v^1}{\partial x}, \frac{\partial w^1}{\partial x}, \left(1 + \frac{\partial u^1}{\partial x}\right), \frac{\partial v^1}{\partial x}, \frac{\partial w^1}{\partial x}\right]$$

at $t = 0$, $\quad u^1 = v^1 = w^1 = 0$

hence

$$\underline{B}_L = [-1 \quad 0 \quad 0 \quad 1 \quad 0 \quad 0]$$

and

$$\underline{k}_e = \frac{E_T A_o}{L_o} \underline{B}_L^T \underline{B}_L$$

$$= \frac{E_T A_o}{L_o} \begin{bmatrix} -1 \\ 0 \\ 0 \\ 1 \\ 0 \\ 0 \end{bmatrix} [-1 \quad 0 \quad 0 \quad 1 \quad 0 \quad 0]$$

$$\underline{k}_e = \frac{E_T A_o}{L_o} \begin{bmatrix} 1 & 0 & 0 & -1 & 0 & 0 \\ 0 & 0 & 0 & 0 & 0 & 0 \\ 0 & 0 & 0 & 0 & 0 & 0 \\ -1 & 0 & 0 & 1 & 0 & 0 \\ 0 & 0 & 0 & 0 & 0 & 0 \\ 0 & 0 & 0 & 0 & 0 & 0 \end{bmatrix}$$

which is the standard bar stiffness matrix.

$$\underline{k}_g = \frac{P^1}{L_o}\begin{bmatrix} 1 & 0 & 0 & -1 & 0 & 0 \\ 0 & 1 & 0 & 0 & -1 & 0 \\ 0 & 0 & 1 & 0 & 0 & -1 \\ -1 & 0 & 0 & 1 & 0 & 0 \\ 0 & -1 & 0 & 0 & 1 & 0 \\ 0 & 0 & -1 & 0 & 0 & 1 \end{bmatrix}$$

which is the invariant form of truss bar geometric stiffness.

5.1.3 State Determination

The state determination for the truss bar element with the small displacement option assumes the original element geometry for state determination calculations. When the large displacement option is used, the final configuration is used for state determination. The large displacement theory is embedded in the fundamental assumptions of the element formulation.

5.2 Large Displacement Beam Element

This element has a rigorous three-dimensional geometric stiffness which makes it capable of modeling complete rigid body motions and moderately large deformations.

5.2.1 Applications

The element is appropriate for modeling virtually all large displacement beam behavior in which the material remains linear. If large element deformations are to be resolved, it is important to include K_{gi}, the internal geometric stiffness. The beam is only modestly more expensive computationally than the nonlinear truss bar and provides more stability to the solution because of the additional flexural stiffness it provides.

5.2.2 Basic Assumptions

The basic assumptions are stated as follows:

1. The material is linearly elastic.
2. Plane sections remain plane.
3. Element deformations are small at all times.
4. Increments of nodal rotations are small.
5. Cross-sections are prismatic and doubly symmetric and remain so at all times.
6. Warping of cross-sections and changes in cross-sectional shapes are negligible.

Note that the assumption of small element deformations does not imply small displacements. Nodal displacements in each load step (or iteration) can be large as long as the element deformations are small.

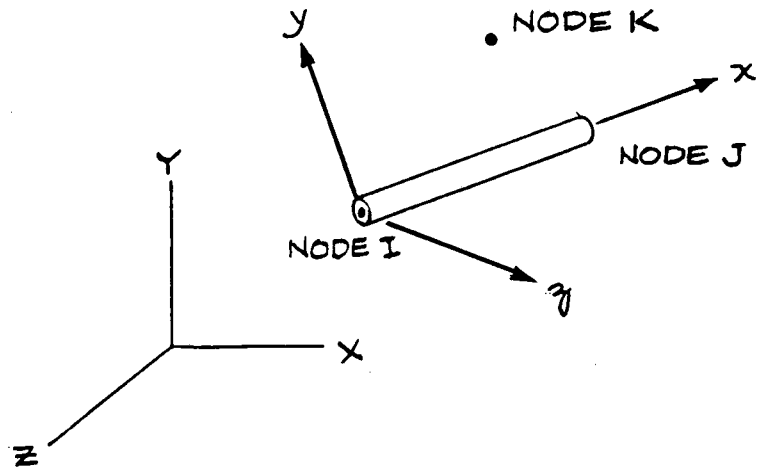

FIG. 5.2-1 ELEMENT COORDINATE AXIS

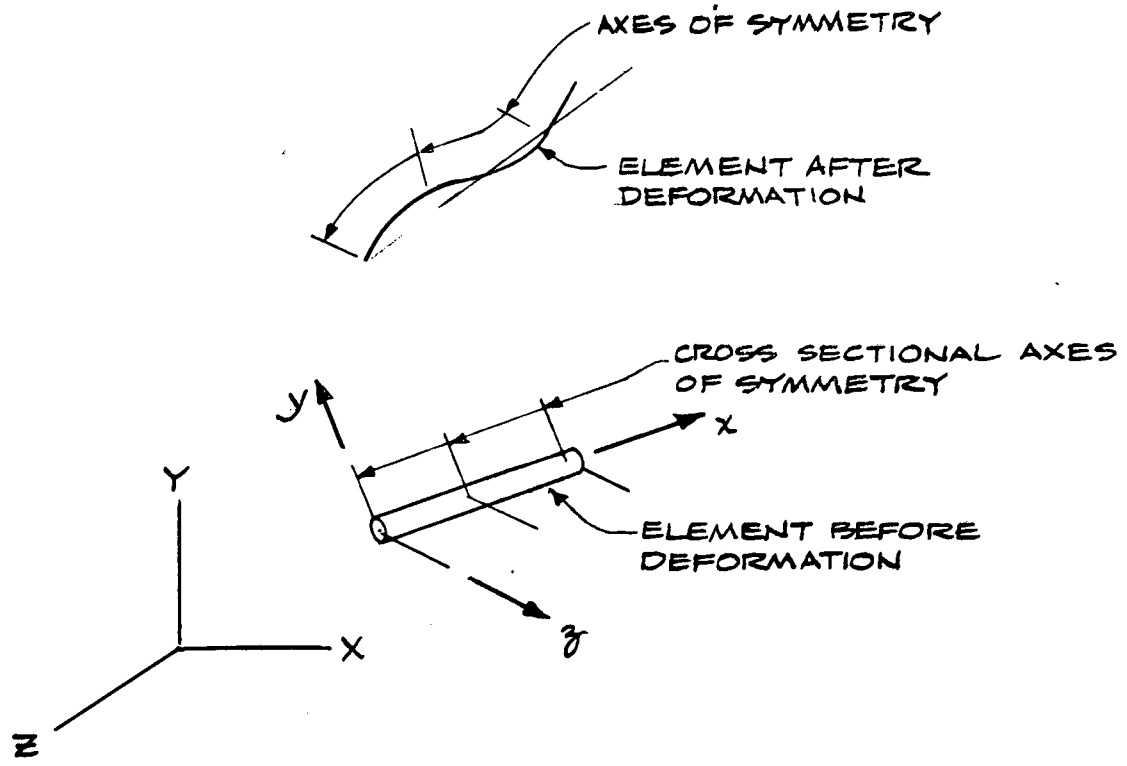

FIG. 5.2-2 ELEMENT BEFORE AND AFTER DEFORMATION

Increments in nodal rotations (and translations) are represented by vectors and therefore transformations from global to local axes are permissible. Since finite rotations cannot be represented as vectors, the assumption of small increments in nodal rotation is necessary.

Note that no restriction is placed on total rotations and translations. Total rotations and translations can be large provided that assumptions 3 and 4 are not violated.

5.2.3 Element Local Axes

The initial orientation of an element in space is defined by three nodes I, J and K as shown in Figure 5.2-1. Each element has a local Cartesian coordinate axis. The 1 axis passes through nodes I and J. The 2 axis is in the plane of nodes I, J and K and is perpendicular to the 1 axis. The 3 axis is perpendicular to both 1 and 2 axes (by the right-hand rule).

Initially cross-sectional centroids coincide with the 1 axis and cross-sectional axes of symmetry coincide with 2 and 3 axes.

After an element has undergone some displacement and rotation, the initial element axes can no longer define the new orientation of the element in space. Furthermore, a typical element may deform as shown in Figure 5.2-2 and in general a single set of element axes can no longer define the geometry of the element.

If the element deformations are small, however, a single set of element axes can define the orientation and geometry of a deformed element. In this formulation, a single moving element coordinate axis is considered. As an element displaces, the element coordinate axis also moves with the element.

5.2.4 Element Degrees of Freedom

Each element has 12 degrees of freedom, three translations and three rotations at each node. Increments in nodal displacements and rotations, $\underline{q}$, with respect to the global coordinate system are shown in Figure 5.2-3.

The same increments in nodal displacements and rotations with respect to the element local axes, $\underline{u}$, are shown in Figure 5.2-4.

5.2.5 Element Relative Deformations and Forces

Element relative deformations, $\Delta\underline{v}$ can be defined by six quantities, as shown in Figure 5.2-5. Increments in element relative deformations and forces referred to the element local axes are shown in Figure 5.2-6.

5.2.6 Transformations

Increments in nodal displacements and forces referred to element coordinate axes and global coordinate axes are related as follows:

$$\Delta\underline{u} = \underline{T}\ \Delta\ \underline{q} \qquad (5.2-1)$$

$$\Delta\underline{v} = \underline{A}\ \Delta\ \underline{u} \qquad (5.2-2)$$

$$\Delta\underline{Q} = \underline{T}^T\ \Delta\ \underline{P} \qquad (5.2-3)$$

$$\Delta\underline{P} = \underline{A}^T\ \Delta\ \underline{F} \qquad (5.2-3)$$

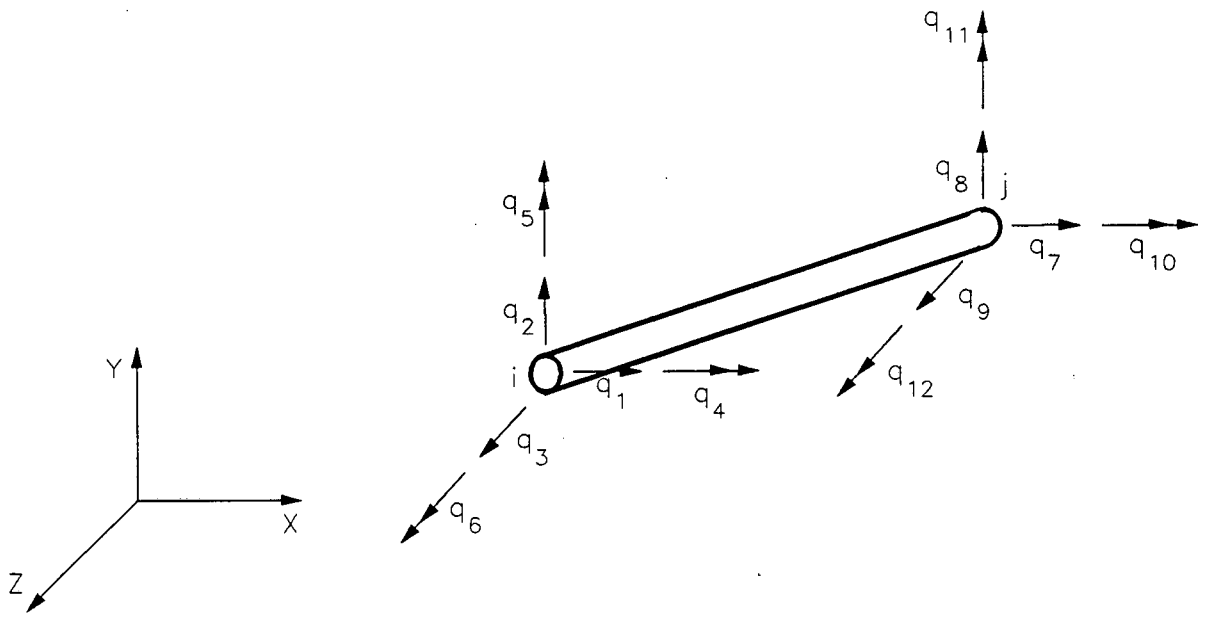

FIG. 5.2-3 INCREMENTS IN NODAL DISPLACEMENTS ($\Delta\underline{q}$) AND FORCES ($\Delta\underline{Q}$) REFERRED TO GLOBAL COORDINATE AXIS

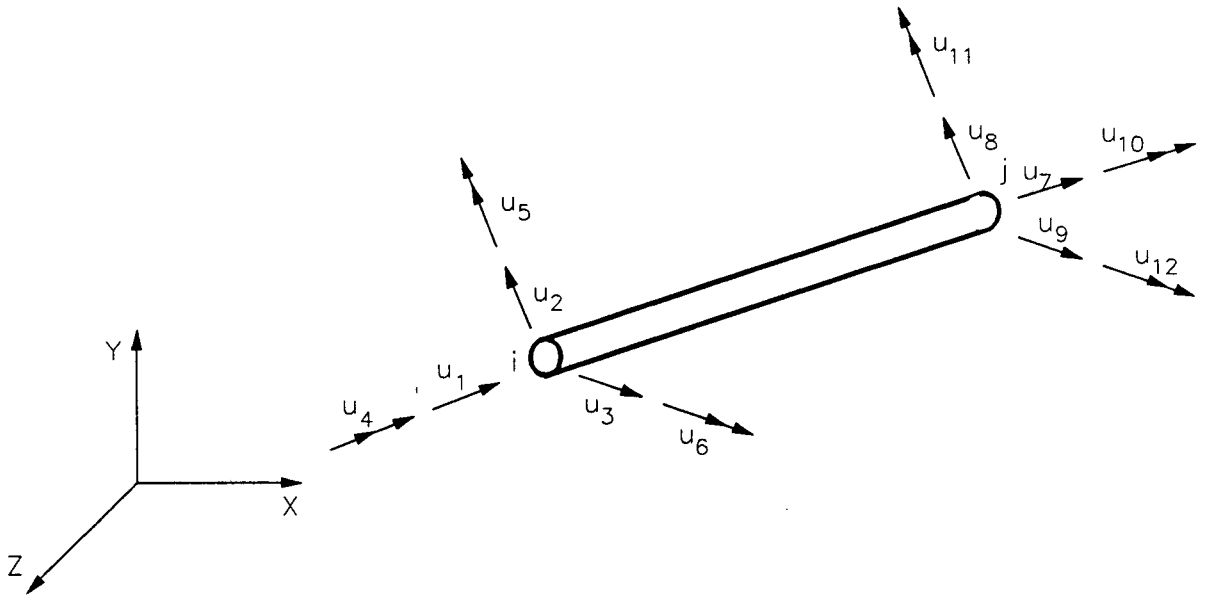

FIG. 5.2-4 INCREMENTS IN NODAL DISPLACEMENTS ($\Delta\underline{u}$) AND FORCES ($\Delta\underline{P}$) REFERRED TO ELEMENT COORDINATE AXIS

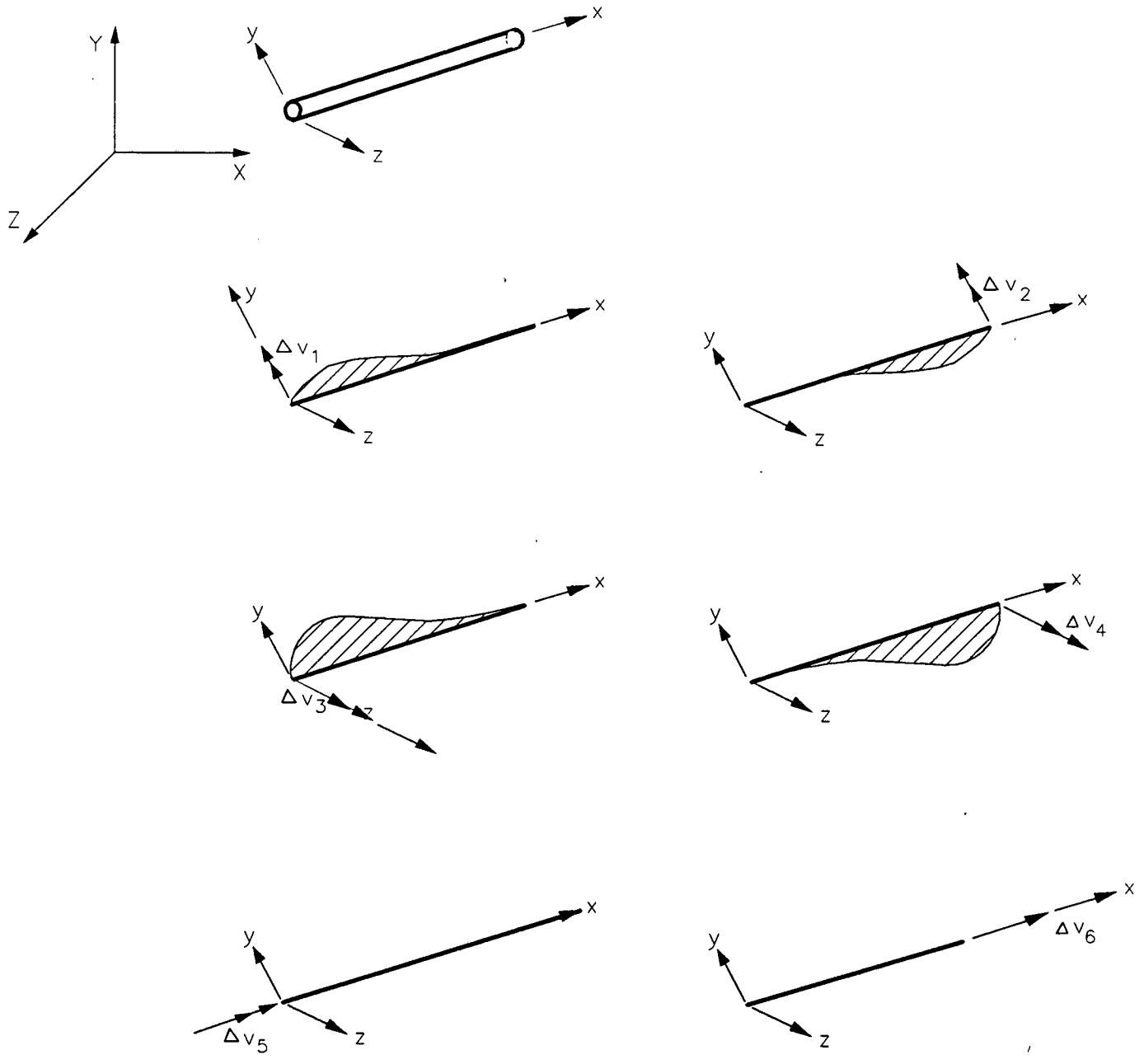

FIG. 5.2-5 INCREMENTS IN ELEMENT RELATIVE DEFORMATIONS $\Delta \underline{v}$

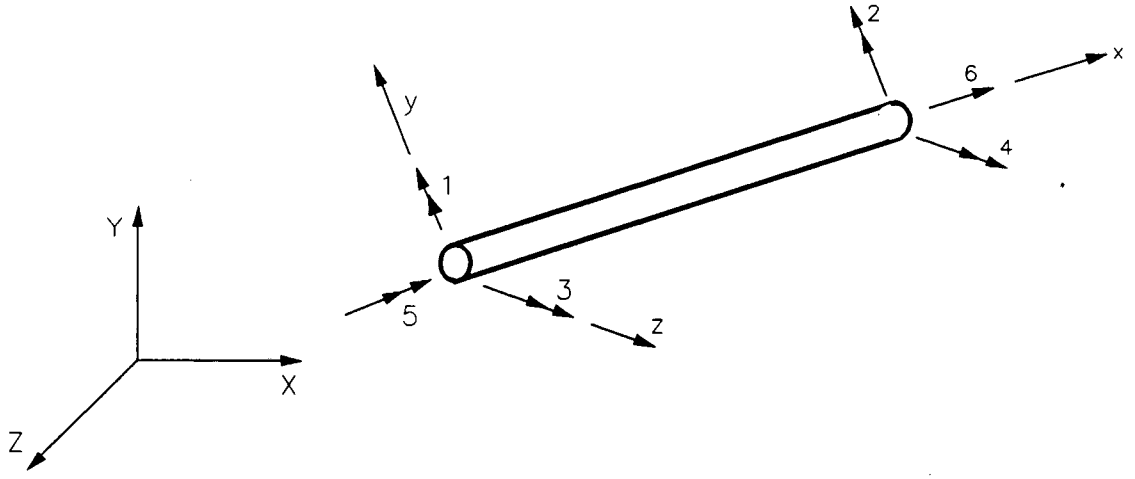

FIG. 5.2-6 INCREMENTS IN ELEMENT RELATIVE DEFORMATIONS $\Delta \underline{v}$ AND FORCES $\Delta \underline{f}$

where

$\Delta\underline{q}$, $\Delta\underline{Q}$ = increments in nodal displacements and forces referred to global coordinate axes, see Figure 5.2-3.

$\Delta\underline{u}$, $\Delta\underline{P}$ = increments in nodal displacements and forces referred to element local axes, see Figure 5.2-4.

$\Delta\underline{v}$, $\Delta\underline{F}$ = increments in nodal relative deformations and forces referred to element local axes, see Figures 5.2-5 and 5.2-6.

$\underline{T}$ = coordinate transformation matrix.

$$= \begin{bmatrix} \underline{t} & & zeros \\ & \underline{t} & \\ zeros & & \underline{t} \\ & & & \underline{t} \end{bmatrix} \qquad (5.2-5)$$

$\underline{t}$ = direction cosine matrix

$$= \begin{bmatrix} l_1 & m_1 & n_1 \\ l_2 & m_2 & n_2 \\ l_3 & m_3 & n_3 \end{bmatrix}$$

where l_i, m_i, n_i are direction cosines of the local axis i.

$\underline{A}$ = displacement-deformation transformation matrix.

$$\underline{A} = \begin{bmatrix} 0 & 0 & -1/L & 0 & 1 & 0 & 0 & 0 & 1/L & 0 & 0 & 0 \\ 0 & 0 & -1/L & 0 & 0 & 0 & 0 & 0 & 1/L & 0 & 1 & 0 \\ 0 & -1/L & 0 & 0 & 0 & 1 & 0 & 1/L & 0 & 0 & 0 & 0 \\ 0 & -1/L & 0 & 0 & 0 & 0 & 0 & 1/L & 0 & 0 & 0 & 1 \\ 0 & 0 & 0 & 1 & 0 & 0 & 0 & 0 & 0 & -1 & 0 & 0 \\ -1 & 0 & 0 & 0 & 0 & 0 & 1 & 0 & 0 & 0 & 0 & 0 \end{bmatrix} \quad (5.2-6)$$

L = current element length.

5.2.7 Stiffness Terms

The total element stiffness matrix for the large displacement beam consists of three distinctive contributions as represented by the following expression:

$$\underline{k}_t = \underline{k}_e + \underline{k}_{ge} + \underline{k}_{gi} \quad (5.2-7)$$

where

$\underline{k}_t$ = total element stiffness.

$\underline{k}_e$ = linear elastic material element stiffness

$\underline{k}_{ge}$ = external geometric stiffness (two options available).

$\underline{k}_{get}$ = truss bar form.

$\underline{k}_{gei}$ = invariant form.

$\underline{k}_{gi}$ = internal geometric stiffness.

For large displacement problems the external geometric stiffness controls the nodal displacement response. The internal geometric stiffness is primarily important in the refinement of internal moment resolution and secondary in controlling global structure displacements. For detailed derivations of the element, refer to Riahi (1979).

$\underline{k}_e$, Linear Elastic Material Element Stiffness

The linear elastic material element stiffness is given by Eq. 5.2-8.

$$\underline{k}_e = \begin{bmatrix}
\frac{AE}{L} & & & & & & -\frac{AE}{L} & & & & & \\
 & \frac{12EI_y}{L^3} & & & & \frac{6EI_y}{L^2} & & \frac{-12EI_y}{L^3} & & & & \frac{6EI_y}{L^2} \\
 & & \frac{12EI_z}{L^3} & & \frac{-6EI_z}{L^2} & & & & \frac{-12EI_z}{L^3} & & \frac{6EI_z}{L^2} & \\
 & & & \frac{GJ}{L} & & & & & & -\frac{GJ}{L} & & \\
 & & & & \frac{4EI_z}{L} & & & & \frac{-6EI_z}{L^2} & & \frac{2EI_z}{L} & \\
 & & & & & \frac{4EI_y}{L} & & \frac{-6EI_y}{L^2} & & & & \frac{2EI_y}{L} \\
 & & & & & & \frac{AE}{L} & & & & & \\
 & & & & & & & \frac{12EI_y}{L^3} & & & & \frac{-6EI_y}{L^2} \\
 & & & & & & & & \frac{12EI_z}{L^3} & & \frac{-6EI_z}{L^2} & \\
 & & & \text{Symmetric} & & & & & & \frac{GJ}{L} & & \\
 & & & & & & & & & & \frac{4EI_z}{L} & \\
 & & & & & & & & & & & \frac{4EI_y}{L}
\end{bmatrix} \tag{5.2-8}$$

Linear Elastic Stiffness Matrix

where

I_y, I_Z = cross-sectional moment of inertia about element local y and z axes.

J = cross-sectional torsional moment of inertia.

L = initial element length.

$\underline{k}_{get}$, External Geometric Stiffness (truss bar form)

Eq. 5.2-9 lists the individual terms of the external geometric stiffness matrix in terms of the element local axes.

$$\underline{k}_{get} = \frac{P}{L}$$

	1						-1				
		1						-1			
	-1						1				
		-1						1			

(5.2-9)

P = current element axial force (tension positive).

L = current element length.

The term external stems from the fact that the matrix is addressing the effect of the external nodal forces on equilibrium due to large displacements. This stiffness matrix is independent of the element characteristics and deformations occurring within the element. It is commonly referred to as the P-Δ stiffness associated with gravity loads on buildings causing overturning moments. Figure 5.2-7 provides a more visual interpretation of the contribution.

$\underline{k}_{gei}$, External Geometric Stiffness (invariant form)

Eq. 5.2-10 lists the individual terms of the external geometric stiffness in the invariant form in terms of element local axes. The four new matrix elements arise from the inclusion of the nonlinear axial strain term

$$\frac{1}{2}\left(\frac{\partial u}{\partial x}\right)^2$$

which is of course only significant if axial strains are not small.

$$\underline{k}_{gei} = \frac{P}{L}$$

1						-1					
	1						-1				
		1						-1			
-1						1					
	-1						1				
		-1						1			

(5.2-10)

L = current element length.

It is invariant from the fact that the global stiffness is unchanged, no matter what the element orientation in space, whereas the global stiffness associated with the truss bar form changes with element orientation. The invariant from is important when large axial member extensions are being considered.

k_{gi}, Internal Geometric Stiffness

Eq. 5.2-11 lists the individual terms of the internal geometric stiffness matrix in terms of element deformations.

k_{gi} =

$\frac{2PL}{15}$	$\frac{-PL}{30}$				
	$\frac{2PL}{15}$				
		$\frac{2PL}{15}$	$\frac{-PL}{30}$		
			$\frac{2PL}{15}$		
				0	
					0

(5.2-11)

P = current element axial force (tension positive).

L = current element lengths.

Figure 5.2-8 illustrates the physical interpretation of the matrix. In (a), the simply-supported beam is loaded with equal end moments resulting in the uniform moment (and curvature) distribution along the beam length. An axial load, P, is added in (b) and the moment distribution is altered by the moment developed by the axial force combined with the lateral (flexural) deformation of the beam. The result is a nonuniform moment distribution along the beam length. The potential energy associated with

this modification of the internal strain energy results in the internal geometric stiffness term. Figure 5.2-8(c) emphasizes a modeling consideration in regard to the internal geometric stiffness term. If the simply supported beam is modeled with multiple elements as opposed to a single element, the relative lateral flexural deformation within a single element is greatly reduced and the importance of including this stiffness is greatly diminished. Both models would give the same results, but the multi-element model would accommodate the internal geometric stiffness effects shown in Figure 5.2-8(b) through the external geometric stiffness. The multi-element model reduces the complexity of the individual element stiffness matrices, but, of course, at the expense of requiring more elements to model the system.

5.2.8 Computational Steps

For each load step or iteration within each load step, the following computations are performed:

1. Element tangent stiffness is formed and returned to the base program.

    a. Elastic and internal geometric stiffnesses are formed and transformed from element deformation degrees of freedom to local degrees of freedom.

$$\underline{k}^e = \underline{A}^T (\underline{k}_e + \underline{k}_{gi}) \underline{A} \qquad (5.2-12)$$

    b. Global tangent stiffness, $\hat{\underline{k}}_T$ is formed by adding the external geometric stiffness and transforming to global coordinates.

$$\underline{\hat{k}}_T = \underline{T}^T (\underline{k}_e + \underline{k}_{ge})\, \underline{A} \qquad (5.2-12)$$

$$= \underline{T}^T \left(\underline{A}^T (\underline{k}_e + \underline{k}_{gi})\, \underline{A} + \underline{k}_{ge} \right) \underline{T}$$

2. Increments in element displacements in the local coordinates, $\Delta \underline{u}$, are computed from increments in the nodal displacements in the global coordinates, $\underline{q}$, (which are computed in the base program and returned to element subroutine) as shown below.

Two procedures are considered:

Procedure 1

Eq. 5.2-1 is:

$$\Delta \underline{u} = \underline{T}^1 \Delta \underline{q} \qquad (5.2-14)$$

where $\underline{T}^1$ = transformation matrix for the current (beginning of the step) orientation of the element.

Procedure 2

Alternatively, $\Delta \underline{u}$ can be computed using the geometry at the middle of the step, i.e.,

$$\Delta \underline{u} = \underline{T}_{ms} \Delta \underline{q} \qquad (5.2-15)$$

where $\underline{T}_{ms}$ = transformation matrix for the middle of step orientation of the element.

The first procedure corresponds to the Euler method and the second to the midpoint method. The midpoint method is a predictor-corrector method and is of the second order.

3. Increments in nodal forces are computed using Eq. 5.2-12.

$$\Delta \underline{P} = \underline{A}^T (\underline{k}_e + \underline{k}_{gi}) \underline{A} \Delta \underline{u} \qquad (5.2-16)$$

4. Nodal forces are updated.

$$\underline{P}^2 = \underline{P}^1 + \Delta \underline{P} \qquad (5.2-17)$$

where

$\underline{P}^1$ = current forces.

$\Delta \underline{P}$ = increment in nodal forces.

$\underline{P}^2$ = final forces.

5. Orientation of the element axes is updated as follows:

The element x axis is assumed to pass through the element ends. The final positions of the element ends are determined from their current positions and the increments in end displacements; thus, the orientation of the element x axis is determined.

The orientation of the element y and z axes are considered next. For simplicity, first consider the 2D case shown in Figure 5.2-9. The final position of the element x axis can easily be determined.

The element y axis remains in the xy plane and its final orientation is perpendicular to the final orientation of the x axis. Orientation of the element z axis does not change and remains perpendicular to the xy plane. This process can be expressed by a single rotation as follows:

$$\underline{t}_{k+1} = \underline{d}\ \underline{t}_k \qquad (5.2-18)$$

where

t_k = (3x3) direction cosine matrix of the element local axes for configuration k.

$\underline{d}$ = rotation matrix.

$$= \begin{bmatrix} \cos\alpha_k & \sin\alpha_k & 0 \\ -\sin\alpha_k & -\cos\alpha_k & 0 \\ 0 & 0 & 1 \end{bmatrix} \qquad (5.2-19)$$

where α_k = angle between x_k and x_{k+1}.

$\underline{t}_{k+1}$ = direction cosine matrix of element local axes for configuration k+1.

Note that the increments in nodal rotations do not affect the final orientation of the element axes.

Next consider the same 2D example, but assume that some small end rotations (β_i and β_j) along the x_k are present as shown in Figure 5.2-10. Orientation of x_{k+1} can be determined as before. The new orientation of the y axis will be inclined to the XY plane.

It is assumed that the inclination angle of the element y axis to the XY plane, angle $\bar{\beta}$, is the average of the longitudinal rotations β_i and β_j, i.e.

$$\bar{\beta} = \frac{\beta_i + \beta_j}{2}$$

To obtain the final position of the element axes, first the element axes are rotated about x_k by the angle $\bar{\beta}$, then a second rotation by the angle α (as in the previous case) in the XY plane is performed.

Therefore,

$$\underline{t}_{k+1} = \underline{d}\ \underline{\beta}\ \underline{t}_k \qquad (5.2-20)$$

where $\underline{t}_k$, $\underline{t}_{k+1}$ and $\underline{d}$ are defined in Eq. 5.2-19 and $\underline{\beta}$ = matrix of longitudinal rotation

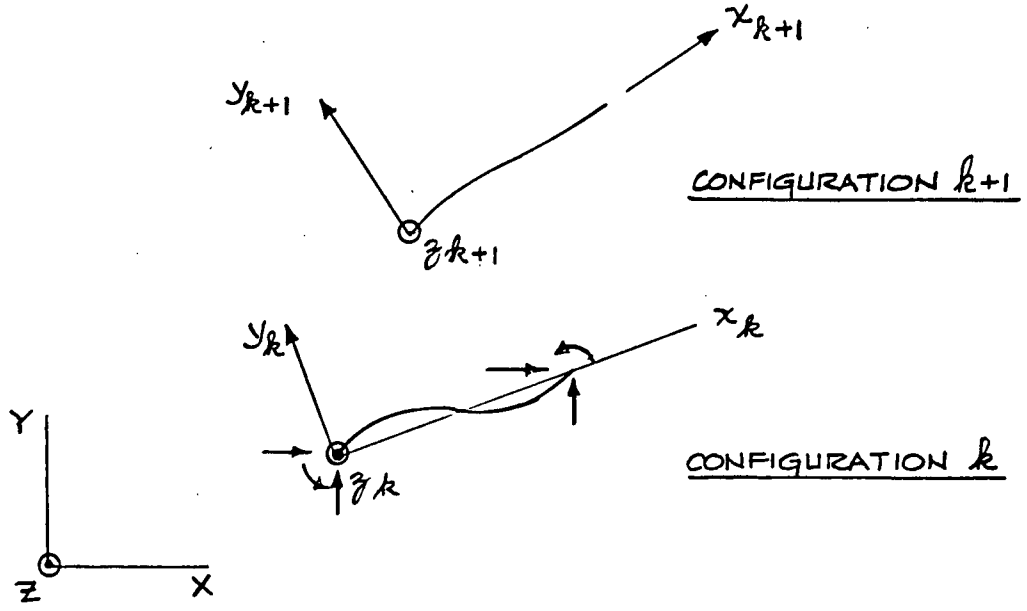

FIG. 5.2-9 TWO-DIMENSIONAL EXAMPLE 1

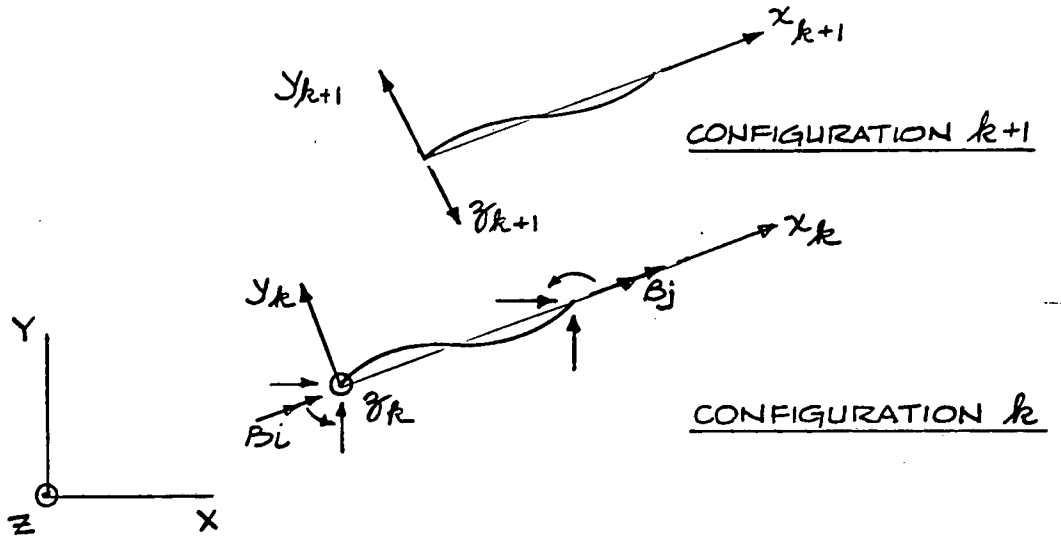

FIG. 5.2-10 TWO-DIMENSIONAL EXAMPLE 2

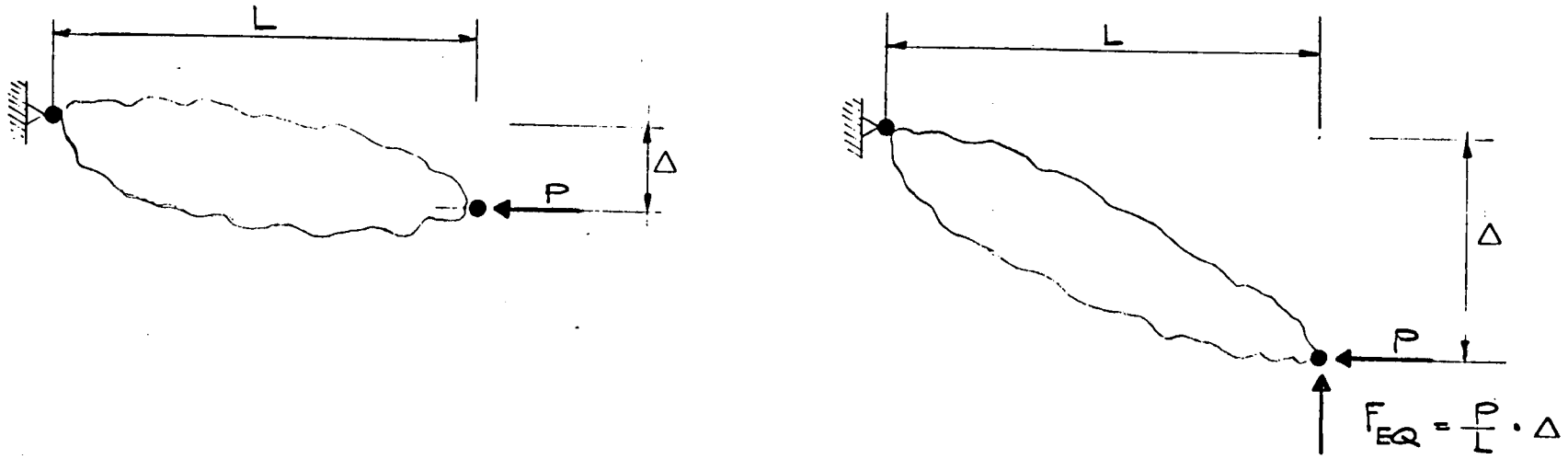

FIG. 5.2-7 EXTERNAL GEOMETRIC STIFFNESS
(EXTERNAL EQUILIBRIUM)

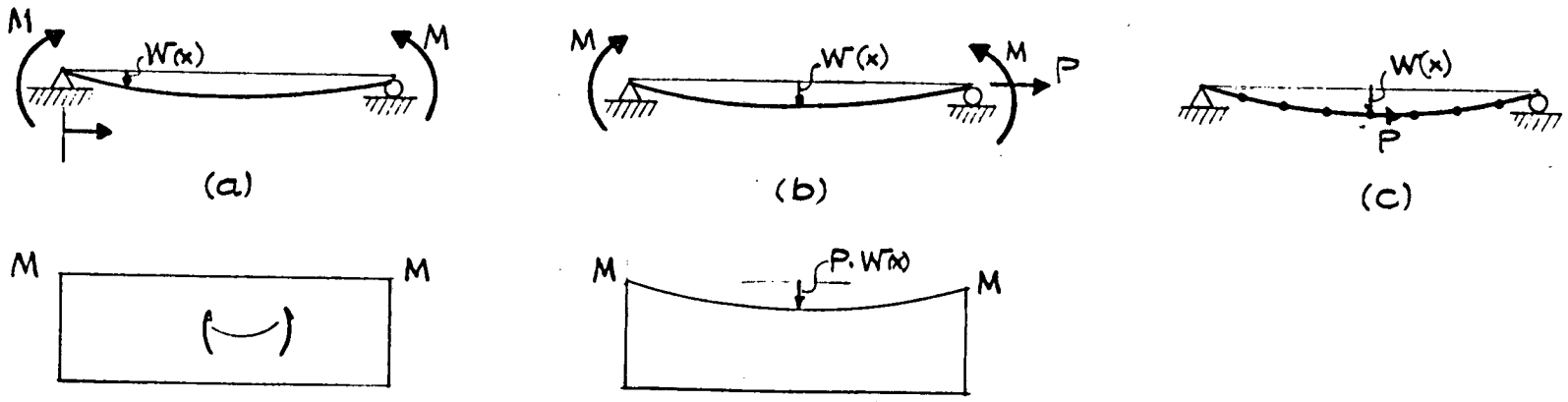

FIG. 5.2-8 INTERNAL GEOMETRIC STIFFNESS

$$\underline{\beta} = \begin{bmatrix} \cos\bar{\beta} & \sin\bar{\beta} & 0 \\ -\sin\bar{\beta} & \cos\bar{\beta} & 0 \\ 0 & 0 & 1 \end{bmatrix} \qquad (5.2-21)$$

Note that the second rotation does not induce any longitudinal rotation. Also note that the nodal rotations in the XY plane do not affect the final orientation of element coordinate axes.

Now consider the 3D case as shown in Figure 5.2-11. The final orientation of the element axes are determined (as with the 2D cases considered above) by successive rotations. First, nodal rotations in global coordinate axes are transformed to element local x_k axis (at current position) to compute the longitudinal rotations β_i and β_j. Coordinate axes are then rotated by the average nodal longitudinal rotation

$$\frac{\beta_i + \beta_j}{2}$$

Next, element axes are rotated by the angle α_k (the angle between x_k and x_{k+1}) about an axis which is perpendicular to both the current and the final positions of element x axes. Therefore

$$\underline{t}_{k+1} = \underline{d}\ \underline{\beta}\ \underline{t}_k \qquad (5.2-22)$$

where $\underline{\beta}$, $\underline{t}_k$ and $\underline{t}_{k+1}$ are defined in Eqs. 5.2-21 and 5.2-5.

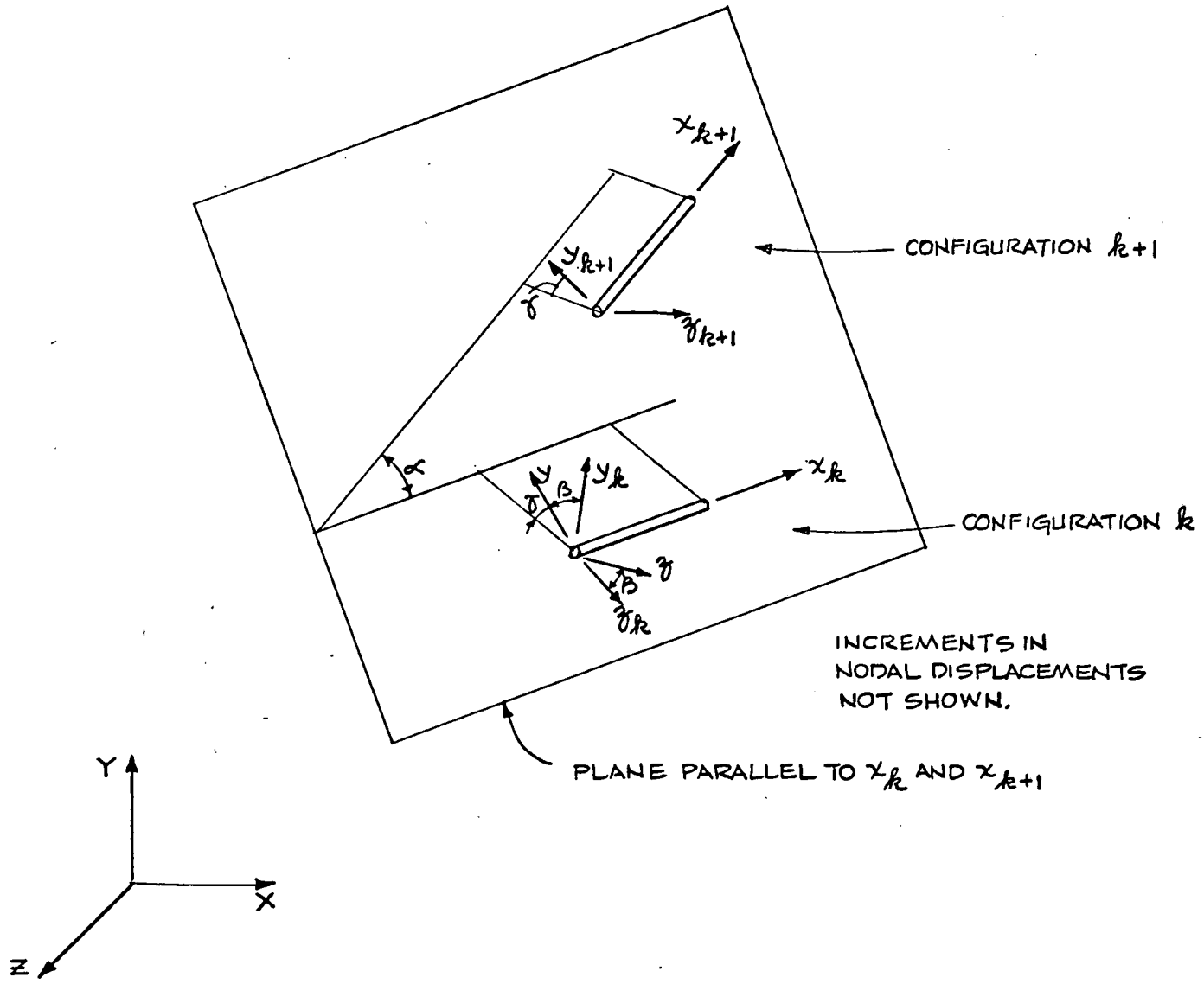

FIG. 5.2-11 THREE DIMENSIONAL EXAMPLE

$\underline{d}'$ = matrix of rotation about an axis perpendicular to x_k and x_{k+1}.

$$= \begin{bmatrix} \cos\alpha_k & n_3 \sin\alpha_k & -n_2 \sin\alpha_k \\ -n_3 \sin\alpha_k & n_2^2 + n_3^2 \cos\alpha_k & n_2 n_3 (1 - \cos\alpha_k) \\ n_2 \sin\alpha_k & n_2 n_3 (1 - \cos\alpha_k) & n_3^2 + n_2^2 \cos\alpha_k \end{bmatrix}$$

(5.2-23)

$\underline{n}$ = $(0, n_2, n_3)$ = unit normal to x_k and x_{k+1}. Components measured in current coordinate axes.

α_k = angle between x_k and x_{k+1}.

Note that the second rotation as shown in Figure 5.2-9 will not induce any additional longitudinal rotation.

In the procedure outlined above, it is assumed that the element will undergo a longitudinal rotation equal to the average nodal longitudinal rotations referred to the current position of the element x axis. This procedure is approximate, since the orientation of the element x axis changes from x_k to x_{k+1} within a step. A more accurate procedure may be devised by applying the increment in displacements and rotations in a number of steps. A two-step procedure as follows is considered here.

In this two-step procedure, the element axes are first rotated by the angle $\alpha_k/2$ (by the same procedure as explained for the above 3D case, but with no longitudinal rotation) to obtain the middle of step orientation of the element x axis. Then the element nodal rotation increments are transferred to the middle of the step x axis to compute the longitudinal rotations β_i and β_j. Finally, a third rotation, similar to the first one, by the angle α is applied to obtain the final position of the element local axes. In matrix notation,

$$\underline{t}_{k+1} = \underline{d}_2 \, \underline{\beta} \, \underline{d}_1 \, \underline{t}_k \qquad (5.2-24)$$

where $\underline{\beta}$, $\underline{t}_k$ and $\underline{t}k+1$ are defined in Eq. 5.2-19 and 5.3-21.

$\underline{d}_1$ and $\underline{d}_2$ = rotation matrices similar to Eq. 5.2-23.

Note that $\alpha_k/2$ is used and that

$\underline{d}_1 \neq \underline{d}_2$ due to different $\underline{n}$ vectors.

Both procedures as given by Eqs. 5.2-22 and 5.2-24 are implemented in the program.

In the second procedure for computation of the element deformations, the middle of step direction cosine matrix is used. The middle of step direction cosine matrix (t_{ms}) is computed as follows:

$$\underline{t}_{ms} = \underline{\beta} \, (\bar{\beta}/2) \, \underline{d}_1 \, \underline{t}_k \qquad (5.2-25)$$

where $\underline{t}_k$ and $\underline{d}_l$ are defined in Eq. 5.2-19.

$\underline{\beta}(\bar{\beta}/2)$ = is as defined in Eq. 5.2-21, with $\bar{\beta}/2$ angle of longitudinal rotation.

6. Nodal loads in equilibrium with element nodal forces are computed as follows and returned to the base program.

$$\underline{Q} = \underline{T}^T \underline{P} \qquad (5.2-26)$$

where

$\underline{Q}$ = equivalent nodal loads.

$\underline{T}$ = coordinate transformation matrix referred to end of step (final) position of the element axes.

$\underline{P}$ = updated nodal forces.

5.3 Linear Beam

The three-dimensional linear beam element is a straight member of uniform cross-section capable of resisting axial force, torque and bending moments. This element can be arbitrarily oriented in space and is defined by three nodes i, j and k. Nodes i and j define the centroidal beam axis or the local-1 axis. The 2-axis is defined normal to the 1-axis and resides in the plane containing the k-node and the 1-axis. The local-3 axis is defined orthogonal to the local 1 and 2 axis, using the right hand rule.

The element forces and deformations are defined as follows for the i and j ends, respectively.

	Deformations	Forces
Axial	u_1, u_7	P_1, P_7
2-axis shear	u_2, u_8	P_2, P_8
3-axis shear	u_3, u_9	P_3, P_9
Torque	u_4, u_{10}	P_4, P_{10}
2-axis moments	u_5, u_{11}	P_5, P_{11}
3-axis moments	u_6, u_{12}	P_6, P_{12}

The end deformations u_1 through u_{12} are indicated in Figure 5.3-1. The corresponding forces are not shown; however, the positive force and deformation directions coincide.

5.3.1 Element Stiffness Matrix

The beam element stiffness, $\underline{\hat{k}}$, in the global coordinate system is given by

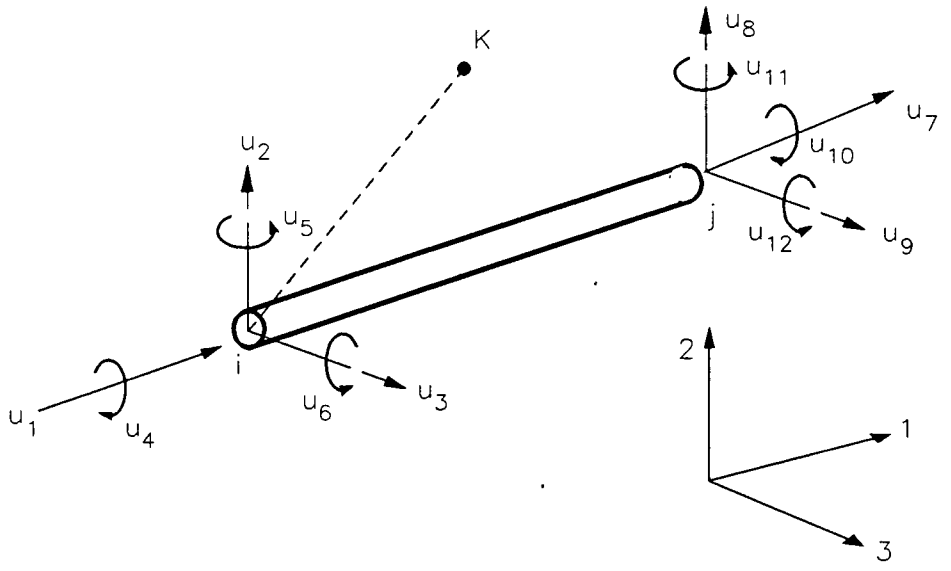

FIG. 5.3-1 END DEFORMATIONS OF THREE-DIMENSIONAL BEAM

$$\underline{\hat{k}} = \underline{T}^T \; \underline{k} \; \underline{T} \qquad (5.3-1)$$

The matrix $\underline{T}$ transforms the local stiffness $\underline{k}$ to a global orientation for assembly into the global stiffness matrix.

The element local stiffness matrix, $\underline{k}$, is symmetric and is defined as

$$\begin{bmatrix} P1 \\ P2 \\ P3 \\ P4 \\ P5 \\ P6 \\ P7 \\ P8 \\ P9 \\ P10 \\ P11 \\ P12 \end{bmatrix} = \begin{bmatrix} k1 & & & & & & & & & & & \\ 0 & k2 & & & & & & & & & & \\ 0 & 0 & k3 & & & & & & & & & \\ 0 & 0 & 0 & k4 & & & & \text{Symmetric} & & & & \\ 0 & 0 & -k5 & 0 & k6 & & & & & & & \\ 0 & k7 & 0 & 0 & 0 & k8 & & & & & & \\ -k1 & 0 & 0 & 0 & 0 & 0 & k1 & & & & & \\ 0 & -k2 & 0 & 0 & 0 & -k7 & 0 & k2 & & & & \\ 0 & 0 & -k3 & 0 & k5 & 0 & 0 & 0 & k3 & & & \\ 0 & 0 & 0 & -k4 & 0 & 0 & 0 & 0 & 0 & k4 & & \\ 0 & 0 & -k5 & 0 & k9 & 0 & 0 & 0 & k5 & 0 & k6 & \\ 0 & k7 & 0 & 0 & 0 & k10 & 0 & -k7 & 0 & 0 & 0 & k8 \end{bmatrix} \begin{bmatrix} u_1 \\ u_2 \\ u_3 \\ u_4 \\ u_5 \\ u_6 \\ u_7 \\ u_8 \\ u_9 \\ u_{10} \\ u_{11} \\ u_{12} \end{bmatrix}$$

(5.3-2)

where

$$k1 = \frac{AE}{L} = \text{axial stiffness}$$

$$k2 = \frac{12EI_3}{L^3(1+\phi_2)} = \text{2-axis shear stiffness}$$

$$k3 = \frac{12EI_2}{L^3(1+\phi_3)} = \text{3-axis shear stiffness}$$

$$k4 = \frac{GJ}{L} = \text{torsional stiffness}$$

$$k5 = \frac{6EI_2}{L^2(1+\phi_3)} = \text{flexural (about local-2 axis) - shear coupling stiffness}$$

$$k6 = \frac{(4+\phi_3)EI_2}{L(1+\phi_3)} = \text{flexural stiffness about local-2 axis}$$

$$k7 = \frac{6EI_3}{L^2(1+\phi_2)} = \text{flexural (about local-3 axis) - shear coupling stiffness}$$

$$k8 = \frac{(4+\phi_2)EI_3}{L(1+\phi_2)} = \text{flexural stiffness about local-2 axis}$$

$$k9 = \frac{(2-\phi_3)EI_2}{L(1+\phi_3)}$$

$$k10 = \frac{(2-\phi_2)EI_3}{L(1+\phi_2)}$$

The shearing deformation terms are defined as follows:

$$\phi_2 = \frac{12EI_3}{GA_{s_2}L^2}$$

$$\phi_3 = \frac{12EI_2}{GA_{s_3}L^2}$$

where A_{s2} and A_{s3} are shear areas for element 2 and 3 axes. Shear deformations may be neglected by specification of ϕ_2 or ϕ_3 equal to zero.

The transformation from global to local displacements and forces, given by $\underline{T}$ in Eq. 5.3-1, is obtained as follows:

The local element axes are defined by three unit vectors $\underline{s}_1$, $\underline{s}_2$, and $\underline{s}_3$, and the subscript denotes the local axis.

The $\underline{s}_3$ vector is given by the cross product of $\underline{s}_1$ and the vector, $\underline{g}$, between the i and k nodes.

The vectors s_1 and g are defined by:

$$\underline{s}_1 = l_1 \hat{i} + m_i \hat{j} + n_1 \hat{k}$$

$$\underline{g} = g_x \hat{i} + g_y \hat{j} + g_z \hat{k}$$

where

$i, \hat{j}, \hat{k}$ = unit vectors in the global X, Y Z directions, respectively.

$$l_1 = \frac{L_x}{L} = \frac{X_j - X_i}{L}$$

$$m_1 = \frac{L_y}{L} = \frac{Y_j - Y_i}{L}$$

$$n_1 = \frac{L_z}{L} = \frac{Z_j - Z_i}{L}$$

$$g_x = \frac{G_x}{L_g} = \frac{X_k - X_i}{L_g}$$

$$g_y = \frac{G_y}{L_g} = \frac{Y_k - Y_i}{L_g}$$

$$g_z = \frac{G_z}{L_g} = \frac{Z_k - Z_i}{L_g}$$

where

$$L = \sqrt{L_x^2 + L_y^2 + L_z^2}$$

$$Lg = \sqrt{G_x^2 + G_y^2 + G_z^2}$$

Hence

$$\underline{s}_3 = \frac{\underline{s}_1 \times \underline{g}}{|\underline{s}_1 \times \underline{g}|} = l_3\,\hat{i} + m_3\,\hat{j} + n_3\,\hat{k}$$

The $\underline{s}_2$ unit vector resides in the same plane as $\underline{g}$ and $\underline{s}_1$ and is orthogonal to $\underline{s}_1$ and $\underline{s}_3$

The $\underline{s}_2$ unit vector is given by the cross product

$$\underline{s}_2 = \underline{s}_3 \times \underline{s}_1 = l_2\,\hat{i} + m_2\,\hat{j} + n_2\,\hat{k}$$

The direction cosine matrix $\underline{t}$ is defined by

$$\underline{t} = \begin{bmatrix} l_1 & m_1 & n_1 \\ l_2 & m_2 & n_2 \\ l_3 & m_3 & n_3 \end{bmatrix}$$

The local to global transformation matrix $\underline{a}$ is given by (12x12)

$$\underline{a} = \begin{bmatrix} \frac{t}{3x3} & & & 0 \\ & \frac{t}{3x3} & & \\ & & \frac{t}{3x3} & \\ 0 & & & \frac{t}{3x3} \end{bmatrix}$$

The global stiffness can then be formulated as:

$$\underset{12\overline{x}12}{\hat{k}} = \underset{12\overline{x}12}{T^T} \quad \underset{12\overline{x}12}{k} \quad \underset{12\overline{x}12}{T}$$

5.4 Inelastic Three-Dimensional Beam-Column Element

This is intended primarily for modeling inelastic effects in beams and columns. The element takes account of moment-force interaction for columns and of bending moment interaction for biaxial bending. Yielding is assumed to take place only in concentrated (i.e., zero length) plastic hinges located at the element ends. The part of the element between the hinges is assumed to remain linearly elastic.

Initial elastic stiffnesses must be specified for axial extension, torsional twist, and bending about two axes. Flexural shear deformations and the effects of eccentric end connections can be considered, if desired. The element strengths may be different at the two ends, and the elastic stiffnesses can include the effect of varying cross section along the element length.

5.4.1 Element Features

1. The element may be arbitrarily oriented in space but must be straight.

2. Inelastic behavior is confined to zero-length plastic hinges at the element ends.

3. The hinges are assumed to have rigid-plastic-strain-hardening behavior. Strain hardening stiffnesses must be specified for the moment-rotation and force-extension relationships of the hinges. Multi-linear relationships (maximum four segments) are assumed.

4. Interaction between bending moments, torque, and axial force is considered by means of four-dimensional yield surfaces. A

kinematic hardening rule (extended Mroz theory) is assumed for post-yield behavior (i.e., translation of yield surface without change of size or shape).

5. Options are available for small displacements, second order (P-Δ) theory and full large displacement effects. Large displacements are considered using an "engineering" theory.

6. Eccentric end connections may be specified to model rigid joint regions.

5.4.2 Element Axes

Element properties and results are specified in the local coordinate system x, y, z, defined as shown in Figure 5.4-1. If node K is not specified, its location is assumed as follows:

1. If IJ is not vertical, node K is at $Y = +\infty$. The xy plane is then the vertical plane containing the element.

2. If IJ is vertical, node K is at $X = +\infty$. The xy plane is then parallel to the XY plane.

5.4.3 Degrees of Freedom and Forces

The element has two external nodes and two internal nodes, as shown in Figure 5.4-2. The external nodes connect to the complete structure and have six degrees of freedom each, namely X, Y, Z global translations and X, Y, Z global rotations. The element nodal displacements in the global coordinates are written as

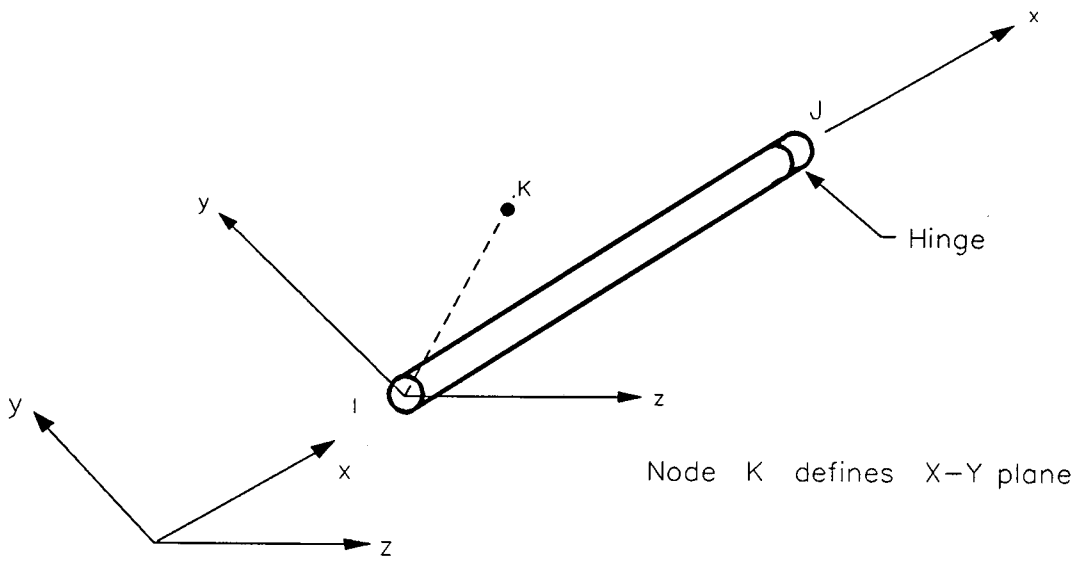

(a) Element Axes

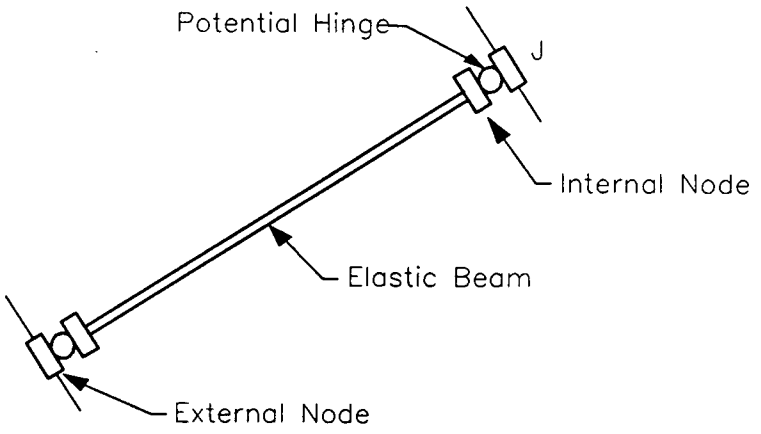

(b) Element Idealization

FIG. 5.4-1 ELEMENT AXES AND IDEALIZATION

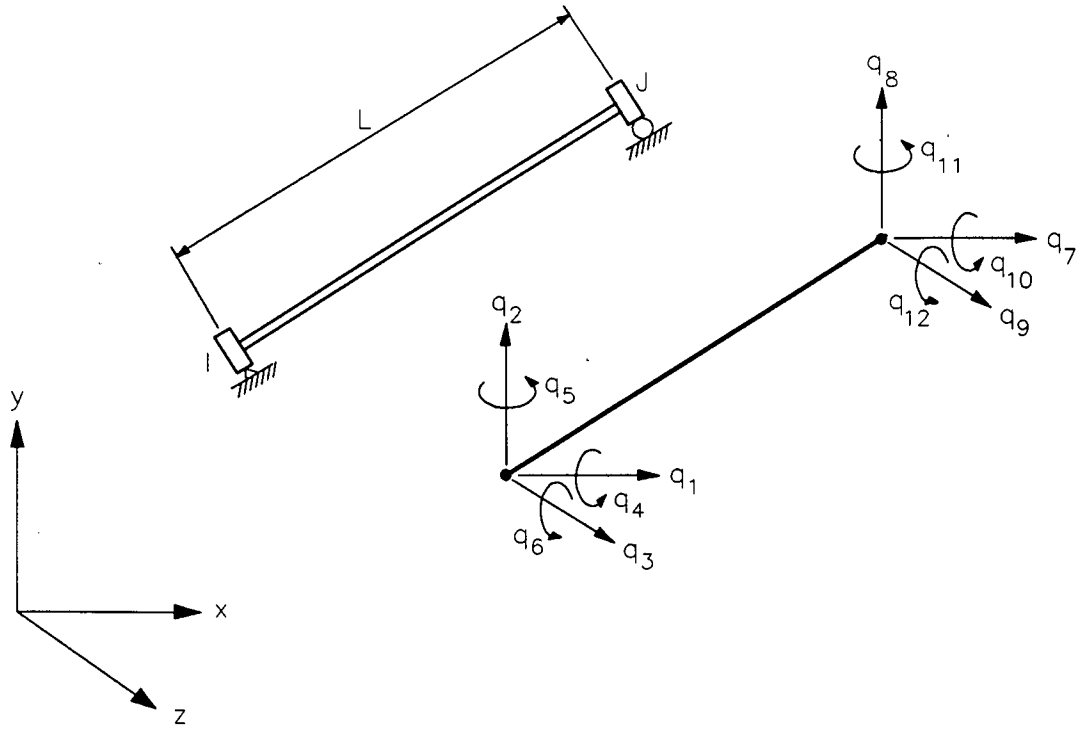

(a) Global Displacements

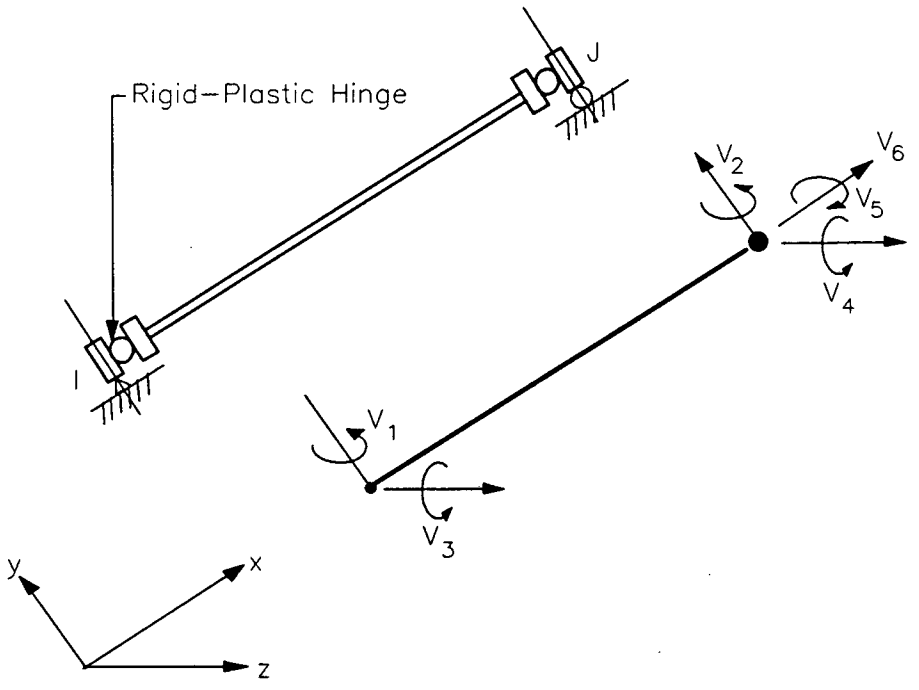

(b) Local Deformations

FIG. 5.4-2 ELEMENT DEGREES OF FREEDOM

$$\underline{q} = \{q_1 \ldots q_{12}\}$$

After deletion of the six rigid body modes for the complete element and transformation to the local element coordinates, the six deformation degrees of freedom shown in Figure 5.4-2(b) remain. Each hinge has four deformations, namely an axial deformation plus rotations about each of the local x, y, z axes (i.e., shear deformations in the hinges are zero).

The transformation from global displacements to element deformations is:

$$\underline{v} = \underline{a}\,\underline{q} \qquad (5.4-1)$$

in which

$\underline{v}^T = [v_1, v_2, \ldots, v_6]$ = element deformations (Figure 5.4-2(b)).

$\underline{q}^T = [q_1, q_2, \ldots, q_{12}]$ = element nodal displacement (Figure 5.4-2(a)).

and the transformation matrix $\underline{a}$ is well known.

The element internal degrees of freedom $\underline{w}$ are shown in Figure 5.4-3.

The element nodal forces corresponding to the internal degrees of freedom, $\underline{F}$, are written as

$$\underline{F} = \{M_{yi} \;\; M_{yj} \;\; M_{zi} \;\; M_{zj} \;\; M_x \;\; F_x\}^T$$

5.4.4 Element Stiffness

The beam element connecting the internal nodes remains elastic, but the tangent stiffnesses of the hinges may change. For any state of the

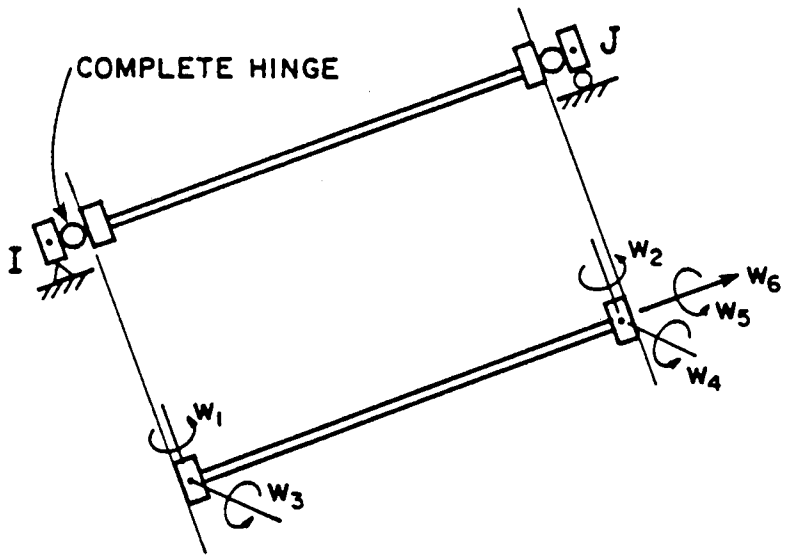

(a) INTERNAL DEGREES OF FREEDOM

FIG. 5.4-3 INTERNAL DEGREES OF FREEDOM

complete element, a 6x6 flexibility matrix is first formed for the elastic beam in terms of the degrees of freedom w_1 through w_6. This matrix is then modified by adding the flexibilities of the hinges to give a complete element flexibility matrix in terms of v_1 through v_6. This matrix is inverted to obtain a 6x6 element stiffness (computationally, the Sherman-Morrison formula is used, not direct inversion). Finally, this stiffness is transformed to the 12x12 global stiffness.

Beam Element Elastic Flexibility

The local y, z axes are assumed to be the principal axes of the beam cross section. The local x axis is assumed to be both the centroidal axis and the axis of torsional twist.

The incremental beam element force-deformation relationships for the internal degrees of freedom can be written as follows:

$$\begin{bmatrix} dM_{yi} \\ dM_{yj} \end{bmatrix} = \frac{EI_y}{L} \begin{bmatrix} K_{iiy} & K_{ijy} \\ K_{ijy} & K_{jjy} \end{bmatrix} \begin{bmatrix} dw_1 \\ dw_2 \end{bmatrix} \qquad (5.4-2)$$

$$\begin{bmatrix} dM_{zi} \\ dM_{zj} \end{bmatrix} = \frac{EI_z}{L} \begin{bmatrix} K_{iiz} & K_{ijz} \\ K_{ijz} & K_{jjz} \end{bmatrix} \begin{bmatrix} dw_3 \\ dw_4 \end{bmatrix} \qquad (5.4-3)$$

$$dM_x = \frac{GJ}{L} dw_5 \quad , \qquad (5.4-4)$$

$$dF_x = \frac{EA}{L} dw_6 \qquad (5.4-5)$$

where

k_{ii}, k_{ij}, k_{jj} = flexural stiffness factors.

EI_y, EI_z = effective flexural rigidities.

M_y, M_z = bending moments.

i,j = element ends.

M_x = torsional moment.

F_x = axial force.

L = element length.

EA = effective axial rigidity.

GJ = effective torsional rigidity.

The flexural stiffness factors can be used to account for non-uniform elements. For a uniform element, $K_{ii} = K_{jj} = 4.0$ and $K_{ij} = 2.0$.

Eqs. 5.4-2 and 5.4-3 are inverted to obtain flexibilities and are modified, if necessary, to allow for shear deformations by adding the shear flexibility matrices, f_{sy} and f_{sz}, where

$$\underline{f}_s = \frac{1}{GAL} \begin{bmatrix} 1 & 1 \\ 1 & 1 \end{bmatrix} \qquad (5.4-6)$$

5.4.5 Modeling of Inelastic Behavior

Yield is monitored at the potential hinges. Tangent stiffness relationships between the actions and deformations at a yielding hinge are established using a plasticity theory which is an extension of the Mroz theory for yield of metals. Each hinge is initially rigid, so that the initial stiffness of the complete element is the stiffness of the

elastic beam. As the moments and forces at the element ends (the hinge actions) increase, the hinges can yield, causing a stiffness reduction in the element. Under increasing deformation, the hinges strain harden, following multi-linear action-deformation relationships. If the actions at a hinge decrease, the hinge becomes rigid again and the element unloads. The overall element behavior is thus multi-linearly inelastic, as illustrated in Figure 5.4-4.

Hinge Properties

The rigid-plastic-strain-hardening relationships between hinge actions and deformations must be defined for the two hinges. The relationships at the two hinges in any element may be different, if desired.

Relationships as shown in Figure 5.4-5 must be defined for each of four action-deformation pairs, namely

1. Bending moment, M_y, and the corresponding rotation, θ_y.

2. Bending moment, M_z, and the corresponding rotation, θ_z.

3. Torque, M_x, and the corresponding twist, ϕ_x.

4. Axial force, F_x, and the corresponding extension, δ_x.

Each relationship is rigid-plastic-strain-hardening and may have up to three linear segments, as shown in Figure 5.4-5. The relationships may be of different shapes for each action. For material with an elastic-perfectly plastic stress-strain relationship, the torque-twist and force-extension relationships will be rigid-perfectly plastic,

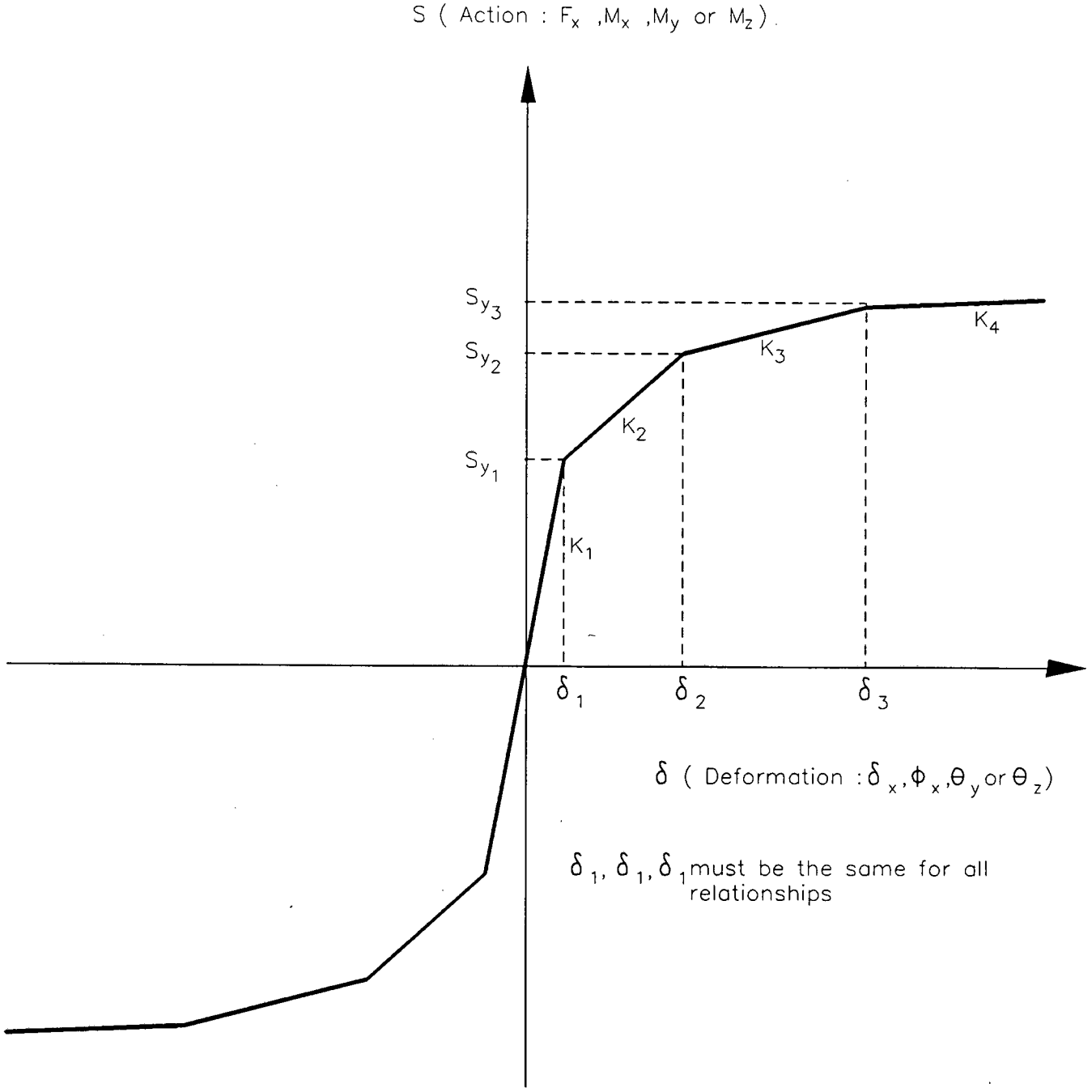

FIG. 5.4-4 ACTION VS. DEFORMATION FOR THE COMPLETE ELEMENT

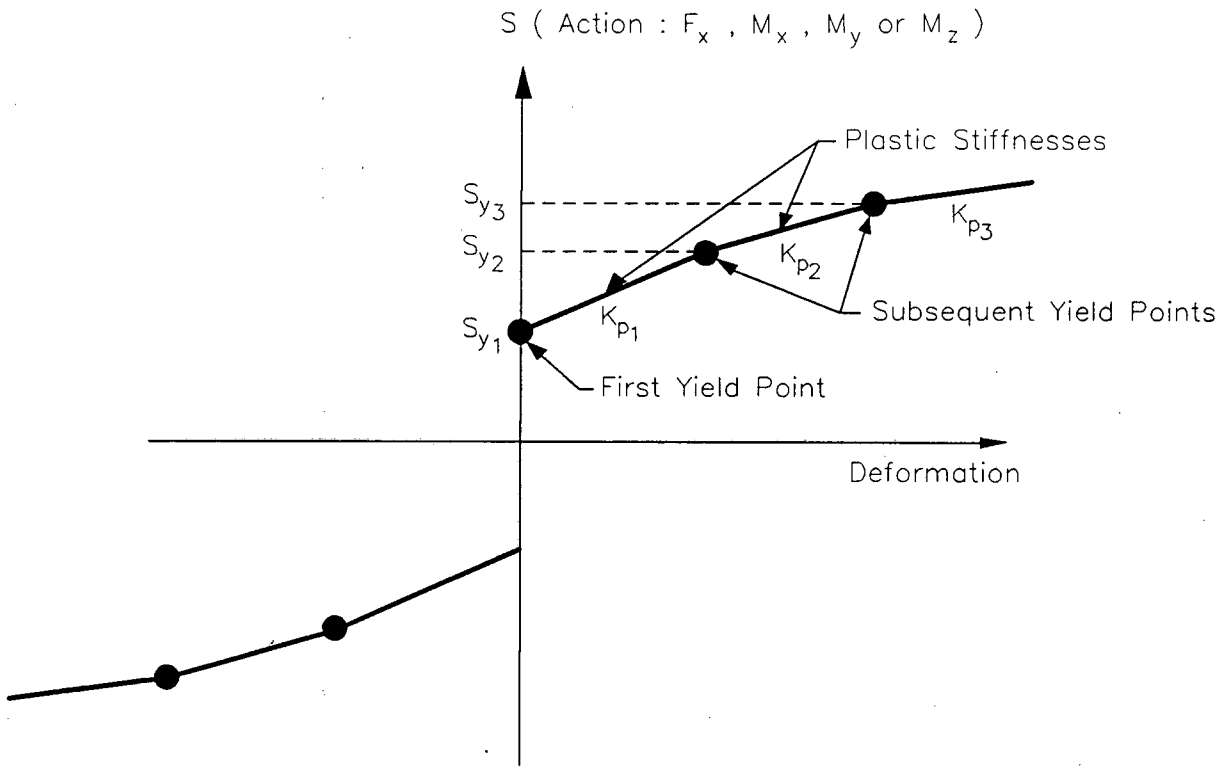

(a) Action vs. Deformation Relationship

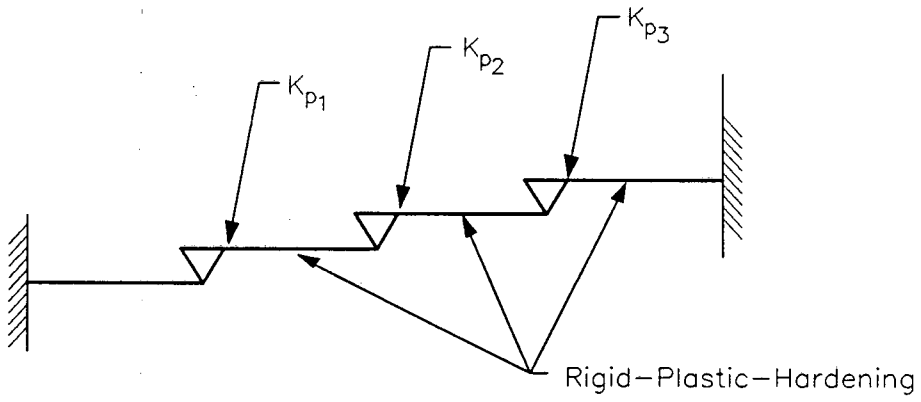

(b) I-D Model

FIG. 5.4-5 1-D MODEL FOR A HINGE

whereas the moment-rotation relationships will usually exhibit strain hardening behavior (Figure 5.4-6). It is required that the deformations at changes in stiffness have the same ratios for all relationships, as indicated in Figure 5.4-4. This restriction is necessary to avoid inconsistencies in the plasticity theory.

It may be noted that the assumption of a zero-length hinge implies infinitely high strains as a hinge deforms. This is inherent in any plastic hinge type of theory.

Interaction Surfaces for First Yield

The actions M_y, M_z, M_x, and F_x interact with each other to produce initial yield of the hinge. The interaction effect is determined by a yield (interaction) surface. To allow for a variety of applications, provision is made in the theory for five different yield surfaces. These surfaces are all four dimensional (i.e., M_y, M_z, M_x, and F_x), and hence, cannot be shown easily using diagrams. The surfaces differ, however, mainly in the way in which the axial force interacts with the three moments. Hence, the differences can be illustrated using the three-dimensional diagrams in Figure 5.4-7. In these figures, the M_i and M_j axes indicate any two of the moments, and the F_x axis indicates axial force. The origin of the yield surface can be shifted along the axial force axis, if it is desired to have greater compressive capacity than tension capacity. The F-M interaction surface can then approximate that for a reinforced concrete column. The equations defining the yield surfaces are shown in the figure.

Surface 1 is elliptical and is the simplest mathematically. Surfaces 2, 3 and 4 allow more realistic modeling of moment-force interaction for

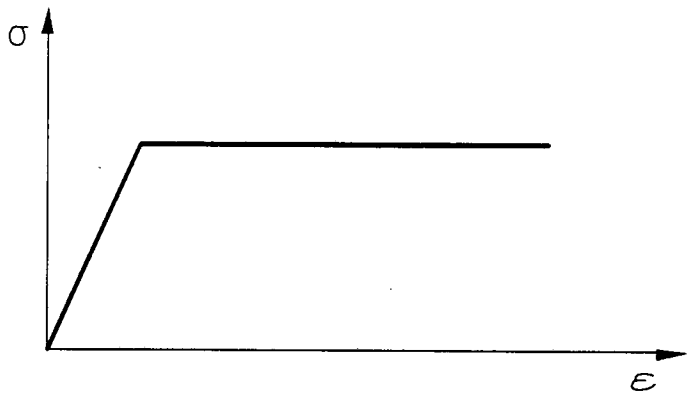

(a) Elastic-Plastic Stress-Strain Relationship

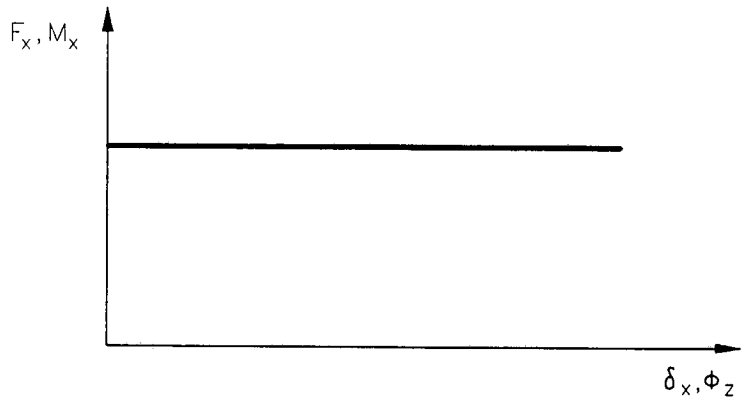

(b) Force-Extension and Torque-Twist

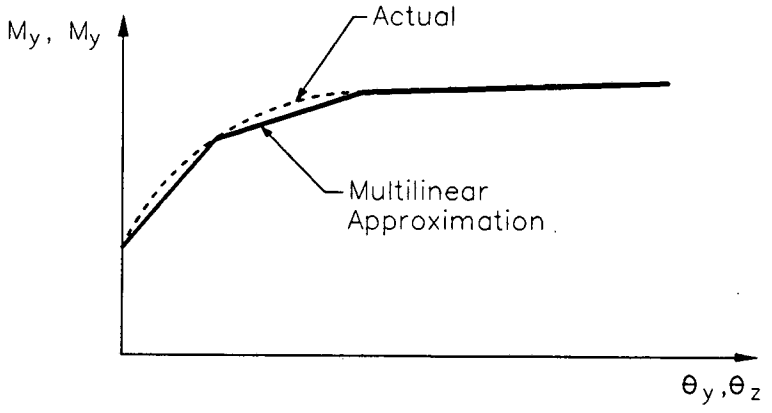

(c) Moment-Curvature

FIG. 5.4-6 DIFFERENCES IN SHAPES OF RELATIONSHIPS

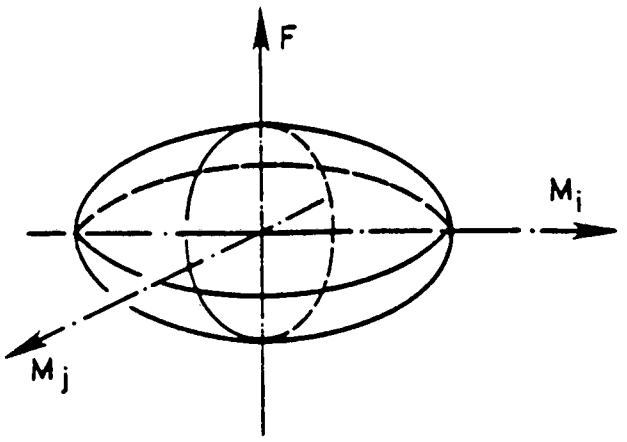

$$\phi = \left(\frac{M_y}{M_{yu}}\right)^2 + \left(\frac{M_z}{M_{zu}}\right)^2 + \left(\frac{M_x}{M_{xu}}\right)^2 + \left(\frac{F}{F_u}\right)^2 = 1$$

(A) SURFACE TYPE 1

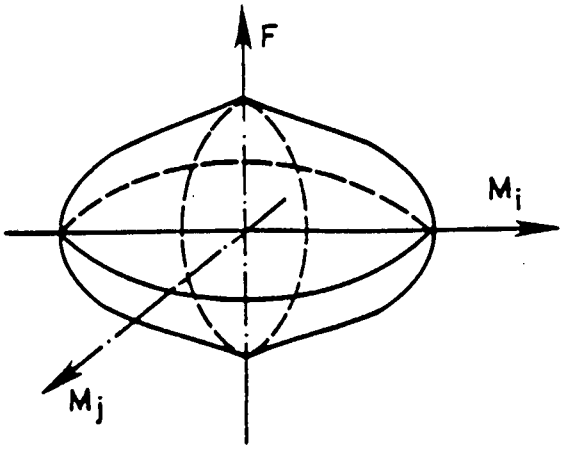

$$\phi = \left[\left(\frac{M_y}{M_{yu}}\right)^2 + \left(\frac{M_z}{M_{zu}}\right)^2 + \left(\frac{M_x}{M_{xu}}\right)^2\right]^{1/2} + \left(\frac{F}{F_u}\right)^2 = 1$$

(B) SURFACE TYPE 2

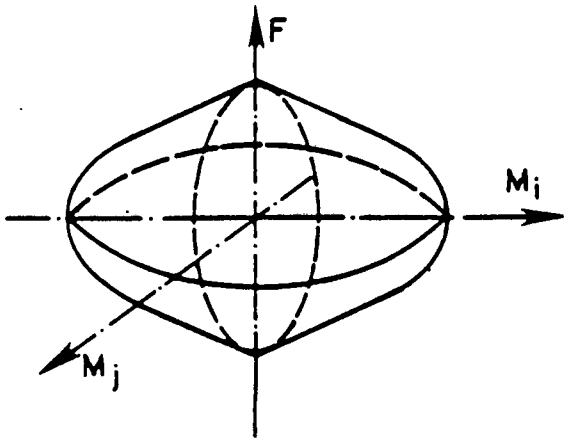

$$\phi = \left[\left(\frac{M_y}{M_{yu}}\right)^2 + \left(\frac{M_z}{M_{zu}}\right)^2 + \left(\frac{M_x}{M_{xu}}\right)^2\right]^{1/2} + \left(\frac{F}{F_u}\right)^{a_1} = 1$$

(C) SURFACE TYPE 3

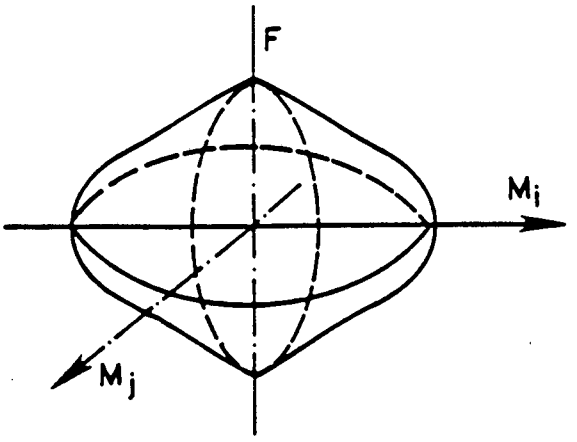

$$\phi = \left[\left(\frac{M_y}{M_{yu}}\right)^2 + \left(\frac{M_z}{M_{zu}}\right)^2 + \left(\frac{M_x}{M_{xu}}\right)^2\right]^{a_1} + \left(\frac{F}{F_u}\right)^{a_2} = 1$$

(D) SURFACE TYPE 4

FIG. 5.4-7 **INTERACTION SURFACES**

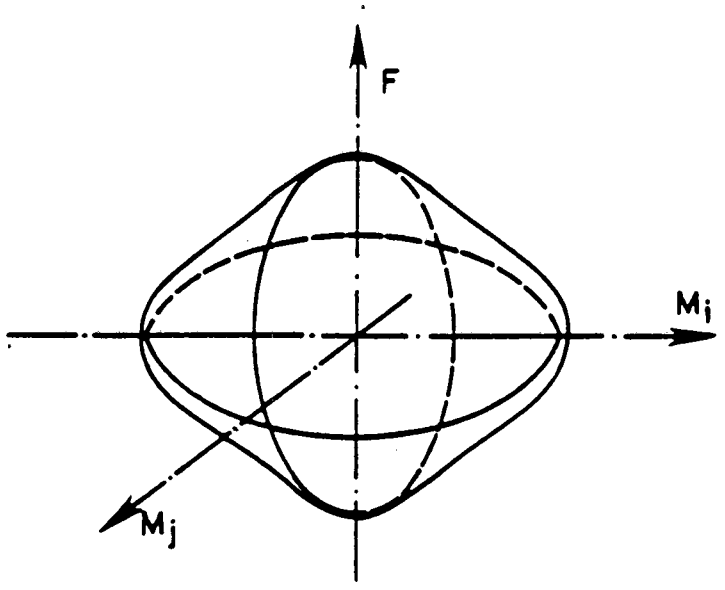

$$\phi = \left(\frac{M_y}{M_{yu}}\right)^{a_1} + \left(\frac{M_z}{M_{zu}}\right)^{a_2} + \left(\frac{T}{T_u}\right)^{a_3} + \left(\frac{F}{F_u}\right)^{a_4} = 1$$

(E) SURFACE TYPE 5

FIG. 5.4-7 INTERACTION SURFACES (CONT'D)

cases in which axial force effects are substantial. For all of these four surfaces, the interaction among M_y, M_z and M_x is elliptical and only the force-moment interaction changes. Surface 5 is of a different form than the other four and is included for greater generality in special cases.

Interaction Surfaces for Subsequent Yield

For modeling a hinge with nonlinear material properties, it is assumed that the behavior is rigid-plastic-strain-hardening for each action individually, as shown in Figure 5.4-5(a). In one dimension, the rigid-plastic-strain-hardening behavior can be modeled using a series rigid-plastic subsprings, as shown in Figure 5.4-5(b). This model can be extended to the multidimensional case using a series of rigid-plastic "subsprings," with the yield of any subhinge governed by a yield surface.

First yield occurs at the first subhinge and is governed by the initial yield surface. For each change of stiffness, there is a corresponding yield surface, each corresponding to a subhinge. These surfaces are assumed to have the same basic form as the surface for first yield. However, because the action deformation relationships may be of different shape for each action, the surfaces for the first and subsequent subhinges will not have, in general, identical actual shapes.

Plastic Stiffness and Torque

The hinge yield strengths and the plastic stiffnesses of the hinge action-deformation relationships (K_{p1}, K_{p2} and K_{p3} in Figure 5.4-5) must

be specified to provide appropriate post-yield stiffening of the complete element. The procedure is straightforward for axial force and torque but more complex for bending.

Consider axial force, and let the force-extension relationship for the complete element be as shown in Figure 5.4-8(b). The steps are as follows:

a. Elastic axial rigidity of beam = EA = $K_{F1} \cdot L$.

b. Strength at first yield surface = F_{y1}.

c. Plastic stiffness after first yield surface =

$$K_{p1} = \frac{K_{F1} \cdot K_{F2}}{K_{F1} - K_{F2}}$$

d. Strength at yield surface i = F_{yi}.

e. Plastic stiffness after yield surface i =

$$K_{pi} = \frac{K_{Fi} \cdot K_{F(i+1)}}{K_{F1} - K_{F(i+1)}}$$

The same procedure applies for the torque, M_X, as follows (Figure 5.4-8(d).

a. Elastic torsional rigidity of beam = GJ = $K_{T1} \cdot L$.

b. Strength at first yield surface = T_{y1}.

c. Plastic stiffness after first yield surface =

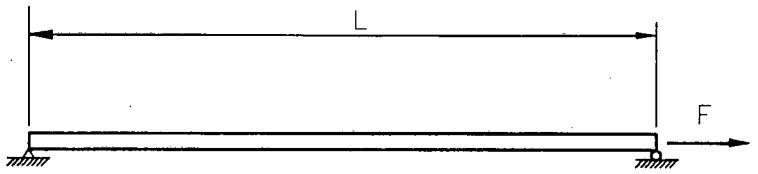

(a) Beam Under Axial Force

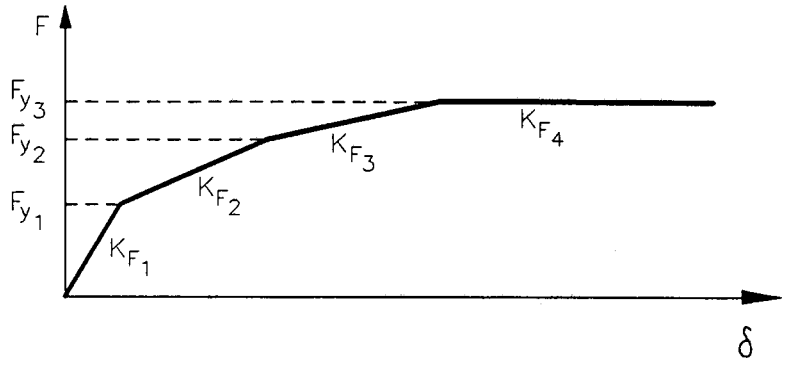

(b) F-δ Relationship

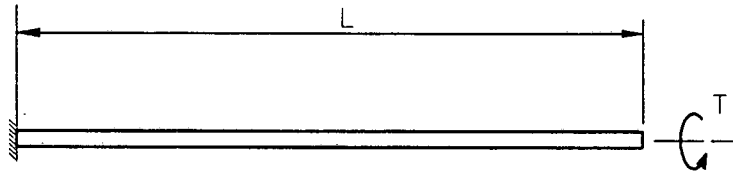

(c) Beam Under Torque

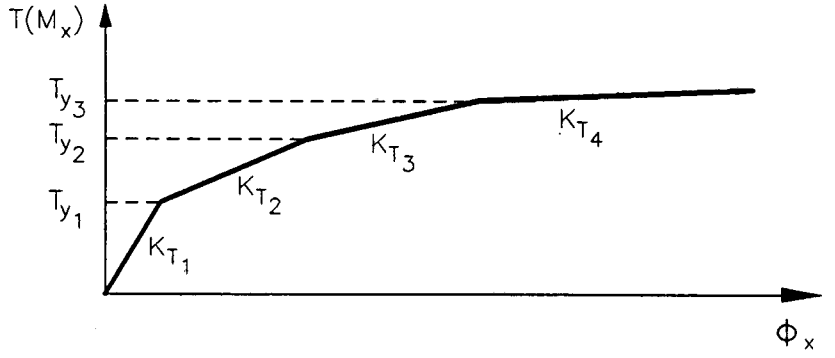

(d) M_x-Φ_x Relationship

FIG. 5.4-8 FORCE-EXTENSION AND TORQUE-TWIST

$$K_{p1} = \frac{K_{T1} \cdot K_{T2}}{K_{T1} - K_{T2}}$$

d. Strength at yield surface i = T_{yi}.

e. Plastic stiffness after yield surface i =

$$K_{pi} = \frac{K_{Ti} \cdot K_{T(i+1)}}{K_{T1} - K_{T(i+1)}}$$

Plastic Stiffnesses: Bending

A complication in specifying the flexural plastic stiffnesses arises from the fact that moment-curvature nonlinearities are modeled using concentrated hinges. In an actual beam, the moment typically varies along the length, and plastic deformations occur over finite regions. Consequently, the flexural stiffness depends on the moment variation along the beam. In a concentrated hinge model, it is not possible to account for all possible moment variations; and hence, assumptions must be made in specifying the hinge properties.

Three options are available in the computer program for assigning bending stiffness properties to the hinges. The first option is for a uniform beam with essentially constant moment along the element (Figure 5.4-9(a). This option is applicable, in general, only for a structure which is modeled using short beam-column elements, such that the bending moment does not vary greatly over a single element. The relationships between bending moment and end rotation for the initial loading of the element is as shown in Figure 5.4-9(b). The steps in establishing the hinge properties are as follows:

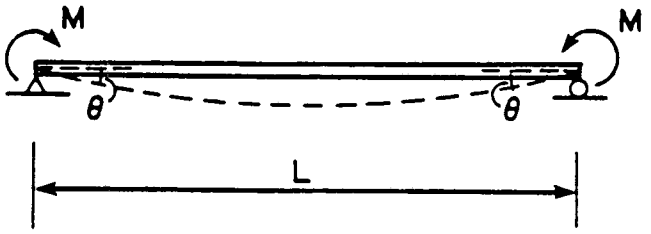

(a) BEAM WITH CONSTANT MOMENT

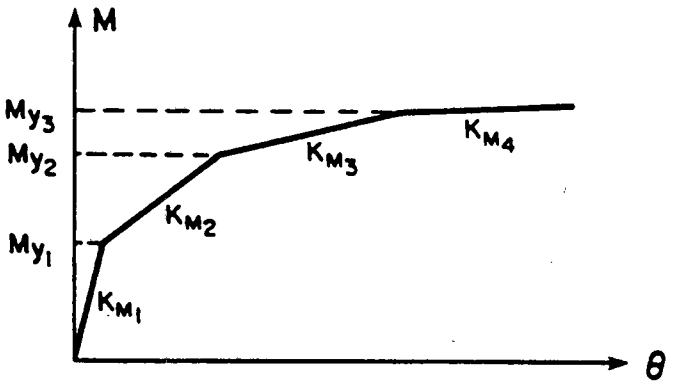

(b) MOMENT-ROTATION RELATIONSHIP

FIG. 5.4-9 MOMENT–ROTATION RELATIONSHIP

a. Elastic flexural rigidity of beam = EI = $K_{M1} \cdot L/2$.

b. Shear rigidity of beam assumed to be infinite (no shear deformations).

c. Hinge strength at first yield = M_{y1}.

d. Plastic stiffness after first yield surface =

$$K_{p1} = \frac{K_{M1} \cdot K_{M2}}{K_{M1} - K_{M2}}$$

e. Strength at yield surface i = M_{yi}.

f. Plastic stiffness after yield surface i =

$$K_{pi} = \frac{K_{Mi} \cdot K_{M(i+1)}}{K_{M1} - K_{M(i+1)}}$$

The second option is applicable for a uniform beam in which a linear variation of bending moment can be assumed over the element length, with equal and opposite values at the ends (Figure 5.4-10). This option will typically apply for columns in an unbraced frame building. An equivalent cantilever for each half of the element is used, as shown in Figure 5.4-10(b). It is required that the relationships between the tip load and tip displacement of the cantilever be known (Figure 5.4-10(c). This relationship can then be used to obtain hinge stiffness as follows:

a. Elastic flexural rigidity of beam = EI = $K_1 L^3/24$.

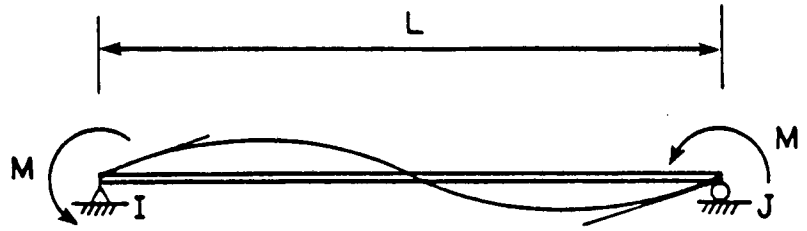

(a) BEAM WITH END MOMENTS

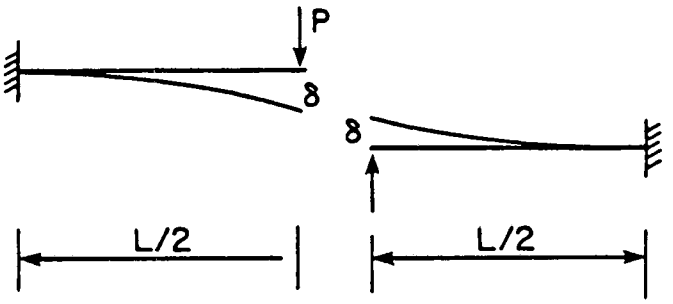

(b) EQUIVALENT CANTILEVERS

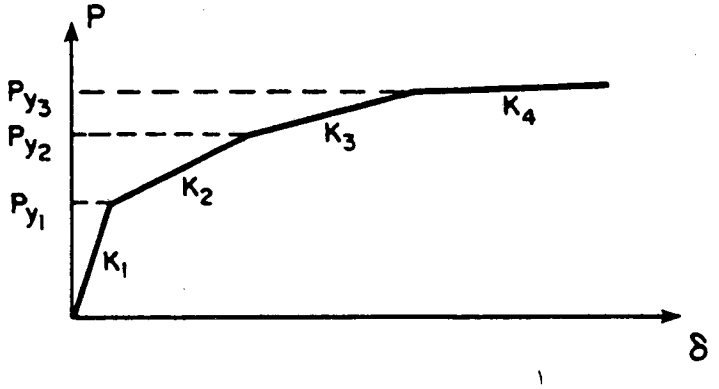

(c) P-δ RELATIONSHIP

FIG. 5.4-10 REPRESENTATION OF CANTILEVER BEHAVIOR

b. Shear rigidity of beam assumed to be infinite (no shear deformations).

c. Hinge strength at first yield = $P_{y1} \cdot L/2$.

d. Plastic stiffness after first yield surface =

$$K_{p1} = \frac{K_1 \cdot K_2 \cdot L}{2(K_1 - K_2)}$$

e. Strength at yield surface i = $P_{y1} \cdot L/2$.

f. Plastic stiffness after first yield surface i =

$$K_{p1} = \frac{K_i \cdot K_{i+1} \cdot L}{2(K_i - K_{i+1})}$$

For these first two options, the computer program calculates the K_p values, given the moment-rotation relationships (for Option 1) or load-deflection relationship (for Option 2). The third option provides the user with more flexibility by requiring that the EI/L and K_p values be specified directly. In addition, with this option it is not necessary for the element to be of uniform section. Flexural stiffness coefficients K_{ii}, K_{jj} and K_{ij}, which depend on the variation of the beam cross section, may be specified (for example, for a uniform element, $K_{ii} - K_{jj} = 4.0$ and $K_{ij} = 2.0$). Also, an effective shear stiffness (GA_s) can be specified.

Plastic Flow

Interaction among the actions is considered as shown diagrammatically in Figure 5.4-11. Yield begins when the yield surface of the first subhinge is reached. The surface then translates in action space, the motion being governed by the plastic flow of the first subhinge. Translation of the first surface continues until the second surface is reached. Both surfaces then translate together, governed by a combination of plastic flow on both yield subhinges. For any subhinge, plastic flow is assumed to take place normal to the yield surface of that subhinge. If two or more subhinges are yielded, their yield surfaces move together, and the total plastic deformation is equal to the sum of the individual plastic deformations for each subhinge, directed along the normal directions of their respective yield surfaces at the action point. After some arbitrary amount of plastic deformation, the situation might be as illustrated in Figure 5.4-11(b).

On unloading, the elastic stiffness values, K_1, govern until the yield surface of the first subhinge is again reached. The surface then translates as before.

Hardening Behavior

After first yield, the yield surfaces of the yielded subhinges are assumed to translate in action space, obeying a kinematic hardening rule (translation without change of shape or size). An extension of the Mroz theory of material plasticity is used to define the hardening behavior. Because the yield surfaces of the yielded subhinges are generally not exactly similar, overlapping of the surfaces can occur. As a result, the hardening behavior is more complex than in the basic Mroz theory. For

example, in Figure 5.4-11(b), the current action point, A, lies on yield surfaces YS_1, YS_2 and YS_3. Hence, all three subhinges have yielded, and the direction of plastic flow is a combination of the normal vectors $\underline{n}_1$, $\underline{n}_2$ and $\underline{n}_3$. Details of the theory are given by Chen (1982).

5.4.6 End Eccentricity

Plastic hinges in frames and coupled frame-shear wall structures will form near the faces of the joints rather than at the theoretical joint centerlines. This effect can be approximated by postulating rigid, infinitely strong connecting links between the nodes and the element ends, as shown in Figure 5.4-12.

5.4.7 Initial Forces

For structures in which static analyses are carried out separately, initial member forces may be specified. The sign convention for these forces is as shown in Figure 5.4-13. These forces are not converted to loads on the nodes of the structure, but are simply used to initialize the element end actions. For this reason, initial forces need not constitute a set of actions in equilibrium. The only effects they have on the behavior of the system are (a) to influence the onset of plasticity and (b) to affect the geometric stiffnesses.

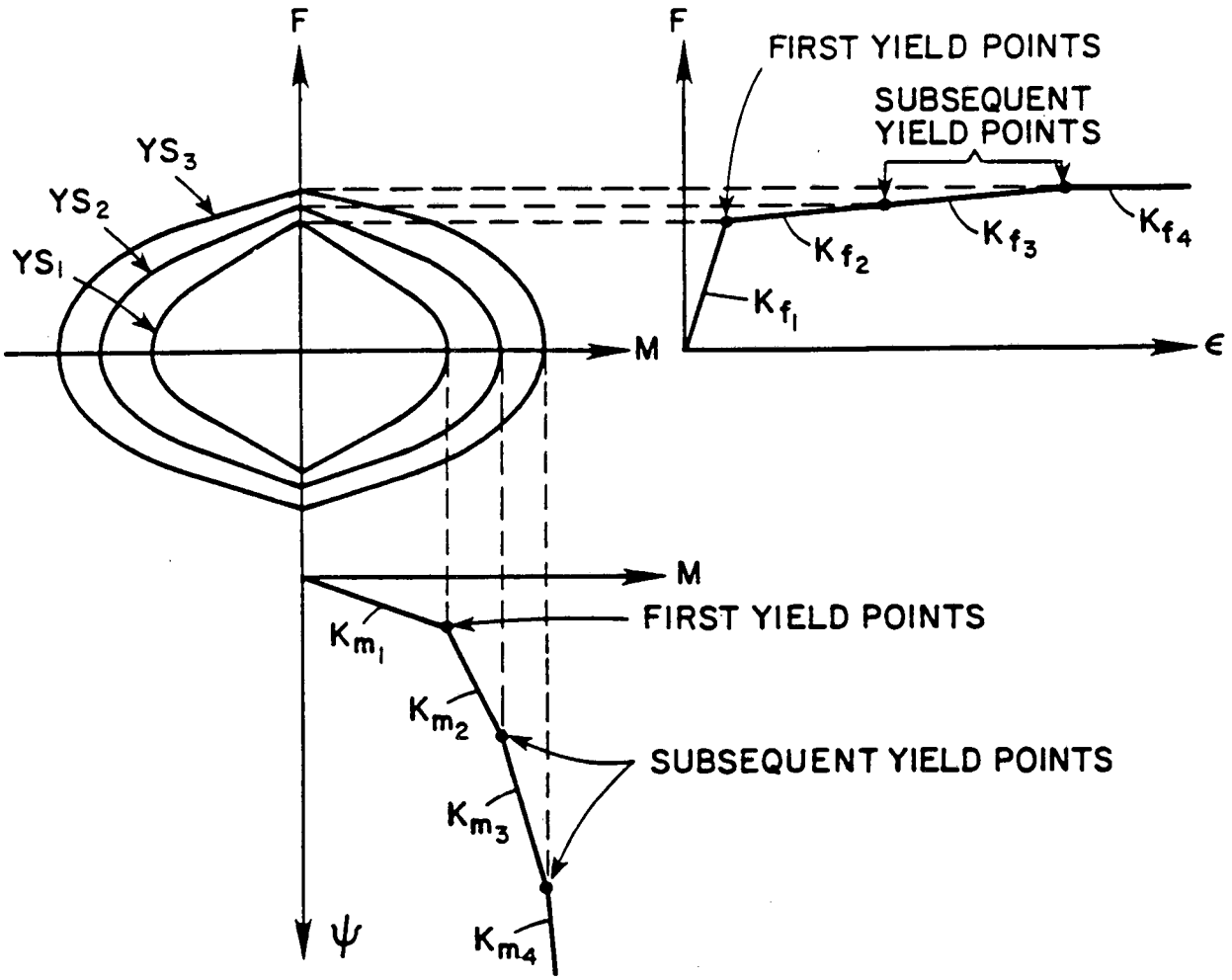

(a) INITIAL LOCATIONS OF SURFACES

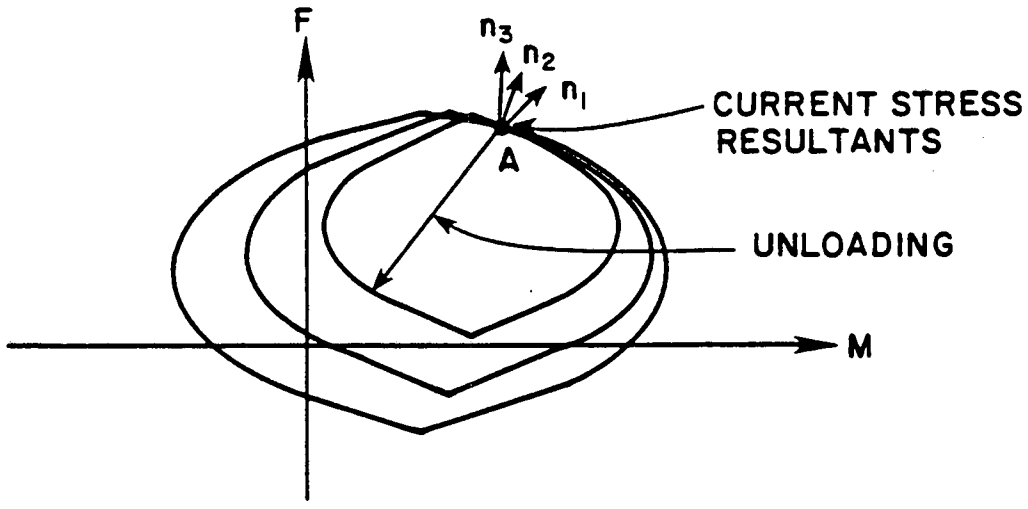

(b) DISPLACED SURFACES AFTER HARDENING

FIG. 5.4-11 STRAIN HARDENING BEHAVIOR

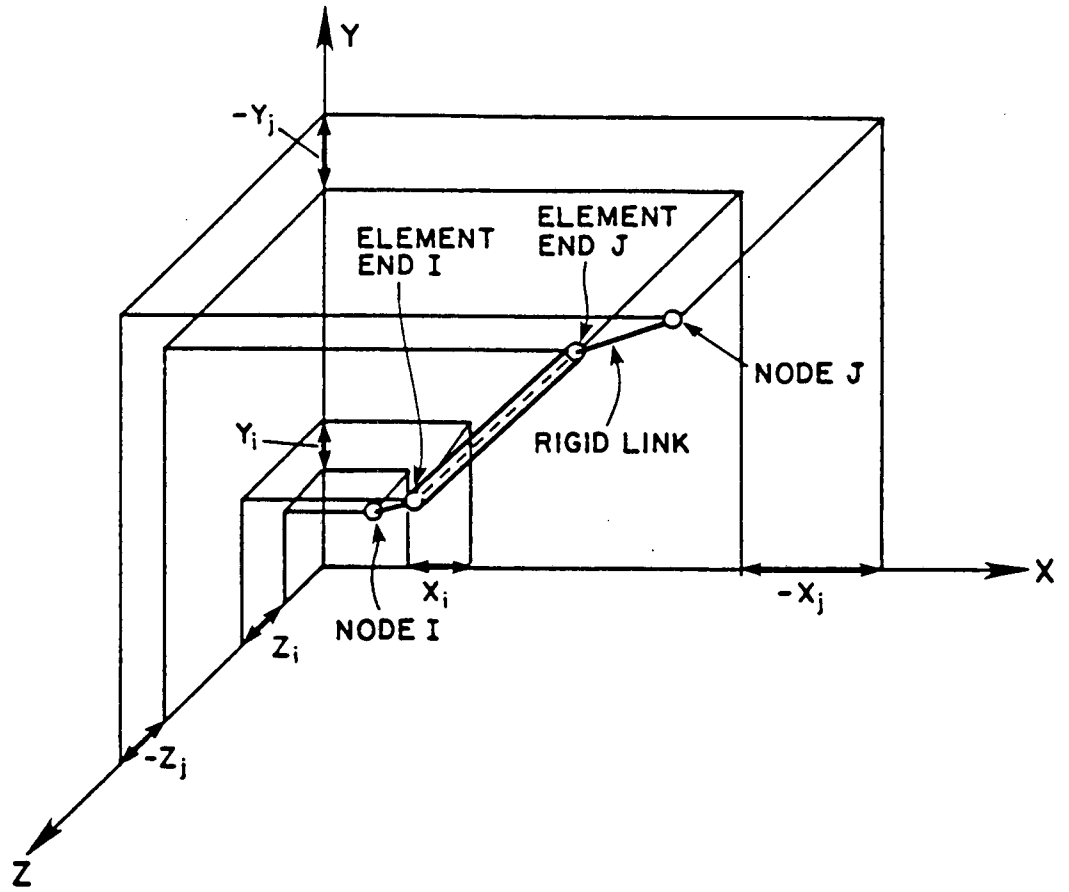

FIG. 5.4-12 END ECCENTRICITIES

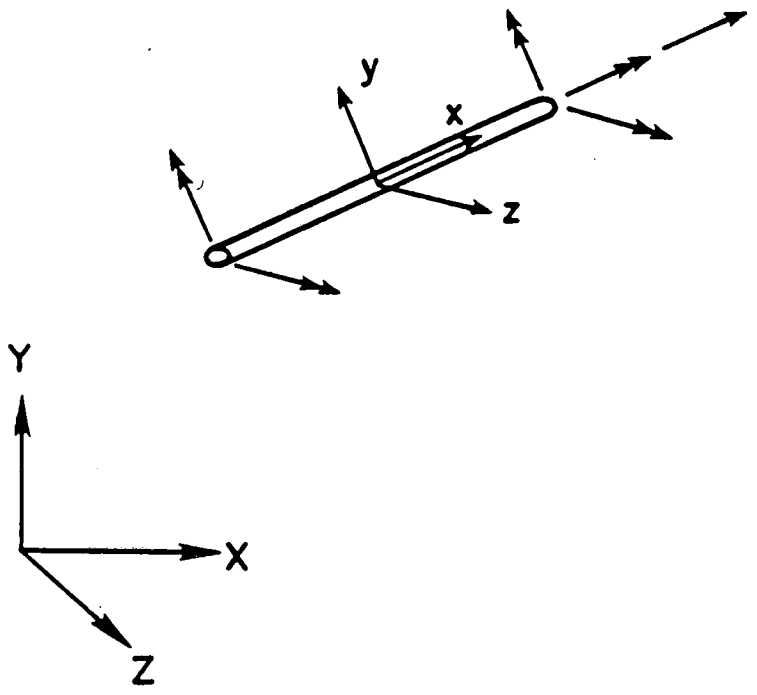

FIG. 5.4-13 POSITIVE DIRECTION OF INITIAL ELEMENT ACTIONS

5.5 Three-Dimensional Gap Friction (Support Element)

This element is designed to model contact problems. It can only sustain loads in compression, and has no stiffness in tension. Also, it models friction caused by the normal reaction on the element. The limiting frictional force is directly proportional to the value of normal reaction.

5.5.1 Applications

The element is capable of modeling contact problems such as the support of flowlines on the seafloor. The inelastic nonlinear spring in compression allows better modeling of nonlinear soils supporting the flowlines. An initial gap allows modeling of an uneven seafloor for unsupported sections of the flowlines.

5.5.2 Element Features

The element has the following features:

1. Arbitrary orientation of the bearing plane in 3-D space.

2. Zero stiffness perpendicular and tangential to the bearing plane when the gap is open.

3. Trilinear inelastic force-deformation relationship for deformation perpendicular to the bearing plane following gap closure.

4. Frictional behavior tangential to the bearing plane when the gap is closed, with constant friction coefficient.

5. Linear rotational springs in the global coordinate systems.

5.5.3 Element Properties

The element resists deformation normal and tangential to a specified bearing plane. The bearing plane may be arbitrarily oriented in space.

The element consists of three components, namely (a) a bearing component, acting normal to the bearing plane, (b) a friction component, acting parallel to the bearing plane, and (c) a rotational component providing rotational stiffness in the global directions uncoupled with the direction of the bearing plane.

The element is connected to the structure at node N (as shown in Figure 5.5-1). The bearing plane is defined by three nodes, I, N and J, as shown. The normal component is oriented along the local z-axis, normal to the bearing plane. The local x-axis lies in the bearing plane, direction from node J to node N. The local y-axis, also in the bearing plane, is perpendicular to the z-x plane.

The force deformation relationships of the normal component is shown in Figure 5.5-2. The stiffness in tension is zero. The element stiffness after the closure of the gap is modeled by a trilinear inelastic force-deformation relationship. If the element yields in compression upon unloading, the element unloads with the initial stiffness. The size of the initial gap is increased for further reloading.

The force-deformation relationship of the tangential component is as shown in Figure 5.5-3. For a force less than that required to cause slip, the behavior is elastic with stiffness K_f. When the force equals the slip value (normal component force multiplied by the friction

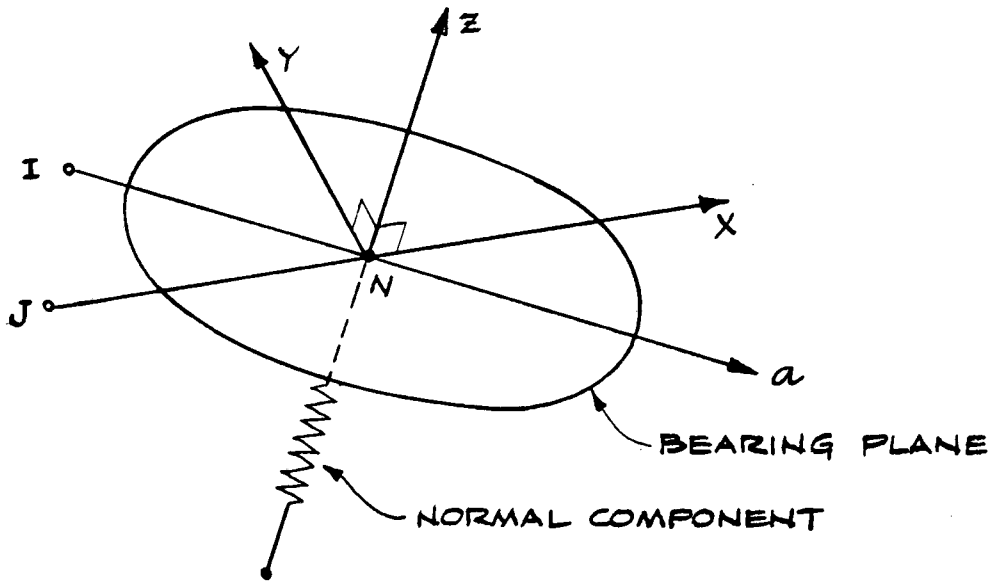

FIG. 5.5-1 ORIENTATION OF SUPPORT ELEMENT

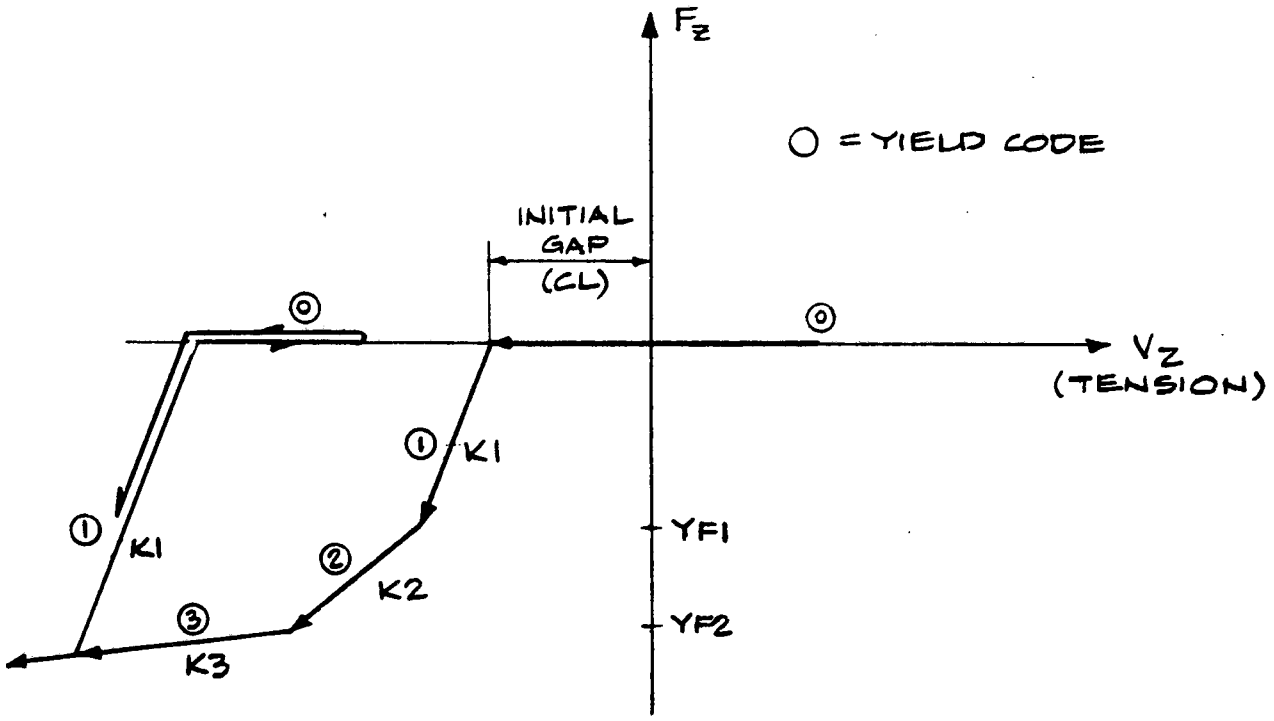

FIG. 5.5-2 FORCE-DEFORMATION BEHAVIOR OF NORMAL COMPONENT

coefficient), slip takes place. If the force in the normal component is zero (i.e., open gap) both the normal and tangential components have zero stiffnesses.

5.5.4 Element Stiffness

The element has three local deformations, namely (a) deformation v_z, along the local z-axis of the normal component; and (b) deformations v_x and v_y along the local x and y axes, respectively, of the tangential component. The increments in element deformations are related to the increments in nodal displacements, referenced to the global coordinates as follows (Figure 5.5-4):

$$d\underline{v} = \underline{T}\ d\underline{q} \qquad (5.5-1)$$

in which

$$\underline{v}^T = (v_x, v_y, v_z) \qquad (5.5-2)$$

$$\underline{q}^T = (q_x\ q_y\ q_z) \qquad (5.5-3)$$

The transformation matrix $\underline{T}$ contains the direction cosines of the local x-y-z axes with respect to the global X-Y-Z axes.

The tangent force-deformation relationship for the normal component is

$$dF_z = K_z\ dv_z \qquad (5.5-4)$$

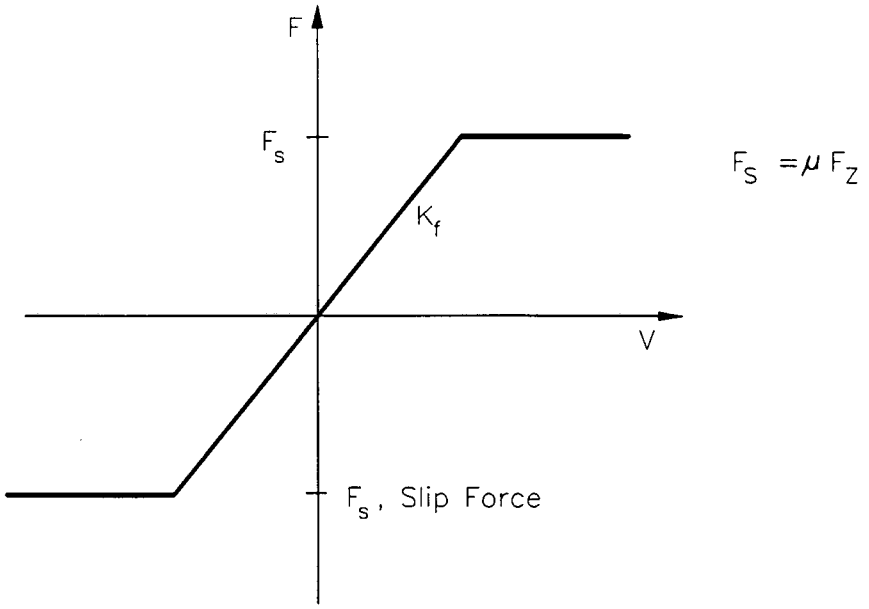

FIG. 5.5-3 FORCE-DEFORMATION BEHAVIOR OF TANGENTIAL COMPONENT

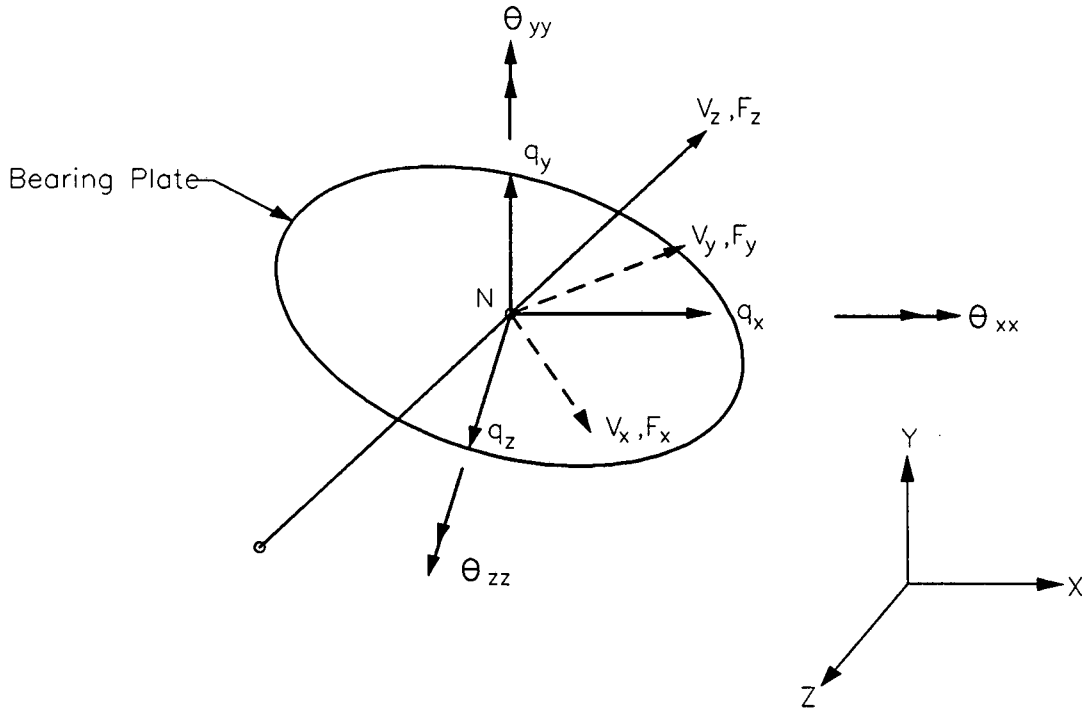

FIG. 5.5-4 DEFORMATIONS AND DISPLACEMENTS

in which dF_Z is the increment in force, and K_Z is the tangent stiffness of the normal component. The tangent stiffness, K_Z, may be equal to zero, K1, K2 or K3, depending on the state of the normal component (Figure 5.5-2).

The force states required to produce slip of the tangential component are defined by a "slip circle" in the bearing plane (Figure 5.5-5). The radius, F_X, of the circle is equal to the normal component force multiplied by the friction coefficient.

If the local x and y forces, F_X and F_Y, of the tangential component are such that $\sqrt{(F_x)^2 + (F_y)^2}$ is less than F_S, the behavior of the tangential component is elastic. The tangent stiffness of this component is then given by

$$\begin{bmatrix} dF_x \\ dF_y \end{bmatrix} = \begin{bmatrix} K_f & 0 \\ 0 & K_f \end{bmatrix} \begin{bmatrix} dv_x \\ dv_y \end{bmatrix} \qquad (5.5-5)$$

This tangent stiffness assumes two springs, each with stiffness K_f, along the local x and y axis in the bearing plane (Figure 5.5-5(a)).

If the forces F_X and F_Y are such that $\sqrt{(F_x)^2 + (F_y)^2}$ is equal to F_S, the tangential component is assumed to be slipping along the radial direction of the slip circle (Figure 5.5-5(b)). The tangent stiffness of the component is then given by

$$\begin{bmatrix} dF_r \\ dF_t \end{bmatrix} = \begin{bmatrix} 0 & 0 \\ 0 & K_f \end{bmatrix} \begin{bmatrix} dv_r \\ dv_t \end{bmatrix} \qquad (5.5-6)$$

in which r and t are the radial and tangential directions, respectively, at the point on the clip circle (Figure 5.5-5(b)). This tangent stiffness assumes a spring with stiffness K_f along the tangent to the slip circle. The tangent stiffness in the local x and y axes is thus given by

$$\begin{bmatrix} dF_x \\ dF_y \end{bmatrix} = K_f \begin{bmatrix} \sin^2\alpha' & -\sin\alpha'\cos\alpha' \\ -\sin\alpha'\cos\alpha' & \cos^2\alpha' \end{bmatrix} \begin{bmatrix} dv_x \\ dv_y \end{bmatrix} \tag{5.5-6}$$

$$= \begin{bmatrix} K_{xx} & K_{xy} \\ K_{xy} & K_{yy} \end{bmatrix} \begin{bmatrix} dv_x \\ dv_y \end{bmatrix}$$

in which $\cos\alpha' = F_x/F_s$; and $\sin\alpha' = F_y/F_s$.

The tangent stiffness matrix of the complete element, K_{xyz}, is obtained by combining Eqs. (5.5-4) and (5.5-5) or Eqs. (5.5-4) and (5.5-7), giving

$$\underline{k}_T = \begin{bmatrix} K_f & 0 & 0 \\ 0 & K_f & 0 \\ 0 & 0 & K_z \end{bmatrix}$$

or

(5.5-8)

$$\underline{k}_T = \begin{bmatrix} K_{xx} & K_{xy} & 0 \\ K_{xy} & K_{yy} & 0 \\ 0 & 0 & K_z \end{bmatrix}$$

The tangent stiffness matrix in the global coordinates axes is then given by

$$\underline{\hat{k}}_T = \underline{T}^T \ \underline{k}_T \ \underline{T} \qquad (5.5-9)$$

In addition, three uncoupled global rotational springs are added to the element stiffness. The global rotational springs are user defined. The complete element stiffness is given by

$$\underline{\hat{k}}_T = \begin{bmatrix} \underline{T}^T \ \underline{k}_T \ \underline{T} & & 0 \\ & k_{xx} & \\ 0 & & k_{yy} \\ & & & k_{zz} \end{bmatrix}$$

in which k_{xx}, k_{yy} and k_{zz} are rotational springs in the three global directions.

5.5.5 State Determination

Increments of element deformation are computed using Eq. 5.5-1. The force increment in the normal component is then obtained by following the force-deformation relationship shown in Figure 5.5-2. The computation of force increments for the tangential component is more complex, because during any load or time step the state of force can change in many ways, and because the slip circle may change in size.

As an example, consider Figure 5.5-6. At the beginning of the step, let the tangential force be at point A, within the slip circle, so that the

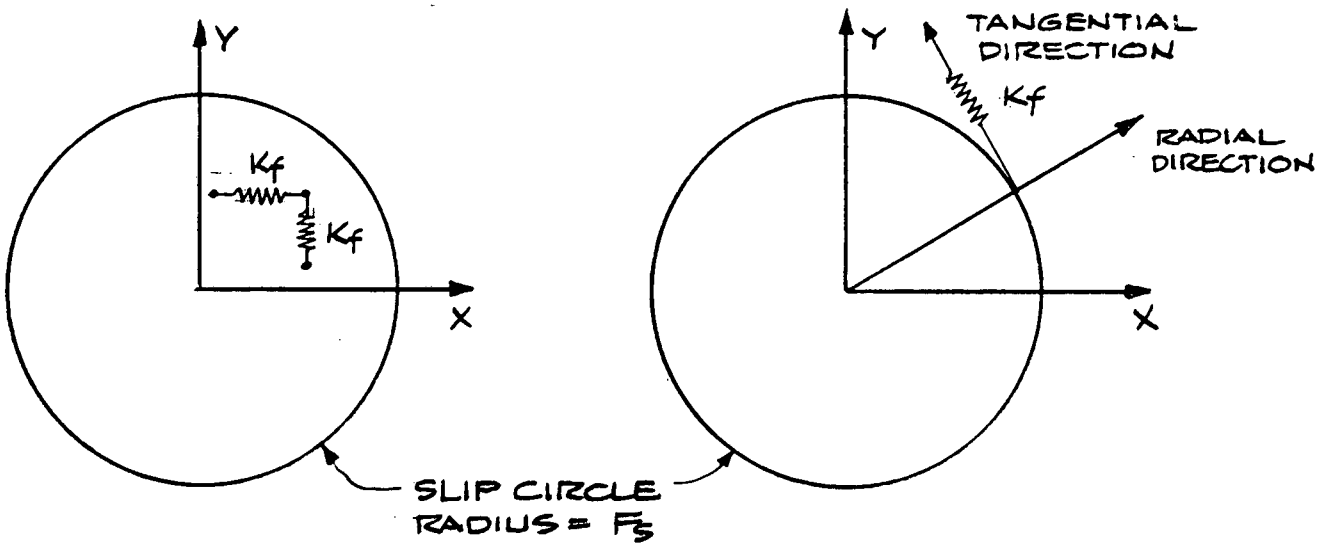

(a) ELASTIC (b) SLIPPING

FIG. 5.5-5 STIFFNESS OF TANGENTIAL COMPONENT

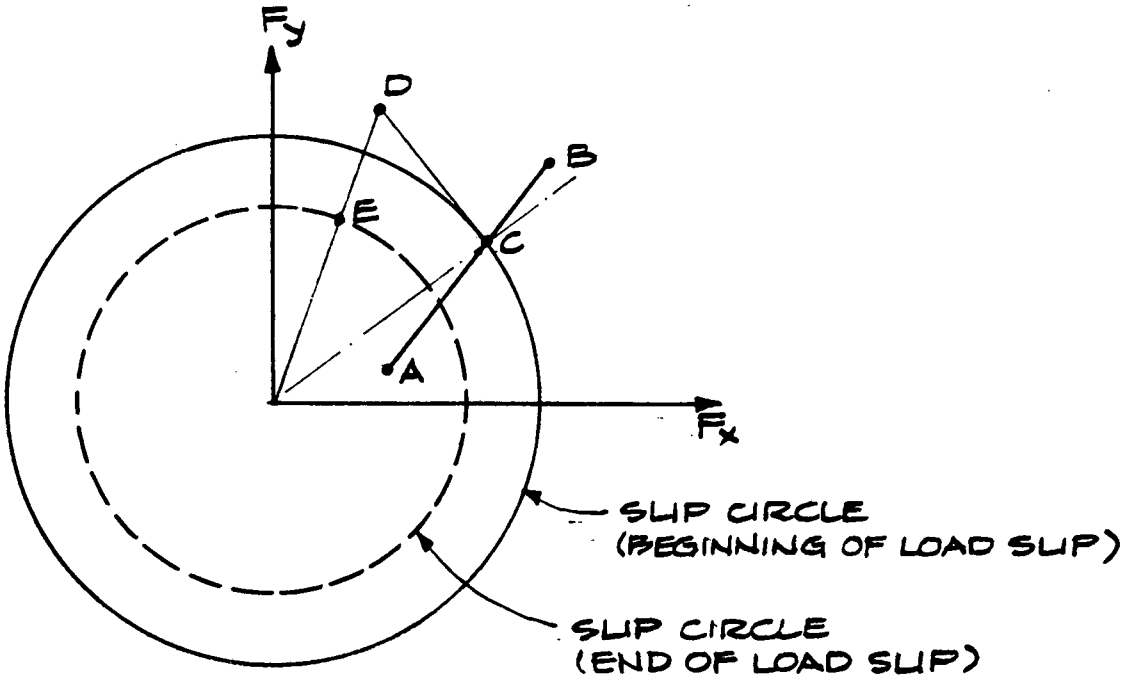

FIG. 5.5-6 STATE DETERMINATION EXAMPLE

state is elastic. The radius of the slip circle is equal to the normal force at the beginning of the step multiplied by the friction coefficient. Assuming linear behavior within the step, let the tangential force at the end of the step be at point B. This point is outside the slip circle, which is incorrect. If the tangential deformations are assumed to increase proportionately, and if the slip circle is assumed not to change, point C on path AB can be found such that the tangential force state lies on the slip circle. For the remainder of the deformation increment, slip occurs, with zero restraint along the radial direction at any time. The tangential force increment for this remainder of the deformation increment is computed using Eq. (5.5-7). In general, the coefficients in Eq. 5.5-7 will not be constant throughout the step. In the computer program, however, constant coefficients are assumed, and a force state at D is found. This point lies outside the circle. Further, in computing the forces at point D, it has been assumed that the slip circle does not change during the step, which is not generally correct. The slip circle corresponding to the normal force at the end of the step might, for example be as shown in Figure 5.5-6. The fores at point D must be corrected to correspond to the new slip circle. If the force state at D is within the new slip circle, the forces are left unchanged, and the new state is set to be elastic. If the force state is outside the new slip circle, the forces are scaled radially, as shown, to give point E on the slip circle, and the new state is set to be slipping.

If large deformations occur within a single load or time step, this procedure may be inaccurate, and may lead to large unbalanced loads.

5.5.6 Angle Tolerance for Stiffness Reformulation

If slip continues to occur in the tangential component over several load steps, the element stiffness will generally change continuously, because angle α' (Figure 5.5-7) and Eq. (5.5-7) will generally change. If the change in α' is small, the change in stiffness can be ignored, and computer costs for reforming the stiffness can be saved. In the computer program, an option is provided for the user to specify a tolerance for the angle α'. If a nonzero tolerance is specified, the element stiffness is reformed only when the change in state is such that the angle between the current state and that at which the stiffness was last reformed exceeds the tolerance.

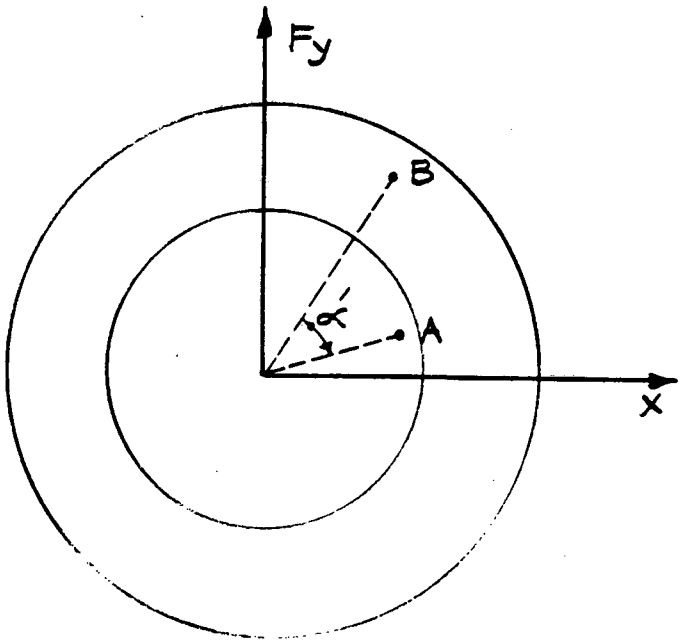

FIG. 5.5-7 STIFFNESS REFORMULATION ANGLE

5.6 Linear 4 to 8 Node Quadrilateral Element

The element may lie in any of the three global planes, except for the axisymmetric solid element which must lie in the XY plane with the global Y axis as the axis of revolution.

Each element can have from four to eight nodes. The element maps into a rectangular element in a local r-s coordinate system, such that nodes 1 through 4 are located at the four corners and nodes 5 through 8 are located at the midsides of the rectangle (Figure 5.6-1). The four corner nodes must always be specified, and any one or more of the midside nodes may be specified.

Three different types of behavior may be specified, namely plane stress, plane strain, and axisymmetric solid behavior. In the plane strain formulation it is assumed that the element has unit thickness, whereas in the axisymmetric formulation a unit radian segment ($\theta = 1$) is considered. The applied nodal loads for plane strain and axisymmetric structures must be computed accordingly. In the plane stress formulation, each element may be assigned an average thickness.

The element matrices (stiffness, resisting nodal loads, etc.) are computed using Gauss quadrature integration. The integration orders (numbers of integration points) in the local r-direction and s-directions may be specified separately. Any integration order up to 4 may be specified in either direction; however, 2x2 integration is recommended for most cases.

Large displacement effects may be included or ignored. If large displacements are considered, a total Lagrangian formulation is used.

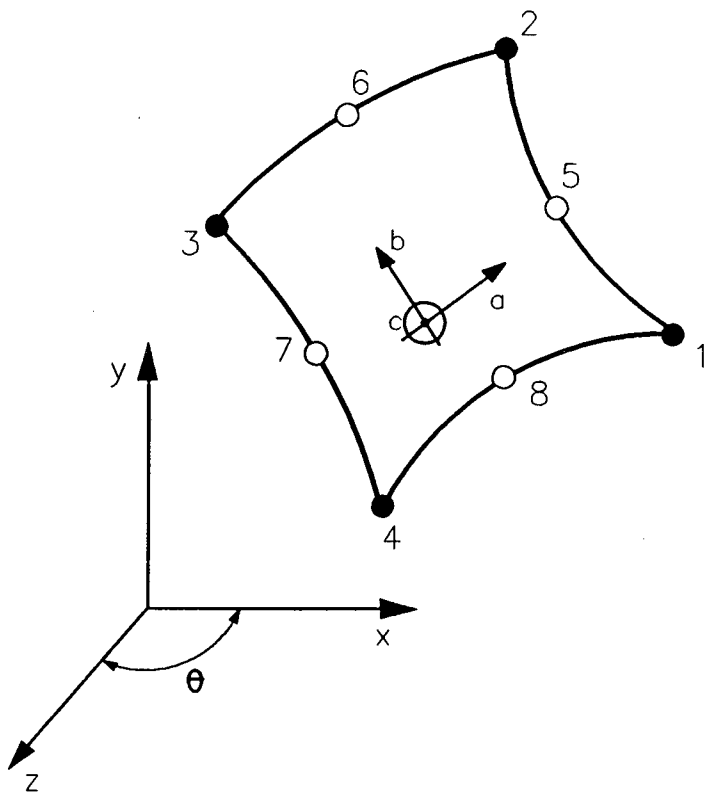

(a) 2D Element in Global x-y-z System

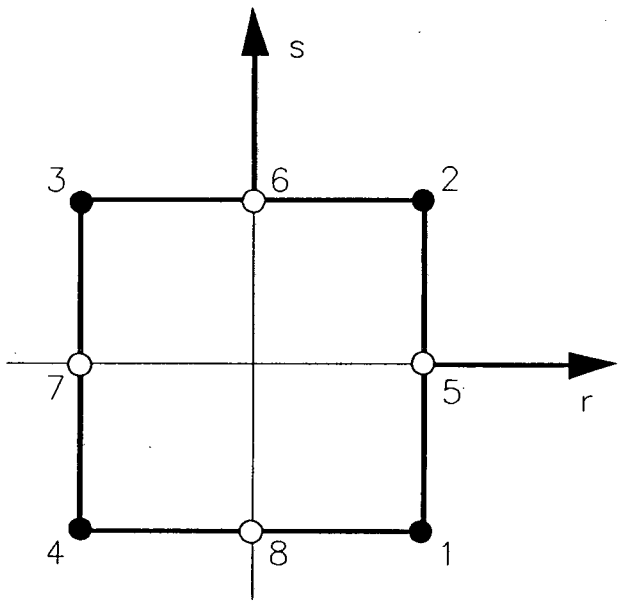

(b) 2D Element in Local r-s System

FIG. 5.6-1 TWO-DIMENSIONAL QUADRILATERAL FINITE ELEMENT

5.6.1 Element Features

The element has the following features:

1. Two-dimensional orientation in any of the three global planes except the axisymmetric solid element which must lie in the XY plane.

2. Plane stress, plane strain or axisymmetric behavior.

3. Isoparametric quadrilateral element with variable number of nodes (from 4 to 8).

4. Variable Gauss integration order (from 2 to 4 points).

5. For dynamic analysis, damping proportional to initial elastic stiffness and/or current tangent stiffness.

6. Isotropic, linearly elastic material.

5.6.2 Element Stiffness

The strain-displacement relationships and element stiffness matrices are developed as the structure deforms from a known state (configuration 1, time t) to a neighboring state (configuration 2, time $t + \delta t$). All strain and stress quantities in the deformed configuration are referred to the undeformed state (configuration 0, time = 0).

Shape Functions

The X and Y displacements at any point within the element in the current deformed state (state 1) u_x^1 and u_y^1 are related to the nodal displacements, 1_q, as follows:

$$\begin{Bmatrix} u_x^1 \\ u_y^1 \end{Bmatrix} = \begin{bmatrix} \underline{N} & 0 \\ 0 & \underline{N} \end{bmatrix} \begin{Bmatrix} \underline{q}_x^1 \\ \underline{q}_y^1 \end{Bmatrix} \qquad (5.6-1)$$

or

$$\underline{u}^1 = \underline{N}^* \ \underline{q}^1$$

where $\underline{N}$ is the vector of shape functions and $\underline{N}^*$ is the shape function matrix. Similarly, displacement increments are related to the nodal displacement increments as

$$\Delta \underline{u} = \underline{N}^* \ \Delta \underline{q}$$

For an 8-node isoparametric element (Figure 5.6-1), the shape functions can be written as follows:

1. For corner nodes (m = 1 to 4; $r_m = \pm 1$ and $S_m = \pm 1$)

$$N^m(r,s) = \frac{1}{4}(1 + rr_m)(1 + ss_m) - \frac{1}{4}(1 + rr_m)(1 - s^2) - \frac{1}{4}(1 - r^2)(1 + ss_m) \qquad (5.6-2)$$

2. For midside nodes (m = 5 to 8)

$$N^m(r,s) = \frac{1}{2}(1 + rr_m)\ (1 - s^2), \qquad s_m = 0 \qquad (5.6-3)$$

$$N^m(r,s) = \frac{1}{2}(1 - r_m^2)\ (1 + ss_m), \qquad r_m = 0 \qquad (5.6-4)$$

For a variable (4 to 8) node element, the shape functions for the midside nodes are included only for those nodes which are present. For the corner nodes, terms involving $(1 - s^2)$ and $(1 - r^2)$ in Eq. 5.6-2 are included only if corresponding midside node(s) are present (e.g., if only node 5 is present, the shape functions for nodes 1 and 2 will have only the corresponding terms included).

In subsequent relationships, derivatives of shape functions with respect to the global X and Y axes will be needed. These derivatives are obtained by the usual Jacobian transformation.

Strain-Displacement Transformation

The total strain increment, $\underline{\epsilon}$, is decomposed into linear and nonlinear components, e and η, respectively. That is

$$\begin{Bmatrix} \epsilon_{xx} \\ \epsilon_{yy} \\ 2\epsilon_{xy} \\ \epsilon_{zz} \end{Bmatrix} = \begin{Bmatrix} e_{xx} \\ e_{yy} \\ 2e_{xy} \\ e_{zz} \end{Bmatrix} + \begin{Bmatrix} \eta_{xx} \\ \eta_{yy} \\ 2\eta_{xy} \\ \eta_{zz} \end{Bmatrix} \qquad (5.6-4)$$

or

$$\underline{\epsilon} = \underline{e} + \underline{\eta}$$

For plane stress (strain) behavior, terms involving stress S_{zz} (strain ϵ_{zz}) are neglected, and appropriate modifications are made to the stress-strain relationship.

The linear component is related to the nodal displacement increments through the following relationship:

$$\underline{e} = \underline{F}^1 \ \underline{u}_\partial \tag{5.6-5}$$

and

$$\underline{u}_\partial = \underline{N}_\partial \ \Delta\underline{q} \tag{5.6-6}$$

where

$$\underline{F}^1 = \begin{bmatrix} \left(1 + \frac{\partial u_x^1}{\partial x}\right) & 0 & \frac{\partial u_y^1}{\partial x} & 0 & 0 \\ 0 & \frac{\partial u_y^1}{\partial y} & 0 & \left(1 + \frac{\partial u_y^1}{\partial y}\right) & 0 \\ \frac{\partial u_y^1}{\partial y} & \left(1 + \frac{\partial u_x^1}{\partial x}\right) & \left(1 + \frac{\partial u_y^1}{\partial y}\right) & \frac{\partial u_y^1}{\partial x} & 0 \\ 0 & 0 & 0 & 0 & \left(1 + \frac{\partial u_x^1}{\partial x}\right) \end{bmatrix} \tag{5.6-7}$$

$$\{u_\partial\}^T = < \frac{\partial (\Delta u_x)}{\partial x} \quad \frac{\partial (\Delta u_x)}{\partial y} \quad \frac{\partial (\Delta u_y)}{\partial y} \quad \frac{\partial (\Delta u_y)}{\partial y} \quad \frac{\Delta u_x}{x} > \tag{5.6-8}$$

and

$$[N_\partial] = \begin{bmatrix} \frac{\partial \underline{\underline{N}}}{\partial x} & 0 \\ \frac{\partial \underline{\underline{N}}}{\partial y} & 0 \\ 0 & \frac{\partial \underline{\underline{N}}}{\partial x} \\ 0 & \frac{\partial \underline{\underline{N}}}{\partial y} \\ \frac{\underline{\underline{N}}}{x} & 0 \end{bmatrix} \tag{5.6-9}$$

From a combination of Eqs. 5.6-5 and 5.6-6, the following strain-displacement relationship is obtained

$$\underline{e} = \underline{F}^1 \; \underline{\underline{N}}_\partial \; \Delta \underline{q}$$

$$\underline{e} = \underline{B}^1 \; \underline{q} \tag{5.6-10}$$

Element Stiffness Matrix

The element stiffness matrix is given by

$$\underline{k}_o = \int_{V_o} \underline{B}^1 \; \overline{\underline{C}} \; \underline{B}^1 \; dV \qquad (5.6-11)$$

in which $\overline{\underline{C}}$ is the constitutive matrix, and integration is carried out over the volume V_0 of the element in the undeformed state.

The integration in Eq. (5.6-11) is carried out numerically using Gauss quadrature.

Geometric Stiffness Matrix

The nonlinear component of the strain increment is given by

$$\eta_{xx} = \frac{1}{2}\left[\left(\frac{\partial(\Delta u_x)}{\partial x}\right)^2 + \left(\frac{\partial(\Delta u_y)}{\partial x}\right)^2\right]$$

$$\eta_{yy} = \frac{1}{2}\left[\left(\frac{\partial(\Delta u_x)}{\partial y}\right)^2 + \left(\frac{\partial(\Delta u_y)}{\partial x}\right)^2\right] \qquad (5.6-12)$$

$$2\eta_{xy} = \left[\left(\frac{\partial(\Delta u_x)}{\partial x}\right)\left(\frac{\partial(\Delta u_x)}{\partial y}\right) + \left(\frac{\partial(\Delta u_y)}{\partial x}\right)\left(\frac{\partial(\Delta u_y)}{\partial y}\right)\right]$$

$$\eta_{zz} = \frac{1}{2}\left(\frac{\Delta u_x}{x}\right)^2$$

The element geometric stiffness $\underline{k}_G$ is obtained from the following virtual work equation.

$$\{\delta q\}^T [\underline{k}_g]\{q\} = \int_{V_o} (S^1_{xx}\delta\eta_{xx} + S^1_{yy}\delta\eta_{yy} + 2S^1_{xy}\delta\eta_{xy} + S^1_{zz}\delta\eta_{zz})dV \tag{5.6-13}$$

in which $\delta(\cdot)$ is a variation on the undesignated variable, and S^1_{xx}, S^1_{yy}, S^1_{xy}, and S^1_{zz} are stresses in the deformed state at time t. By combining Eqs. 5.6-12 and 5.6-13 and simplifying, it can be shown that

$$\underline{k}_g = \int_{V_o} \underline{N_\partial}^T \ \underline{S}^1 \ \underline{N_\partial} \ dV \tag{5.6-14}$$

in which the matrix $\underline{N_\partial}$ is given in Eq. 5.6-9 and the matrix $\underline{S}^1$ is as follows:

$$\underline{S}^1 = \begin{bmatrix} S^1_{xx} & S^1_{xy} & 0 & 0 & 0 \\ S^1_{xy} & S^1_{yy} & 0 & 0 & 0 \\ 0 & 0 & S^1_{xx} & S^1_{xy} & 0 \\ 0 & 0 & S^1_{xy} & S^1_{yy} & 0 \\ 0 & 0 & 0 & 0 & S^1_{zz} \end{bmatrix} \tag{5.6-15}$$

As for the element stiffness matrix, the integral in Eq. 5.6-14 is evaluated numerically using Gauss quadrature.

Equilibrium Nodal Loads

Nodal loads in equilibrium with the state of stress in the deformed state at time t are given by

$$\underline{R}_I^1 = \int_{V_o} (\underline{B}^1)^T \, \overline{\underline{S}}^1 \, dV \qquad (5.6-16)$$

in which $\overline{\underline{S}}^1 = \{S_{xx}^1 \; S_{yy}^1 \; S_{xy}^1 \; S_{zz}^1\}^T$; and the strain-displacement matrix $\underline{B}^1$ is given in Eq. 5.6-10. Again, the integral in Eq. 5.6-16 is evaluated numerically.

Material Models

The constitutive relationship between stress and strain can be written as

$$\begin{Bmatrix} S_{xx} \\ S_{yy} \\ S_{xy} \\ S_{zz} \end{Bmatrix} = \begin{bmatrix} C_{11} & C_{12} & C_{13} & C_{14} \\ & C_{22} & C_{23} & C_{24} \\ & & C_{33} & C_{34} \\ & \text{Symmetric} & & C_{44} \end{bmatrix} \begin{Bmatrix} \epsilon_{xx} \\ \epsilon_{yy} \\ 2\epsilon_{xy} \\ \epsilon_{zz} \end{Bmatrix} \qquad (5.6-17)$$

That is, $\underline{S} = \overline{\underline{C}} \, \underline{\epsilon}$.

It should be noted that for large displacements, the above relationship is assumed to be between the (second) Piola-Kirchhoff stress and Green-Lagrange strain. The (4x4) matrix given in Eq. 5.6-17 is for

axisymmetric behavior. To obtain the constitutive matrix for plane stress the matrix is condensed to a (3x3) matrix using the condition that stress $s_{zz} = 0$. For plane strain, $E_{zz} = 0$, and the last row and column are ignored.

The matrix coefficients in Eq. 5.6-17 are as follows:

$$C_{11} = C_{22} = C_{44} = 2\bar{\mu} + \bar{\lambda}$$

$$C_{12} = C_{14} = C_{24} = \bar{\lambda}$$

$$C_{33} = \bar{\mu} \qquad (5.6-18)$$

$$C_{13} = C_{23} = C_{34} = 0$$

in which

$$\bar{\mu} = \frac{E}{2(1+\nu)} \quad \text{and} \quad \bar{\lambda} = \frac{\nu E}{(1+\nu)(1-2\nu)}$$

E = Young's modulus of elasticity.

ν = Poisson's ratio.

5.7 Linear Beam Wave Loading Element

This element is intended to model pertinences which are subjected to wave loads but do not contribute to the stiffness of the structure. Examples of such nonstructural members are boat landings, barge bumpers and disposal caissons. This element is called the linear beam wave loading element since it is modeled as a linear beam element with zero stiffness.

5.8 Marshall Strut

Since postbuckling of all but very slender elements is poorly represented by the nonlinear truss element, an element that will adequately follow the inelastic bending and straightening of a strut after buckling is included in the element library. The response of this strut to axial loads is defined in Figure 5.8-1 by the envelope curve ABCDFA, and the additional lines DED and AG. These points are all input by the user.

The basic response consists of

1. Linear elastic extensions of the straight strut, shown as AB.
2. Inelastic buckling under compressive load, as in BC and CD.
3. Inelastic straightening along DFA.

Continued compressive loading after reaching the point D, results in reversible axial shortening (with very large inelastic bending) under no load along DED.

More complex loading patterns may be derived by following two basic assumptions:

1. When unloading or loading away from an envelope curve, the strut follows the line colinear with the point A and the envelope reversal point. If the other envelope is intersected, continued unloading or loading is along the envelope path.

2. The element loads beyond its first tension yielding (P_y) without strain-hardening, and the whole envelope shifts to the right.

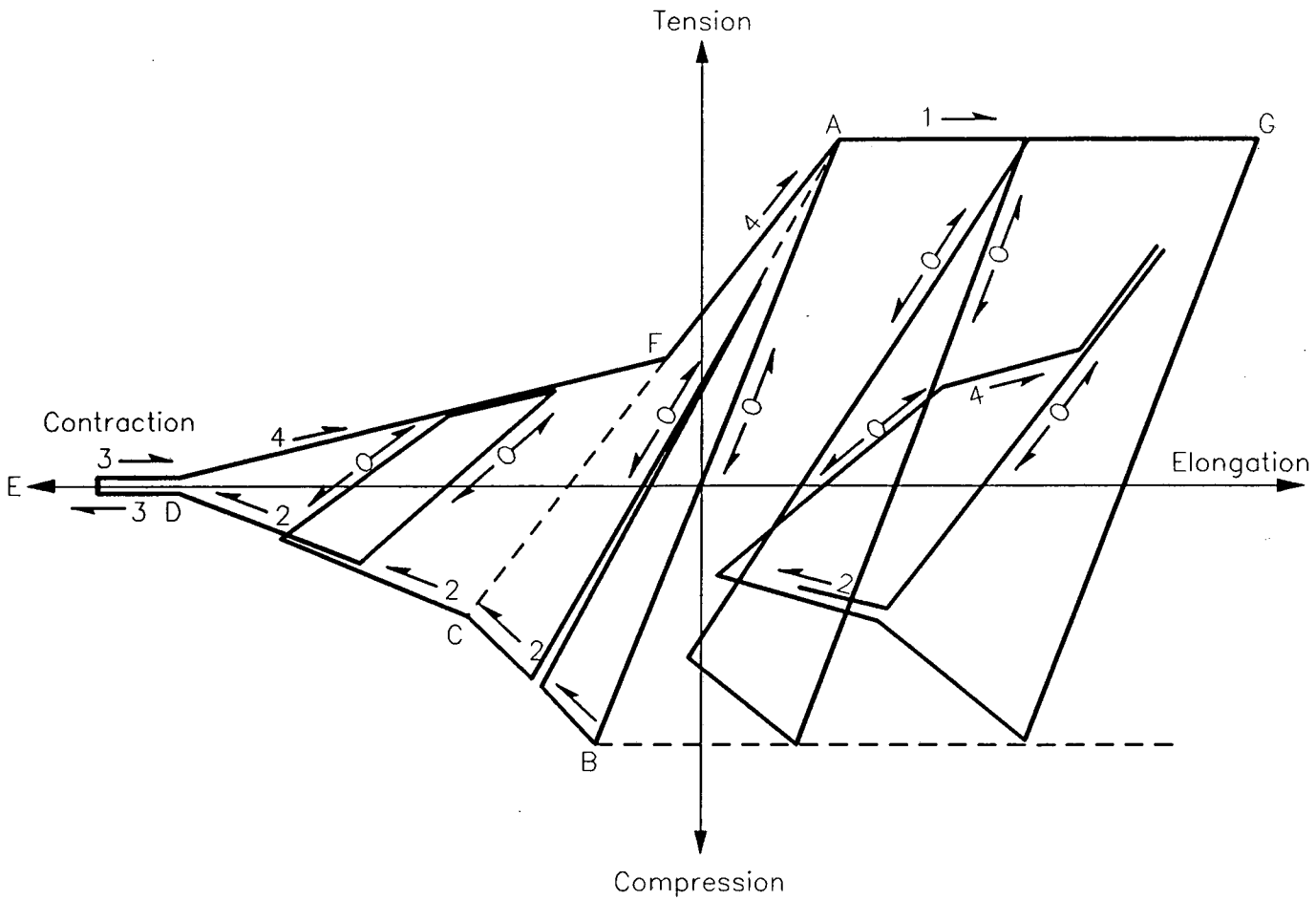

FIG. 5.8-1 FORCE-DEFLECTION ALGORITHM FOR MARSHALL STRUT

By following these rules, any complex loading and unloading sequence may be simulated. Figure 5.8-1 indicates various such sequences.

5.8.1 Element Stiffness Matrix

The element stiffness is formulated in the local coordinate system, then transformed to the global coordinate system. The stiffness is the slope of the appropriate trace on the stress-strain diagram. The envelope stiffnesses are user-defined and the stiffnesses between envelopes are computed as shown in Figure 5.8-1. The stiffness will be negative when following the envelope BCD.

5.8.2 Element Loading

Initial axial forces can be specified as in the case of the linear truss and the nonlinear truss.

5.8.3 Energy Ductility Ratios and Failure Algorithms

Energy ductility ratios are computed and printed for each element from

$$\mu_h = \frac{E_h}{P_y \Delta_y} + 1 \qquad (5.8-1)$$

where

μ_h = energy ductility ratio.

E_h = accumulated energy absorbed within the hysteresis loops.

P_y, Δ_y = tensile yield load and tensile yield extension for each member.

If we have a member that is subjected to a monotonically increasing load, and has a force-deformation relationship corresponding to an elastic perfectly plastic system, then μ_h reduces to the conventional definition of ductility.

In addition, a Marshall strut can be allowed to fail. The failure criteria used is given by

$$\left(\frac{E_f}{E_{cf}}\right)^2 + \left(\frac{E_s}{E_{cs}}\right)^2 \geq 1 \qquad (5.8-2)$$

where

E_f = cumulative flexural energy at plastic hinges.

E_{cf} = a reference flexural energy for failure.

E_s = cumulative inelastic stretch energy.

E_{cs} = a reference inelastic stretch energy for failure.

E_{cf} and E_{cs} may be input by the user directly or, for tubular sections, are computed by the program internally. In the latter case, these values are found as follows:

Flexural Energy for Failure, E_{cf}:

For a fixed-end beam, with plastic hinges at the ends and the middle, failure occurs when

$$E_{cf} = 4 M_{fp} \theta_{hinge}$$

where

θ_{hinge} = the plastic rotation at failure at the ends.

M_{fp} = the fully plastic moment.

Marshall [1974] has shown experimentally that

$$\theta_{hinge} = (\theta_{cr} - \theta'_y)\ (L_h + L_p)$$

where

θ_{cr} = critical curvature.

θ'_y = M_{fp}/EI.

L_h = additional finite hinge length to account for additional hinge rotation observed in test results.

L_p = length of plastic hinge.

Extensional Energy for Failure, E_{cs}

Marshall [1976] indicates that we can write

$$E_{cs} = P_y(0.01L + \Delta_{joint}) \qquad (5.8-3)$$

where

P_y = tensile yield load.

L = length of member.

Δ_{joint} = joint distortion at failure.

The above experimental results can thus be used to determine E_{cf} and E_{cs}.

The failure process is as follows. Once the strut has failed, the force (ordinate) of the envelope curve is reduced at each subsequent time step by a percentage which is input by the user. This leads to a progressive failure of the element that is numerically stable. When the curve has dropped to 1/100 of its original size, the stiffness is removed entirely.

5.9 PSAS (Pile Soil Analysis System) Element

5.9.1 Introduction

The PSAS element is used to model the soil-pile interaction in a foundation system. Pile-soil-pile interaction (displacement of one pile due to the displacement of a neighboring pile) is not taken into account by PSAS.

The PSAS element is a line element with two nodes. One of the two nodes is fixed because of the boundary condition of zero soil deformation at an infinite distance from the pile and the other node is attached to the pile (Figure 5.9-1). The PSAS elements model the soil resistance to the pile displacement by load-deflection relationships in the axial direction (shaft T-Z curves and tip Q-Z curves) and in the lateral direction (P-Y curves).

The basic load deflection relationship is called the "backbone curve" and represents the virgin soil (loaded for the first time) deformation under a load applied at a reference rate. The load deflection relationship under actual loading conditions is obtained by adjusting the backbone curve to taken into account the hysteretic behavior, cyclic loading effects, loading rate effects and gapping effects.

5.9.2 Backbone Curve

The backbone curve used by PSAS to define the load deflection relationship is typically a multilinear curve defined by up to 9 points as shown in Figure 5.9-2. The user can specify the input for PSAS to be either Automatic (where only basic pile and soil properties are input) or generalized (where the points defining the backbone curve and damping

effects of each element are input). For an Automatic input, the backbone curve is constructed according to the relationships specified in the American Petroleum Institute (1987) Recommended Practice for Planning, Designing and Construction of Fixed Offshore Platforms.

In the rest of this section, the construction of the backbone curves for different types of soil according to the API guidelines will be discussed.

API (1987) Load Deflection Curves

The API guidelines provide the formulae needed to construct the backbone curves for lateral (P-Y) load-deflection relationships, and several key values for the vertical-shaft (T-Z) and vertical-tip (Q-Z) load-deflection relationships. Stiff clay requires a more complex formulation which the API references to Reese and Cox (1975).

PSAS also uses this reference to construct the appropriate backbone curves.

API (1987) and Reese and Cox (1975) provide techniques for constructing continuous curves. These curves are approximated in PSAS as multi-segment curves, where the last segment of each curve is always perfectly plastic (zero-slope). Both references define backbone curves for virgin and fully-degraded cyclic conditions with no gap.

Shaft and Tip Load Deflection Curves

The axial capacity of a pile, Q_d, is the sum of the shaft resistance, T_f, and the end bearing resistance, Q_p:

$$Q_d = T_f + Q_p = f\bar{A}_s + \bar{q}A_p$$

where

f = unit skin friction along the pile shaft.

$\bar{A}_s$ = embedded shaft area of the pile.

$\bar{q}$ = unit end bearing capacity.

A_p = gross end area of the pile.

The values of f and $\bar{q}$ are specified per API (1987) for both cohesive and cohesionless soils. The displacements at which T_f and Q_p are mobilized, however, are not defined by API. The next sections discuss how PSAS forms the T-Z and Q-Z curves.

Shaft Load-Deflection Curve (T-Z)

The shaft load deflection (T-Z) curve is shown in Figure 5.9-3. Notice that a compressive axial load on the pile (which is applied in the negative global z-direction) produces a positive deflection in the soil element (to the right in Figure 5.9-3).

For the compressive cycle, the behavior is characterized by five values:

T_C = the value of maximum shaft resistance.

Z_C = the displacement required to mobilize that resistance.

Z_{dc} = the displacement at which the maximum resistance starts to decrease due to strain softening.

T_{rc} = the residual shaft resistance.

Z_{rc} = the displacement at which that resistance is mobilized.

For the tensile cycle, the behavior can be characterized in a similar way. In general, the five values for the tensile cycle are different than for the compressive cycle.

Cohesive Soils - Values for Shaft Resistance

The values of T_c and T_t are calculated by PSAS per the API guidelines. T_{rc} in Figure 5.9-3 represents the value of the residual resistance for the shaft after a specific deflection, Z_{rc}, has been reached. The residual response is not specified in API (1987); however its influence on the overall pile behavior was found to be potentially important for some combinations of soil-pile conditions, e.g., Murff (1980) and Kraft et al. (1981).

Residual resistance values in the range of 0.7 to 1.0 times the maximum static resistance were found by Coyle and Reese (1966) for piles in marine clays with sensitivities of 2 to 4. Holmquist and Matlock (1976) found similar values in their laboratory pile-soil tests (T_r/T = 0.87 for static loading).

The method available for the definition of the static residual resistance is that of a ratio of residual resistance to maximum shaft resistance $\frac{T_r}{T}$. Unless soil data is available, selection of $\frac{T_r}{T}$ should be based on field and laboratory pile and soil test condition results.

Cohesive Soils - Control Values of Axial Pile/Soil Deflection

The **Maximum Displacement Factor** value in PSAS is used to define the value of Z_C, where Z_C is calculated by multiplying the **Maximum Displacement Factor** by the pile diameter.

Values of the **Maximum Displacement Factor** have been found to range from 0.005 to 0.03. PSAS uses 0.01 for both tension and compression.

Cohesionless Soils - Values of Shaft Resistance

For cohesionless soils, PSAS uses API (1987) guidelines for the shaft resistance values. The static residual resistance, T_{rc}, is taken as equal to the static maximum resistance, T_c. The tensile resistance is also taken as equal to the compressive resistance, $T_t = T_c$.

Cohesionless Soils - Control Values of Axial Pile/Soil Deflection

Similar to cohesive soils, the **Maximum Displacement Factor** value is also used to define the value of Z_C for cohesionless soils. PSAS uses 0.01 as the value for the **Maximum Displacement Factor**.

Tip Load-Deflection Curve (Q-Z)

The shape of the Q-Z curve is assumed in PSAS to be similar to Figure 5.9-3. Very little data is available on the load-deflection characteristics of the Q-Z curve, other than the unit bearing capacity, $\bar{q}$. PSAS assumes that the ultimate bearing capacity for both tension and compression is identical and mobilized at a **Maximum Displacement Factor** of 0.10.

5.9.3 Hysteretic Behavior

Lateral Loading

At shallow soil depths along the pile, soils that are subjected to cyclic lateral loads may form a gap between the soil interface and the pile wall. This gap may result from a soil "wedge" being pushed up and away from the pile during loading. At the onset of the next loading cycle, the pile must move through the gap and contact the soil before the soil can resist the pile load. The depth at which this wedge-type of soil failure can occur (and where gapping can occur) is the "critical depth".

When gapping is used in PSAS, the soil elements above the critical depth track the gap that forms between the pile wall and soil interface. Load reversal causes the element response to slide back through the gap with reduced resistance until bearing on the other side of the gap occurs. The resistance level during the gap can be set to any value.

For elements below the critical depth, where no gap is allowed to occur, the hysteretic behavior of a PSAS element under lateral loading is shown in Figure 5.9-4. Notice that on unloading, the origin of the P-Y curve is shifted to the load reversal point. For a full gap (zero gap strength) and for a partial gap (non-zero gap strength), the origin remains at zero deformation.

Figure 5.9-5 shows the hysteretic behavior with full gap effects. For this case, when unloaded to P = 0, some pile movement is required to pick up the soil resistance in the direction of pile movement.

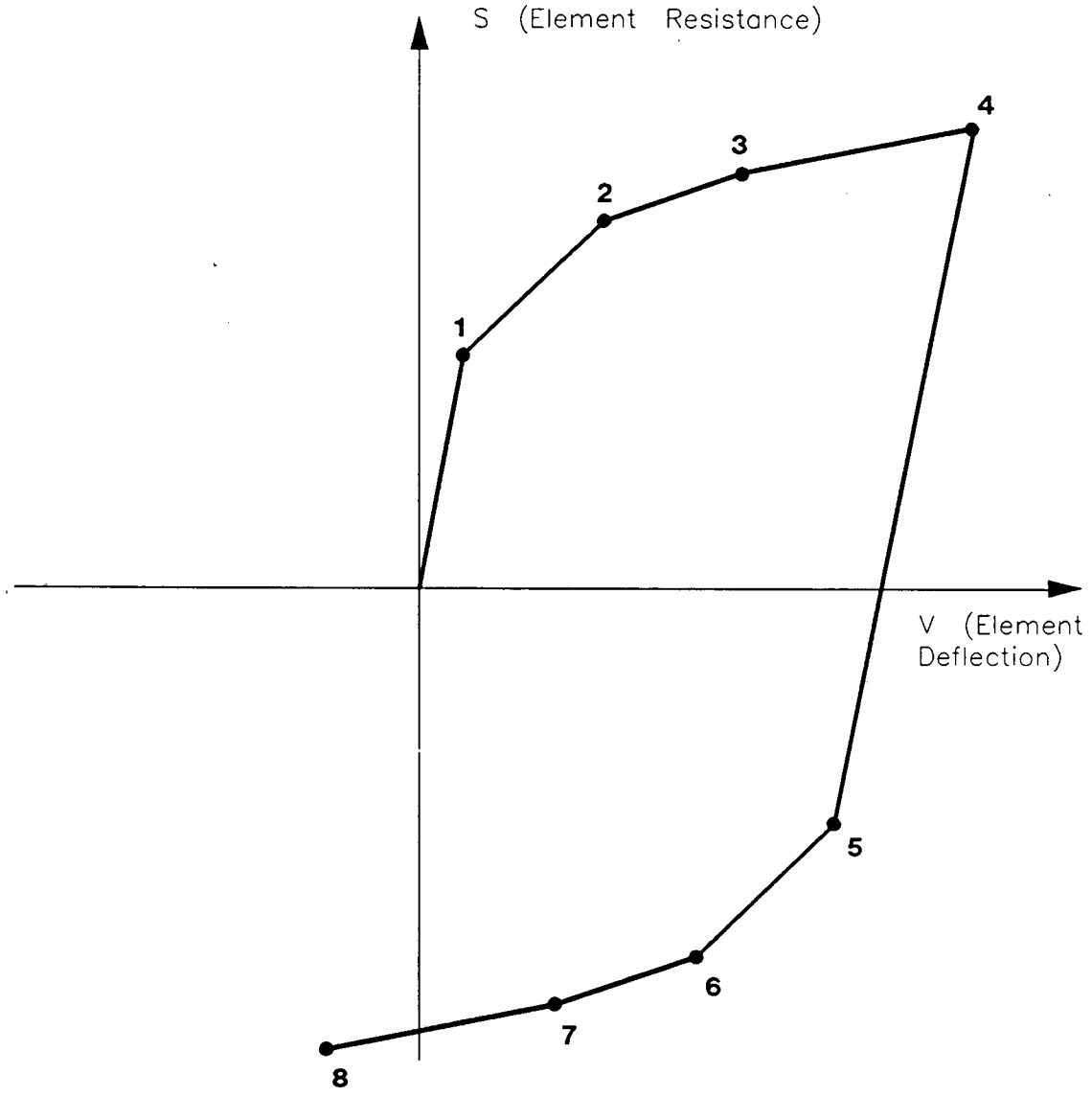

FIG. 5.9-4 HYSTERETIC BEHAVIOR-LATERAL DIRECTION, NO GAP

Figure 5.9-6 shows the hysteretic behavior with partial gap effects. Similar to the case with full gap effects, when unloading to certain force levels, some pile movement is required before the soil resistance can increase. A constraint on the partial gap strength is that it be less than the strength for point 1.

Axial Loading

The hysteretic behavior of the load deflection curve in the axial direction is shown in Figure 5.9-3. Notice that the origin is shifted to the new load reversal point every half load cycle.

Lateral-Axial Interaction Effects

When gapping (partial or full) occurs in the lateral load-deflection (P-Y) curve, the resistance of the associated load-deflection (T-Z) curve is set to zero. This represents the loss in axial strength resulting from the soil being pushed away from the pile during lateral response.

5.9.4 Cyclic Loading Effects

Laboratory and field tests have shown that cyclic loading may cause a reduction in the load capacity and an increase in the settlement of piles.

A consistent feature of the cyclic response of piles is that after a full two-way cycle, significant reduction in strength is obtained. Another important aspect of cyclic loading is that the amount of degradation per cycle reduces significantly after a certain number of cycles have taken

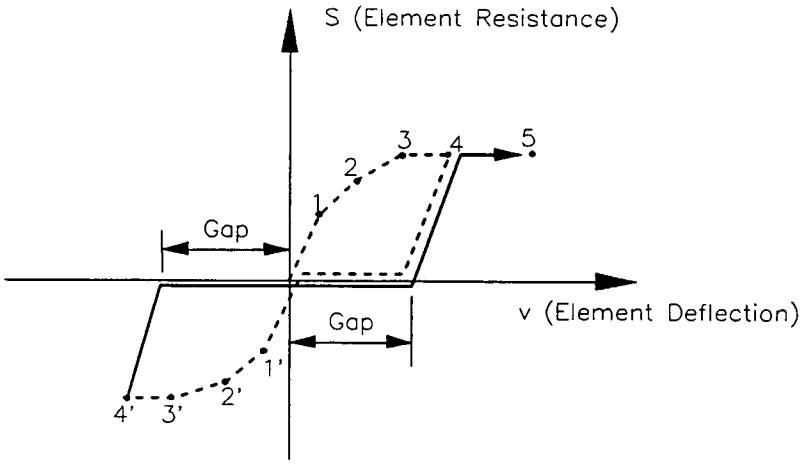

FIG. 5.9-5 HYSTERETIC BEHAVIOR-LATERAL LOADING, FULL GAP

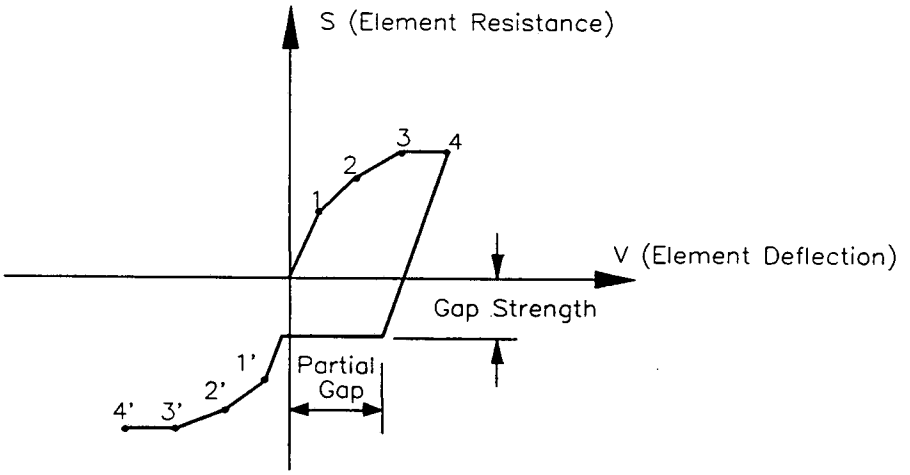

FIG. 5.9-6 HYSTERETIC BEHAVIOR-LATERAL LOADING, PARTIAL GAP

place. This phenomenon leads to the definition of a "fully degraded curve", where the strength remains fairly constant with continuing cycles.

The cyclic degradation is characterized in PSAS by using a degradation factor λ, which is applied to the current strength of the backbone curve whenever a full two-way cycle has occurred. A full two-way cycle is counted in PSAS whenever the total pile displacement (peak to peak) exceeds a **Significant Deflection** value. In the Automatic soil generation option, the **Significant Deflection** is defaulted to $2 \times Y_D$ where Y_D is the displacement corresponding to the load equal to 75 percent of the ultimate capacity for any given soil element. In the Generalized soil input option, the **Significant Deflection** is input by the user.

In PSAS, the following procedure outlined by Matlock and Foo (1980) is adopted for the cyclic degradation (Figure 5.9-7):

$$P_2 = P_{min} + (1 - \lambda)\ (P_1 - P_{min})$$

where

P_1 = the existing ultimate strength for the previous loading cycle.

P_2 = the new ultimate strength for the current loading cycle.

P_{min} = the strength at the fully degraded limit.

λ = the cyclic degradation factor.

Guidelines for Selection of Lambda

The key for predicting the cyclic degradation characteristics of a given soil/pile system is the selection of the Lambda parameter. The best method is to use the results of an actual cyclic pile load test, with similar soil, pile and loading properties. Given the values of P_1, P_2 and P_{min} for a load test, the appropriate value of Lambda can be back calculated.

One common method for determining Lambda is from load test data that gives the number of cycles required to cause 50 percent degradation. This value of lambda can be given by:

$$\lambda = 1 - 10^{\left(\frac{\log 2}{1-N_{50}}\right)}$$

where N_{50} is the number of load cycles required to cause 50 percent degradation.

Obviously, cyclic load test data is not always available. In this case, published values of Lambda can be used. Various authors have published results of cyclic field and lab load tests, including:

Figure 5.9-8 shows a compilation of results derived from the cyclic axial loading tests performed on a small scale pile by Grosch and Reese (1980). A typical cyclic load resulted in displacement of the pile of 10 times the initial yield level displacement.

Figure 5.9-9 gives a compilation of results of cyclic load tests on a variety of piles. All piles in these tests were repeatedly failed in

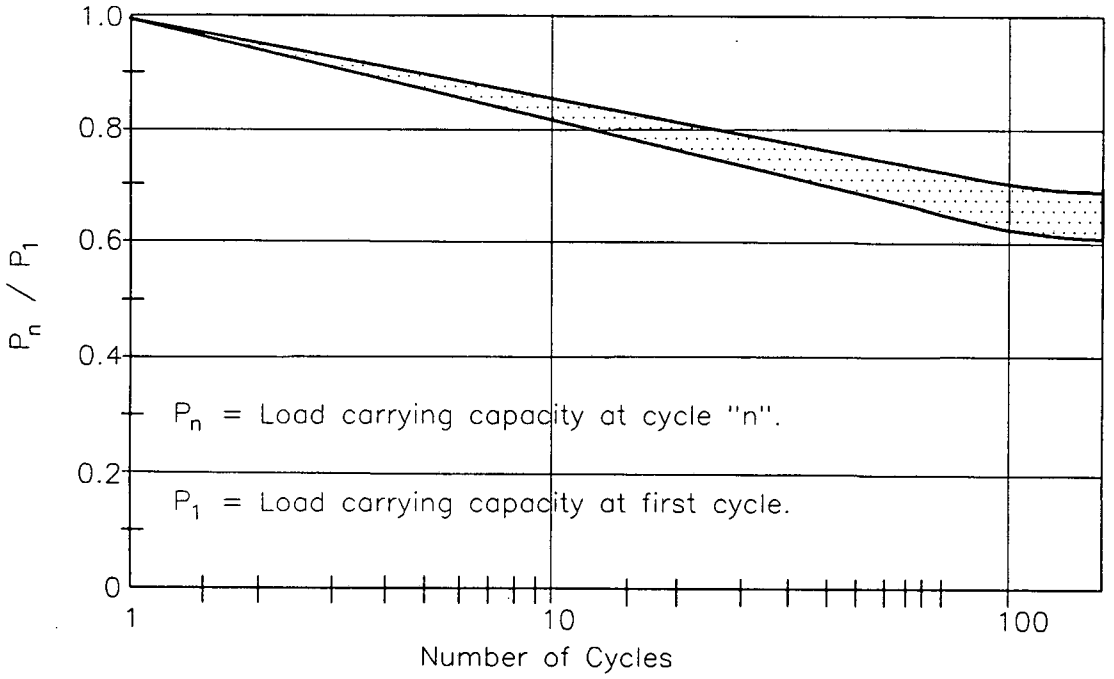

FIG. 5.9-8 SUMMARY OF CYCLIC AXIAL LOAD TEST RESULTS (After Grosch and Reese, 1980)

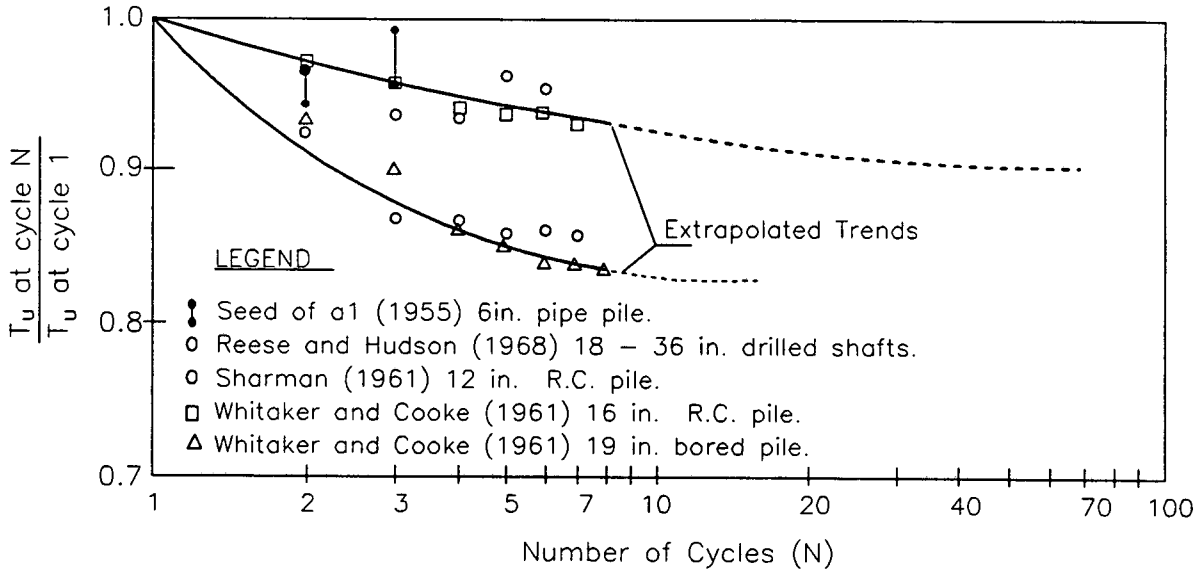

FIG. 5.9-9 COMPILATION OF VARIOUS AXIAL PILE TESTS (COHESIVE SOILS) (After Audibert and Dover, 1982)

compression. The ultimate capacity of the piles at the "n^{th}" cycle normalized by the capacity at the first cycle are plotted against the number of cycles.

The results of other cycling load tests on piles are published in Holmquist and Matlock (1976) and Sangray (1977).

5.9.5 Loading Rate Effects

The rate at which axial or lateral loads are applied to a pile affect the load deflection characteristics of the soil-pile system. The resistance and stiffness of the soil increases for higher rates of loading and vice versa for lower rates.

The review of literature on the soil strain rate effects suggests that the best method available is to use a loading rate factor β_R, which scales the ultimate strength and stiffness of soil load-deflection curves.

The loading factor β_R is defined as the ratio of dynamic resistance (P_d), to static resistance (P_s) and is expressed in the following form:

$$\beta_R = \frac{P_d}{P_s} = F_1 + F_2 \log \frac{t_r}{t_s}$$

in which

t_s = the static or standard rate of loading.

t_r = the actual (dynamic) rate of loading.

F_1, F_2 = numerical constants.

Based on the results of several investigators, numerical values for the constant F_2 have been found to range from 0.01 to 0.03 for sands, 0.02 to 0.07 for silts, 0.02 to 0.12 for clays, and 00 to 0.03 for calcareous soils. A value of 1.0 for F_1 is typically used.

Figure 5.9-10 shows lateral load test results on piles in cohesive soils compiled by Bea et al (1980). Soils with higher OCR values tend to have greater values of β_R. Several tests showed a value of F_2 ranging from 0.02 to 0.06 at OCR = 1 to 0.04 to 0.24 at OCR = 4.

In the "static" soil tests, about 10 to 100 per cent of ultimate load capacity is applied per hour. This gives a reference value of $\beta_R = 1.0$. For coastal environments dominated by wave loading, 100 to 1000 cycles of load could be applied per hour. This gives us a corresponding ordinate of 10^4 to 10^5 and a β_R about 1.2 to 1.7. Note that for low "creep" loading rates (less than the static reference rate), β_R is smaller than 1.0.

Values for β_R corresponding to axial loading conditions were also summarized by Bea, et. al. (1980), and are shown in Figure 5.9-11. Similar β_R factors to lateral load tests were found for axial loads, however tests for creep type loadings were not reported.

Very little published data is available regarding the effect of loading rate on strength or stiffness of cohesionless soils. In fact, some investigators have suggested that the strength of cohesionless soils is largely unaffected by loading rate.

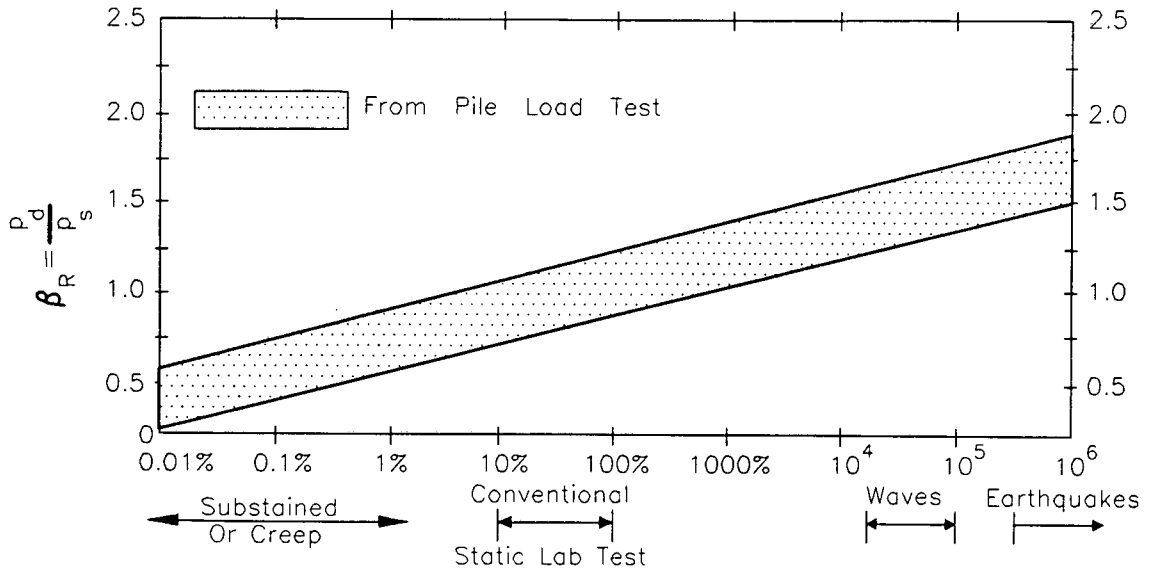

FIG. 5.9-10 COMPILATION OF β_R VALUES FOR LATERAL LOADS (After Bea, et. al., 1980)

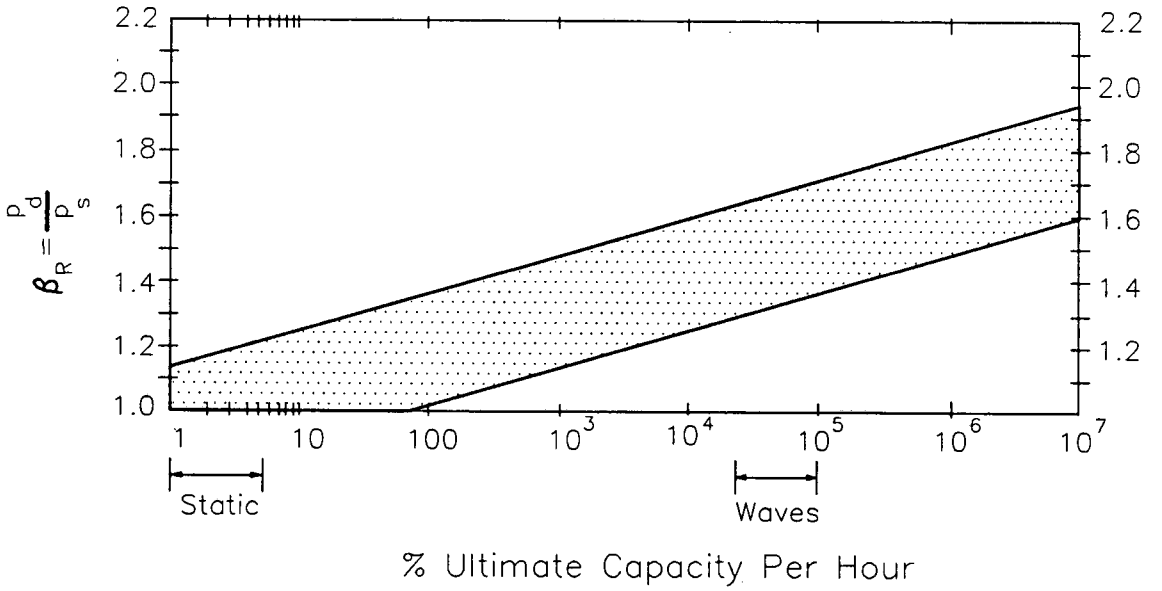

FIG. 5.9-11 COMPILATION OF β_R VALUES FOR AXIAL LOADS (After Bea, et. al., 1980)

5.9.6 Radiation Damping

Energy is dissipated in pile foundations subjected to cyclic loads through two sources: the hysteretic damping due to inelastic behavior of soils and the radiation damping due to elastic wave propagation in the soil away from the pile. Incorporating this energy loss is important to accurately determine the response of a pile system. The hysteretic soil behavior and the associated loss of energy is illustrated in Section 5.9.3.

The approach used in PSAS to approximate the effects of radiation damping was formulated by O'Rourke and Dobry (1979). In this approach, the coefficient of radiation damping, C_h, per unit length is given by

$$C_h = 2d\,\rho_s\,(v_s + v)$$

where

d = the pile diameter.

ρ_s = the soil mass density.

v_s = the shear wave velocity.

v = a velocity satisfying $v_s \leq v \leq v_c$, where v_c is the compression wave velocity in the soil.

The dashpot coefficient used in PSAS is based on a concept which is valid for a one-dimensional wave propagation. A dashpot with a damping coefficient $C = \rho A V_c$ will fully absorb the energy of a wave traveling

with velocity V_c along a bar with cross-sectional area A and mass density ρ_p. O'Rourke and Dobry have shown that the radiation damping can be reasonably approximated by the above formulation.

The use of the lower bound shear wave velocity for v in the expression of radiation damping is a conservative assumption and simplifies the expression for the radiation damping coefficient to the following:

$$C_h = 4d\rho_s v_s.$$

The shear wave velocity v_s is given by:

$$v_s = \sqrt{\frac{G}{\rho_s}}$$

where G_s is the shear modulus of the soil.

Shear Modulus

The shear modulus of a soil is a function of the level of strain, so in determining a reasonable value, the average level of strain in the soil element during the analysis should be estimated.

The shear modulus can be evaluated either from field measurements or from laboratory experiments. The advantage of field measurements is that the soil shear modulus is evaluated in the undisturbed state which is ideal for the purpose of estimating the radiation damping. On the other hand, conducting laboratory experiments allows for the variation in confining

pressure and strain level. Field methods for the evaluation of shear modulus are classified into surface techniques and bore hole techniques. These methods depend on the evaluation of the shear wave velocity, V_s.

The different field and laboratory methods for the evaluation of soil shear wave velocity are discussed in Auld (1977) and Richart and Woods (1970).

Interaction Between Radiation Damping and Gapping

The coefficient of radiation damping in the lateral and axial directions is set to zero for a full gap. As the gap closes, the value of the coefficient is set at half of its original value. A partial gap does not affect the initially specified coefficient value, however.

5.10 Cable-Spring Element

This element models the nonlinear restoring force of a cable system. The force is defined at the cable attachment point.

5.10.1 Applications

This element can be used to replace a system of cable-anchor-support elements, once the force-displacement characteristics at the cable attachment point are known. Thus all of the cable, anchor, and support elements can be replaced with a single element, greatly simplifying the computer model.

5.10.2 Element Features

The element has the following features:

1. Arbitrary orientation in 3-D space.

2. The multi-linear force-displacement curve may be up to 19 segments.

3. Vertical and horizontal preloads may be specified.

5.10.3 Element Properties

Typical force-deformation curves for a cable-spring element are as shown in Figure 5.10-1.

Each curve is defined by a force-deformation pair (e.g., horizontal projection and corresponding force). Curves must be defined in

increasing order of horizontal projections. For each cable element, the program calculates preloads in the element corresponding to its initial horizontal projection.

Each cable-spring element is defined by three nodes as shown in Figure 5.10-2. The element end I is connected to the structure, and end J is the anchor node. A third node K is designated to define the plane of the element. The initial horizontal projection of the element is the distance IJ in a horizontal plane normal to the plane of the element, i.e., plane IJK. The subsequent horizontal projections are also defined with respect to the initial horizontal plane. Therefore, it is important to specify the node J correctly at a distance of initial horizontal projection. Node K can be any node used to define the cable element cable.

5.10.4 Element Stiffness

The element stiffness is formulated in the local coordinate system and is transformed to the global coordinate system. The stiffness is obtained from the force-displacement relationship in Figure 5.10-1.

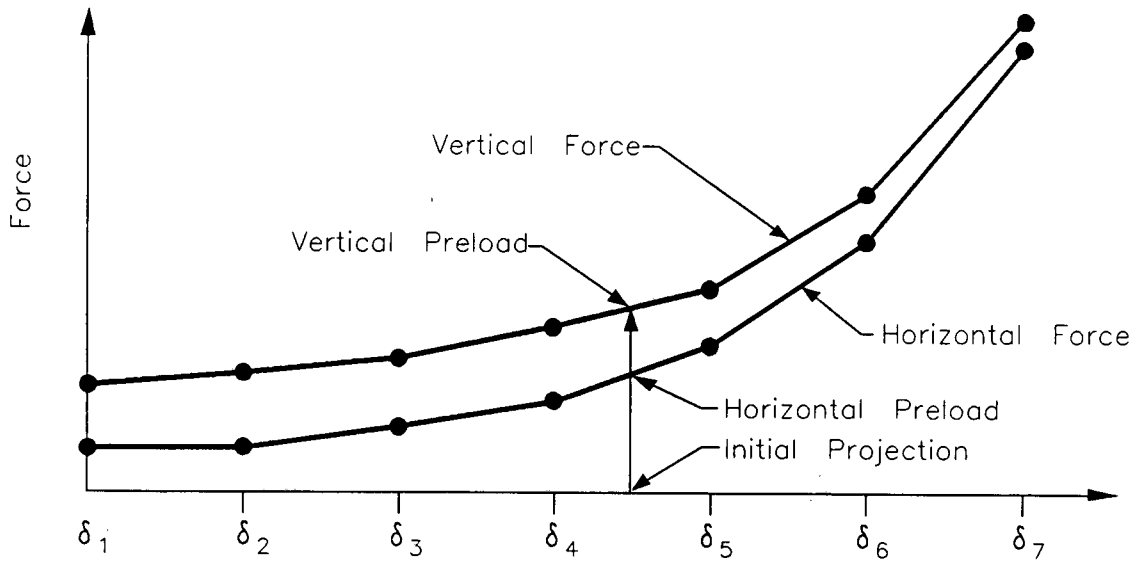

FIG. 5.10-1 FORCE-DEFORMATION CURVES FOR CABLE-SPRING ELEMENT

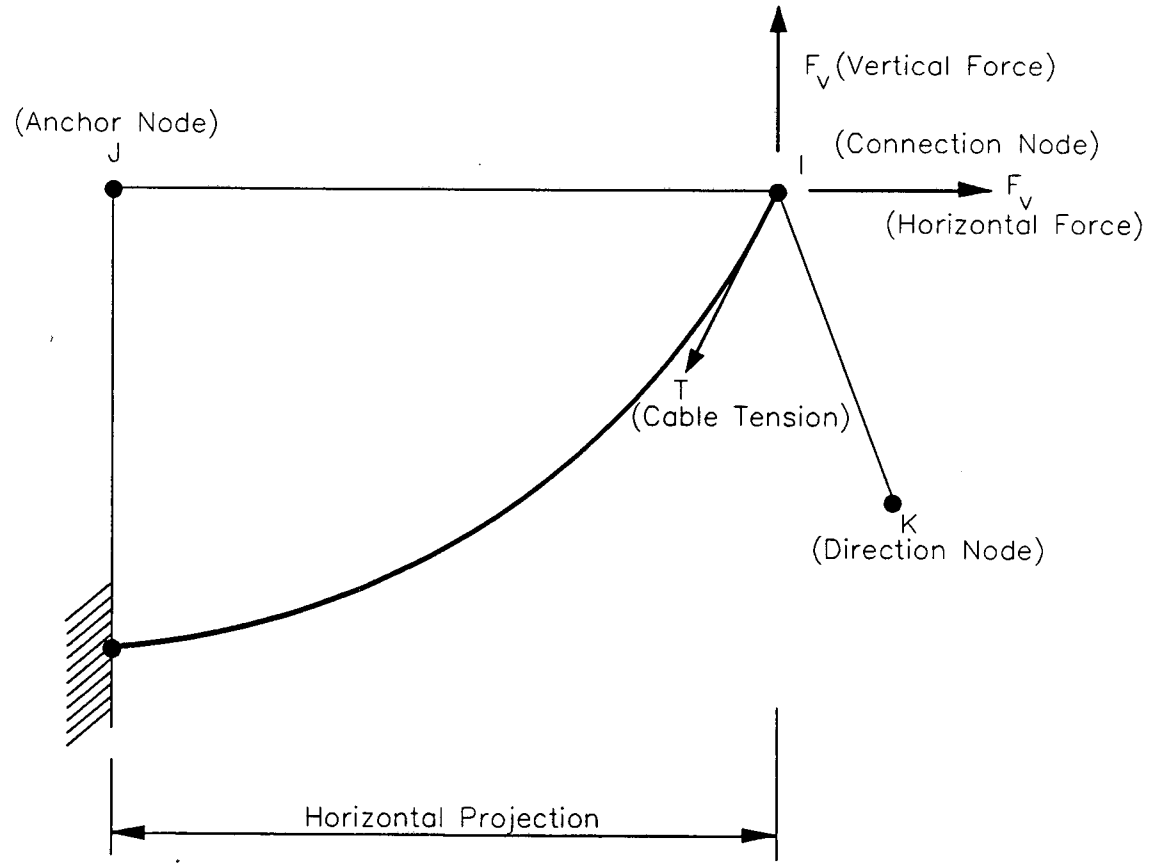

FIG. 5.10-2 CABLE-SPRING ELEMENT GEOMETRY

5.11 Shear Transfer Element (SHER)

The shear transfer element is a two-node element simulating the effect of the shim connection between the pile and the tower leg. The pile direction node defines the direction of zero stiffness. The plane normal to the pile direction offers high rigidity, forcing the pile and casing nodes to move together in the plane but slip along the pile direction. (See Figure 5.11-1). The element has three translational degrees of freedom associated with each of its two nodes.

From the pile direction vector, two orthogonal unit vectors a_1 and a_2 are formed. Truss bars with high stiffness ($K = 1 \times 10^{10}$) are placed along these two directions to give the high in-plane stiffness. The global element stiffness is found by adding the stiffness of the two bars, after transforming them to global directions.

$$[a_1^T - a_1^T] \; K \begin{bmatrix} a_1 \\ -a_1 \end{bmatrix} \quad \text{and} \quad [a_2^T - a_2^T] \; K \begin{bmatrix} a_2 \\ -a_2 \end{bmatrix}$$

The output consists of resultant shear transferred, relative total deformation between the pile and casing node, and the direction cosines of the resultant shear.

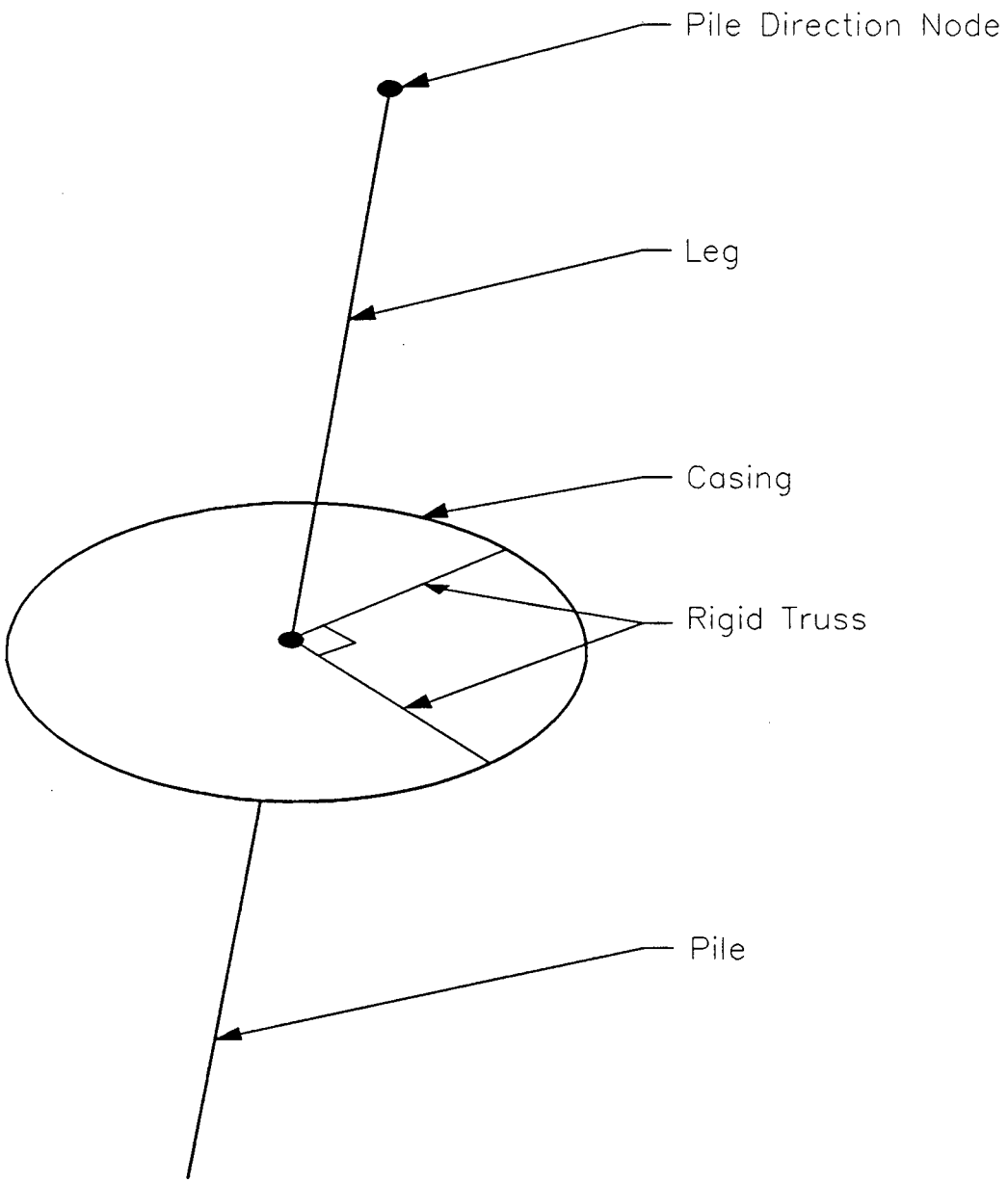

FIG. 5.11-1 SHEAR TRANSFER ELEMENT

5.12 Inelastic Buckling Beam-Column Element

This element is intended primarily to model inelastic pre-buckling and post-buckling behavior in tubular beams and columns. The element is 3-dimensional and is able to take into account the effects of section damage, joint cans, joint flexibility, and eccentric end connections.

Unlike a typical beam element, this element is multi-segmented and is composed of other beam elements. The total element constitutes a structural system and is called a "super-element"; the basic elements which compose it are hereafter called "sub-elements." Action-deformation response of the element will be obtained by performing a finite element analysis on the super-element system.

The large-displacement, distributed plasticity beam-column element as described in Section 5.13 is chosen as the sub-element of this element. This type of sub-element enables the super-element to exhibit inelastic buckling behavior.

5.12.1 Element Capabilities

The element has the following capabilities:

1. The element is multi-segmented and can be straight or curved in space. A curved member, often used in modeling out-of-straightness effects, is specified in the shape of a half-cycle sine curve.

2. Element deformation can be large for every step as long as the element behaves stably.

3. All element input properties are automatically generated from basic, user-supplied data.

4. The nonlinear force-displacement relationship of the tubular element is constructed based on the behavior of elastic-perfectly plastic material.

5. Element load is applied along the length of the element; its effect on instantaneous buckling load can be studied.

6. Damaged sections with holes and/or dents can be represented along the length of the element.

7. Joint cans, bi-linear flexible joints, and eccentric end connections can be specified near the element ends.

8. Displacement and force results along the length of the element, in addition to element end displacements and forces, can be displayed.

The various super-elements that may be generated are shown in Figure 5.12-1.

5.12.2 Element Axes

The local coordinate system x, y and z of the super-element is defined by three nodes i, j, and k, as shown in Figure 5.12-2. Nodes i and j define the local x axis. The local y axis is normal to the local x axis and resides in the plane containing the k node and the local x axis. The local z axis is defined orthogonal to the local x and y axes, using the right hand rule.

The local coordinate system x′, y′ and z′ of the sub-elements is defined by i′, j′ and k′ nodes in the way same as to define the super-element axes. Each sub-element has its own i′, j′ and k′ nodes. Node i′ is located on the sub-element end, close to the i node; node j′ is on the other end. Node k′ is in the position same as the k node.

In Figure 5.12-2, capital X, Y, and Z are for the global coordinate system.

5.12.3 Element Degrees of Freedom

The element has two external nodes and several internal nodes, as shown in Figure 5.12-2. The external nodes connect to the complete structure and have six degrees of freedom each; namely, X, Y, Z global translation and X, Y, Z global rotation. The element nodal displacements in the global coordinates are written as in vector $q = [q_1, q_2, \ldots, q_{12}]$, and are related to the element end deformations in vector $u = [u_1, u_2, \ldots, u_{12}]$ by a direction transformation matrix. The nodal displacements and end deformations are shown in Figure 5.12-3. The local element forces written as in vector $p = [p_1, p_2, \ldots, p_{12}]$ are defined in a way similar to the end deformations, i.e., the subscript numbers in the vector "p" correspond to those of the vector "u", and the positive forces coincide with the deformation directions.

The internal nodes (sub-nodes) are needed for constructing the sub-elements. Each sub-element connecting two sub-nodes has twelve degrees of freedom. The nodal displacements, q′, the end deformations, u′, and the end forces, p′, of each sub-element are defined similarly to the super-element. Thus, by adding a prime symbol to every designated letter, the sub-element system can be indicated as well (Figure 5.12-3).

Clearly, for a super-element system with "n" sub-elements, "n+1" sub-nodes are needed and "6n+6" degrees of freedom are generated.

5.12.4 Section Properties

The basic data required to define the material and section properties of the element are the diameter, D, the thickness, t, Young's modulus, E, and the yield stress, σ_y, as shown in Figure 5.12-4. Based on these data and assuming elastic-perfectly plastic material, four basic nonlinear action-deformation pairs, i.e., M_y - ψ_y, M_z - ψ_z, M_x - ψ_x, and F-ϵ, as defined in Section 5.13.5, can be obtained. Because the input parameters required by the distributed plasticity beam-column element are forces and stiffnesses, they are constructed instead.

Bending Properties

The bending capacities which must be constructed are M_{Y1}, M_{Y2} and M_{Y3}. M_{Y1} is the first yield bending moment capacity, when the section just starts to yield; M_{Y3} is the full capacity as when the full section reaches the yield stress; and M_{Y2} is the capacity at an intermediate stage as when the maximum strain of the section gets to two times the yield strain. These bending capacities, as illustrated in Figure 5.12-5(a), are expressed as

$$M_{Y1} = \sigma_y \frac{2I}{D}$$

$$M_{y2} = \sigma_y\left(0.147D^3 - \frac{\pi}{d}\left(\frac{D}{2-t}\right)^4\right) \qquad \text{if } t \geq \frac{d}{4}$$

$$= \sigma_y\left(0.147D^3 - \left(\frac{D}{2-t}\right)^3\left(\frac{\cos 3B}{3} + \cos(B) + \left(1-\frac{2t}{d}\right)\left(B - \frac{\sin 4B}{4}\right)\right)\right) \quad \text{if } t < \frac{d}{4}$$

and

$$M_{y3} = \sigma_y \frac{D^3 - (D-2t)^3}{6}$$

where A and I are the section area and the moment of inertia, respectively, and

$$B = \sin^{-1}\left(\frac{1}{2-\frac{4t}{D}}\right)$$

The stiffnesses which must be constructed are K_{My1}, K_{My2}, K_{My3} and K_{My4}. K_{My1} represents the elastic stiffness while K_{My2}, K_{My3} and K_{My4}, respectively, are the softening stiffnesses after M_{y1}, M_{y2} and M_{y3} are reached. These four stiffnesses are expressed as

$$K_{M_{Y1}} = EI$$

$$K_{M_{Y2}} = \frac{M_{Y2} - M_{Y1}}{M_{Y_1}} EI$$

$$K_{M_{Y3}} = \frac{M_{Y3} - M_{Y2}}{20 M_{Y1}} EI$$

and

$$K_{M_{Y4}} = 0.05 K_{M_{Y3}}$$

Note that K_{My3} is calculated by assuming that the full capacity of the section is reached, when the maximum strain get to 22 times the yield strain, and K_{My4} is arbitrarily chosen to represent a very small residual stiffness.

The bending action-deformation relationships for the local y and z axes are the same for a tubular section. The above relationship, therefore, can be used to define the bending relationship of the local z axes as well.

Torsional Properties

The torsional capacities which must be constructed are M_{x1}, M_{x2} and M_{x3}. The first and third torsional capacities, M_{x1} and M_{x3}, are defined in a way similar to the bending capacities (see Figure 5.12-5(b)) and M_{x2} is assigned as the average of M_{x1} and M_{x3}. These torsional capacities, thus, can be expressed as

$$M_{X1} = \sigma_y \frac{2J}{D}$$

$$M_{X2} = \frac{M_{X1} + M_{X3}}{2}$$

and

$$M_{X3} = \sigma_y \frac{2\pi}{3}\left(\frac{D^3}{8} - \left(\frac{D}{2} - t\right)^3\right)$$

where J is the polar moment of inertia.

Subject to the constraints of the deformation values at changes in stiffness to have the same ratios for all action-deformation relationships (see Section 5.13.5), the four torsional stiffnesses are

$$K_{M_{X1}} = GJ$$

$$K_{M_{X2}} = \frac{M_{X2}-M_{X1}}{M_{Y2}-M_{y1}} \frac{M_{Y1}}{M_{X1}} \frac{K_{M_{Y2}}}{K_{M_{Y1}}} K_{M_{X1}}$$

$$K_{M_{X3}} = \frac{(M_{X3}-M_{X1})\, K_{M_{X1}}\, K_{M_{X2}}}{K_{M_{X1}}\,(M_{X2}-M_{X1}) - RM_{X1}\, K_{M_{X2}}}$$

and

$$K_{M_{X4}} = 0.05\, K_{M_{X3}}$$

where

$$R = \frac{KM_{Y1}}{M_{Y1}}\left(\frac{M_{Y2}-M_{Y1}}{K_{M_{Y2}}} + \frac{M_{Y3}-M_{Y2}}{K_{M_{Y3}}}\right)$$

Note that K_{MX4} is arbitrarily chosen to represent a very small residual stiffness.

Axial Properties

The axial capacities which must be constructed are F_1, F_2 and F_3. When elastic-perfectly plastic material is assumed, these three forces should be all the same. However, because the input of the distributed plasticity beam-column element requires the magnitudes of F_1, F_2 and F_3 in an increasing order, these axial capacities are assumed to be

$$F_1 = \sigma_Y A$$

and

$$F_2 = 1.01\, F_1$$

$$F_3 = 1.02\, F_1$$

The derivation of the axial stiffnesses, K_{F1}, K_{F2}, K_{F3} and K_{F4}, is also subject to the constraints as stated above. Thus, these four stiffnesses have the following form:

$$K_{F_1} = EA$$

$$K_{F_2} = \frac{F_2 - F_1}{M_{Y_2} - M_{Y_1}} \frac{M_{Y_1}}{F_1} \frac{K_{M_{Y_2}}}{K_{M_{Y_1}}} K_{F_1}$$

$$K_{F_3} = \frac{(F_3 - F_1)\, K_{F_1} K_{F_2}}{K_{F_1}(F_2 - F_1) - R F_1 K_{F_2}}$$

and

$$K_{F_4} = 0.05\, K_{F_3}$$

Note that the above force capacities and stiffnesses do not take account of the effects of ovalization and local buckling. As a result, they could be unconservative, particularly for a thin wall tube.

5.12.5 Element Stiffness

The process to form the super-element stiffness begins at a sub-element level. First, the 12 x 12 global stiffness matrix of each sub-element is computed as described in Section 5.13.6. Second, all sub-element stiffness matrices are added together to create a total stiffness matrix,

which has "6*n*+6" degrees of freedom for an "*n*" sub-elements system. Finally, static condensation is performed to obtain a 12 x 12 element stiffness matrix, retaining the degrees of freedom q_1 through q_{12}. This final element stiffness matrix can then be incorporated into the total structural stiffness matrix.

5.12.6 State Determination

One of the major steps in the general nonlinear solution procedure for structural analysis is the state determination of element response (see Figure 5.12-6). The state determination for a beam-column element is mainly to find element end forces response and then to determine the force equilibrium status, provided that the element displacements increment and the element state at the previous state are known.

For a typical beam-column element, the relationship of the force displacements is explicitly known or assumed, though it may not be simple. For the super-element, which is a structure system with many sub-elements, the relationship becomes more complicated and, in most cases, cannot be directly formulated and explicitly stated. This is particularly true when nonlinear behavior is also involved. However, because each sub-element is clearly defined, the response of the super-element can be determined by performing the finite element analysis on the super-element system.

An analysis solver to perform nonlinear finite element analysis is thus created for the super-element. The solver, by itself, is able to perform the solution procedure as illustrated in Figure 5.12-6; and the role of the solver, in conjunction with the global SEASTAR solver, is also illustrated in Figure 5.12-7. This solver, specifically tailored to solve for the buckling of the nonlinear beams, uses either an adaptive

load stepping or a displacement control scheme.

The displacement control scheme is applied when the given incremental displacements are not all zero. In this case, the end displacements are imposed, either in one or several sub-steps, and the corresponding response forces are computed. If the end displacements are all zero and the element load occurs, the load stepping control is used to evaluate the response.

5.12.7 Initial Out-of-Straightness

To consider the initial out-of-straightness effect, the element is modeled as piece-wise linear, by connecting the points on the half cycle of a sine curve. The curve is controlled by two parameters, DELT and ANGL, as shown in Figure 5.12-8. The amplitude control parameter, DELT, represents the ratio of the maximum deflection at midspan to the initial element length, and the position control parameter, ANGL, defines the angle, measured from the local x-y plane to the plane containing the curve element according to the local x axis using the right hand rule.

The initial shape of the element may also be used to take account of the effects of other imperfects of the element, such as residual stress.

5.12.8 Damaged Sections

The damaged sections can be any place along the length of the element, and are defined by the damage length, the damage width, the damage depth, the damage distance, and the damage angle, as shown in Figure 5.12-9. The distance is measured from the center of the damage to the i node, and the damage angle is from the local y axis to the damage center according to the right hand rule. Up to 5 damaged sections can be specified for

each element. Damage may be a hole or a dent. Analytically, each damaged section is represented by a single sub-element. Four sets of action-deformation relationships for two bending, torsional, and axial properties, respectively, should be constructed for each sub-element to represent the damaged section.

To construct the action-deformation relationships, a simplified reduction factor method is used. This method replaces the dented (or holed) portion of the section by an equivalent eccentrically placed circular tube and reduces the capacity and stiffness of the equivalent tube from a virgin section according to an evaluated factor. The factor differs for the damage of a hole or dent type and is considered separately in the following sections:

Hole

A hole in a tubular section is assumed to have a rectangular shape with the damage width and the damage length, as shown Figures 5.12-9 and 5.12-10(a). It is reasonable to assume the reduction factor, h_p, of the axial capacity is the ratio between the damaged and virgin section areas, A′ and A:

$$h_p = \frac{A'}{A} = \frac{\pi - \alpha}{\pi}$$

where $\alpha = \sin^{-1}(1 - W_d/D)$. W_d is the damage width.

The reduction factor, h_m, of the bending capacity is determined using the following equation:

$$h_m = \cos\left(\frac{\alpha}{2}\right) - \frac{\sin(\alpha)}{2}$$

For simplicity, the reduction factor of the torsional capacity is assumed to be "h_m" as well.

By assuming a thin wall tubular section, the eccentricity or the shift of the gravity center of the section (see Figure 5.12-10(a)), due to a hole is determined as

$$e = \frac{D \sin(\alpha)}{2(\pi - \alpha)}$$

Dent

For the damage of dent type, the effect of the occurrence of the plastification in the dented region, as shown in Figure 5.12-10(b), should be incorporated into the reduction factor. The plastification stress is

$$\sigma_p = \sigma_y \frac{D}{t}\left(\sqrt{1.778\delta^2 + \frac{t^2}{D^2}} - 1.3334\delta\right)$$

where $\delta = D_d/D$. D_d is the damage depth.

Thus, by including the plastification effect, the axial force and bending moment capacities, P_d, and M_d, respectively, become

$$P_d = h_p F_3 + \sigma_p A_d \qquad < F_3$$

and

$$M_d = h_m M_{y_3} + \sigma_p A_d \left(\frac{D}{2} - D_d - e \right) \qquad < M_{y_3}$$

where h_p and h_m are the reduction factors for the damaged section of a hole type, $A_d = t * D * \sin(\alpha)$ is the approximate area of the dented region, and F_3 and M_{Y3} are the maximum axial force and bending moment capacities for a corresponding virgin section. Hence, the reduction factors of the dented section become

$$h_p = \frac{P_d}{F_3}$$

and

$$h_m = \frac{M_d}{M_{y_3}}$$

For simplicity, the eccentricity due to a dent (see Figure 5.12-10(b)) is assumed to be the same as that of a hole-type damage.

Note that only the local damage to the section is formulated here. The overall deflection due to the damage is not considered. To take this effect into account, the initial out-of-straightness option can be used.

A comparison of the buckling load histories between the laboratory test data of a dented brace and the SEASTAR result of the super-element is shown in Figure 5.12-11. The comparison indicates that the maximum capacity of the damaged brace can be predicted fairly well, while the post-buckling strain of the super-element behaves stiffer than a real damaged brace. This is caused by the fact that dent growth is not

considered when the super-element reaches beyond the post-buckling part of its load history.

5.12.9 Joint Can

Joint cans, stiffened sections at the proximity regions to the element ends as shown in Figure 5.12-12, can be specified. Similar to the main span, the joint can is also assumed to have a tubular cross-section and is defined by its own diameter, thickness, Young's modulus and yield stress. Analytically, each joint can is represented by a single sub-element. Thus, the input properties of the sub-element to represent the joint can be determined in a way similar to those of the main span.

5.12.10 Flexible Joint

Bi-linear flexible joints can exist at both ends of the element. The stiffness and capacity of the joint are defined through three action-deformation relationships for axial force and two bending moments, respectively. The input data needed for each relationship include the elastic stiffness, K_e, the yield force, F_y, and the stiffness after yield, K_y, as shown in Figure 5.12-13(a). The axial forces and the bending moments are assumed to be uncoupled while the two moments are coupled through an elliptical interaction surface.

In the analytical model, each flexible joint is represented by a single sub-element of a relatively small length (about one hundredth of the total length of the super-element), as shown in Figure 5.12-13(b). The input properties of the sub-element to represent the flexible joint are calculated from the basic, user-provided data. Because the flexible joint often does not consider a torsional failure, the torsional effect

is ignored by assigning large torsional capacity and stiffnesses (20 times bending capacity) to the sub-element.

Interaction surface type 4, described in Section 5.13.7 and shown in Figure 5.13-4, is chosen to model the force interaction of the joint. This surface, with very large control constants, a_1 and a_2, enables the axial force and bending moments almost uncoupled. For example, when a_1=5.0 and a_2=10.0 are used, the occurrence of a bending moment with a half magnitude of the yield capacity only reduces the axial force to reach the yield surface by 0.01 percent, or vice versa. This surface assumes two bending moments are coupled through an elliptical interaction surface.

To define a flexible joint, which is not right at the location of the end node (e.g., which may be located at the face of the members to which this element connects), the end eccentricity option can be combined.

5.12.11 End Eccentricity

A flexible joint is often assumed at near the faces of the large stiffer member, which the super-element connects to, rather than at the theoretical centerlines of the member. This effect can be approximated by postulating rigid, infinitely strong connecting links between the nodes and the element ends, as shown in Figure 5.12-14.

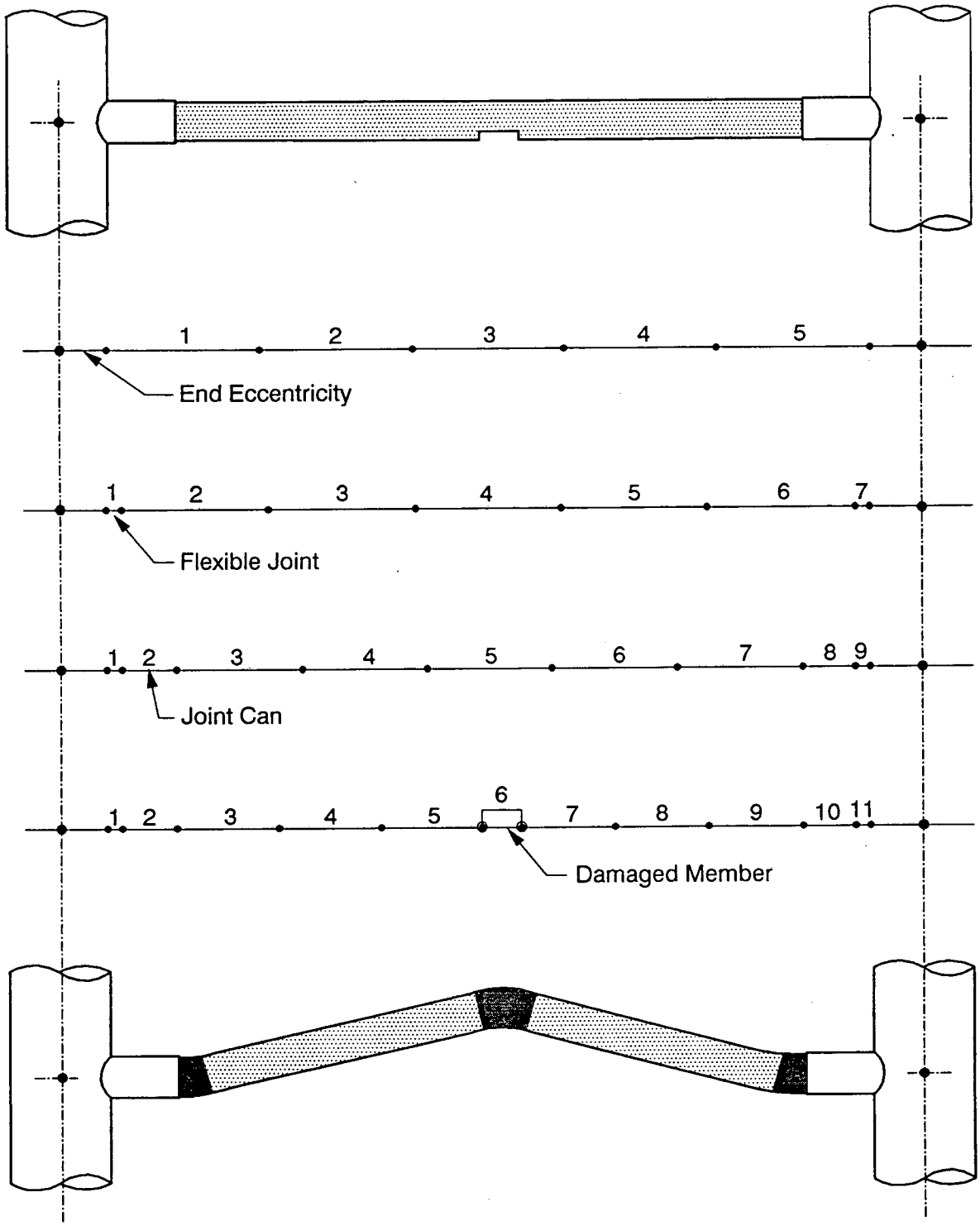

Figure 5.12-1 BUCKLING BEAM MODELS

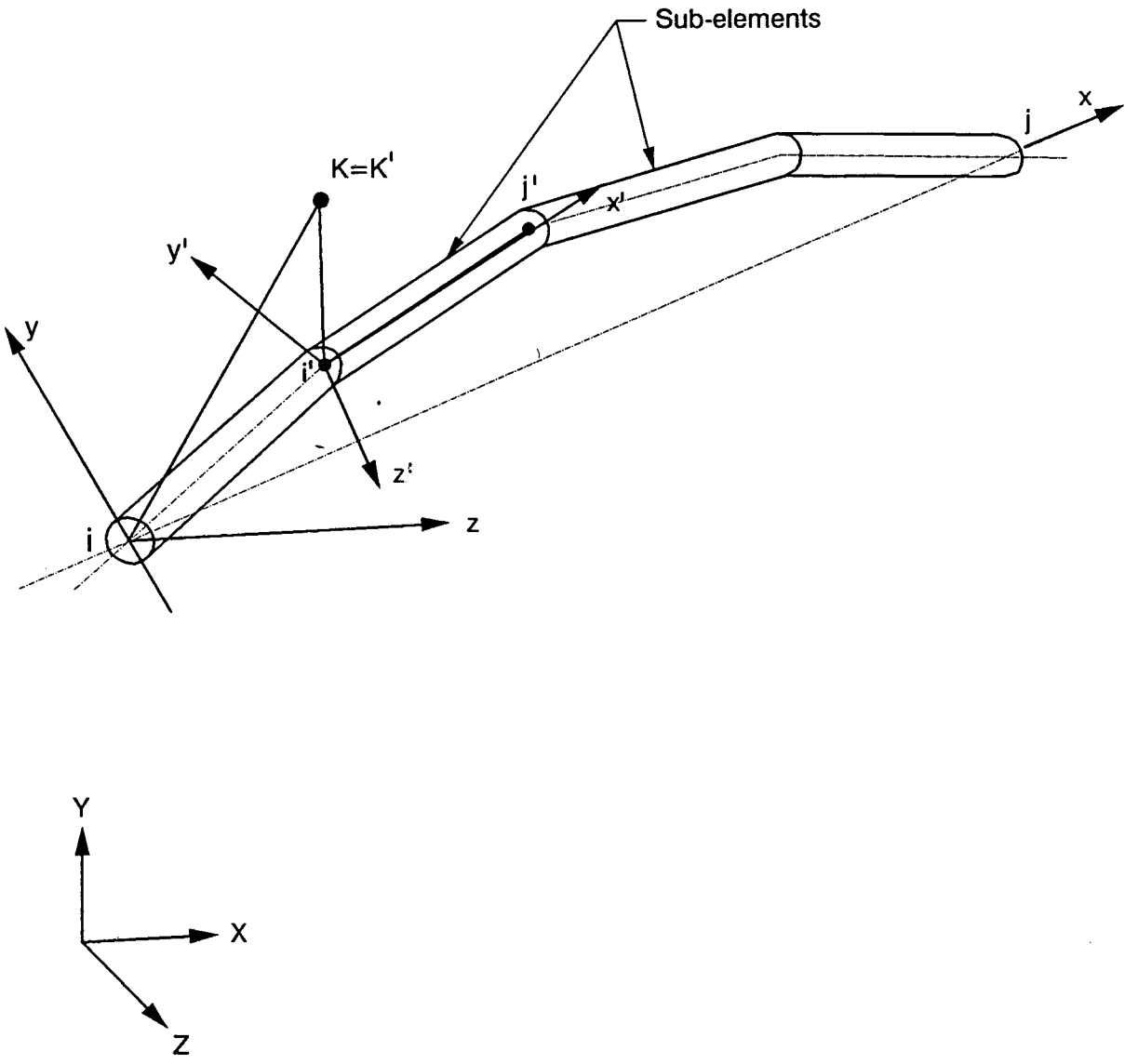

Figure 5.12-2 ELEMENT AXES

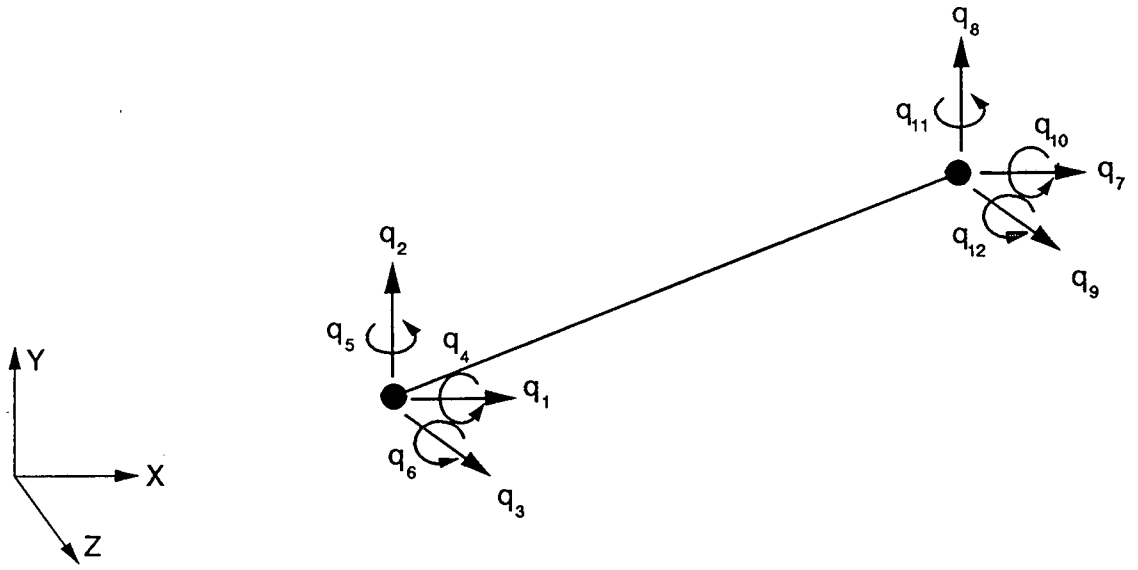

(a) GLOBAL DISPLACEMENTS

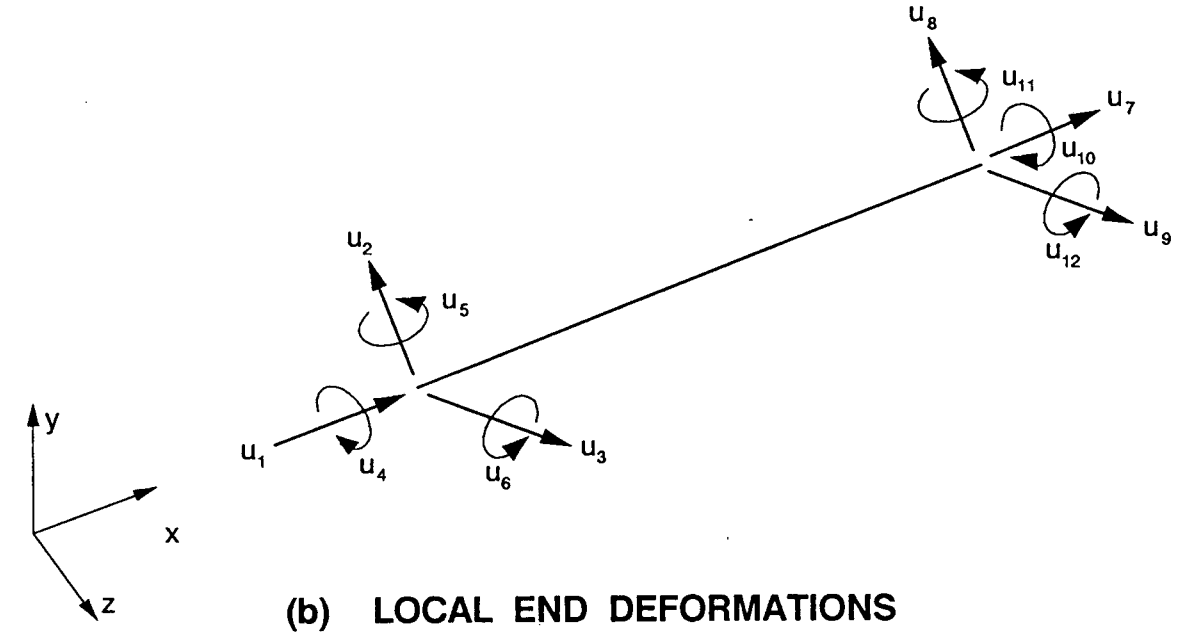

(b) LOCAL END DEFORMATIONS

Figure 5.12-3 ELEMENT DEGREES OF FREEDOM

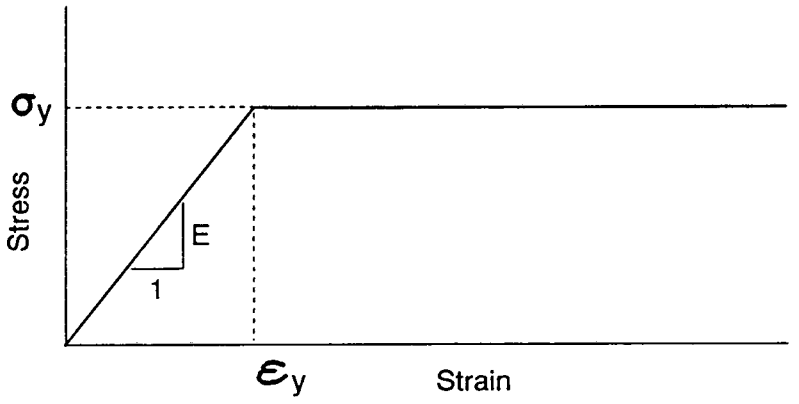

(a) STRESS-STRAIN RELATIONSHIP

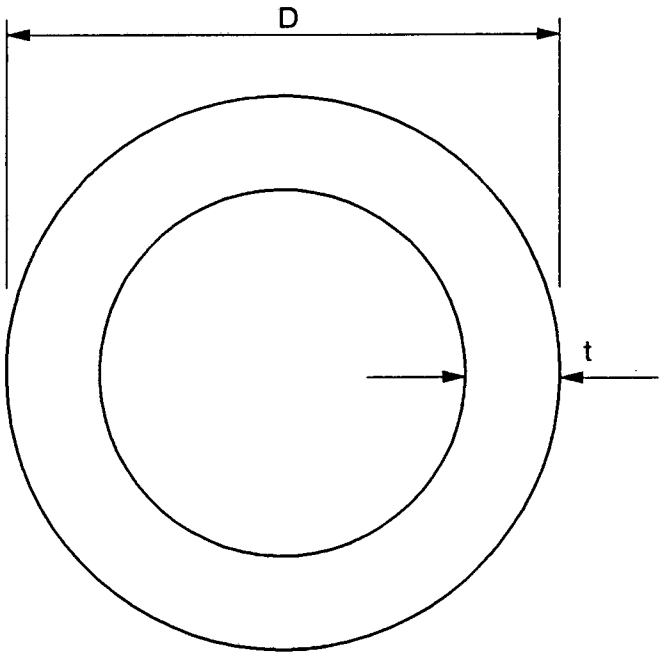

(b) SECTION PROPERTIES

Figure 5.12-4 MATERIAL AND SECTION PROPERTIES

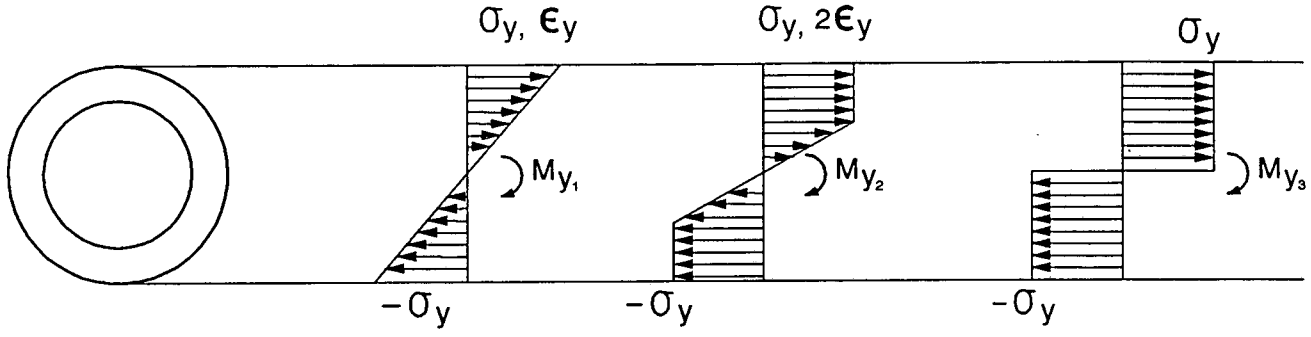

(a) BENDING CAPACITIES

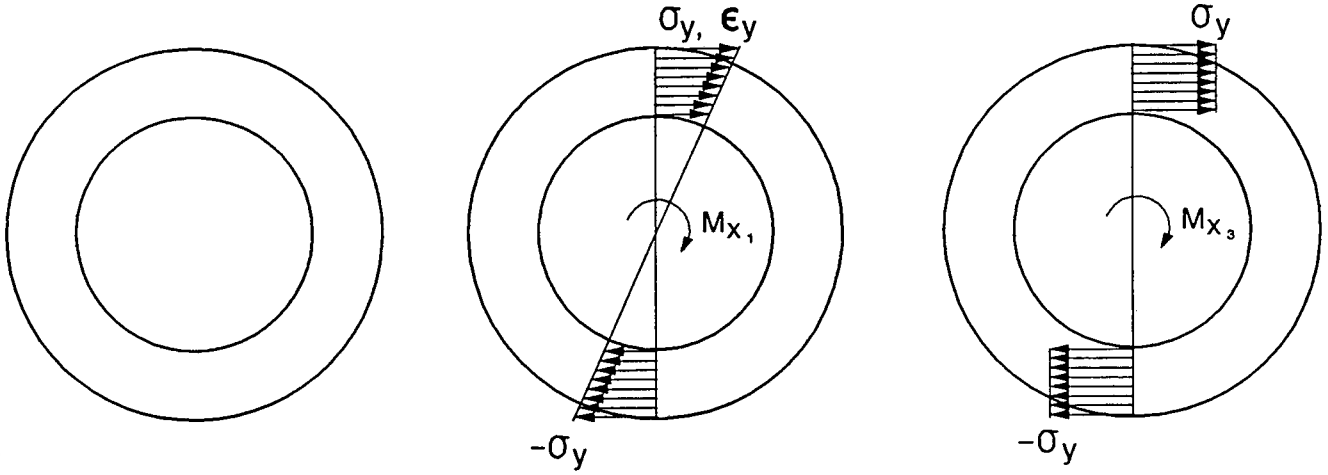

(b) TORSIONAL CAPACITIES

Figure 5.12-5 YIELD CAPACITIES OF DIFFERENT STAGES

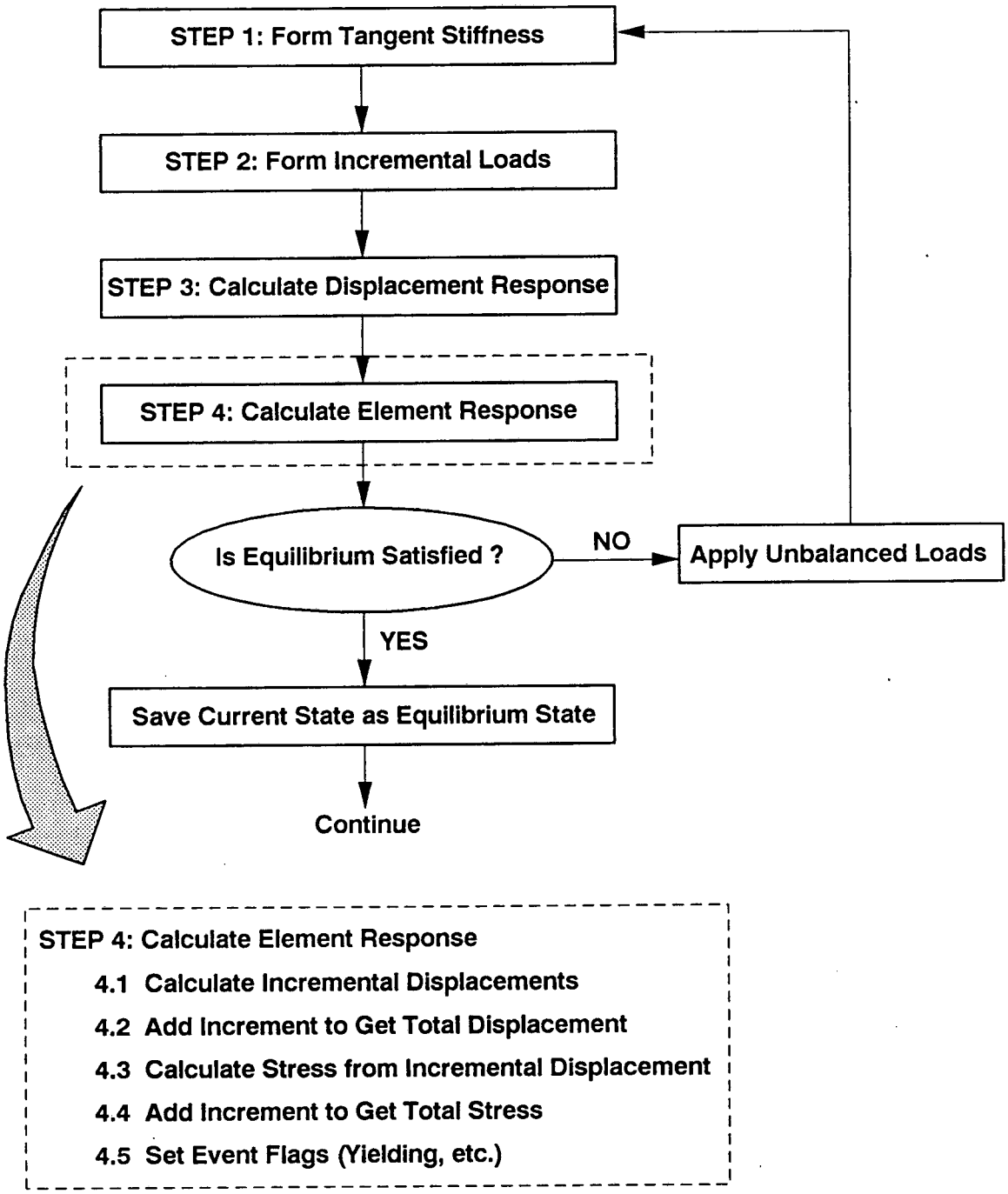

Figure 5.12-6 GENERAL NONLINEAR SOLUTION PROCEDURE

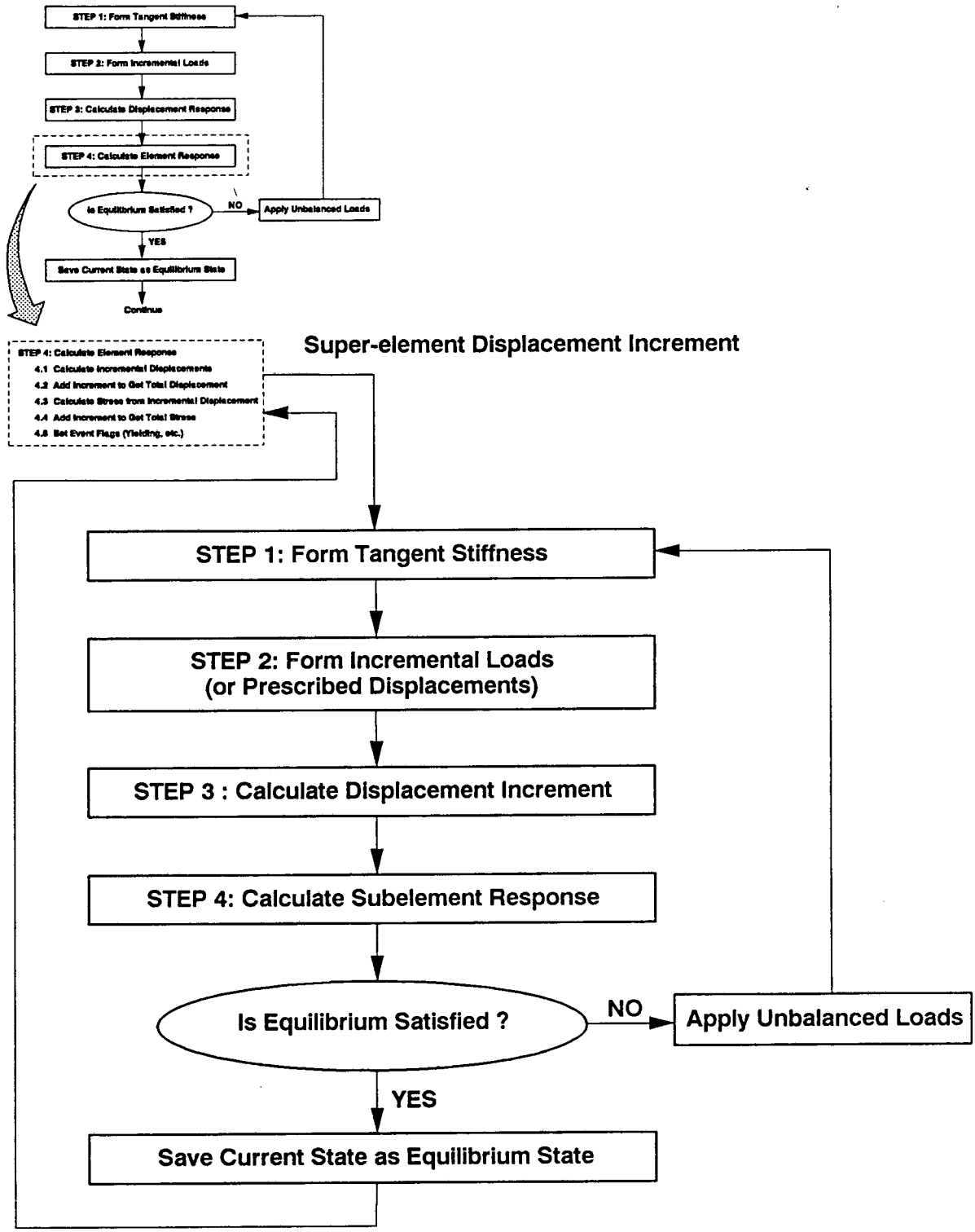

Figure 5.12-7 SUPER-ELEMENT SOLUTION PROCEDURE

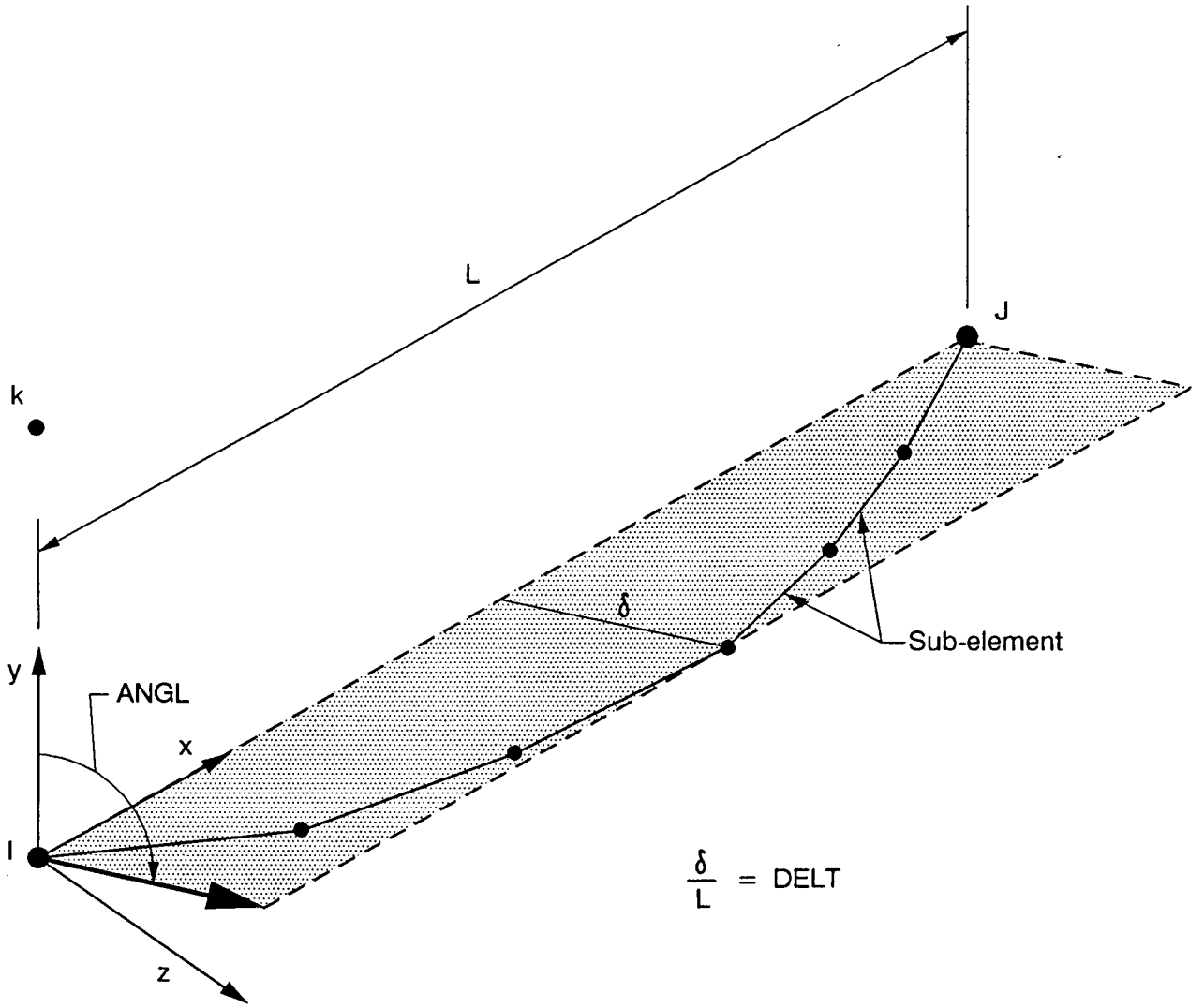

Figure 5.12-8 - ELEMENT OUT-OF-STRAIGHTNESS CONFIGURATION

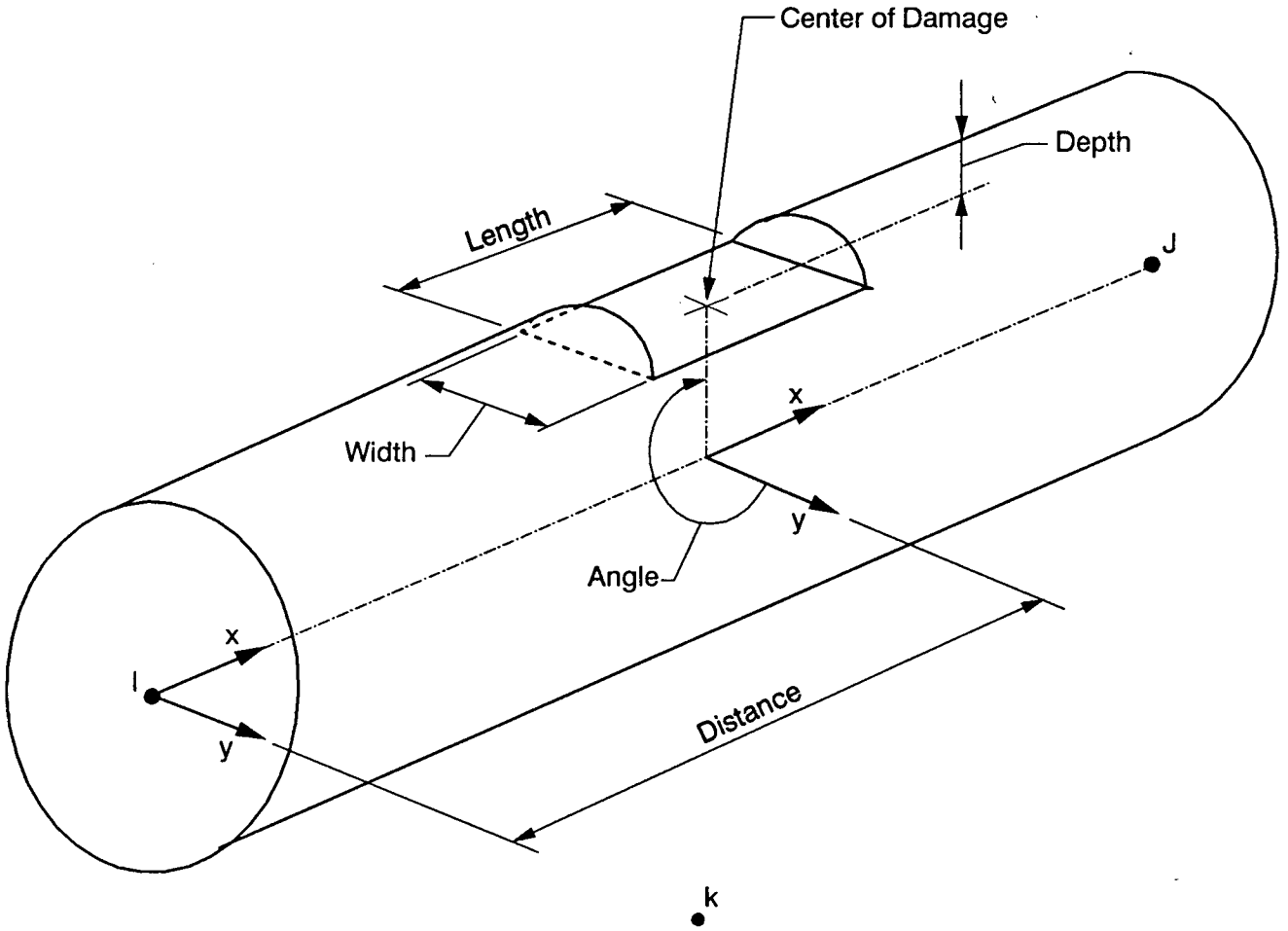

Figure 5.12-9 MEMBER DAMAGE

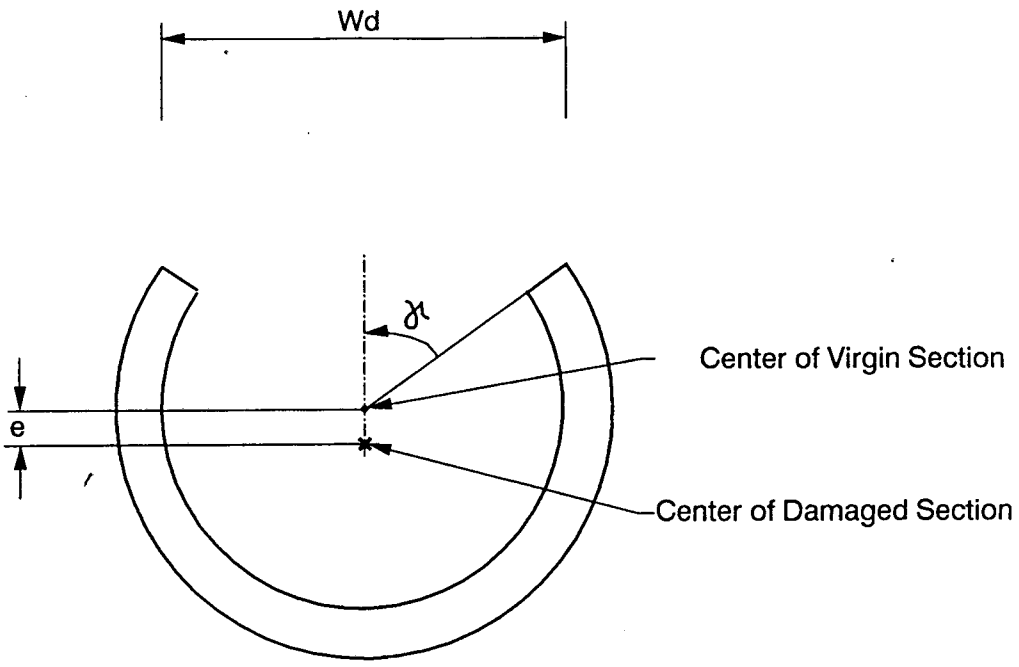

(a) SECTION WITH HOLE

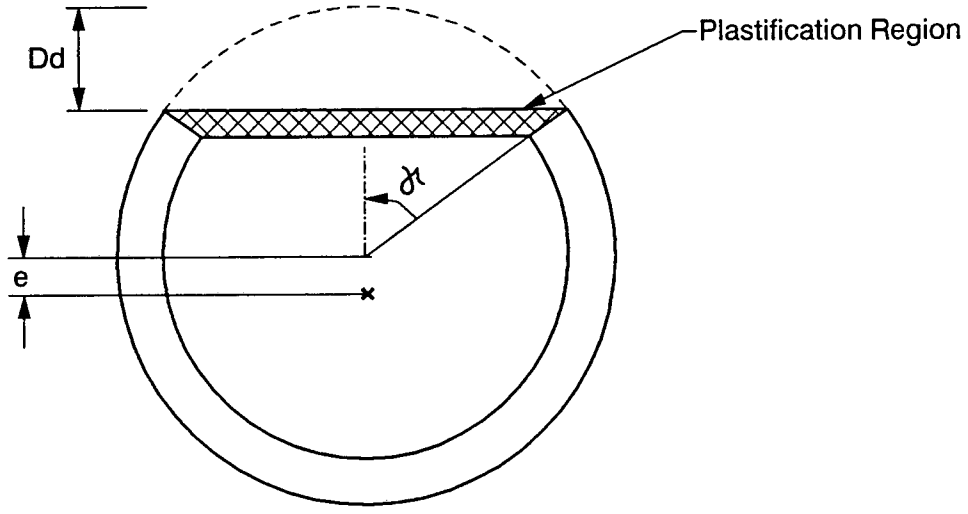

(b) SECTION WITH DENT

Figure 5.12-10 CROSS SECTIONS OF DAMAGED MEMBER

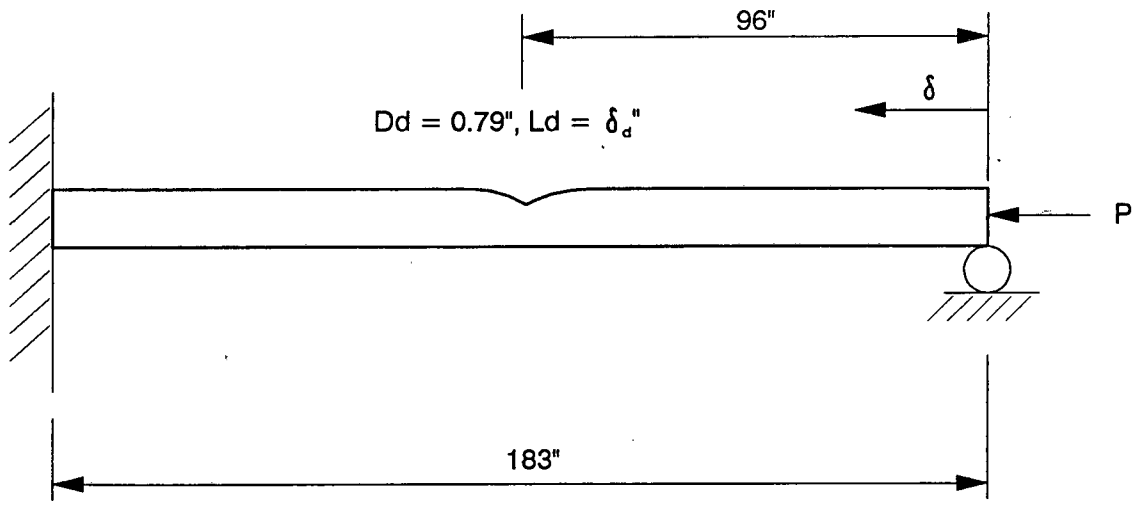

D = 10.34", t = .2045", E = 24243 ksi, σ_y = 62.27 ksi

(a) BERKELEY TEST BRACE CONFIGURATION

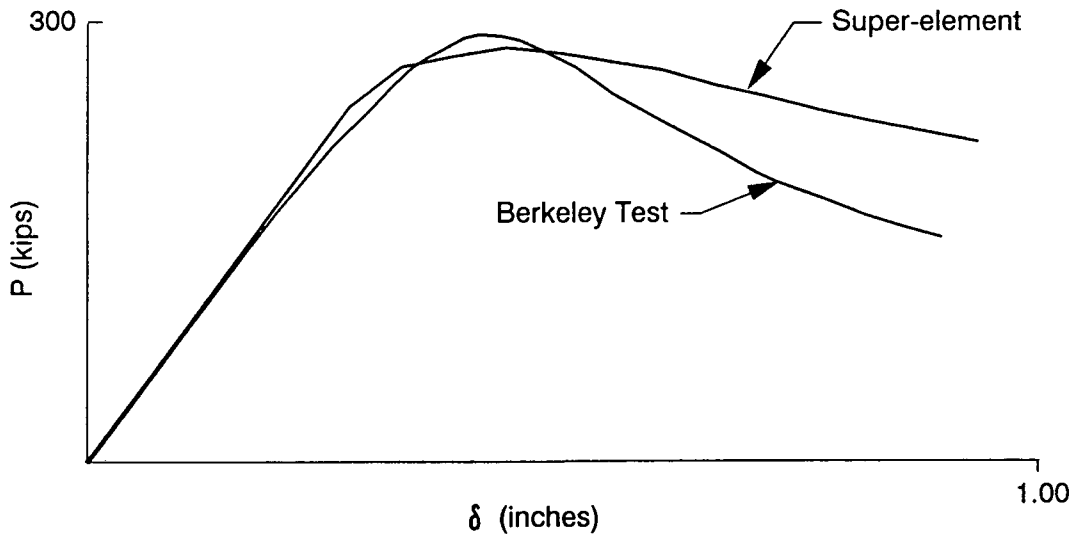

(b) AXIAL LOAD VERSUS AXIAL SHORTENING

Figure 5.12-11 COMPARISON OF BERKELEY TEST BRACE AGAINST SUPER-ELEMENT

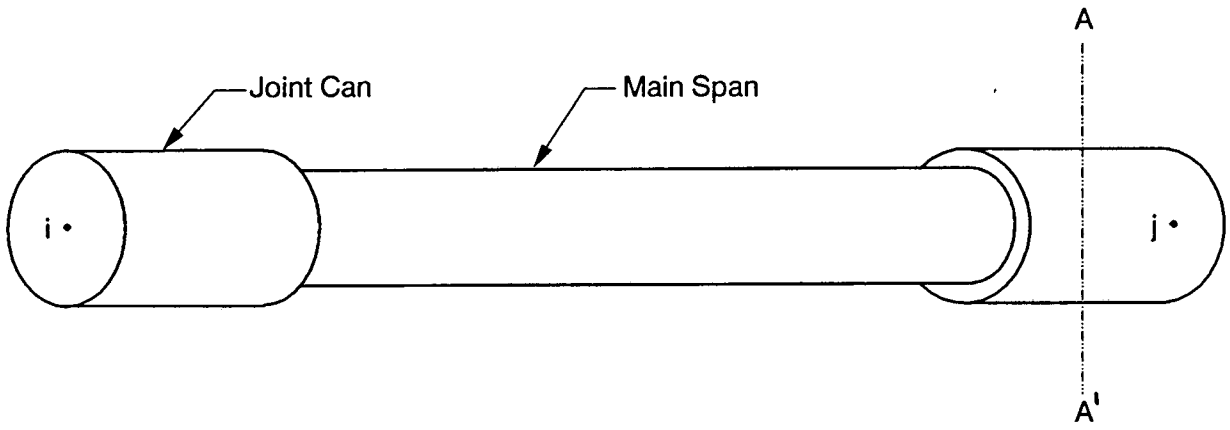

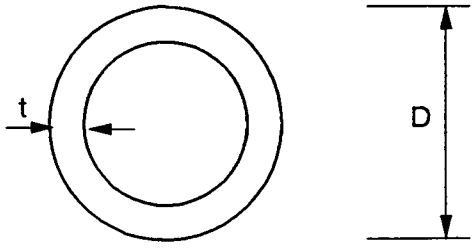

CROSS SECTION A-A'

Figure 5.12-12 JOINT CANS

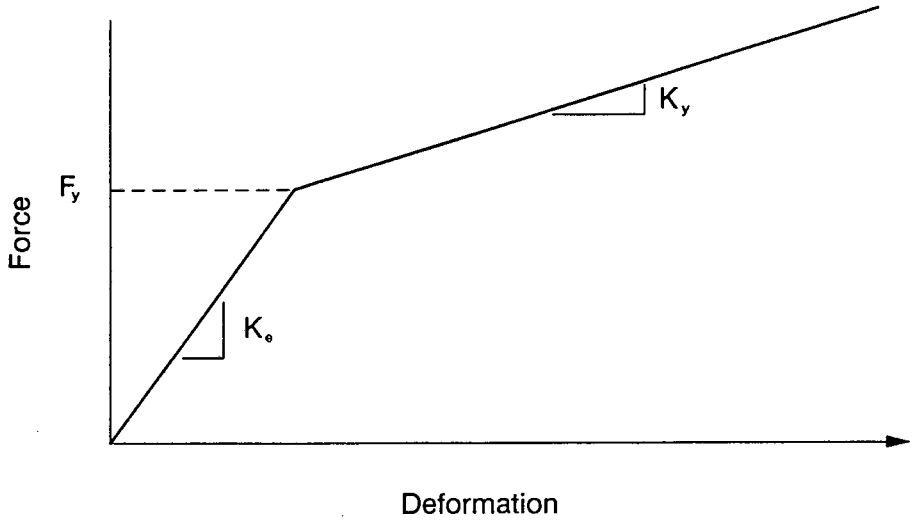

(a) JOINT ACTION VERSUS DEFORMATION

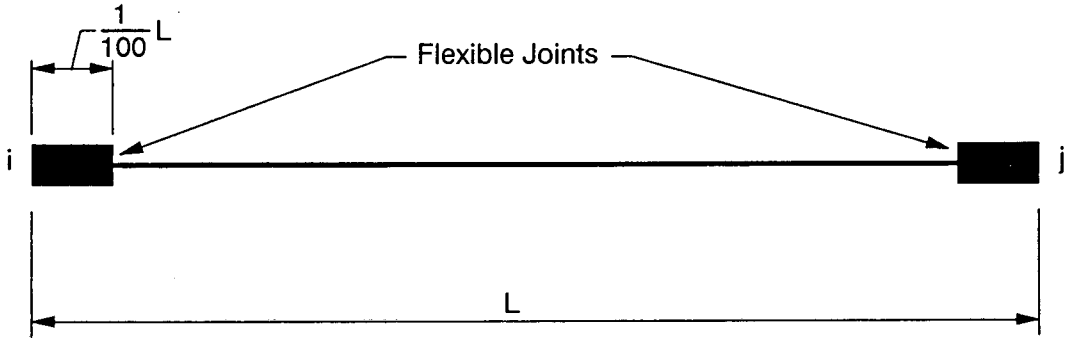

(b) FLEXIBLE JOINT MODEL

Figure 5.12-13 FLEXIBLE JOINTS

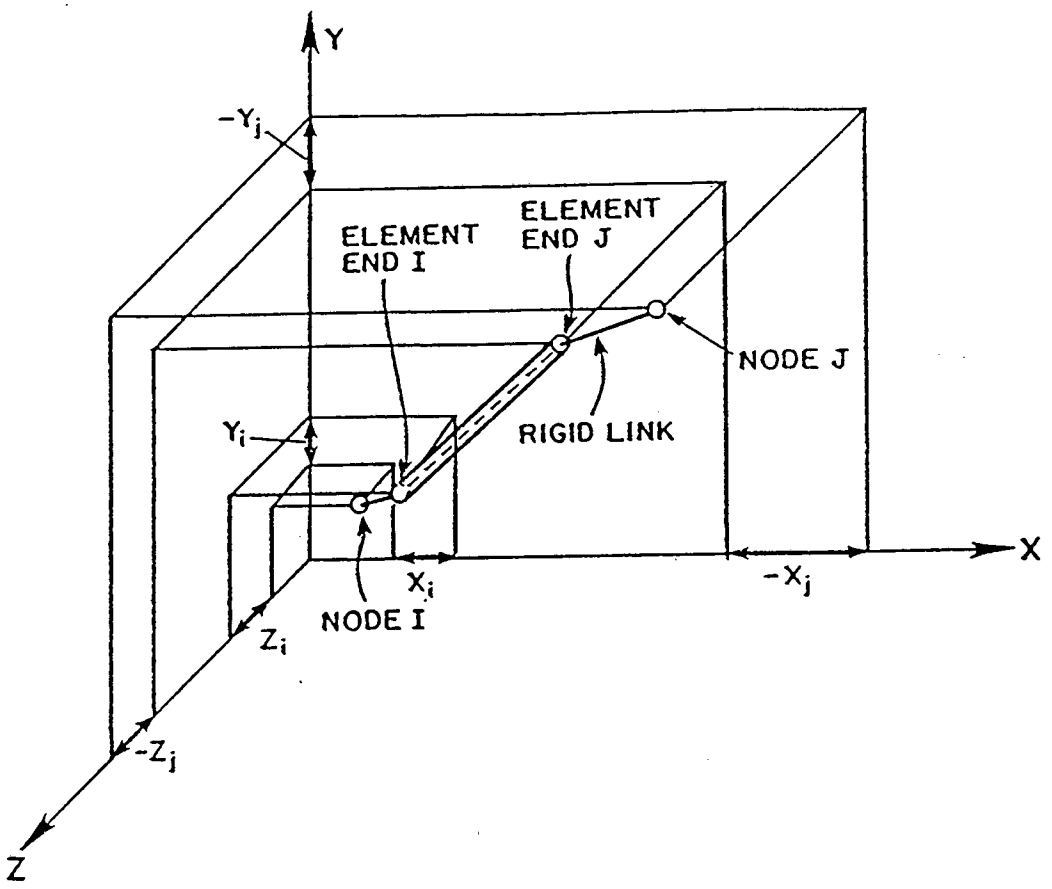

Figure 5.12-14 END ECCENTRICITIES

5.13 Distributed Plasticity Beam-Column Element

This element is intended primarily to model inelastic effects in beams and columns. The element takes account of moment-force interaction for columns and of bending moment interaction for biaxial bending.

Nonlinear action-deformation (stiffness) properties in axial, torsional, and two bending directions can be separately defined. The interaction of action forces can be described.

The effects of eccentric end connections and varying cross section along the element length can be considered if desired. Initial force of the element can be also assigned.

Response of the element is monitored at two cross sections, located at two Gauss points and is integrated over the element with use of shape functions. From testing, it shows that this element, in computation aspects, is more stable than a lumped type element described in Section 5.4.

5.13.1 Basic Assumptions

The basic assumptions of the element are stated as follows:

1. The element is straight and can be arbitrarily oriented in space.
2. Element deformation should be small for each step.
3. Inelastic behavior is defined using multi-linear stress resultant-strain resultant relationships for axial, torsional, and two bending properties, separately.

4. Bending moments, torque and axial force are interacted by means of yield interaction surfaces.
5. Kinematic strain hardening is assumed for cyclic loading. The kinematic hardening rule corresponds to translation of the yield surface without change of size or shape.
6. Cross section plasticity is monitored at two cross sections in the element and is assumed to be distributed over the element length.
7. If considered, large displacement effects are based on an engineering theory (i.e. not a consistent continuum mechanics approach).

5.13.2 Element Axes

Element properties and results are specified in the local coordinate system x, y, and z, which is defined by three nodes i, j, and k and as shown in Figure 5.13-1. Nodes i and j define the local x axis. The local y axis is normal to the local x axis and resides in the plane containing the k node and local x axis. The local z axis is defined orthogonal to the local x and y axes, using the right hand rule. In Figure 5.13-1, capital X, Y, and Z are for the global coordinate system.

5.13.3 Degrees of Freedom

The element has two external nodes and two internal Gauss stations, as shown in Figure 5.13-2(a). The external nodes connect to the complete structure and have six degrees of freedom, each, namely X, Y, Z global translations and X, Y, Z global rotations. The element nodal displacements in the global coordinates are written as

$$q = (q_1, q_2, \ldots, q_{12})$$

After deletion of the six rigid body modes for the complete element and transformation to the local element coordinates, the six deformation degrees of freedom shown in Figure 5.13-2(b) remain.

The transformation from global displacements to element deformations is

$$v = \alpha\, q$$

in which

$v^T = (v_1, v_2, \ldots, v_6)$ = element deformations (Figure 5.13-2(b)).

$q^T = (q_1, q_2, \ldots, q_{12})$ = element nodal displacement (Figure 5.13-2(a)).

and the transformation matrix "α" is well known.

5.13.4 Shape Functions

Response of the element is monitored at two cross sections or "slices", located at Gauss stations. Each slice has six deformations, namely, axial deformation, rotational deformations about each of the local x, y, z axes, and shear deformations along the y and z axes. The deformations are arranged in the vector w,

$$w^T = (w_1, w_2, \ldots, w_6)$$

The Deformation vector "w" at any location can be related to the end deformation vector "v" through shape functions, which are obtained based on the assumption of a uniform elastic beam. The shape functions are assumed to be applicable, in both the elastic and yield states.

With use of the shape functions, the element performance can be determined by Gauss integration (i.e. conventional finite element techniques).

5.13.5 Section Properties

The relationships between actions (stress resultants) and deformations (strain resultants) must be provided for the two cross sections at the Gauss points. Relationships are shown in Figure 5.13-3 for each of four action-deformation pairs, namely (1) bending moment in the local y axis, M_y, and corresponding curvature, ψ_y; (2) bending moment in the local z axis, M_z, and corresponding curvature, ψ_z; (3) torque, M_x, and corresponding rate of twist, ψ_x; and (4) axial force, F, and corresponding strain, ϵ. Each relationship may have up to four linear segments, as shown. The relationships may be of different shape for each stress resultant. It is necessary, however, for the deformation values at changes in stiffness to have the same ratios for all relations.

5.13.6 Element Stiffness

To compute element stiffness at any state, a 4 x 4 elastic slice flexibility matrix is first formed, in terms of the section actions M_y, M_z, M_x, and F at each Gauss station. This matrix is then modified by adding the plastic flexibilities on each active yield surface to give a 4 x 4 elasto-plastic slice flexibility. This flexibility is inverted to obtain a 4 x 4 slice stiffness, which is then expanded to a 6 x 6 slice stiffness in terms of the degrees of freedom w_1 through w_6 by adding stiffness to account for shear deformations along the y and z axes. The stiffness matrix in terms of the degrees of freedom v_1 through v_6 is then determined by Gauss integration using the conventional finite element technique. Finally, the stiffness is transformed into the 12 x 12 global

element stiffness matrix and is able to be incorporated into the total structural stiffness matrix.

5.13.7 Modeling of Inelastic Behavior

First Interaction Surfaces

The actions M_y, M_z, M_x, and F interact with each other after the magnitude of the actions reaches a certain level. To model this effect, an interaction surface (yield surface) method is used. And, to allow for a variety of applications, five different yield surfaces are available. These surfaces are all four-dimensional (i.e., M_y, M_z, M_x, and F), and hence cannot be shown easily using diagrams. The surfaces differ, however, mainly in the way in which the axial force interacts with the three moments. Hence, the differences can be illustrated using the three dimension diagrams as Figure 5.13-4 where the Mi and Mj axes indicate any two of the moments, and the F axis indicates axial force. The equations defining the interaction surfaces are shown in the figures too.

Surface 1 is elliptical and is the simplest mathematically. Surfaces 2, 3 and 4 allow more realistic modeling of moment-force interaction for cases in which axial force effects are substantial. Surface 5 is included for greater generality in special cases.

Interaction Surfaces for Subsequent Yield

For modeling a slice with nonlinear material properties, it is assumed that the behavior is elastic-plastic-strain-hardening, as shown in Figure 5.13-5. First yield is governed by the initial yield surface; for each change of stiffness, there is a corresponding "subsequent" yield surface. These surfaces are assumed to have the same basic form as the surface of

first yield. However, because the action-deformation relationships may be different shape for each action, the surfaces for the first and subsequent yield will generally not have identical actual shapes. An example is 2-D stress resultant space is shown in Figure 5.13-5.

Elastic and Plastic Stiffnesses

The initial slopes, K_1, for the action-deformation relationships are defined as the elastic stiffnesses and are expressed as:

$$K_1 = Kse = diag\ (EI_y\ \ EI_z\ \ GJ\ \ EA)$$

where E is Young's modulus, G is shear modulus, I_y and I_z flexural inertias in local x and y axes, respectively, J is torsional inertia, and A is section area. The slopes of subsequent segments of the action-deformation relationships are denoted as K_2, K_3, and K_4 and are defined as the post-yield stiffnesses.

The assumed multi-linear action-deformation relationship for each force component can be modeled as a set of springs, consisting of an elastic spring and a series of rigid plastic springs, as shown in Figure 5.13-6. The plastic stiffnesses, K_p, of the rigid-plastic springs can be related to the post-yield stiffness values, K. The relationship between plastic stiffness, K_{pi} and post-yield stiffnesses, K_i and K_{i+1} can be obtained as:

$$K_{pi} = \frac{K_i K_{i+1}}{K_i - K_{i+1}}$$

For each rigid plastic spring, a plastic stiffness matrix is defined as:

$$K_{sp} = diag(K_{M_y}, K_{M_z}, K_{M_x}, K_F)$$

where KM_y, KM_z, KM_x, and KF are the plastic stiffnesses of the individual action-deformation relationships, obtained from the equation above.

Hardening Behavior

After first yield, the yield surfaces are assumed to translate in stress resultant space, obeying a kinematic hardening rule (translation without change of shape or size). An extension of the Mroz theory of material plasticity is used to define the hardening behavior. Because the interaction surfaces are generally not exactly similar, overlapping of surfaces can occur. As a result, the hardening behavior is more complex than in the basic Mroz theory. For example, in Figure 5.13-5(b), the current stress resultant point, A, lies on yield surfaces YS_1, YS_2, and YS_3. Hence, all three plastic springs have yielded, and the direction of plastic flow is a combination of the normal vectors n_1, n_2, and n_3.

Plastic Flow

Interaction among the stress resultants is considered as shown diagrammatically in Figure 5.13-5. Yield begins when the first yield surface is reached. The surface then translates in stress resultant space, the motion being governed by the plastic flow of this first yield surface. Translation of the first surface continues until the second surface is reached. Both surfaces then translate together, governed by a combination of plastic flow on both of the surfaces. For any yield surface, plastic flow is assumed to take place normal to that surface. If two or more surfaces are moving together, the total plastic

deformation is equal to the sum of the individual plastic deformations for each yield surface, directed along the respective normal directions at the action point. After some arbitrary amount of plastic deformation, the situation might be as illustrated in Figure 5.13-5(b).

On unloading, the elastic stiffness values, K_1, govern until the yield surface of the first subhinge is again reached (Figure 5.13-5(b)). The surface then translates as before.

5.13.8 End Eccentricity

Plastic hinges in frames and coupled frame-shear wall structures will form near the faces of the joints rather than at the theoretical joint centerlines. This effect can be approximated by postulating rigid, infinitely strong connecting links between the nodes and the element ends, as shown in Figure 5.13-7.

5.13.9 Initial Forces

For structures in which static analyses are carried out separately (i.e. outside the SEASTAR program), initial member forces may be specified. The sign convention for these forces is as shown in Figure 5.13-8. These forces are not converted to loads on the nodes of the structure, but are simply used to initialize the element end actions. For this reason, initial forces need not constitute a set of actions in equilibrium. The only effects they have on the behavior of the system are (a) to influence the onset of plasticity and (b) to affect the geometric stiffnesses.

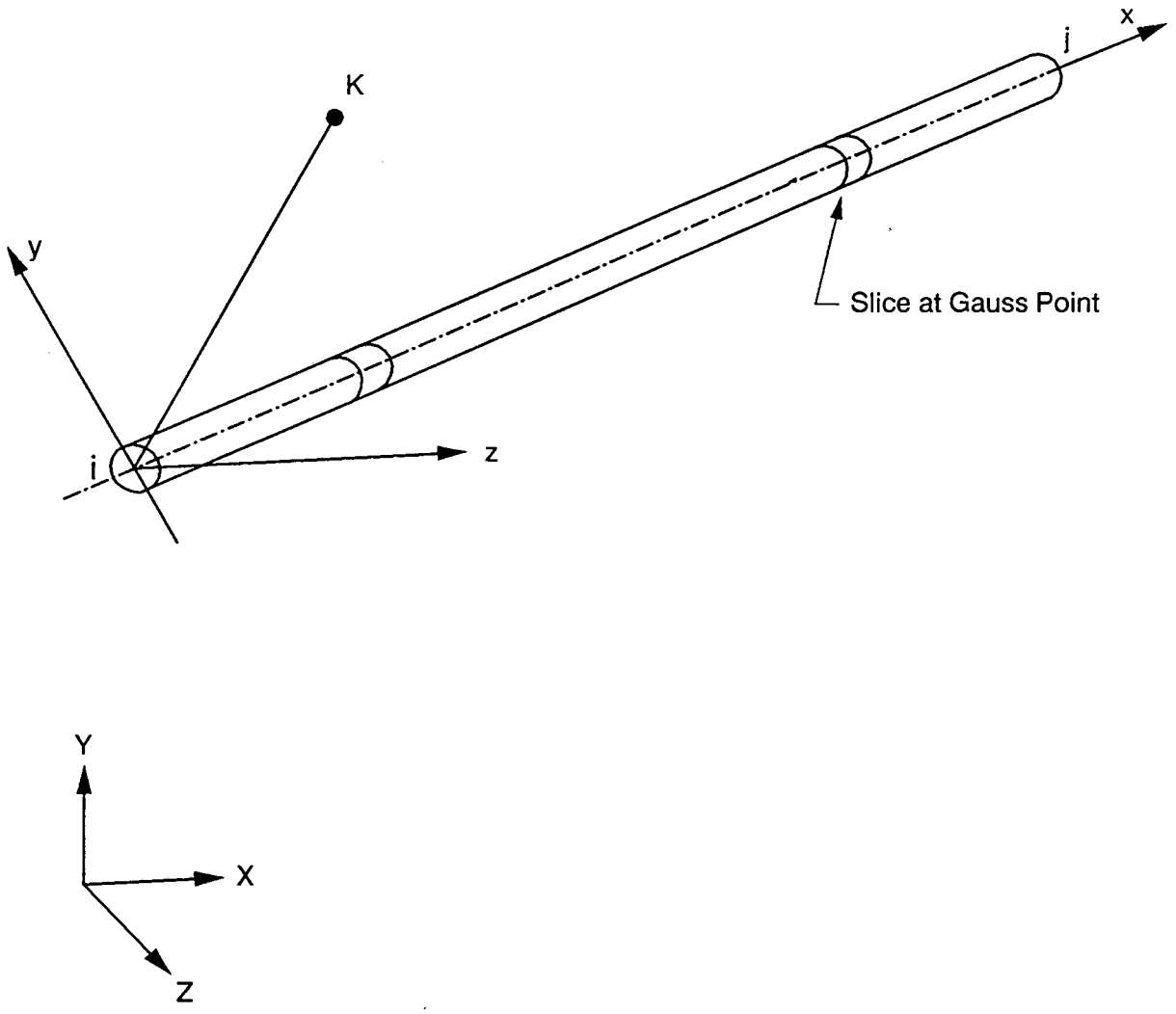

Figure 5.13-1 ELEMENT AXES

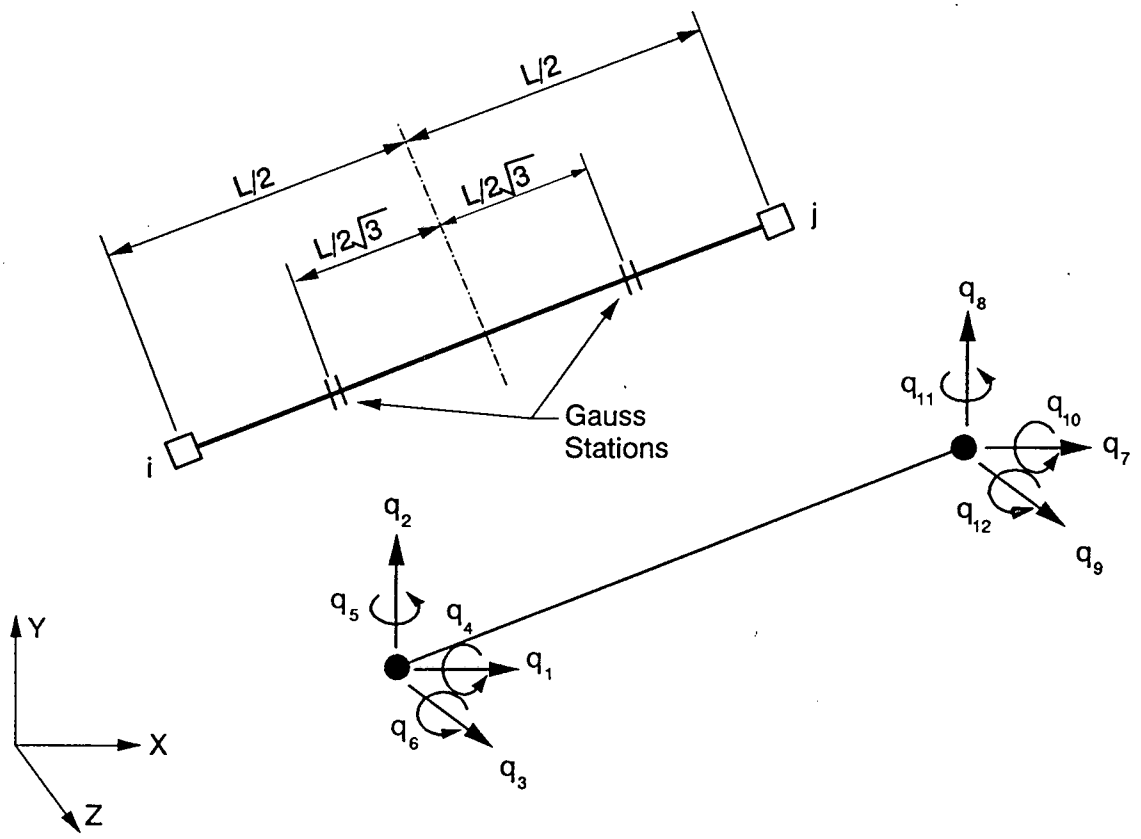

(a) GLOBAL DISPLACEMENTS

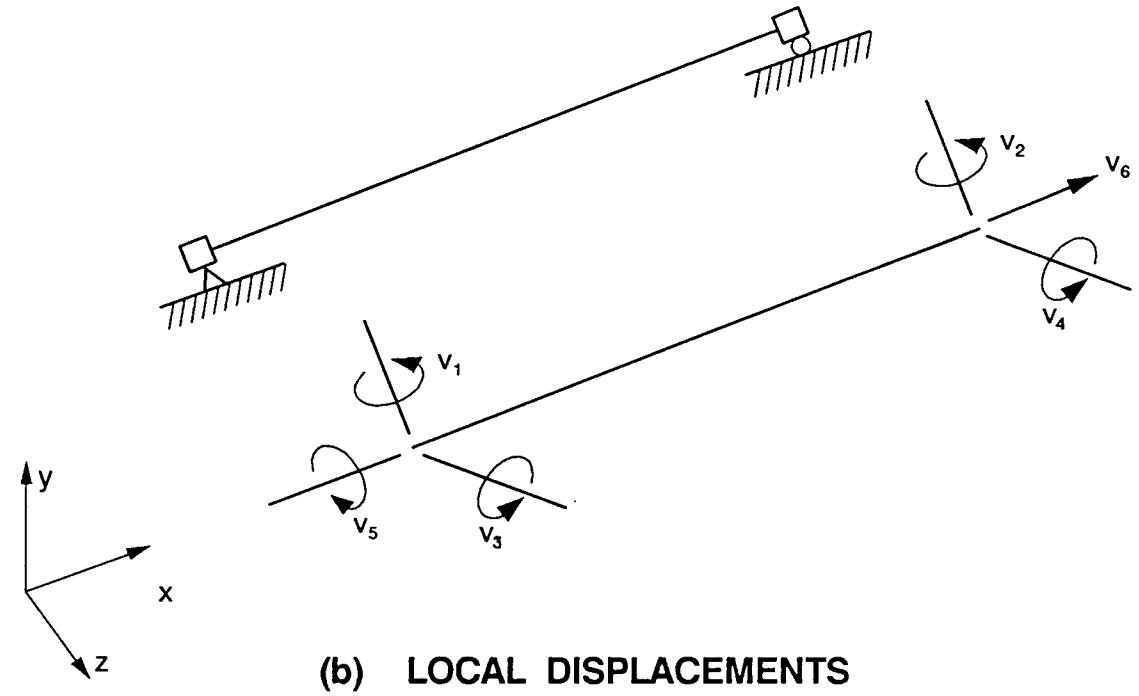

(b) LOCAL DISPLACEMENTS

Figure 5.13-2 ELEMENT DEGREES OF FREEDOM

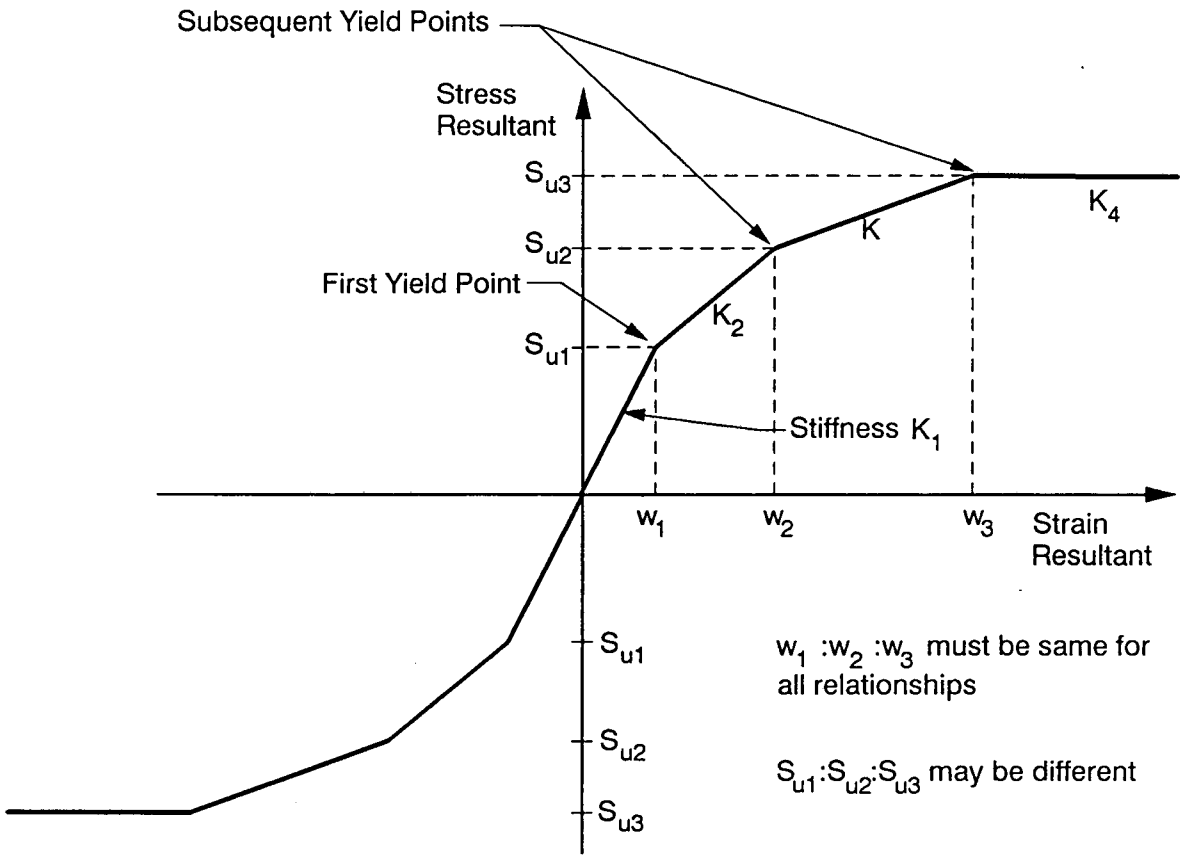

Figure 5.13-3 STRESS VS. STRAIN RESULTANT RELATIONSHIP

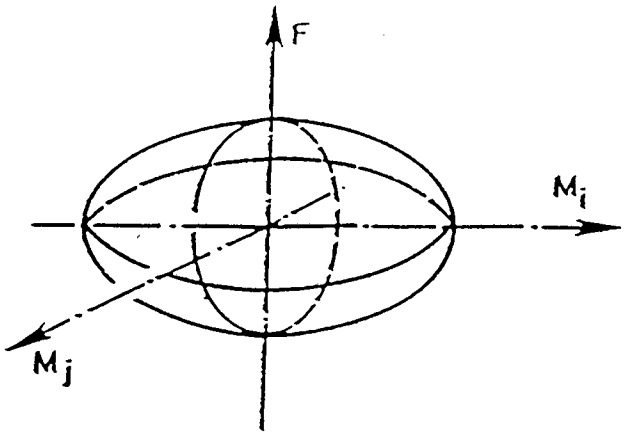

$$\phi = \left(\frac{M_y}{M_{yu}}\right)^2 + \left(\frac{M_z}{M_{zu}}\right)^2 + \left(\frac{M_x}{M_{xu}}\right)^2 + \left(\frac{F}{F_u}\right)^2 = 1$$

(A) SURFACE TYPE 1

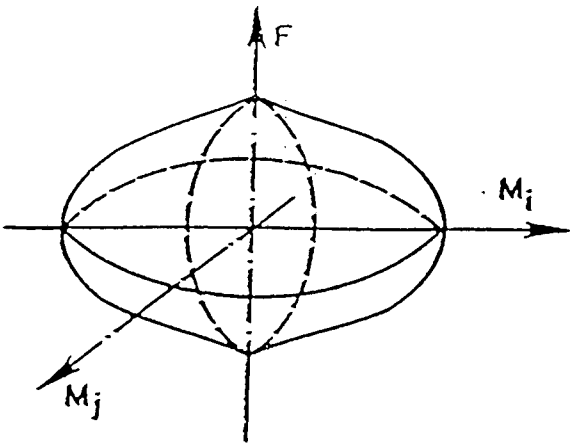

$$\phi = \left[\left(\frac{M_y}{M_{yu}}\right)^2 + \left(\frac{M_z}{M_{zu}}\right)^2 + \left(\frac{M_x}{M_{xu}}\right)^2\right]^{1/2} + \left(\frac{F}{F_u}\right)^2 = 1$$

(B) SURFACE TYPE 2

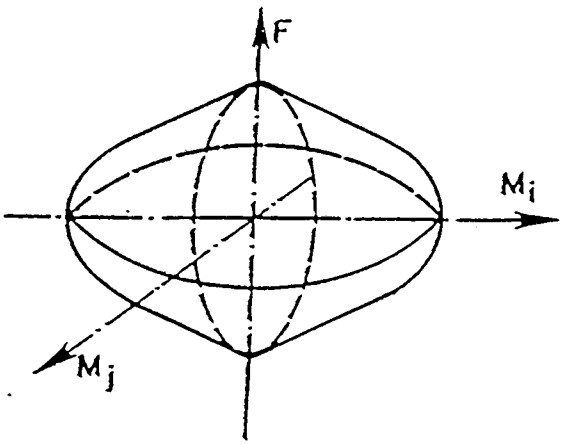

$$\phi = \left[\left(\frac{M_y}{M_{yu}}\right)^2 + \left(\frac{M_z}{M_{zu}}\right)^2 + \left(\frac{M_x}{M_{xu}}\right)^2\right]^{1/2} + \left(\frac{F}{F_u}\right)^{a_1} = 1$$

(C) SURFACE TYPE 3

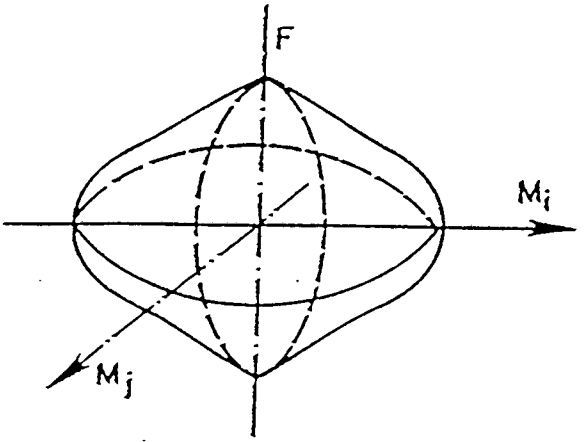

$$\phi = \left[\left(\frac{M_y}{M_{yu}}\right)^2 + \left(\frac{M_z}{M_{zu}}\right)^2 + \left(\frac{M_x}{M_{xu}}\right)^2\right]^{a_1} + \left(\frac{F}{F_u}\right)^{a_2} = 1$$

(D) SURFACE TYPE 4

Figure 5.13-4 INTERACTION SURFACES

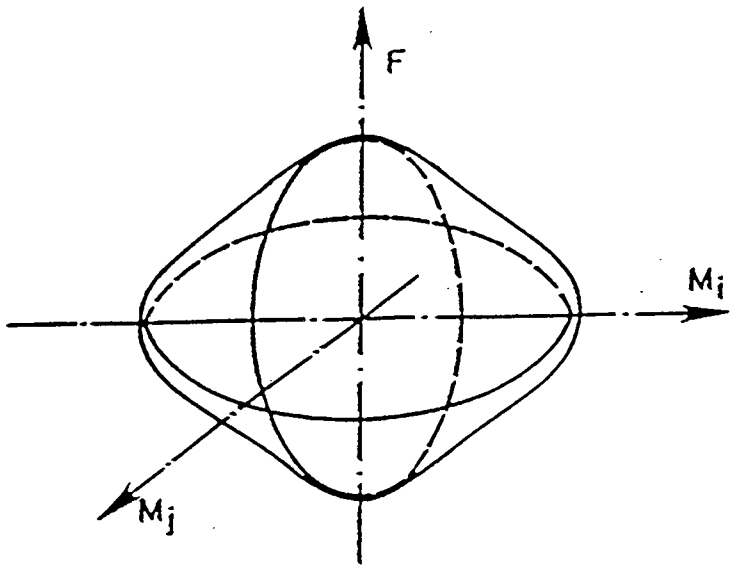

$$\phi = \left(\frac{M_y}{M_{yu}}\right)^{a_1} + \left(\frac{M_z}{M_{zu}}\right)^{a_2} + \left(\frac{T}{T_u}\right)^{a_3} + \left(\frac{F}{F_u}\right)^{a_4} = 1$$

(E) SURFACE TYPE 5

Figure 5.13-4 INTERACTION SURFACES (CONT'D)

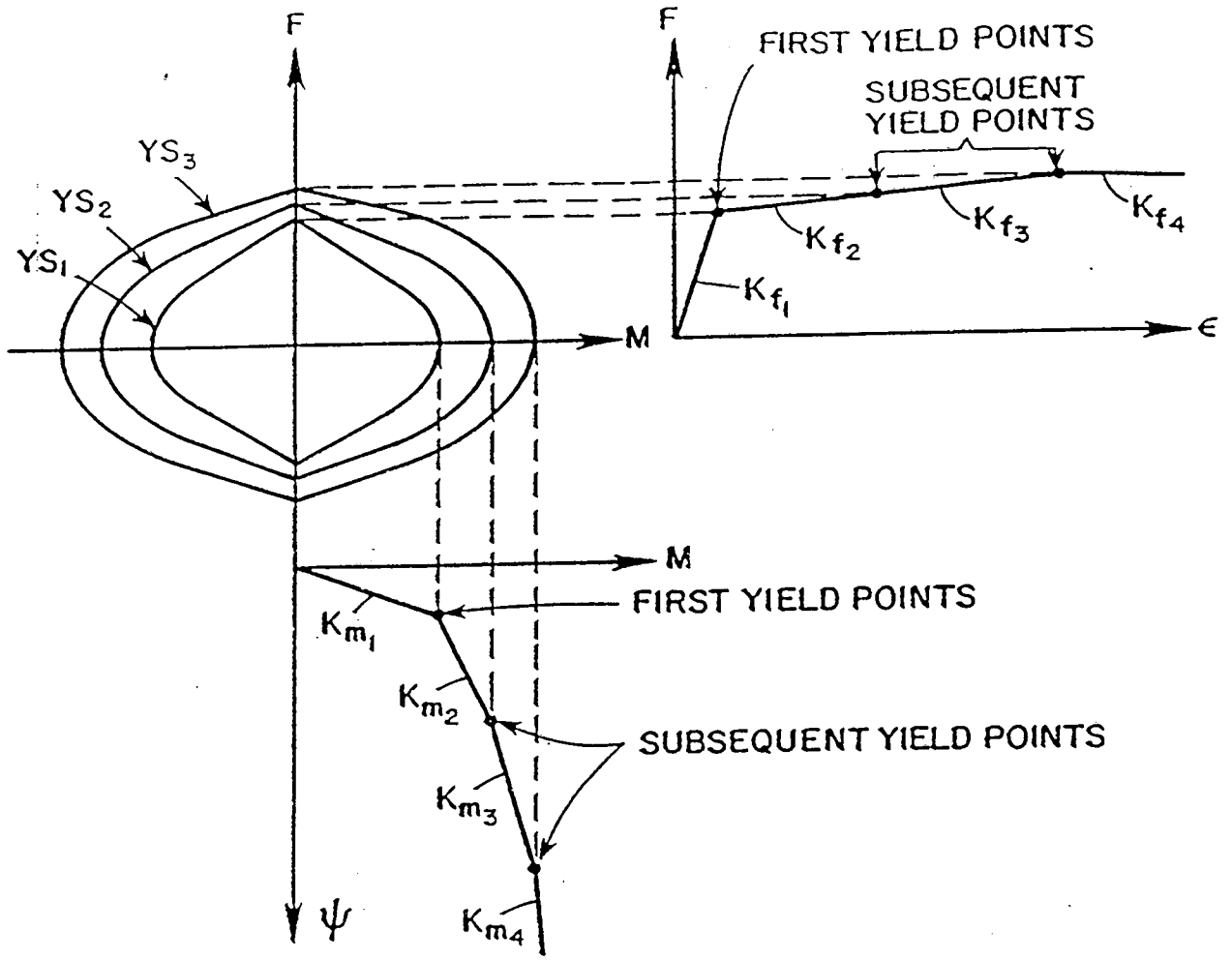

(a) INITIAL LOCATIONS OF SURFACES

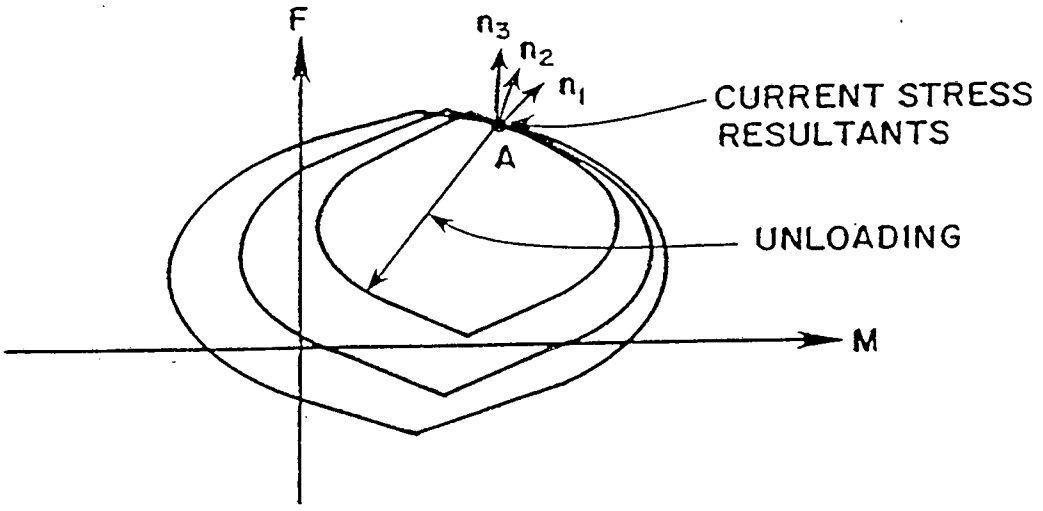

(b) DISPLACED SURFACES AFTER HARDENING

Figure 5.13-5 STRAIN HARDENING BEHAVIOR

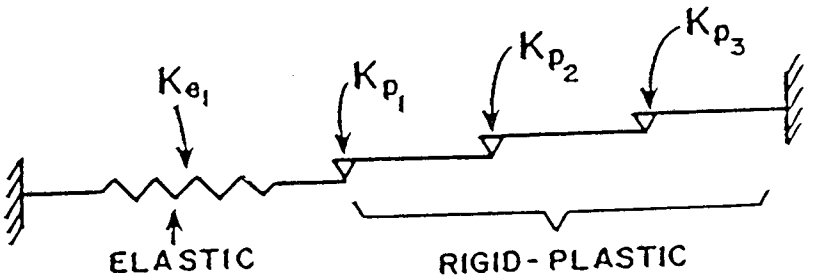

Figure 5.13-6 1-D MODEL

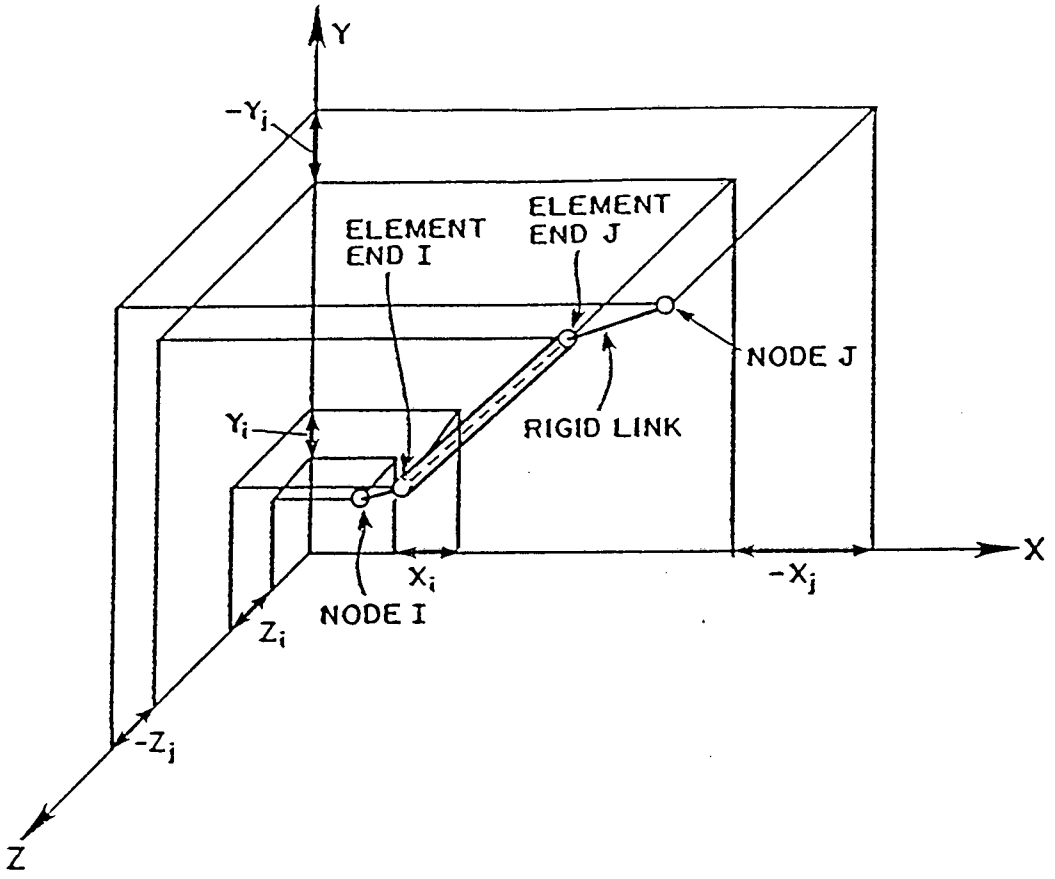

Figure 5.13-7 END ECCENTRICITIES

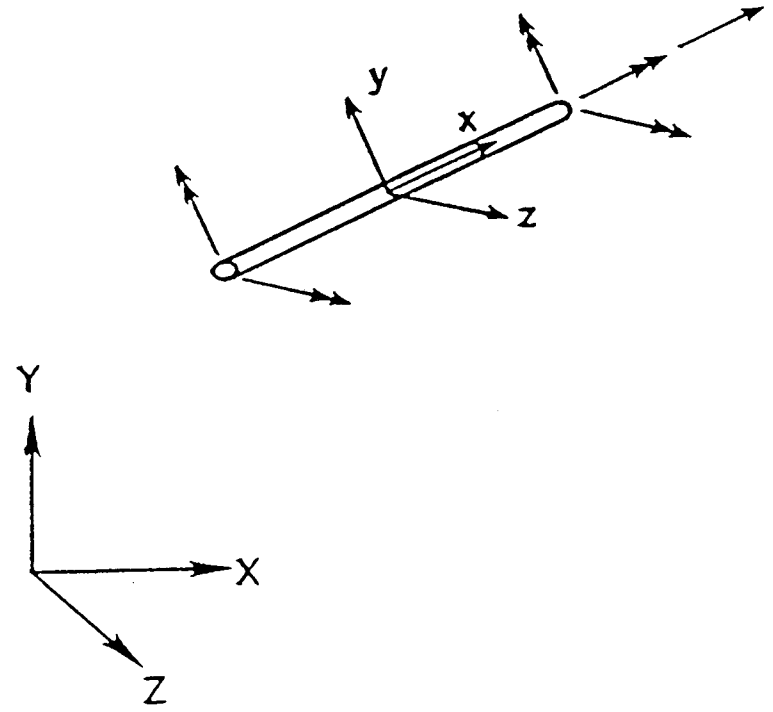

Figure 5.13-8 POSITIVE DIRECTION OF INITIAL ELEMENT ACTIONS

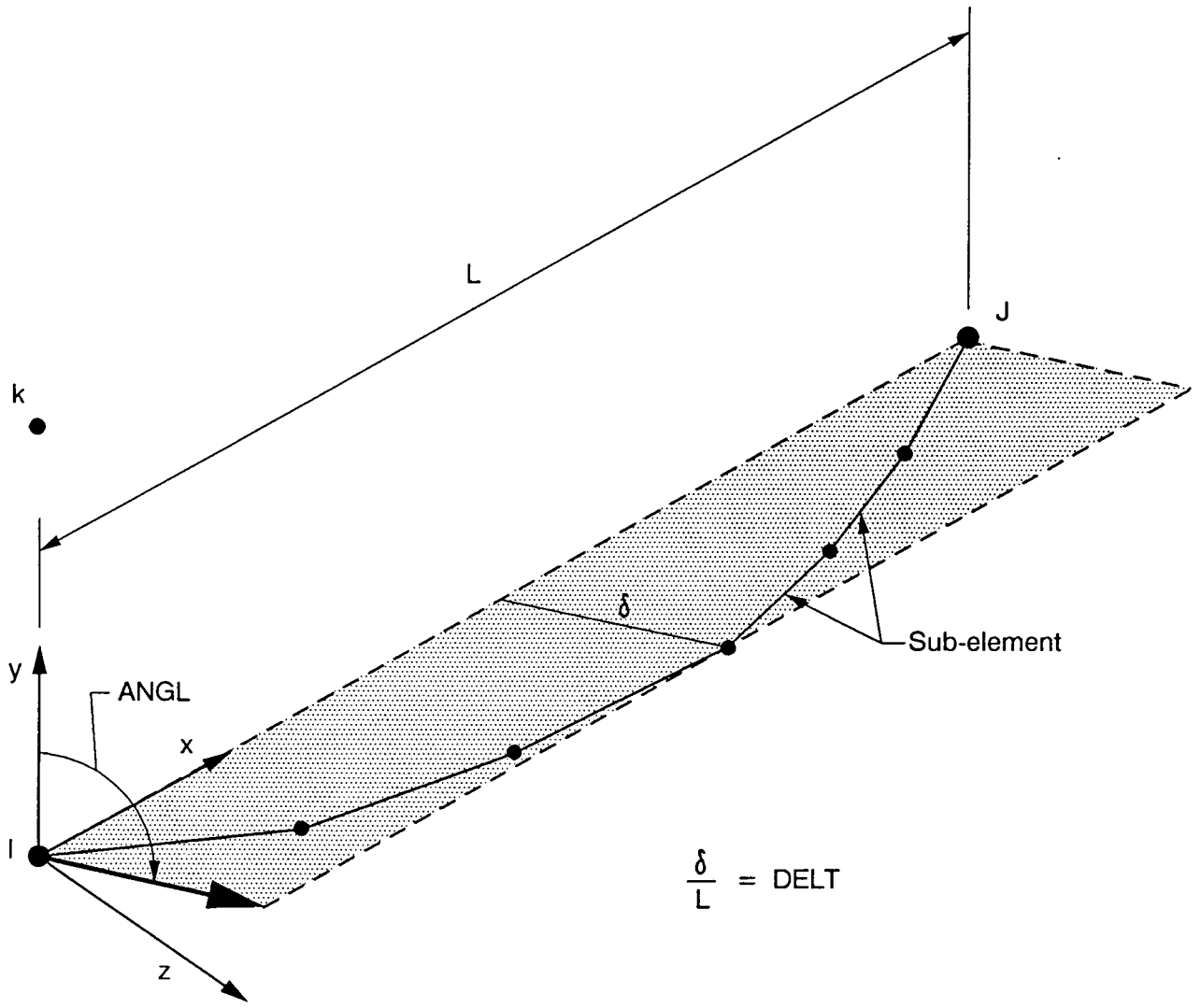

Figure E44 - ELEMENT OUT-OF-STRAIGHTNESS CONFIGURATION

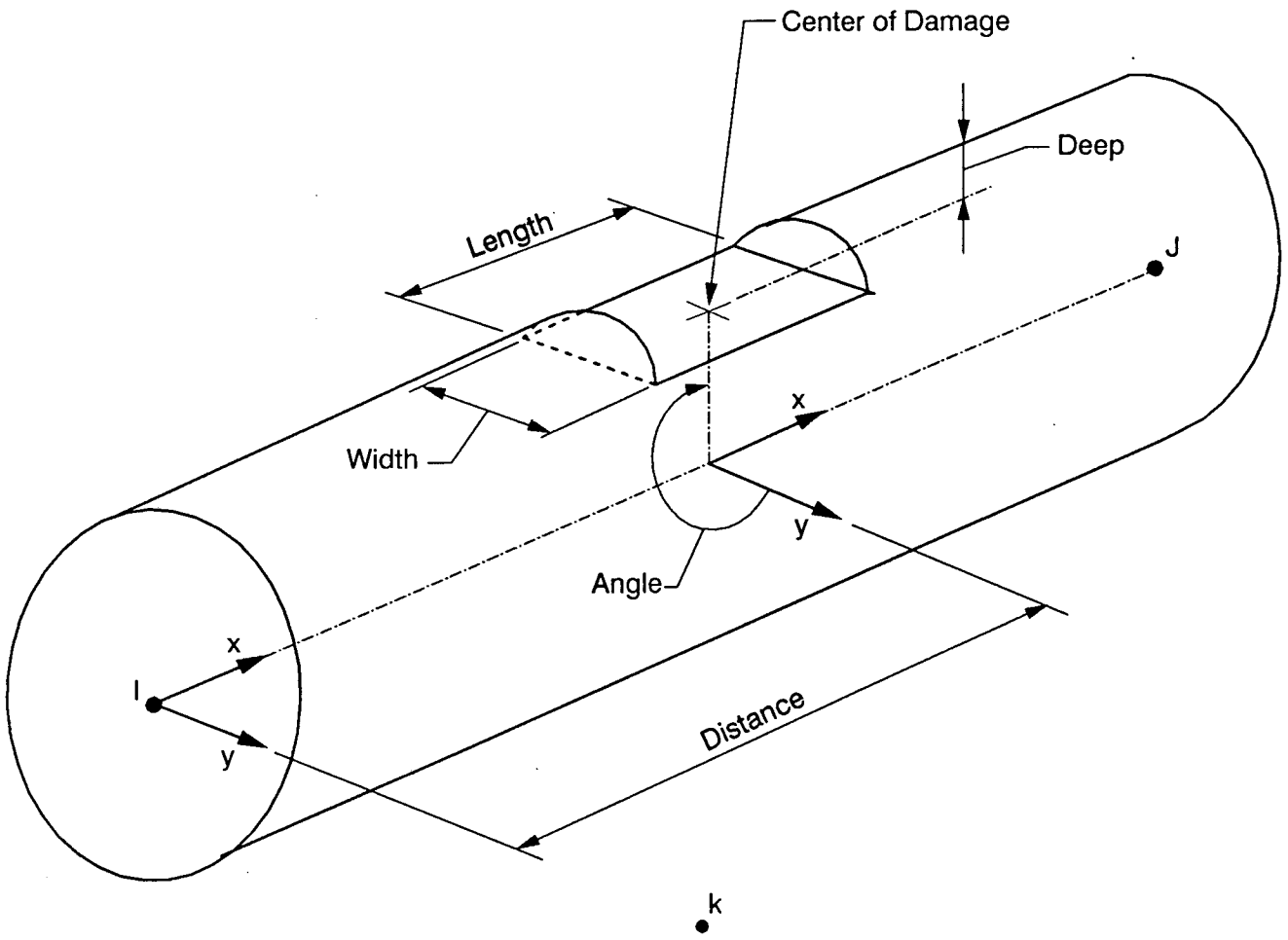

Figure E45 MEMBER DAMAGE

6.0 ELEMENT LOADING

6.1 Introduction

The loads generated at the element level by the program are categorized as element loadings. These include dead load, buoyancy, and hydrodynamic loads. In addition, the generation of the riser mass and hydrodynamic added mass is discussed in this section. The treatment of hydrostatic pressure, Poisson's effect, at the element level is described. In addition, the use of the concept of "effective axial forces" in the computation of element stiffness is outlined. Generation of catenary shapes and initial forces at the element level is also included.

6.2 Dead Load

The dead load is calculated from the weight density of the member in air. This dead load does not include the weight of the internal fluid in the member. The effects of buoyancy and internal fluid are treated separately.

The element dead load is computed as concentrated nodal loads. Effects of moments caused by self-weight are considered. The element dead loads are applied as a static nodal force pattern. The original dead load distribution remains unchanged during the structure motion.

6.3 Element Mass

The mass is calculated using the mass density of the member material. The tributary element mass for each node is calculated by multiplying the member tributary volume (member cross-sectional area multiplied by the tributary length) by the mass density. The tributary element mass for each node is then assigned to the translational degrees of freedom. The rotational inertia associated with the rotational degrees of freedom is neglected. The mass matrix is thus a diagonal one with the rotational mass terms neglected. In case the mass density of the member material is not specified, the mass density defaults to the weight density divided by the gravity acceleration.

If the member contains any internal fluid, its mass could be included by turning on a flag.

6.4 Hydrodynamic Added Mass

At each node, the added mass is calculated for each global direction, as

$$\frac{\pi}{4} \; d_w^2 \; K_M \; \rho_w \; \frac{L}{2} \; (1 \; - \; |\cos \bar{\phi}|) \qquad (6.4-1)$$

where

$\bar{\phi}$ = the angle between member axis and each global axis.

K_M = added mass coefficient.

d_w = effective water diameter (input by user).

The effective water diameter is the diameter used to calculate the hydrodynamic loads on the members.

The added mass for members not aligned with a global axis thus has a spurious component in the axial directions of the members. For partially submerged members, only the portion below mean water level contributes to the added mass.

The added masses are simply added to the other nodal masses and do not change with changing submergence from waves or structure motion.

During dynamic analyses with waves or currents, the user has the option to include the change in added mass as the amount of submergence changes. This is achieved as follows:

The initial nodal added mass term $\underline{AM}\ \ddot{\underline{r}}$ is kept permanently on the left hand side of the equation of motion, to give numerical stability to the problem.

$$(\underline{M} + \underline{AM})\ \ddot{\underline{r}} + \underline{C}\ \dot{\underline{r}} + \underline{K}\ \underline{r} = \underline{R}$$

During dynamic analyses with waves or currents, the updated added mass forces are applied as actual elements forces, $\underline{AM'}\ \ddot{\underline{r}}$. To maintain the original equation, the initial nodal added mass forces $\underline{AM}\ \ddot{\underline{r}}$ must be included as element forces also. Thus SEASTAR solves:

$$(\underline{M} + \underline{AM})\ \ddot{\underline{r}} + \underline{C}\ \dot{\underline{r}} + \underline{K}\ \underline{r} = \underline{R} - \underline{AM'}\ \ddot{\underline{r}} + \underline{AM}\ \ddot{\underline{r}}$$

which is the same as the simpler version of the updated representation

$$(\underline{M} + \underline{AM'})\ \ddot{\underline{r}} + \underline{C}\ \dot{\underline{r}} + \underline{K}\ \underline{r} + \underline{R}$$

This is achieved by explicitly computing $\underline{AM}\ \ddot{\underline{r}}$ using the initial nodal mass $\underline{AM}$ and adding it as a nodal force. At the same time, the updated added mass force $\underline{AM'}\ \ddot{\underline{r}}$ is computed, as an element hydrodynamic force, at force points.

6.5 Buoyancy

The buoyancy load is applied as a distributed load per unit length along the member. The distributed load is always acting normal to the member. This load is given by

$$(\gamma_w A_w - \gamma_i A_i) \sin \phi_v \qquad (6.5-1)$$

in which

γ_w = weight density of sea water.

A_w = member external cross-sectional area.

γ_i = weight density of the internal fluid.

A_i = member internal cross-sectional area.

ϕ_v = the angle between the member axis and the vertical axis.

The member is assumed to remain straight between the end nodes. Coordinates of the member are updated and the buoyancy loads are applied at the element deformed configuration. The fixed end forces caused by the application of the buoyancy load are computed.

A buoyancy force pattern is generated by the program in the member's initial configuration.

A surface-piercing member will experience a change in buoyancy if it displaces vertically. SEASTAR models this change in buoyancy by adding a spring to the submerged end of the member with a stiffness equal to the

buoyancy force per unit length of the element. This "buoyancy spring" has one end attached to the submerged end of the member and the other end is fixed.

When two members of equal diameters are connected to the same node and are in line, the buoyancy forces at the connecting node are equal and opposite and thus cancel out.

6.6 Hydrostatic Pressure

Hydrostatic pressures are applied at the end of all members along the elements. The elements are assumed to remain straight between the end nodes. As the member deforms, the direction of end pressures are updated and are always acting along the element in a straight line between the end nodes. The value of the end force at any node is given by:

$$F_{HS} = P_o A_w - P_i A_i \qquad (6.6-1)$$

in which

P_o = the external water pressure.

P_i = the internal water pressure.

For a continuous straight member, the end forces on adjacent elements cancel out, as shown in Figure 6-1. The net end force acting on a straight member acts at the exposed surface only.

For a continuous curved member in a horizontal plane, the end forces produce a resultant which acts as a restoring force and causes the moment to be zero everywhere along the element (Figure 6-2). The net effect is a compressive stress in the curved member equal to the hydrostatic pressure.

Figure 6-3 shows a member subjected to distributed buoyancy along the member plus the end pressures. The resolution of these forces in the vertical direction results in a net vertical force given by

$$(\gamma_w A_w - \gamma_i A_i) L \qquad (6.6-2)$$

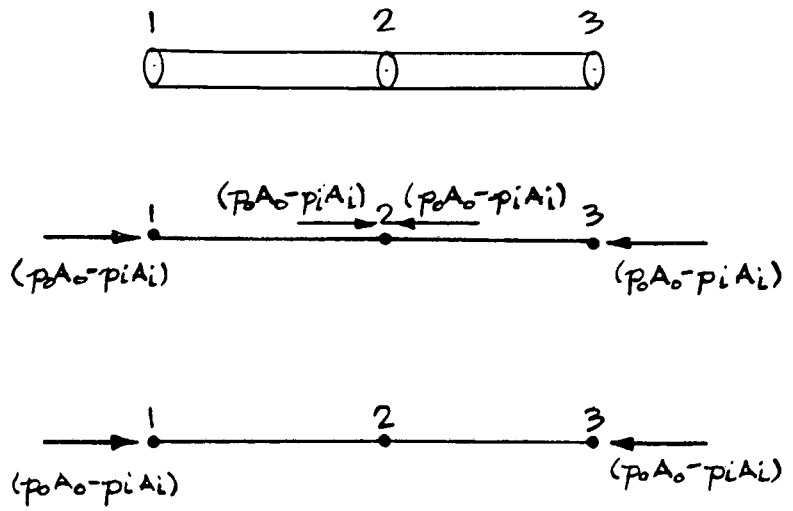

FIG. 6-1 END FORCES ON A STRAIGHT MEMBER

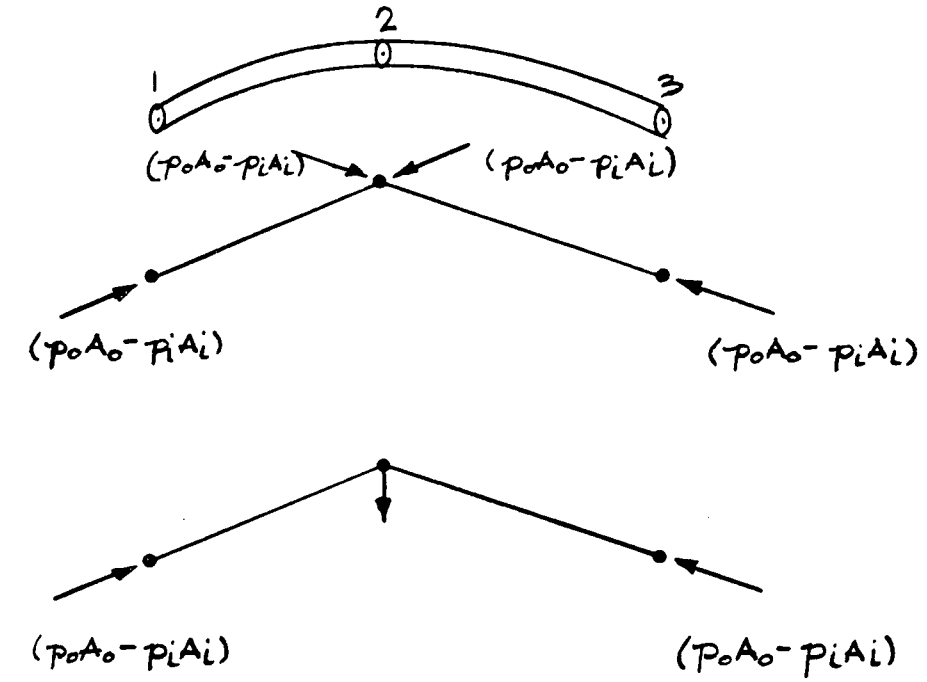

FIG. 6-2 END FORCES ON A CURVED MEMBER

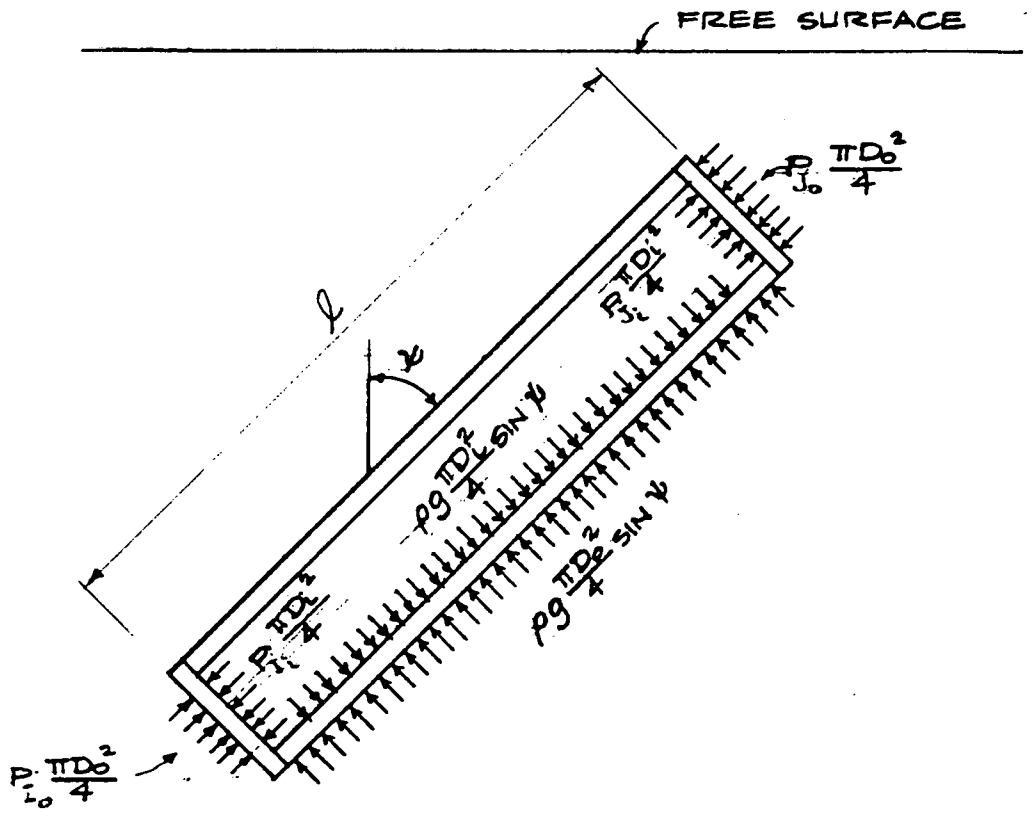

FIG. 6-3 FORCES ON FLOODED MEMBER

This term is simply (the total buoyancy force on the members minus the weight of the inside fluid). The distributed buoyancy along the member plus the end pressure give the correct distribution of buoyancy loads on straight or curved members.

The end pressures are added to the distributed buoyancy along the member.

6.7 Hydrodynamic Forces with Waves or Currents

The equations of motion of the structure are expressed by below:

$$(\underline{M} + \underline{AM})\ \ddot{\underline{r}} + \underline{C}\ \dot{\underline{r}} + \underline{K}\ \underline{r} = \underline{R}_w$$

where $\underline{R}_w$ is the wave load vector. A modified Morison O'Brien equation which takes into account the tangential drag force is used to evaluate the vector of wave loads and is given by:

$$\underline{R}_w = 1/2\ \rho_w\ C_D\ \overline{A}\ (\underline{u}_w - \dot{\underline{r}})\,|\underline{u}_w - \dot{\underline{r}}| + \rho_w\ C_M\ \forall\ \dot{\underline{u}}_w + \frac{1}{2}\ \rho_w\ C_{DS}\ \pi\ d\ (\underline{u}_w - \dot{\underline{r}})\,|\underline{u}_w - \dot{\underline{r}}| \qquad (6.7-1)$$

$$\underline{AM} = \rho_w\ K_M\ \forall$$

where

$\underline{M}$ = structural mass matrix.

$\underline{C}$ = damping matrix.

$\underline{K}$ = stiffness matrix.

$\ddot{\underline{r}}$ = structural acceleration vector

$\dot{\underline{r}}$ = structural velocity vector

$\underline{r}$ = structural displacement vector

$\underline{AM}$ = hydrodynamic added mass matrix.

$\underline{R}_w$ = wave force vector.

ρ_w = fluid mass density.

C_D = hydrodynamic drag coefficient in the normal direction.

C_{DS} = hydrodynamic drag coefficient in the longitudinal tangential direction (parallel to the member axis).

C_M = hydrodynamic inertia coefficient.

K_M = hydrodynamic added mass coefficient.

$\underline{d}_w$ = effective member diameter.

$\overline{A}$ = effective projected area.

$\forall$ = effective displaced volume.

$\underline{u}_w$ = water particle velocity vector (wave and current).

$\dot{\underline{u}}_w$ = water particle acceleration vector (wave and current).

Figure 6-4 shows how the wave force for an inclined tubular member is calculated.

integrating pressure distributions along the element. These forces are actually computed as element resisting forces, rather than as nodal applied forces. Hence, their contributions do not show up in the applied load norm.

An option is available to suppress the generation of fixed end moments for the beams. With this option only, the fixed end shears are computed.

6.8 Poisson's Effect

Poisson's effect due to hydrostatic pressure may be significant with increasing water depth. Forces caused in members due to Poisson's effect depend on the fixed end conditions and water pressure.

Figure 6-5 shows the steps involved in computing forces and displacement caused by external and internal pressure on a section of a pipe with free ends. In the first step, the pipe is assumed to be fixed, and fixed end forces caused by Poisson's effect are computed. Next, the fixed end forces are reversed and applied as external loads. Finally, the forces and displacements from steps 1) and 2) are added.

SEASTAR applies the Poisson forces as internal resisting loads at the element level, and corrects for the fixed end forces.

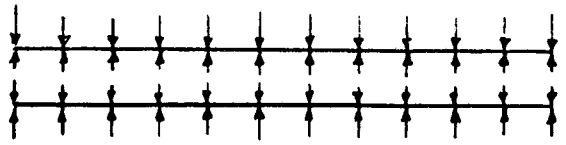

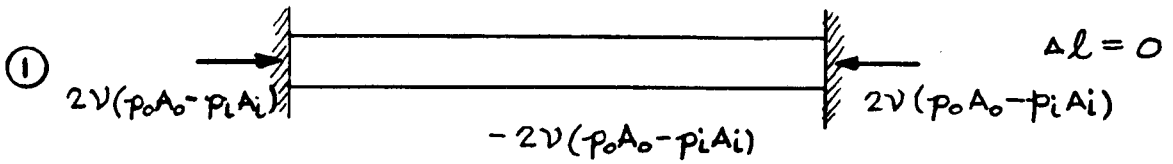

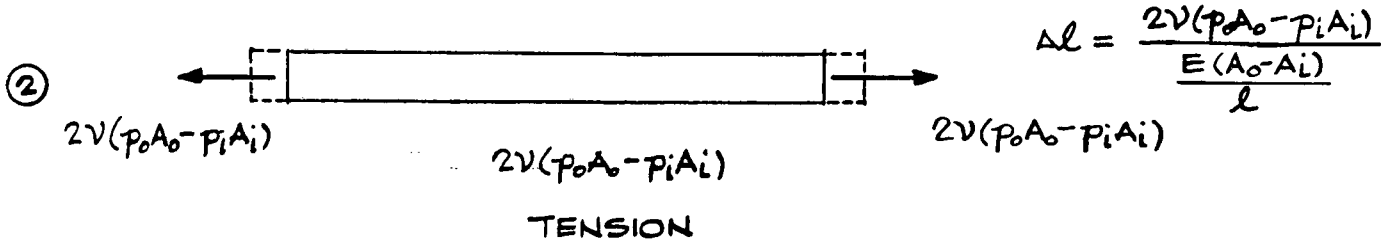

ADD ① + ②

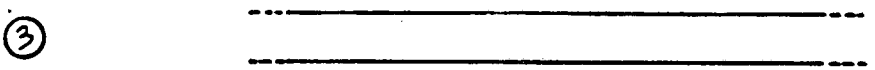

FREE EXPANSION

$$\Delta\ell = \frac{2\nu(p_oA_o - p_iA_i)}{\frac{E(A_o - A_i)}{\ell}}$$

FIG. 6-5 POISSON'S EFFECT DUE TO EXTERNAL & INTERNAL PRESSURE

6.9 Effective Axial Forces

The axial force in a member determines the geometric stiffness of the member and hence its total stiffness. However, when a member is submerged in a fluid with pressure p, the axial force due to the pressure does not contribute to the geometry stiffness. This is most easily explained by a simple example.

Consider first an initially straight beam acted on by an externally applied axial force P. If a small deformation of the element is considered, the "P- Δ effect of the external load is resisted by the bending stiffness of the beam. At some value of P the beam is unable to resist the resulting bending, and buckles.

Next we consider an initially straight beam under hydrostatic pressure p, causing an axial force P. In a displaced position (Figure 6-6), a check of equilibrium at any section across the beam, AA, reveals that there is no bending moment in the beam, and hence the beam is not being called upon to resist the axial pressure force by bending. Thus, axial pressure forces should not appear in geometric stiffness computations.

In SEASTAR, true axial forces are printed, but the effective axial force, found by subtracting pressure forces, is used for the geometric stiffness.

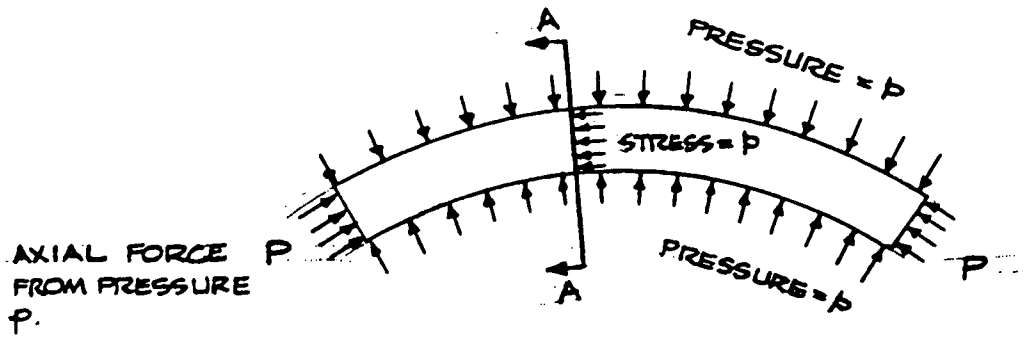

PLAN VIEW

FIG. 6-6 PRESSURE FORCE ON BENT BEAM

6.10 Catenary Generation

The coordinates of the catenary nodes are generated in SEASTAR using six different options:

1. Tension at the top of the catenary (T_B).
2. Horizontal component of tension at the top (H).
3. Catenary length (L_C).
4. Angle with horizontal at lower end (θ_A).
5. Angle with horizontal at upper end (θ_B).
6. Mooring length.

Figure 6-7 shows the definition of these input quantities. The catenary generation is based on the following fundamental equations of catenary:

$$y = \frac{H}{\bar{w}} \cosh\left(\frac{x\bar{w}}{H}\right)$$

$$\bar{T} = H \cosh\left(\frac{x\bar{w}}{H}\right)$$

$$L_c = \frac{H}{3}\left[\sinh\left(\frac{x_B\bar{w}}{H}\right) - \sinh\left(\frac{x_A\bar{w}}{H}\right)\right]$$

$$\theta = \tan^{-1}\left(\sinh\left(\frac{x\bar{w}}{H}\right)\right)$$

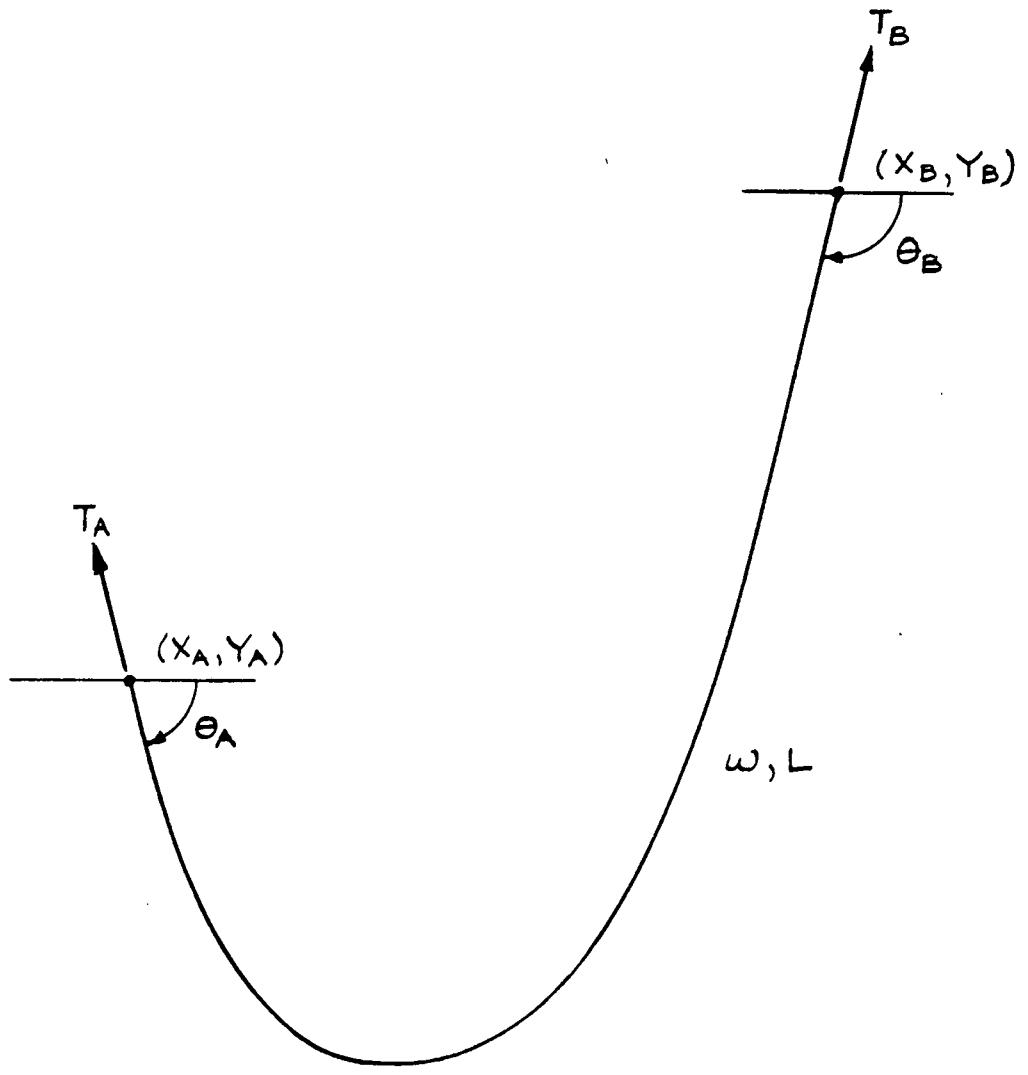

FIG. 6-7 CATENARY GENERATOR INPUT PARAMETERS

These equations are solved numerically using the bisection method. The SEASTAR catenary generator requires the user to distinguish the shape of the catenary generated. This is required because with certain input options, it is possible to get a double root, and by specifying the shape the user helps the generator to converge to the desired root. For example, for a tension T_B at the top of the catenary (Figure 6-8), two solutions are possible.

The catenary generator always assumes that node A is lower than node B. Reversal of the nodes will cause incorrect transformations from local catenary coordinates to global coordinates.

For the sixth option the user specifies the mooring length which differs from option 3. In option six the mooring line is composed of two segments. The first segment is straight and lies on the ocean floor, the second segment is catenary. The solution to this is obtained iteratively. First, the coordinates of the touchdown point of the mooring line is computed. The total length of both segments (the straight line and the catenary) are checked against the length of the mooring line. A new estimate of the length of the catenary part is obtained and new coordinates of the touchdown point are estimated. This process continues iteratively until the total length of both segments is equal to the length of the mooring line. The geometry of the catenary shape is evaluated next.

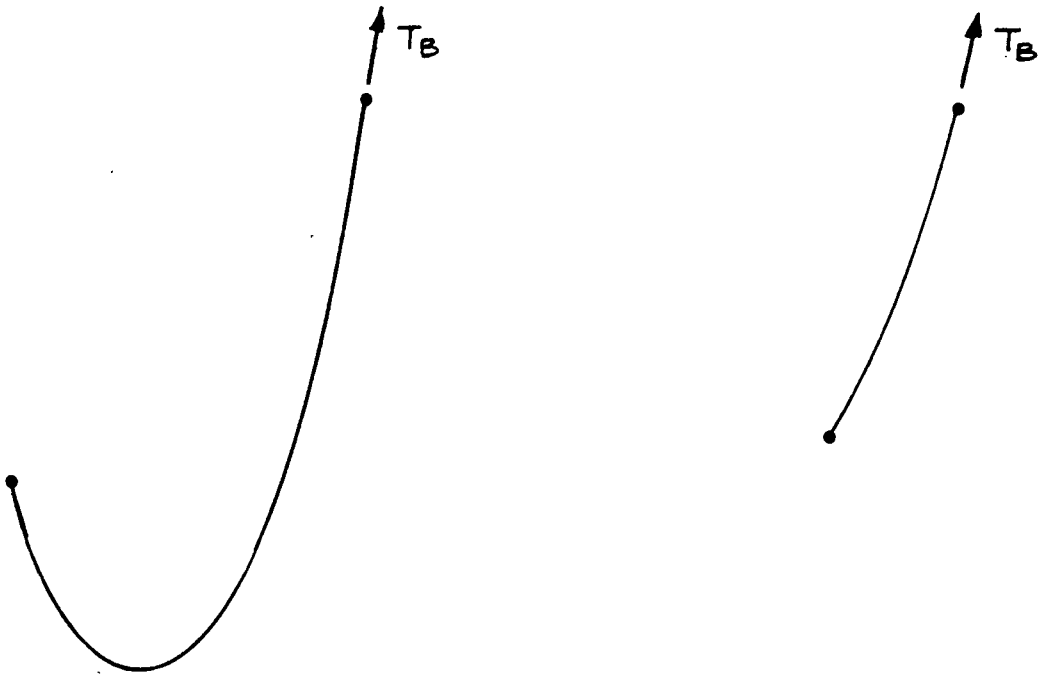

FIG. 6-8 TWO POSSIBLE SOLUTIONS OF A CATENARY WITH SAME TENSION T_B AT THE TOP

7.0 WAVE KINEMATICS

7.1 Available Wave Loading Options

Wave kinematics can be generated from current, Airy waves, Stokes V waves, irregular seas, Stream Function waves or 2-D grid wave loader. A combination of current plus any of the wave types can also be specified. The following six sources of wave kinematics in SEASTAR are described.

1. Current
2. Airy waves
3. Stokes V waves
4. Irregular seas
5. Stream Function waves
6. 2-D grid wave loader

7.2 Current

Current is defined by a series of velocity vectors at different elevations, the velocity between two defined levels being calculated by linear interpolation of two velocity vectors. Current may be combined with regular waves (Airy, Stokes or Stream Function), irregular seas, or 2-D grid wave loader. The current velocity profiles may be time dependent. The current profiles will be stretched to the free water surface if waves and current are both considered.

The current has two effects.

1. Modifications of wave periods for Airy waves, Stokes waves and regular or irregular waves.

2. Modification of kinematics by vector addition of wave and current velocities for all types of wave loading specification.

The effect of a current on a wave is to carry it along with it, thereby changing the period as observed at a stationary point. This is known as the Doppler effect. This is described in detail in Section 7.3.2.

7.3 Airy Waves

An Airy wave is the linearized solution of the boundary value problem

$$\nabla^2 \phi = 0$$

where ϕ is the flow potential function. The free surface boundary condition is linearized by assuming the surface elevation η to be small.

7.3.1 Wave Length

The wave length, λ_w, in still water is found from

$$\lambda_w = \frac{gT^2}{2\pi} \tanh \frac{2\pi D}{\lambda_w} \qquad (7.3.1)$$

where

g = gravity acceleration

D = the water depth

λ_w = the wave length

T = the wave period

7.3.2 Effect of Current on Wave Period

The effect of a current, with velocity component V_C at the surface in the direction of the wave, is to increase the speed of the wave crests. Thus,

$$\frac{\lambda_w}{T_w} + V_c = \frac{\lambda_w}{T_o} \qquad (7.3.2)$$

where

T_o = the period relative to a fixed observer.

T_w = the period relative to a moving current.

From this, equation 7.3-1 is modified to become

$$\lambda_w = \frac{gT_o^2}{2\pi} \frac{1}{\left(1 - \frac{V_c T_o}{\lambda_w}\right)^2} \tanh \frac{2\pi D}{\lambda_w} \qquad (7.3-3)$$

Equations 7.3-2 or 7.3-3 are solved iteratively.

The period of the wave relative to the current is

$$T_w = \frac{T_o}{\left(1 - \frac{V_c T_o}{\lambda_w}\right)} \qquad (7.3-4)$$

7.3.3 Free Surface Profile

The wave profile is given at a point (x, y) and time, t, by

$$\eta = \frac{H_w}{2} \cos 2\pi \left(\frac{x\cos\bar{\theta} + y\sin\bar{\theta}}{\lambda_w} - \frac{t}{T} - \frac{x_o}{\lambda_w} \right) \qquad (7.3-5)$$

where

H_w = the wave height

$\bar{\theta}$ = the angle between the wave direction and the x-axis (Figure 7-1).

x_0 = The distance at time zero from the wave crest to the origin, measured in the direction of wave motion.

7.3.4 Wave Particle Motion

The water particle velocity u and acceleration $\dot{u}$ at the point (x, y, z) where z is measured upwards from MWL are given by

$$\begin{aligned} u_{wx} &= G(z)\ \cos\bar{\theta}\ \cos \\ u_{wy} &= \frac{H_w}{2}\frac{2\pi}{T}\ G(z)\ \sin\bar{\theta}\ \cos\ 2\pi\left(\frac{x\cos\bar{\theta} + y\sin\bar{\theta}}{\lambda_w} - \frac{t}{T} - \frac{x_o}{\lambda_w}\right) \\ u_{wz} &= H(z)\ \ 1\ \ \sin \end{aligned} \tag{7.3-6}$$

$$\begin{aligned} \dot{u}_{wx} &= G(z)\ \cos\bar{\theta}\ \sin \\ \dot{u}_{wy} &= \frac{H_w}{2}\left(\frac{2\pi}{T}\right)^2\ G(z)\ \sin\bar{\theta}\ \sin\ 2\pi\left(\frac{x\cos\bar{\theta} + y\sin\bar{\theta}}{\lambda_w} - \frac{t}{T} - \frac{x_o}{\lambda_w}\right) \\ \dot{u}_{wz} &= H(z)\ \ 1\ -\cos \end{aligned} \tag{7.3-7}$$

Here G(z) and H(z) are the vertical decay functions of horizontal and vertical motion, given by

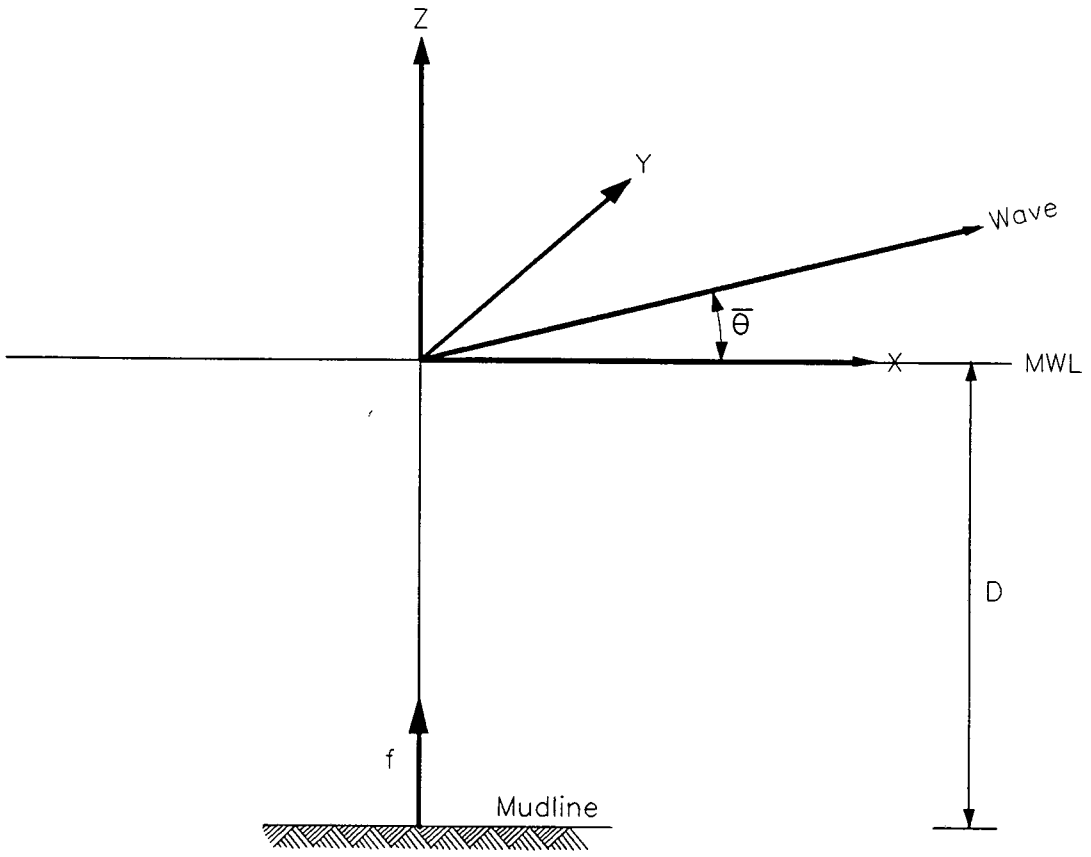

FIG. 7-1 COORDINATE AXES

$$G(z) = \frac{\cosh \frac{2\pi f}{\lambda_w}}{\sinh \frac{2\pi D}{\lambda_w}} \qquad (7.3-8)$$

$$H(z) = \frac{\sinh \frac{2\pi f}{\lambda_w}}{\sinh \frac{2\pi D}{\lambda_w}} \qquad (7.3-9)$$

where f is the distance from the mudline to the point (x, y, z), i.e.,

$$f = D + z \qquad (7.3-10)$$

7.3.5 Stretching of Kinematics

Since the above equations strictly apply only to small values of H, an assumption is required if H_w is not small and values of $z > 0$ are used. Either these equations can be used directly, or the values that strictly apply at the MWL ($z = 0$) can be assumed to apply at the surface ($z = \eta$). Thus kinematics from the MWL are "stretched" up to the free surface at the crest (and compressed to the free surface at the trough). See Figure 7-2. Mathematically this is accomplished by replacing the vertical coordinate f by f′ given by:

$$f' = f \frac{D}{D+\eta} \qquad (7.3-11)$$

This process is shown diagrammatically in Figure 7-2. It is generally not recommended for regular waves.

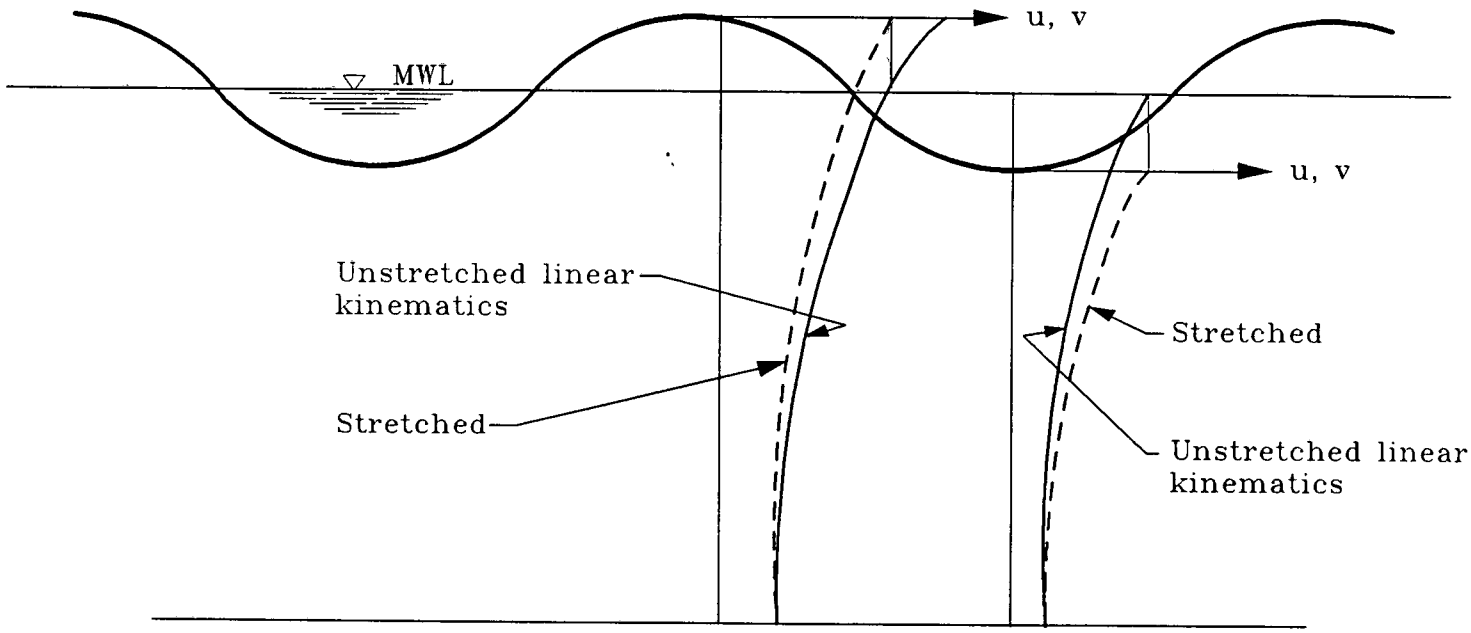

Fig. 7-2 KINEMATICS STRETCHING (REGULAR SEAS)

Another method which is available for stretching the wave kinematics is called the delta stretching. However, the delta stretching does not give good results and is thus not implemented in SEASTAR. The most commonly used method for stretching is the Wheeler stretching.

7.3.6 Effect of Currents on Kinematics

A current modifies the observed period T_o to a period T_w that defines the magnitude of the water particle motion (Section 7.3.2). However, the observer still sees the original period of motion, so the horizontal velocity is

$$u_{wx} = \frac{H_w}{2} \frac{2\pi}{T_w} G(z) \cos\bar{\theta} \cos 2\pi\left(\frac{x\cos\bar{\theta} + y\sin\bar{\theta}}{\lambda_w} - \frac{t}{T_o} - \frac{x_o}{\lambda_w}\right) \quad (7.3-12)$$

Other quantities follow similarly. To these velocities are added the current velocity, vectorially.

7.3.6 Effect of Currents on Kinematics

A current modifies the observed period T_o to a period T_w that defines the magnitude of the water particle motion (Section 7.3.2). However, the observer still sees the original period of motion, so the horizontal velocity is

$$u_{wx} = \frac{H_w}{2} \frac{2\pi}{T_w} G(z) \cos\bar{\theta} \cos 2\pi\left(\frac{x\cos\bar{\theta} + y\sin\bar{\theta}}{\lambda_w} - \frac{t}{T_o} - \frac{x_o}{\lambda_w}\right) \quad (7.3\text{-}12)$$

Other quantities follow similarly. To these velocities are added the current velocity, vectorially.

7.4 Stokes 5th Order Wave

Stokes 5th order wave is an approximation method to solve the Laplace equation $\nabla^2\phi = o$ with nonlinear free surface boundary conditions. Five terms of the trigonometric function are used in the approximation procedure. SEASTAR uses the numerical solution method published by Skjelbreia and Hendricksen (1960).

The solution matches boundary conditions along the free surface more accurately, by assuming that the velocity potential ϕ is a function of five harmonics. They all are assumed to propagate at the same speed. The partial derivatives of ϕ with respect to position are the particle velocities. The partial derivatives of velocity with respect to time are the local (unconvected) accelerations used in the program. (The "total" acceleration includes changes in velocity due to translation, as well as time change.)

Since the Stokes 5th order wave matches the nonlinear free surface boundary condition reasonably, it is valid for large waves and the kinematics stretching is not applicable.

7.4.1 Effect of Current

Currents cause two effects:

1. Modification of the wave period, due to the wave being carried along by the current.

2. Vector addition of water particle velocities from wave and current.

Both effects were described in Section 7.3 and affect Stokes V wave theory similarly. The wave length is a nonlinear function of wave height so the wave length is solved by iterating on a set of nonlinear equations, instead of the simple equation 7.3-3.

7.5 Irregular Sea

The analysis of irregular sea action on marine risers requires information on statistical characteristics of irregular sea which are described with a power spectrum. Various theoretical spectra of ocean waves have been proposed by different investigators. SEASTAR uses two forms of sea spectra: one is user defined and the other is the Pierson-Moscowitz spectrum (1964).

For the user-specified sea spectrum, the user can define a series of linear waves with varying wave heights, periods and directions, i.e., multidirectional spectrum. The ability to specify three-dimensional seas is important since the along-wave forces (i.e., in the mean direction of wave advance) calculated using 3-D waves are less than those calculated using unidirectional waves. Also using 3-D waves takes into account the across-wave forces (i.e., perpendicular to the mean direction of wave advance) which are not accounted for in the unidirectional waves.

For the generated sea spectrum, the Pierson-Moskowitz spectrum is used to generate a series of unidirectional linear waves with varying wave heights and periods. The range and interval of the frequency for generating individual waves is defined by the user. The phase of the individual linear waves is generated by a random number generator.

The irregular sea is obtained by superposition of all the generated linear waves.

7.5.1 Pierson-Moscowitz Spectrum

The Pierson-Moscowitz spectrum is obtained by correlation of observed data with an analytical model for a fully developed sea subjected to wind speeds of 20 to 40 knots. The expression for wave height spectrum is given by

$$S_{hh}(\omega) = \frac{\bar{a} g^2}{|\omega|^5} \exp\left[-\bar{b}\left(\frac{g}{\omega \bar{U}}\right)^4\right] \qquad (7.5-1)$$

in which

ω = the angular frequency

g = acceleration due to gravity

$\bar{a}$ = a dimensionless constant ($\bar{a} = 8.1 \times 10^{-3}$)

$\bar{b}$ = a dimensionless constant ($\bar{b} = 0.74$)

U = the mean wind velocity at a height of 64 feet above the sea surface.

The wave amplitude for a frequency interval $\Delta\omega$ is given by

$$a = \sqrt{2\, S_{hh}(\omega)\, \Delta\omega} \qquad (7.5-2)$$

7.5.2 Wave Number

Using the angular frequency $\omega_n (= 2\pi/T_n)$ instead of the period, T_n, and the wave number $\kappa_n (= 2\pi/\lambda_{wn})$ instead of wavelength λ_{wn}, the wave number of the nth component is defined for any water depth D by

$$\omega_n^2 = g\kappa_n \tanh(\kappa_n D) \qquad (7.5-3)$$

which is exactly equivalent to eqn. 7.3-1 for Airy waves.

7.5.3 Free Surface

The free surface is given by adding contributions from all wave components

$$\eta = \sum_n a_n \cos\{\kappa_n (x\cos\bar{\theta} + y\sin\bar{\theta}) - \omega_n t - \epsilon_n\} \qquad (7.5-4)$$

where

a_n = the amplitude of the nth wave component

x, y = the coordinates of a point

$\bar{\theta}$ = the angle between the x-axis and the direction of wave propagation (Figure 7-1).

t = the time

ϵ_n = the phase of the nth wave component

7.5.4 Wave Kinematics

Water particle motion is found by adding vectorially the kinematics due to each wave component. Thus, the water particle velocity u and acceleration $\dot{u}$ at (x, y, z) are given by the equivalent of equations 7.3-6 and 7.3-7, summed over all components.

$$\begin{aligned} u_{wx} &\qquad G_n(z) \quad \cos\bar{\theta} \quad \cos \\ u_{wy} &= \sum_n \alpha_n \omega_n \quad G_n(z) \quad \sin\bar{\theta} \quad \cos \quad \{\kappa_n(x\cos\bar{\theta} + y\sin\bar{\theta}) - \omega_n t - \epsilon_n\} \\ u_{wz} &\qquad H_n(z) \quad 1 \quad \sin \end{aligned} \tag{7.5-5}$$

$$\begin{aligned} \dot{u}_{wx} &\qquad G_n(z) \quad \cos\bar{\theta} \quad \sin \\ \dot{u}_{wy} &= \sum_n \alpha_n \omega_n \quad G_n(z) \quad \sin\bar{\theta} \quad \sin \quad \{\kappa_n(x\cos\bar{\theta} + y\sin\bar{\theta}) - \omega_n t - \epsilon_n\} \\ \dot{u}_{wz} &\qquad H_n(z) \quad 1 \quad -\cos \end{aligned} \tag{7.5-6}$$

Again, the vertical decay factors are given by

$$G_n(z) = \frac{\cosh \kappa_n f}{\sinh \kappa_n D} \tag{7.5-7}$$

$$H_n(z) = \frac{\sinh \kappa_n f}{\sinh \kappa_n D} \qquad (7.5-8)$$

where

$$f = D + z \qquad (7.5-9)$$

7.5.5 Stretching

The procedure of stretching the kinematics was introduced in Section 7.3.5. While not of much importance in regular waves, it is recommended to be used in irregular waves for the following reason.

Consider two wave components as shown in Figure 7.3, one rather long and one short. If no stretching is used (upper figures), the resulting kinematics at the free surface is incorrectly dominated by the kinematics from the small wave component. Stretching has the effect of transporting the kinematics for the small wave up to the surface, where it "rides" on the larger wave, contributing its kinematics in a more reasonable way (lower figure).

As for regular linear waves, stretching requires replacing f, the elevation of the point relative to the mudline, by f′ given by

$$f' = f \frac{D}{D + \eta} \qquad (7.5-13)$$

Since η is already a function of all wave components, this couples the kinematics of all wave components.

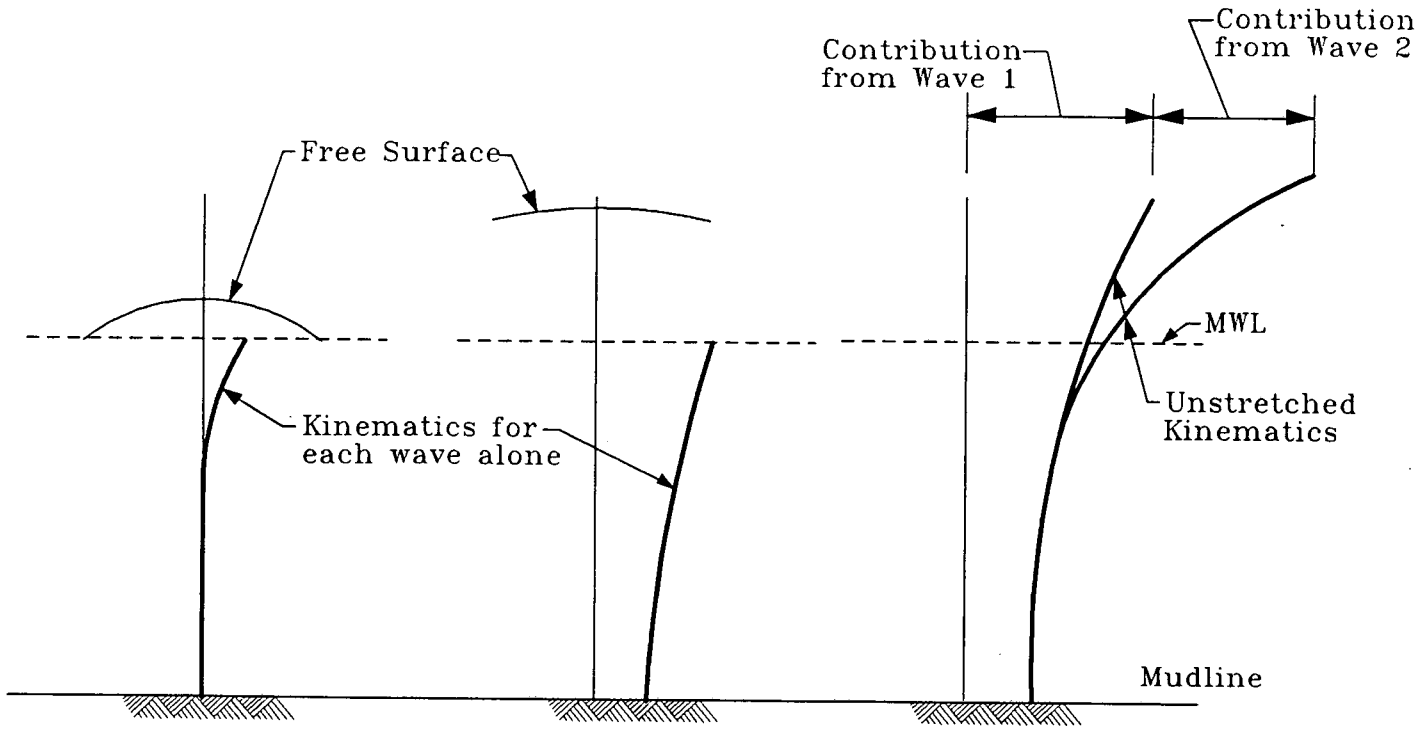

Wave 1 **Wave 2** **Combined, without Stretching**

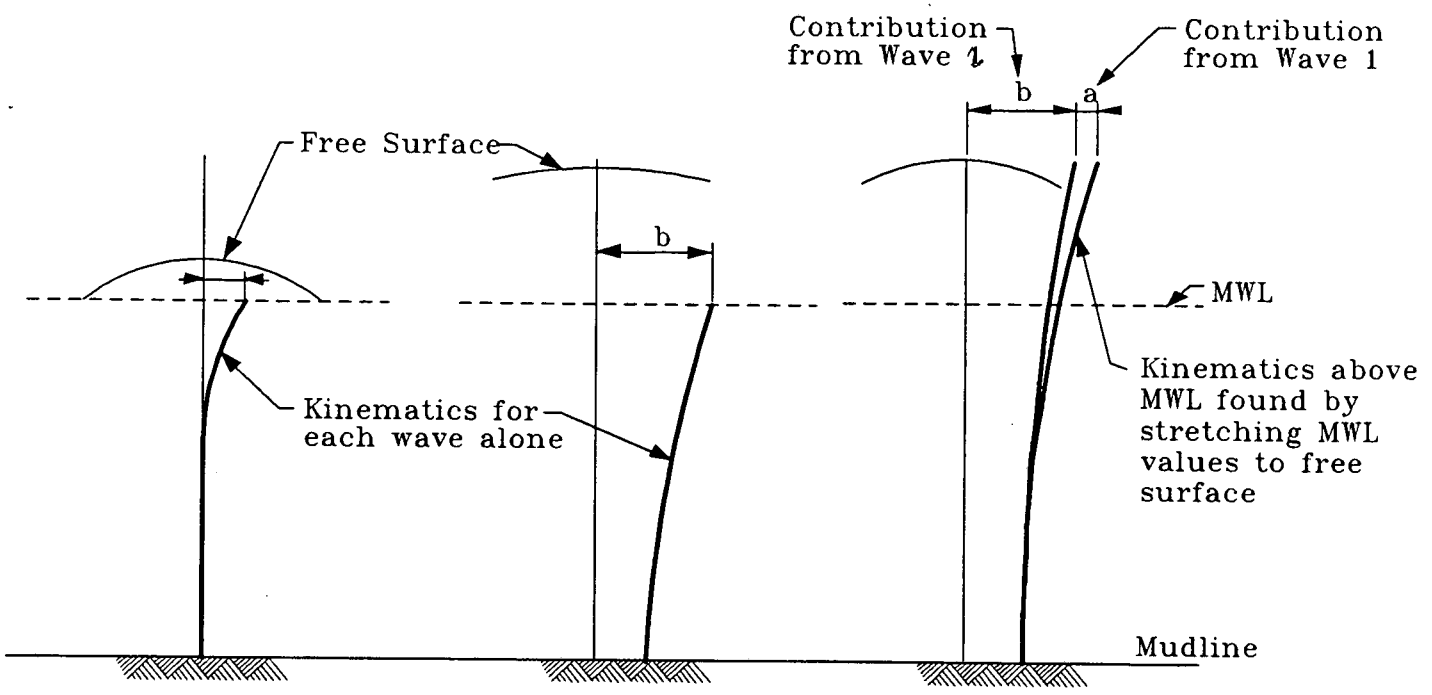

Wave 1 **Wave 2** **Combined, with Stretching**

FIG. 7-3 STRETCHING WITH IRREGULAR SEAS

.014\TEX-STAR\FIG-7-3

7.5.6 Current Interaction

Since each wave is independent of the others, the current modifies the wave length and observed frequency of each wave component, independently, exactly as described in Section 7.3.6 for Airy waves.

Resulting kinematics of wave components and current are added vectorially.

7.6 Stream Function Waves

The Stream Function wave theory, as implied by the name, is based on a Stream Function representation of the flow. For two-dimensional irrotational motion, the Stream Function satisfies Laplace equation

$$\nabla^2 \psi = 0$$

The Stream Function ψ also satisfies the three boundary conditions; 1) no flow through the seabed, 2) constant pressure at the water surface (dynamic free surface boundary condition), and 3) no net change in the mean sea level due to the presence of the wave. Details of the Stream Function wave theory are given in Dean (1965-a).

The Stream Function is expressed as the series sum of waves that are periodic in x. The wave is divided into several discrete points and the dynamic free surface boundary condition is applied at each of these points. The coefficients corresponding to the different components of the series are obtained by minimizing the error resulting from the lack of fit to the free surface boundary condition. An initial set of values for these coefficients is first assumed and then these values are improved through an iterative procedure.

The number of terms (order) necessary for an adequate representation of the nonlinear wave is determined by the relative height parameter H_w/T^2 and the relative depth parameter D/T^2. Figure 7-4, adopted from Dean (1965-b), gives, for different values of the relative depth and height parameters, the minimum order of the Stream Function needed such

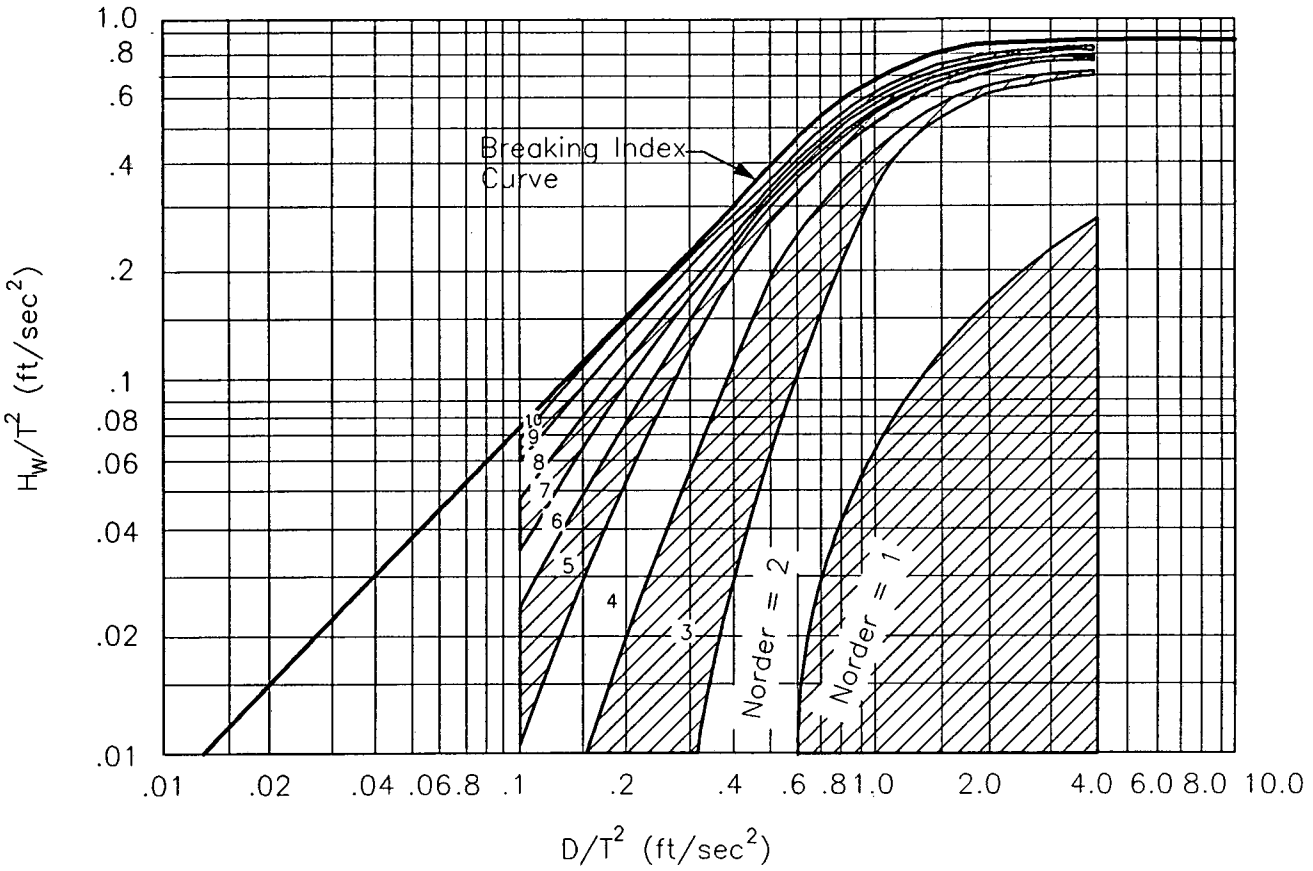

FIG. 7-4 REQUIRED ORDER, NORDER, OF WAVE THEORY SUCH THAT ERRORS IN MAXIMUM VELOCITY AND ACCELERATION ARE LESS THAN ONE PERCENT

.014\TEX-STAR\FIG-7-4

that the errors in the maximum velocities are less than 1 percent between the given order and the next higher one. In SEASTAR, the default order is 9.

As for Stokes wave, the Stream Function wave is valid for large wave heights and the kinematics stretching need not be applied.

Current-wave interaction for the Stream Function wave is considered simply by adding the current water particle velocities vectorially to those of the wave. The effect of the current on the wave period (Doppler effect) is not considered.

7.7 2-D Grid Wave Loader

In this option, the wave kinematics at grid points are generated first by the program SEAGEN and written to a file that is read by SEASTAR. The program SEAGEN calculates wave and current kinematics at points in a rectangular grid as shown in Figure 7-5. Calculation of wave kinematics in SEAGEN is carried out based on any of three options:

1. Direct input of wave heights, periods, and phases.
2. Time history of sea surface elevation.
3. Sea surface elevation power spectral density.

For all the options, the water particle kinematics are computed using the Airy wave theory and stretching is applied.

Current effects in SEAGEN are included by vectorially adding the current water particle velocities to those of the waves. Modification of wave period due to the presence of current (Doppler effect) is not considered in SEAGEN.

If both current and the 2-D grid wave loader options are specified in SEASTAR, the current kinematics are added vectorially to the grid kinematics.

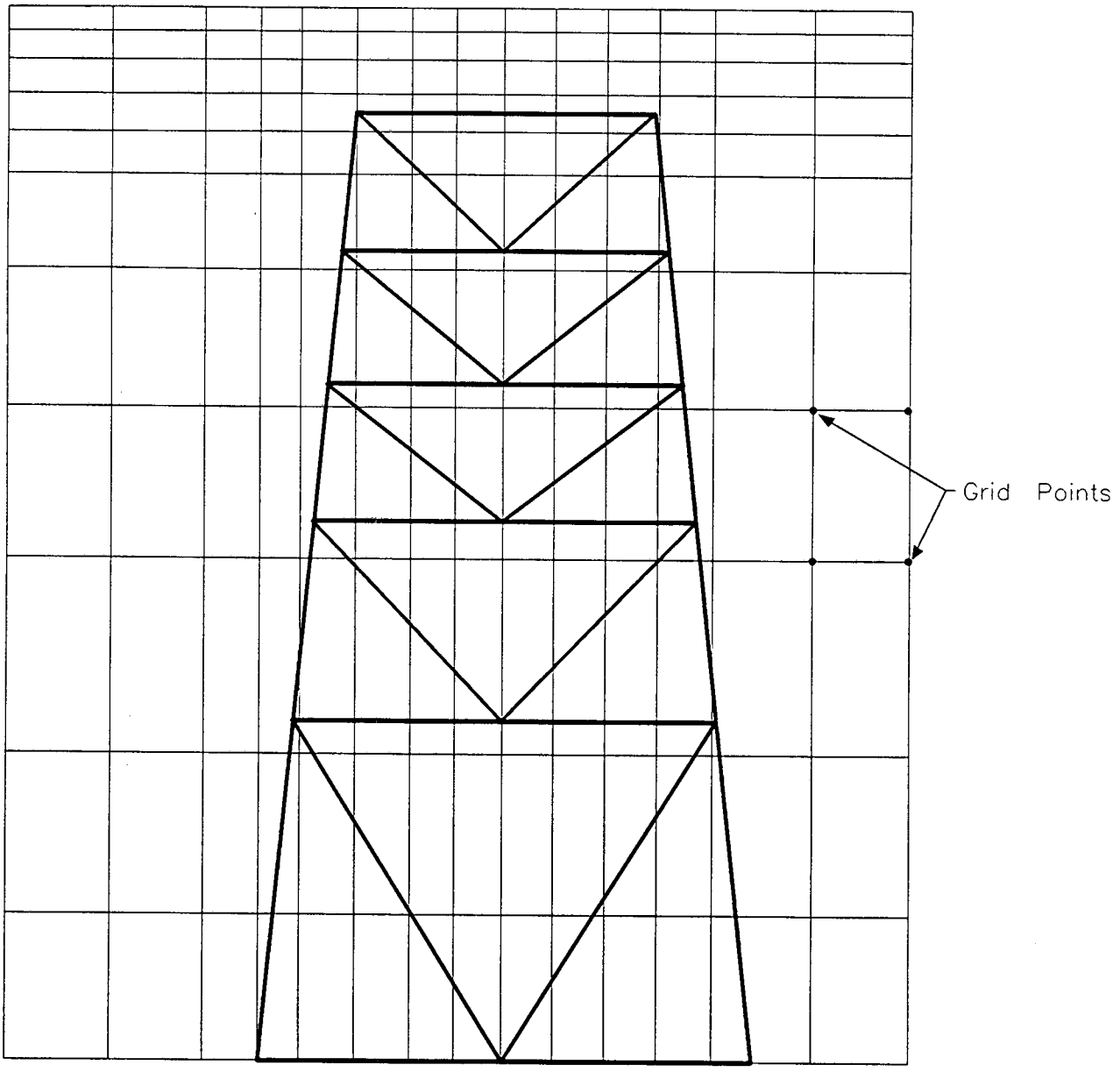

FIG. 7-5 2-D GRID WAVE LOADER

a:\TEX-STAR\FIG-7-5

8.0 VESSEL MOTION

SEASTAR vessel motion is a procedure for defining displacement record time histories for the heave, surge, sway, roll, pitch and yaw of a vessel subjected to "irregular seas." The irregular sea definition is described in detail in Chapter 7. The input or computed irregular seas are used in computing the vessel motions.

For each of the six vessel motions, a response amplitude operator (RAO) is defined by the user. The RAO defines the amplitude and phase with which the vessel responds to a single linear wave of a particular frequency. The RAO's are input for each vessel motion at discrete frequencies for a particular incident angle between the vessel and wave direction. The transfer function or the RAO's are then linearly or parabolically interpolated to the irregular sea wave frequencies.

The cross-coupling effect between various vessel motions is ignored since RAO's are specified independently. For example, cross-coupling between surge and pitch or between roll and sway is ignored.

The vessel motion at various irregular sea frequencies is obtained by a complex product of the RAO's and wave amplitudes, i.e.,

$$Y_i(\omega) = H_i(\omega) \cdot X(\omega) \qquad (8-1)$$

in which

$X(\omega)$ = the irregular sea amplitude for frequency ω.

$H_i(\omega)$ = the interpolated RAO at frequency ω, for the i^{th} vessel motion.

$Y_i(\omega)$ = the vessel motion for frequency ω, for the i^{th} vessel motion.

$Y_i(\omega)$ is a complex number which defines the amplitude and phase of the i^{th} vessel motion at frequency ω.

The time history of the six vessel motions is obtained by linear superposition of individual frequencies. The six vessel motion histories are next resolved in the global axis of the problem. The user has the option of applying these vessel motions as imposed displacement records to any of the structure nodes and degrees of freedom.

Simplified vessel motion can be generated by sinusoidal displacement time histories.

8.1 Imposed Displacement Records

The equilibrium equations to be solved at frequent intervals during the analysis are of the form:

$$\underline{K}^* \cdot \Delta\underline{r} = \Delta\underline{R}^* \qquad (8-2)$$

For dynamic analysis, $\underline{K}^*$ and $\Delta\underline{R}^*$ are effective matrices containing inertia and damping terms.

If all terms in $\Delta\underline{r}$ are initially unknown, the equation solving operation is straightforward. In some cases, however, certain terms in $\Delta\underline{r}$ are specified as imposed displacements (e.g., vessel motions), and can be accounted for during the equation solving. This is done by skipping over the columns and rows of the corresponding equation during the reduction of the stiffness matrix, $\underline{K}^*$, and subtracting from $\Delta\underline{R}^*$ the inner product of the matrix containing the symmetric part of the skipped columns or rows and the vector containing the imposed displacements. The back-substitution to compute the displacements is then done also by skipping over the equations corresponding to imposed displacements.

REFERENCES

American Petroleum Institute, 1987, "Recommended Practice for Planning, Designing and Constructing Fixed Offshore Platforms."

Audibert, J. M. E. and Dover, A. R., 1982, "Pile Load Tests: Cyclic Loads and Varying Load Rates," Discussion, Journal of the Geotechnical Engineering Division, Proceedings of the American Society of Civil Engineers, Vol. 108, March.

Auld, B., 1977, "Cross-Hole and Down-Hole Vs by Mechanical Impulse," Journal of the Geotechnical Engineering Division, ASCE, GT12, December, pp. 1381-1398.

Bea, R. G., Audibert, J. M. E., and Dover, A. R., 1980, "Dynamic Resposne of Laterally and Axially Loaded Piles," Proceedings, Offshore Technology Conference, Vol. 2.

Bergan, P., 1980, "Solution Algorithms for Nonlinear Structural Problems," Proceedings of the International Conference on Engineering Applications of the Finite Element Method, Høvik, Norway, May.

Bergan, P., et a., 1969, "Solution Techniques for Nonlinear Finite Element Problems,", International Journal of Numerical Methods in Engineering, Vol. 12, 1978, pp. 1677-1696.

Chen, P. F., 1982, "Generalized Plastic Hinge concepts for 3-D Beam-Column Elements," Earthquake Engineering Research Center, November.

Coyle, H. M. and Reese, L. C., 1966, "Load-Transfer for Axially Loaded Piles in Clay," Journal of the Soil Mechanics and Foundation Division, ASCE, Vol. 92, March 1966.

Crisfield, M. A., 1981, "A Fast Incremental/Iterative Solution Procedure that Handles 'Snap-Through'," Computers and Structures, Vol. 13, pp. 55-62.

Dean, R. G., 1965a, "Stream Function Representation of Nonlinear Ocean Waves," Journal of Geophysical Research, Sept. 15, Vol., 70, No. 18, pp. 4561-4572.

Dean, R. G., 1965b, Coastal Engineering, Santa Barbara, Specialty Conference, ASCE, October.

Dennis, J. E. and More, J. J., 1977, "Quasi-Newton methods, Motivation and Theory," SIAM Review, Vol. 19, No. 1, pp. 46-89.

Grosch, J. J. and Reese, L. "Field Tests of Small-Scale Pile Segments in a Soft Clay De Repeated Loading," Proceedings, Offshore Technology Confer

Haiser, W. E. and Stricklin 7, "Displacement Incrementation in Nonlinear Structure Analysi f-Correcting Method," International Journal of Nu ods in Engineering, Vol. 11, pp. 3-10.

Hibbit, H. D. and Karlsoon, , "Analysis of Pipe Whip," ASME Pressure Vessels and Piping San Francisco, California, June 25-29.

Hilber, H. J., Hughes, T. J lor, R. L., 1977, "Improved Numerical Dissipation for T on Algorithms in Structural Dynamics," Earthquake Engin ructural Dynamics, Vol. 5, pp. 283-292.

Holmquist, D. V. and Matloc "Resistance-Displacement Relationships for Axially L n Soft Clay," Proceedings, Offshore Technology Conferer 2474, Vol. I.

Irons, B., and Elsawaf, A-F. Conjugate Newton Algorithm for Solving Finite Element Equat ations and Computational Algorithms in Finite Element d. Bathe, Oden and Wunderlich), MIT Press, Cambridge.

Kraft, L. M., Cox, W. R. and ., 1981, "Pile Load Tests: Cyclic Loads and Varying Loa rnal of the Geotechnical Engineering Division, ASCE,

Marshall, P. W., 1974, "Post ty of Tubular Members," Meeting of Column Research Council.

Marshall, P. W., Memo to Dam ased on proprietary information from Shell Oil Company.

Matlock, H. M. and Foo, S. H. xial Analysis of Piles Using a Hysteretic and Degrading Soil rical Methods in Offshore Piling, Institute of Civil En on.

Mattheis, H. and Strang, G., lution of Nonlinear Finite Element Equations," Internati f Numerical Methods in Engineering, Vol. 14, pp. 161

Murff, J. D., 1980, "Pile Cap tening Soil, "International Journal of Numerical and Anal in Geomechanics, Vol. 4.

O'Rourke, M. J. and Dobry, R., 1979, "Spring and Dashpot Coefficients for Machine Foundations on Piles," Paper Presented at the American Concrete Institute Meeting, Milwaukee, Wisconsin, March.

Oughourlian, C. V., 1982, ANSR-III, General Purpose Computer Program for Nonlinear Structural Analysis, Ph.D. Dissertation, University of California, Berkeley.

Pierson, W. J. and Moskowitz, L., 1964, "A Proposed Spectral Form for Fully Developed Wind Seas Based on the Similarity Theory of S. A. Kitaigorodskii," Journal of Geophysical Research, Vol. 69, No. 24, December 15.

Porter, F. and Power, G., 1971, "Static and Dynamic Analysis of Inelastic Frame Structures," EERC Report No. 71-3, Earthquake Engineering Research Center, University of California, Berkeley.

Powell, G. and Simons, J., 1981, "Improved Iteration Strategy for Nonlinear Structures," International Journal of Methods of Engineering, Vol. 17, pp. 1455-1467.

Ramm, E., 1980, "Strategies for Tracing the Nonlinear Response Near Limit Points," Nonlinear Finite Element Analysis in Structural Mechanics, Proceedings of the Europe-U.S. Workshop, Ruhr-Universitat, Bochum, Germany, July 28-31.

Reese, L. C. and Cox, W. R., 1975, "Field Testing and Analysis of Laterally Loaded Piles in Stiff Clay, Proceedings, Offshore Technology Conference, May.

Riahi, A., 1979, "3-D Beam-Column Element for the ANSR-II Program," Earthquake Engineering Research Center, December.

Richart, F. E., Hall, J. R. and Woods, R. D., 1970, Vibrations of Soils and Foundations, Prentice-Hall, p. 414.

Riks, E., 1979, "An Incremental Approach to the Solution of Snapping and Buckling Problems," International Journal of Solids Structures, Vol. 15, pp. 529-551.

Sangray, D. A., 1977, "Response of Offshore Piles to Cyclic Loading," Proceedings, Offshore Technology Conference, OTC Paper 2944.

Simons, J. W., 1982, Solution Strategies for Statically Loaded Nonlinear Structures, Ph.D. Dissertation, University of California, Berkeley.

Skjelbreia, L. and Hendrickson, J. A., 1960, "Fifth Order Gravity Wave Theory," Proceedings of the 7th Coastal Engineering Conference, The Hague, pp. 184-196.